Department of Chemical and
Environmental Engineering

The University of
Nottingham

UNITED KINGDOM · CHINA · MALAYSIA

ENGINEERING OF A THERMOSTABLE ALCOHOL DEHYDROGENASE TOWARDS IMINE REDUCTION

Alanna Mary Nethercott

A thesis submitted to the University of Nottingham
for the degree of Doctor of Philosophy

September 2017

Acknowledgements

Firstly, I would like to express my heartfelt gratitude to my supervisor Dr. Anca Pordea for the constant support throughout my studies and research, for her patience, motivation, and vast knowledge. Her guidance has helped me immensely in all my time at Nottingham University and the writing of this thesis. None of it would not have been possible without her and I could not have wished for a better supervisor.

Besides my supervisor I would like to thank Steve, Rachel, Christof, Gill and Anna for all their help and encouragement at the beginning and throughout. I would also like to thank the Pordea group: Lei, Jaicy, Tim, Camille and Mattias for all their boosts of confidence, knowledge sharing especially with regards to the chemical synthesis and for the many laughs inside and outside of the lab.

I would also like to thank all the wider BECT group especially Luca, Joe and Andy for showing me the ropes and sharing all their knowledge and experience in the beginning and throughout. In addition to the lab technicians, Sam, Amy and Rachel for their help in preparing media, glassware, etc. A huge thank you goes to Doerte for all her help experimentally and performing parts of the work carried out in sections *4.1.6* and *4.2.2.*

Another thank you goes to my lovely Coates ladies Maria and Lois who have shared in this PhD experience and to my housemates, Charlotte and Angela for keeping me sane and for their friendship. Also, my PhD bffs Athina and Juliana who I've have shared many a laugh and plenty of tears with during this whole PhD experience.

To my friends at home, Carrie, Stacey, Amy and Rachael for their encouragement and support especially during the write up period.

A massive thank you goes to my wonderful parents for putting up with me during the write up period and the rest of my family especially my brother and sisters for their

Abstract

The enantioselective reduction of carbon-nitrogen double bonds is a powerful tool for accessing chiral secondary amines. These are important building blocks in the production of many high-added value chemicals, with an estimated 40-45 % of all pharmaceuticals and 20 % of agrochemicals containing a chiral amine intermediate. However, most of their current methods of manufacture are inefficient and wasteful. As a consequence, there is an interest to develop better synthetic routes to chiral amines based on the use of catalytic technologies and of atom efficient reagents. One approach is with the use of enzymes, due to their high activities and selectivities, mild reaction conditions and their renewable origin. The enzymatic reduction of imines is a relatively recent area of research, and the known imine reductases (IREDs) have low activities and limited substrate scope. The research presented here investigates new routes to make imine reduction biocatalysts, whereby an alcohol dehydrogenase is used as a starting point to engineer reaction promiscuity. These enzymes catalyse the reduction of a similar functionality, the carbon-oxygen double bond. The mode of substrate activation differs between the two enzymes: a Brønsted acid is used in imine reductases, while a zinc(II) Lewis acid is used in alcohol dehydrogenases.

The well-characterised thermostable alcohol dehydrogenase from *Thermus* sp. ATN1 (TADH) was selected, due to its broad substrate range and stability. Docking studies with selected imines suggested that these substrates could be accommodated in the hydrophobic binding pocket. Both imines and amines were shown to act as mixed inhibitors of the native TADH activity, and it was suggested that inhibition occurred due to binding elsewhere in the active site. Three approaches were investigated towards the engineering the TADH active site to avoid inhibition and promote imine activation, based on both genetic and chemical modifications.

First, sixteen zinc-devoid TADH mutants containing aspartic acid or tyrosine at selected positions within the active site were created, in an effort to mimic the key features found in existing imine IREDs. Whilst ketone reduction activity was abolished in these mutants, no imine reduction activity could be restored. Second, a chemical modification approach was proposed, involving the replacement of the catalytic

zinc(II) ion by a rhodium(I), which is known to activate imines in synthetic catalysts. Zinc was successfully removed from the active site to yield apo-TADH, as shown by the absence of catalytic activity. Rhodium(I) was observed to non-selectively bind to apo-TADH and to restore a small degree of native activity, however no imine reduction activity was observed. Finally, a novel iridium(III) complex containing a nicotinamide-functionalised *N*-heterocyclic carbene ligand was designed and synthesised. This complex was capable of performing transfer hydrogenation of an aromatic ketone and an aromatic imine, in both organic and aqueous conditions. An increased activity was observed for the imine compared to the ketone in aqueous media employing sodium formate as the hydride source. Inhibition studies showed that the Ir-catalyst acted as a mixed inhibitor for TADH, suggesting that interactions with the protein do not occur at the co-factor binding site.

Table of Contents

List of Abbreviations

ACN	Acetonitrile
ADH	Alcohol dehydrogenase
AEX	Anion exchange chromatography
Ar	Aryl
Bis-tris	*Bis*(2-hydroxyethyl)aminotris(hydroxymethyl)methane
Bn	Benzyl
COD	Cyclooctadiene
Cp*	Pentamethylcyclopentadiene
DCM	Dichloromethane
dH_2O	Deionised water
DA	Dipicolinic acid (2,6-pyridinedicarboxylic acid)
DMF	Dimethyl formamide
DMSO	Dimethyl sulfoxide
E. coli	*Escherichia coli*
EDTA	Ethylenediaminetetraacetic acid
ee	Enantiomeric excess
ESI^+-MS	Electrospray ionisation mass spectrometry (positive mode)
EtOAc	Ethyl acetate
eqv.	Equivalents
HLADH	Horse liver alcohol dehydrogenase
HPLC	High performance liquid chromatography
ICP-MS	Inductively coupled plasma mass spectrometry
IPTG	Isopropyl β-D-1-thiogalactopyranoside
*i*Pr	Isopropyl
IRED	Imine reductase
K_M	Michaelis constant
LB	Lysogeny broth
Me	Methyl
MeOH	Methanol
MES	2-(*N*-morpholino)ethanesulfonic acid
MWCO	Molecular weight cut-off

NAD$^+$ / NADH	Nicotinamide adenine dinucleotide oxidised form / 1,4-reduced form
NADP$^+$ / NADPH	Nicotinamide adenine dinucleotide phosphate oxidised form / 1,4-reduced form
NHC	*N*-heterocyclic carbene
NMR	Nuclear magnetic resonance
OD (OD$_{600}$)	Optical density (measured at 600 nm)
OPA	*Ortho*-phenanthroline (1,10-phenanthroline)
PAGE	Polyacrylamide gel electrophoresis
PDB	Protein Data Bank
Ph	Phenyl
rpm	Rotations per minute
r.t.	Room temperature
SDS	Sodium dodecyl sulphate
SEC	Size exclusion chromatography
TADH	Alcohol dehydrogenase from *Thermus* sp. ATN1
TsDPEN	*N*-tosylated 1,2-diphenyl ethylene diamine
Tris	Tris(hydroxymethyl)aminomethane
U	Unit of activity = μmol substrate / min
U / mg	Specific unit of activity μmol substrate / (min.mg enzyme)
UV	Ultra-violet
v / v	Volume / volume ratio
V$_{max}$	Maximum reaction rate (velocity) of enzyme
WT	Wild type

Chapter 1 Literature review

1.1   Imine reduction as a tool for chiral amine synthesis

1.1.1   Background

Chiral amines are important constituents of many bioactive compounds, such as natural products, pharmaceuticals and agrochemicals. They also have notable use as ligands in transition metal catalysis or as chiral organocatalysts, as well as resolving agents for the separation of enantiomers *via* diastereomeric salt formation.[1] It has been estimated that approximately 40-45 % of pharmaceuticals and 20 % of agrochemicals contain a chiral amine functionality.[2-5] A selection of commercially relevant compounds containing chiral amines is shown in Figure 1.1.

Rivastigmine

Tamsulosin

Repaglinide

Lopinavir

Lariam

Ethambutol

Tubulosine

(S)-Metolachlor
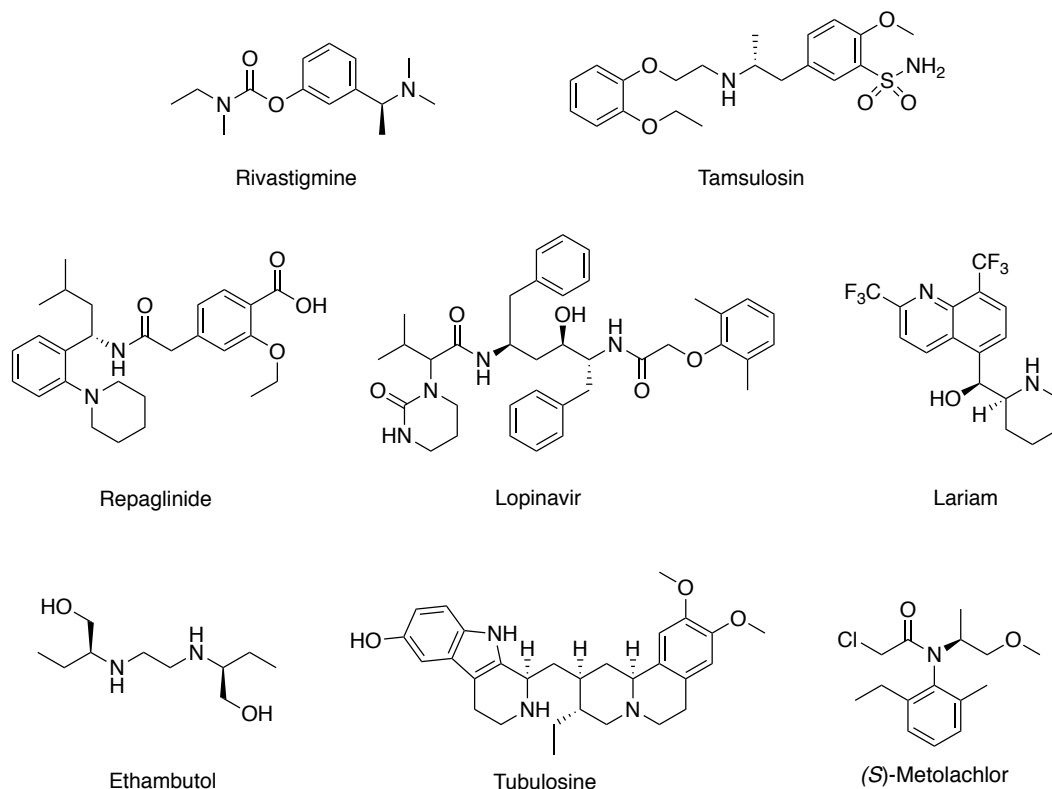
Figure 1.1. Selection of commercially relevant bioactive compounds containing chiral amines.

Current industrial methods to produce enantiomerically pure chiral amines are largely dependent upon the resolution of racemates.[6] With a maximum attainable yield of 50 %, the kinetic resolution route is inefficient in terms of atom economy, especially if the desired racemate requires a multistep synthesis. Consequently, continued

substantial effort has gone into the development of more efficient methods for the synthesis of chiral amines.[7] A particularly efficient route is the reduction of imines, which in turn can be prepared from the corresponding ketones (Figure 1.2). When imine formation and reduction occur sequentially in one pot, the reaction is referred to as reductive amination. Importantly, these reactions give access to secondary amines.
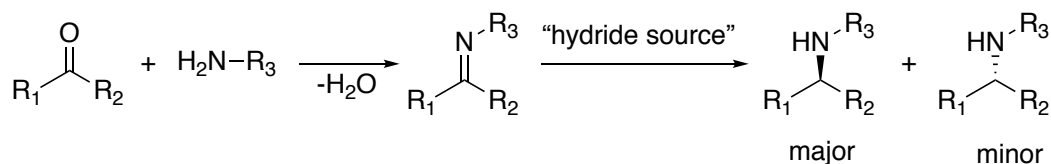
Figure 1.2. General reaction scheme for indirect reductive amination for the synthesis of chiral amines including the enantioselective imine reduction step.

Furthermore, the reductive amination highlighted in Figure 1.2 is performed with a primary amine reacting with the carbonyl group of the ketone. However, when a secondary amine is used, the reaction yields an iminium ion intermediate. This charged species can further tautomerise to the corresponding enamine, if an acidic proton is available in the α-position of the ketone / iminium functionality (Figure 1.3).
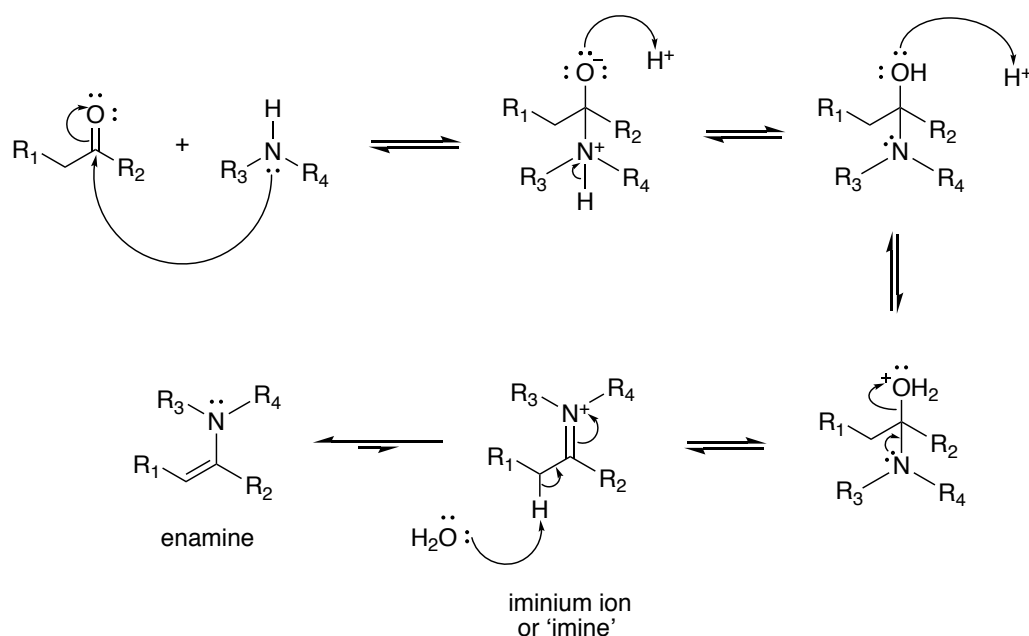
Figure 1.3. Acid-catalysed nucleophilic reaction of a ketone with a secondary amine highlighting enamine formation.

Traditional methods for secondary amine synthesis *via* this route are energy-consuming, not very efficient and generate waste. As a consequence, there is an interest to develop better routes for the reduction of carbon-nitrogen double bonds (C=N), based on the use of catalytic technologies and of atom efficient reagents. During a roundtable discussion of international pharmaceutical companies in 2005, this reaction was highlighted as one of the key research areas needing improvement by the incorporation of 'green chemistry' principles.[8]

The development of efficient processes towards enantioselective imine reduction has been slow, compared to the numerous reduction methods of their carbonyl counterparts. Nonetheless, important advances were made in the early 2000's towards the development of practical approaches, largely based upon synthetic transition-metal catalysts for the reduction of imines using various sources of hydride.

1.1.2 Synthetic catalysts for imine reduction

1.1.2.1 Metal catalysts for imine hydrogenation and transfer hydrogenation

Early efforts to asymmetrically reduce imines focused on the development of transition metal catalysts for asymmetric hydrogenation. The majority of hydrogenation catalysts generally consist of a transition metal ion in a low oxidation state, attached to a chiral ligand. The metal controls the reactivity whilst the ligand is responsible for introducing selectivity into the final product. The hydrogen atoms are accessed from either molecular hydrogen (a reaction known as hydrogenation) or from an organic hydrogen source (Figure 1.4), such as 2-propanol, formic acid or Hantzsch esters (referred to as transfer hydrogenation). The latter structure is an analogue of the biological hydride source nicotinamide adenine dinucleotide (NADH), used as a cofactor by enzymes performing reductions in nature.
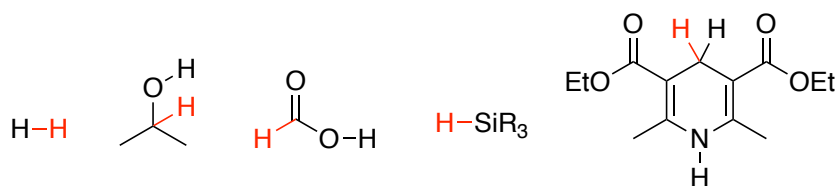
Figure 1.4. Hydride sources used with transition metal catalysts.

The first catalytic example of asymmetric hydrogenation of imines was reported by Levi *et al.* in 1975, using the rhodium-diphosphine catalyst Rh-DIOP (Figure 1.5) and molecular hydrogen. Although the optical purity was relatively low (22 % ee), this work demonstrated the use of a chemical complex based on a transition metal as a new route to enantiomerically enriched chiral amines.[9]
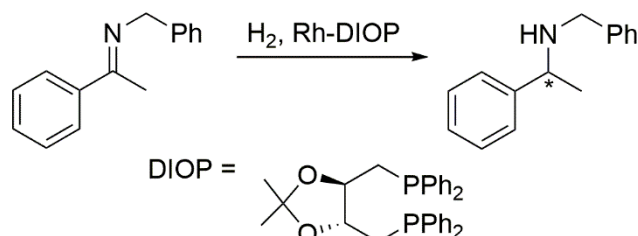
Figure 1.5. Asymmetric imine reduction with the Rh(DIOP) catalyst.[9]

Significantly higher enantioselectivities (60-70 % ee) were obtained a decade later, using a range of other chiral rhodium-based diphosphine ligand complexes.[10] Bakos *et al.* reported the asymmetric hydrogenation of *N*-benzyl imines in a biphasic water ethyl acetate mixture, with a rhodium complex of the sulfonated 2,4-bis(diphenylphosphino)pentane (BDPP) ligand (Figure 1.6).[11]
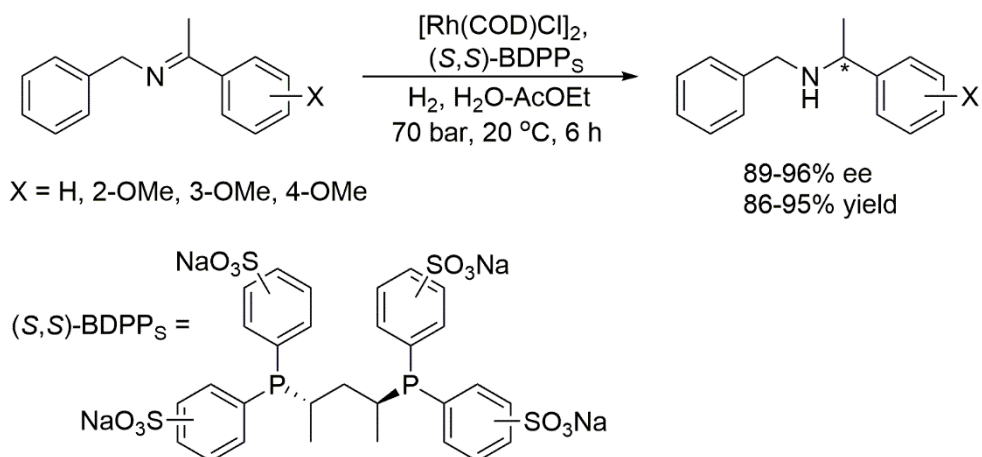
Figure 1.6. Asymmetric imine reduction in biphasic conditions with Rh-BDPPS.

Current existing catalysts for imine hydrogenation most commonly consist of rhodium, ruthenium, iridium or palladium complexes.[12] Amongst these, iridium-based catalysts with bidentate phosphorous ligands are the most efficient. For example, the iridium based complex Ir-xyliphos is employed in the industrial process for the

enantioselective reduction of the imine precursor of the herbicide *(S)*-Metolachlor, commercially known as Dual Mangum® (Figure 1.7).[13]
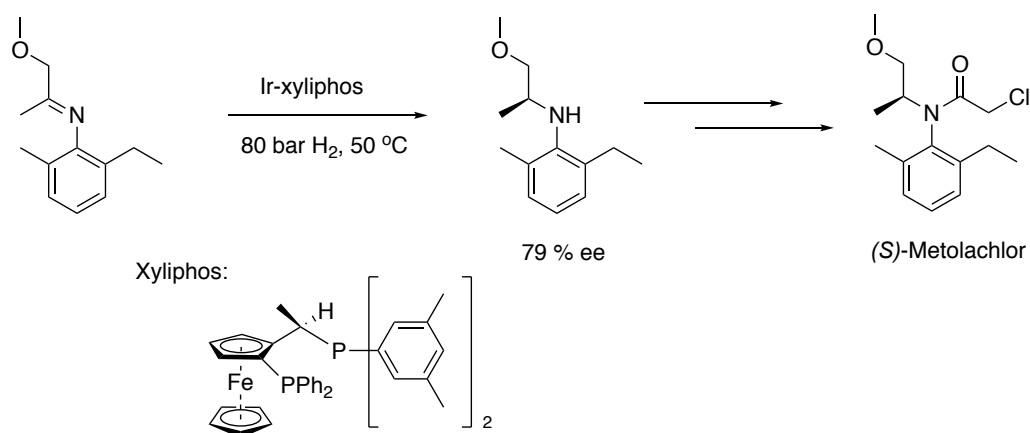
Figure 1.7. Asymmetric imine hydrogenation using Ir-xyliphos, applied to the synthesis of *(S)*-metolachlor. Modified from Blaser *et al.* (1999).[13]

A major breakthrough came in 1996, when Noyori, Ikariya and co-workers reported the first chiral Ru(II) complex for the asymmetric transfer hydrogenation of various imines with high enantioselectivities (77-97 % ee). The same authors had initially developed these complexes for the transfer hydrogenation of ketones. The piano-stool π-complex, [Ru(*p*-cymene) (TsDPEN)Cl], contained *p*-cymene as the capping arene and the *N*-tosylated 1,2-diphenyl ethylene diamine (TsDPEN) as the chiral
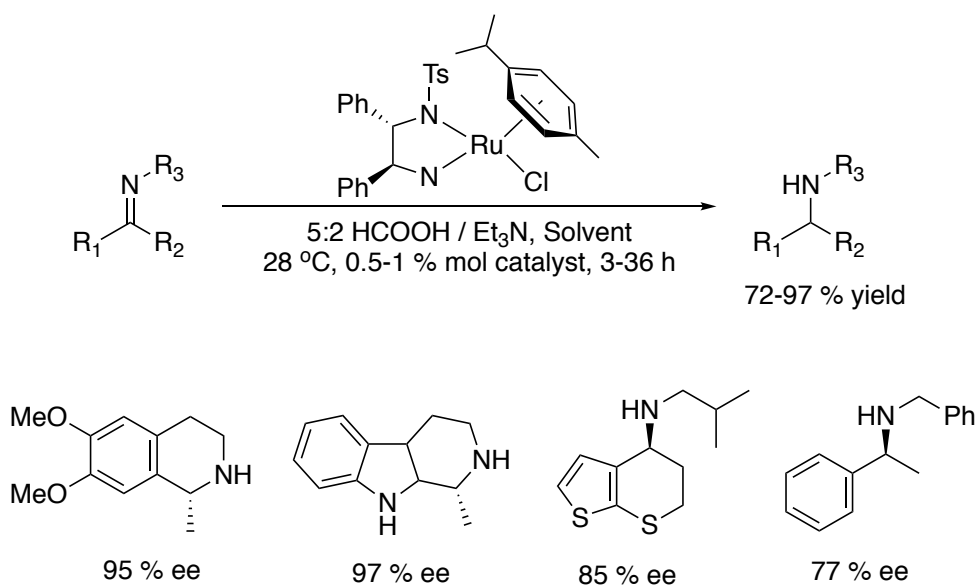
Figure 1.8. Asymmetric transfer hydrogenation of selected imines using the Noyori-Ikariya catalyst. Modified from Wang *et al.* (2011).[14]

ligand. Instead of hydrogen, the formic acid-triethylamine mixture was used as hydride source (Figure 1.8).[14]

Since the discovery of the Ru-aminosulfonamide complexes for imine transfer hydrogenation, a variety of ligands and metal complexes have been developed for the reduction of a range of substrates.[12] The most successful catalytic systems are based on half-sandwich π-complexes of Ru(II), Rh(III) and Ir(III), with a capping arene (usually *p*-cymene) or cyclopentadienyl ligand (Cp or Cp*). The best chiral ligands are bidentate monotosylated 1,2-diamines or 1,2-amino alcohols. An additional ligand, usually a halide, occupies the fourth coordination site, and is displaced during catalysis to allow formation of the active hydride species (Figure 1.9).
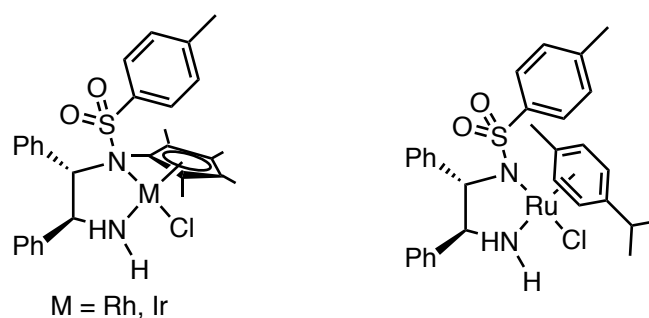
Figure 1.9. General structures of half-sandwich Ru(II), Rh(III) and Ir(III) π-complexes for the asymmetric transfer hydrogenation of ketones and imines.

The most common hydride sources are the azeotropic mixture of formic acid and triethylamine (HCOOH / Et$_3$N)[15] and alcohols such as isopropanol (*i*PrOH).[16] Aqueous sodium formate (HCOONa) can also be used, for reactions taking place in water.[17] When isopropanol is used, a base such as potassium hydroxide is necessary to activate the complex, and the hydride transfer is reversible.[18,19] However, asymmetric transfer hydrogenation of imines does not proceed when isopropanol is used as the hydride souce with Noyori's catalyst.[20] When formate is used in an open system, the reaction proceeds in an irreversible manner, due to the formation and continuous elimination of gaseous CO$_2$.[15,21]

In addition to the bidentate ligands described above, *N*-heterocyclic carbenes (NHCs) have been reported to promote reduction of imines. Efficient catalysts include complexes of NHCs with Ru(II)-arene and Rh(III) / Ir(III)-cyclopentadienyl, but also

Rh(I)- and Ir(I) complexes, bearing diene ligands such as cyclooctadiene (COD) (Figure 1.10).[22-23] Most catalysts are based on Ir and Ru, with less examples available for Rh. Generally, catalysts that perform imine transfer hydrogenation would also be active for the reduction of imines. Few examples are found in aqueous solutions, and isopropanol is the most commonly used hydride donor, in the presence of a base, such as KOH. For example, *N*-benzyl-substituted NHCs based on benzimidazole were shown to promote imine transfer hydrogenation in >99 % yields when complexed to Ir(I),[24] while Ir(III) and Ru(II) complexes with 4-acetylbenzyl-NHCs were active in both ketone and imine reduction.[25]
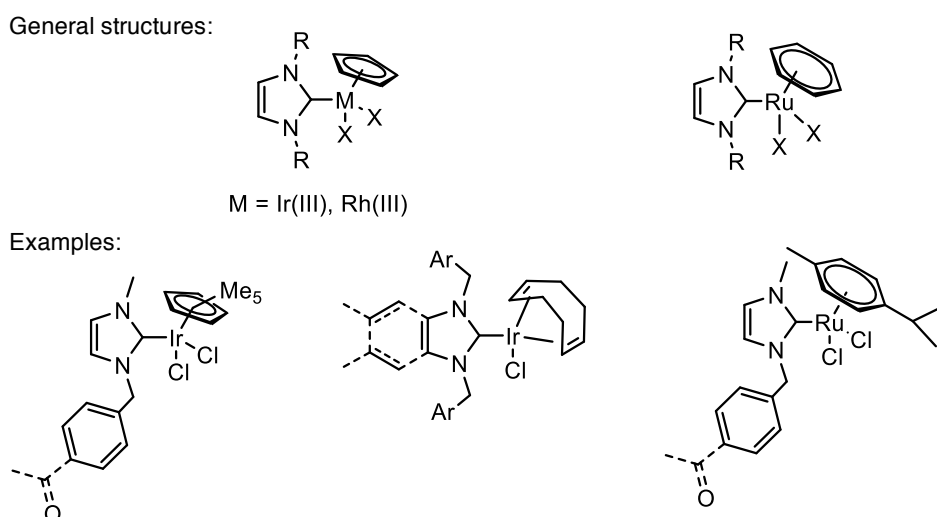
Figure 1.10. Metal complexes of NHCs for imine reduction.

1.1.2.2 Mechanism of imine transfer hydrogenation

The general mechanism for the metal-catalysed reduction of carbonyls and imines involves formation of the metal hydride, followed by its transfer to the substrate.[18,26,27] The mechanisms of ketone and imine reduction are very similar and metal complexes used for this catalysis are generally quite similar too. The full catalytic cycle is shown in Figure 1.11 for the reduction of aromatic imines using [Ru(*p*-cymene)(*R,R*-TsDPEN)Cl] complex. The catalyst precursor **A** first eliminates HCl to form the 16 e⁻ catalytic species **B.** Hydride transfer from the donor leads to the 18 e⁻ Ru-hydride complex **C**, which in turn transfers the hydride to the substrate, to re-form the 16 e⁻ complex **B.**
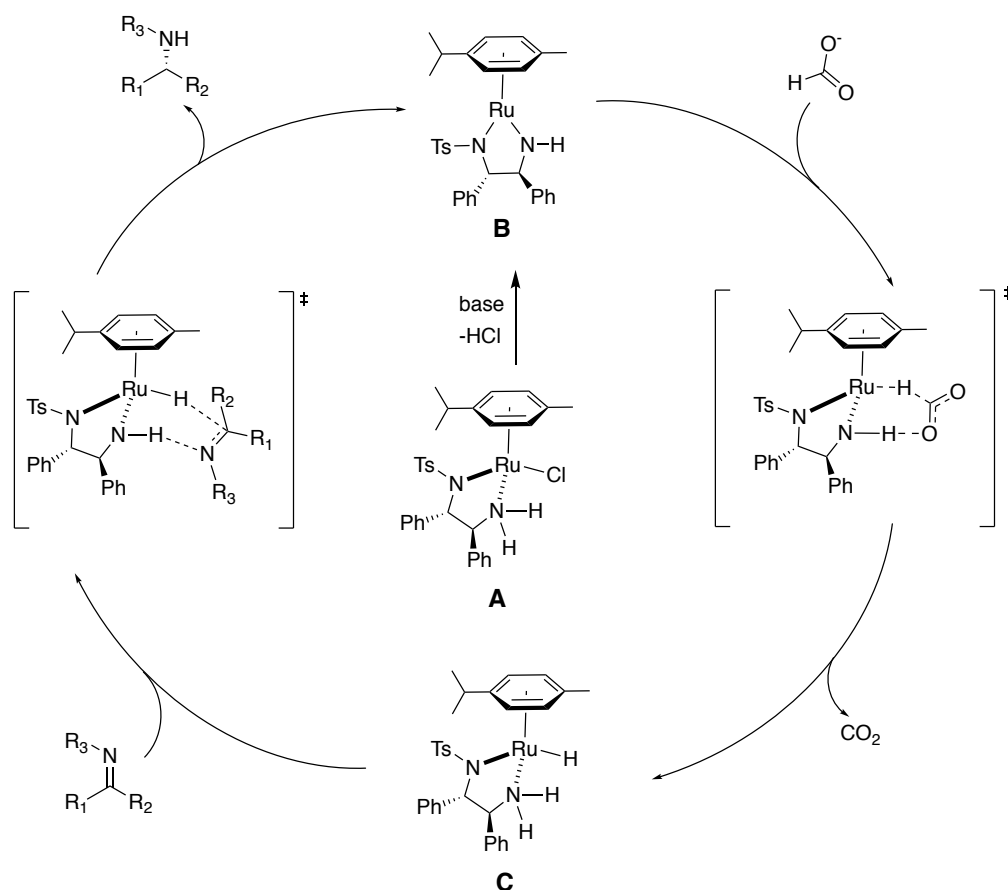
Figure 1.11. Catalytic cycle for the transfer hydrogenation of imines by [Ru(*p*-cymene)(*R,R*-TsDPEN)Cl] with formate as hydrogen donor.

The mechanism of transfer hydrogenation is classified depending on the role played by the substrate: coordination of the substrate to the metal centre is characterised as inner sphere, whereas no direct coordination of the substrate to the metal centre is characterised as outer sphere.[28] In both pathways the metal hydride is transferred onto the sp^2-carbon, which is activated differently depending on the mechanism.

In the inner sphere mechanism, the metal centre acts as a Lewis acid, with imine activation occurring by coordination to the metal centre *via* a vacant coordination site, followed by protonation of the heteroatom by the protic solvent. In the outer sphere mechanism, the hydride and proton are transferred in a concerted polarised or stepwise fashion, upon activation of the heteroatom by hydrogen bonding or by protonation (Figure 1.12).[29] When the proton is acquired from a ligand in the metal complex, as exemplified in Figure 1.11, the outer sphere mechanism is referred to as bifunctional catalysis, a term coined by Noyori.[30] The substrate is activated through

hydrogen bonding with the ligand, a six membered transition state occurs between the complex and the substrate, allowing both proton and hydride transfer to occur in a concerted fashion.[18,26]
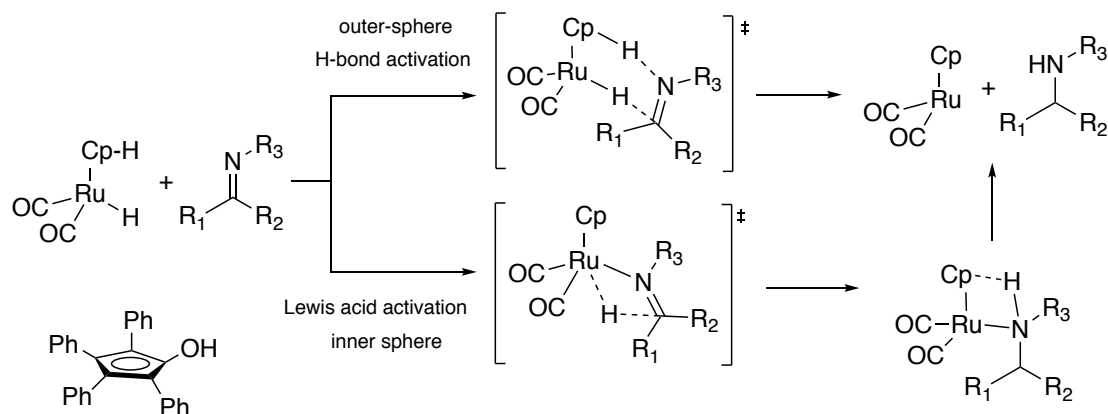
Figure 1.12. Asymmetric imine reduction via inner and outer sphere mechanisms. Modified from Wang *et al.* (2011).[14]

In other studies, Bäckvall and co-workers suggested that that the imine only reacts with the metal hydride complex in the presence of acid, which protonates the imine to yield an iminium ion, which is then reduced to the corresponding amine (Figure 1.13).[31] Others have also confirmed this ionic mechanism.[32,33] Norton clearly defined this mechanism for the asymmetric hydrogenation of iminium salts with Ru-diphosphine catalysts.[34,35]
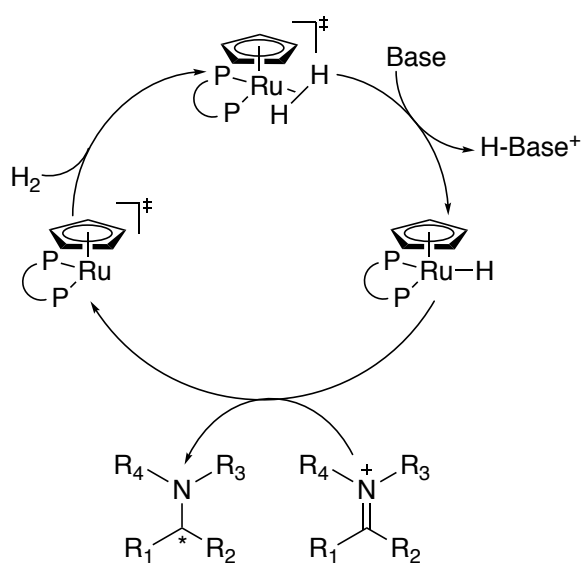
Figure 1.13. Proposed ionic mechanism for imine reduction. Modified from Wang *et al.* (2011).[14]

Several examples of aqueous-phase transfer hydrogenation reactions have been reported.[17,36-39] Generally, water-soluble catalysts contain ligands with sulfonic acid functionalities and sodium formate is employed as the hydrogen source. The low solubility of the substrates in the reaction mixture does not seem to affect the yields.[36] The pH has a critical influence on rate and enantioselectivity as highlighted in investigations by both Ogo *et. al.*[40] and Wu *et. al.*[41] In contrast to ketones, an important issue for aqueous imine reduction is the hydrolysis of imines in water, to form the corresponding carbonyl and amine precursors. The use of cyclic imines minimises this problem.[42] Some acyclic imines derived from aryl ketones have also been successfully used in aqueous systems.

Xiao and co-workers found that the reduction of quinolines by the [(Cp*)Rh(TsDPEN)Cl] catalyst was strongly dependent on the pH, with the maximum conversion obtained at pH 5.[33] The suggested explanation is that a compromised pH had to be achieved, where the protonated quinoline (pKa 5.4) and the formate (pKa 3.6) species were sufficient for the reaction to occur.

Catalysts based on Ru, Rh and Ir- aminosulfonamide complexes have all shown to be active in the aqueous transfer hydrogenation of imines.[17,39,42] (Figure 1.14)

M = Ru, Rh (and Ir) precursor

TsDPEN$_S$ = soluble TsDPEN:
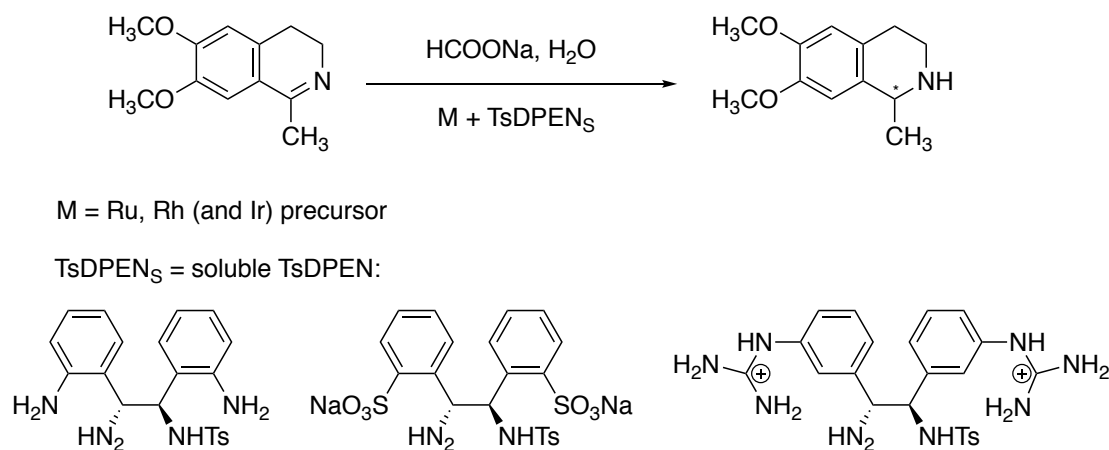
Figure 1.14. Aqueous transfer hydrogenation of imines.

For example, Deng and co-workers reported a range of chiral water-soluble catalysts for the asymmetric transfer hydrogenation of both ketones and imines using

N-aminosulfonated ligands bearing solubilising groups such as sulfonate (guanidinium, or amines).[17]

1.1.2.4 Bioinspired imine transfer hydrogenation

A biologically inspired approach to imine reduction was recently reported, which utilises a rhodium complex tethered to Hantszch ester. Hantszch esters are commonly used in transfer hydrogenation as mimics of the biological NAD(P)H cofactor.[43-46] Colbran and co-workers developed this bio-inspired metal complex as an active site mimic of alcohol dehydrogenase for imine reduction.[47] The basic mechanism involved imine activation by direct coordination to the metal centre acting as a Lewis acid, hydride transfer from the tethered dihydropyridine ligand, followed by proton transfer from the formate proton source (Figure 1.15). The complex produced the corresponding amines in excellent yields (>90 %) from simple aldimines and ketimines in air. Additionally, reduction of the pyridinium ligand to dihydropyridine was possible *via* the rhodium hydride (Rh-H) complex. This is an example of how modern chemistry is moving towards "greener" synthesis with assistance from Nature.
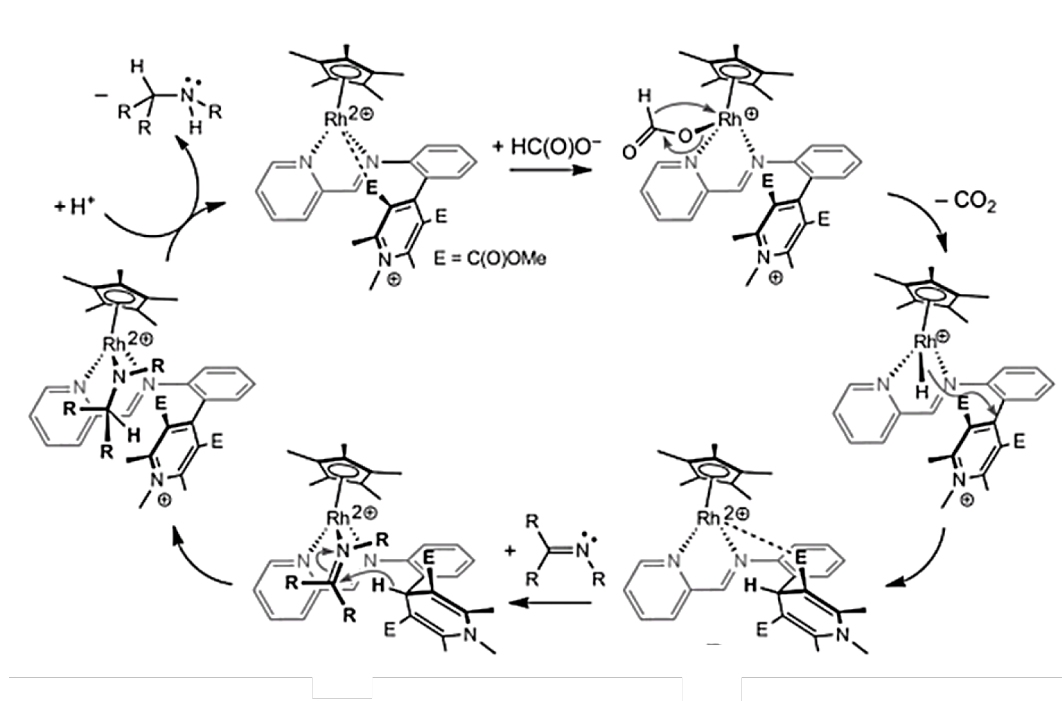
Figure 1.15. Proposed mechanism of imine transfer hydrogenation using the bioinspired Hantzsch pyridine tethered rhodium catalyst. Reproduced from McSkimming *et al.* (2013).[47]

Despite the successful progress of metal catalysts for the asymmetric transfer hydrogenation of imines in aqueous conditions there are still some limitations, such as the use of enantiomerically pure ligands that require a long and difficult synthesis. The metal centre is also quite expensive and can be susceptible to deactivation from any nitrogen or sulphur containing compounds within the reaction. Thus, efforts are still being made towards the development of efficient processes for imine reduction as a way to access enantiopure amines.

1.1.3 Biocatalysts for imine reduction

1.1.3.1 Background and early developments

The potential of enzymes as "green catalysts" has been increasingly recognised and exploited in the past 20 years. As a consequence, much research has focused on the discovery and development of biocatalysts capable of enantioselective imine reduction, as a direct approach to chiral amines. Until recently, this reaction was assumed to be absent from nature's enzymatic toolbox. Currently, various enzymatic routes exist for the synthesis of optically active primary amines, such as (dynamic) kinetic resolution using hydrolases, asymmetric synthesis using amine dehydrogenases and deracemisation using monoamine oxidase.[48] Transaminases[49] and ammonium lyases[50] have recently found applications in industry for the synthesis of optically active primary amines.

On the other hand, the enzymatic routes towards chiral secondary or tertiary amine derivatives are less common. For example, few transaminases can produce secondary amines with smart substrate selection when coupled with chemical catalysts.[51] Thus, efforts into the search and development of biocatalysts for asymmetric imine reduction have been emerging. At the beginning of this thesis, the number of published examples of enzymes exhibiting imine reductase[52] activity was limited to *Candida parapsilosis* (ATCC 7330),[53] *Pseudomonas*[54-56] and *Streptomyces* sp;[52,57,58] strains reported to possess this activity. Since these initial reports, much work has gone into the discovery and development of imine reductases and the number has been increasing over the past few years, along with an understanding of their characteristics and mechanism.

Candida parapsilosis ATCC 7330, a fungal species from the yeast family originally used as a biocatalyst for the asymmetric reduction of α- and β- keto esters[59-60] was investigated for asymmetric imine reduction, due to the chemical analogy between ketones and imines. The functional groups (C=O) and (C=N) of these compounds display similar chemical reactivities, due to their similarity in size and the availability of lone electron pairs. Indeed, resting / living *Candida* cells were found to reduce aryl imines to the corresponding *(R)*-amines with good yields and high enantioselectivities (Figure 1.16).[53] However, low reaction rates were observed with these systems.

R₁= 2-OH, 4-CH₃O, 4-Cl, 2-NO₂
R₂= H, 3-NO₂

55 - 80 % yield
95 - >99 % ee
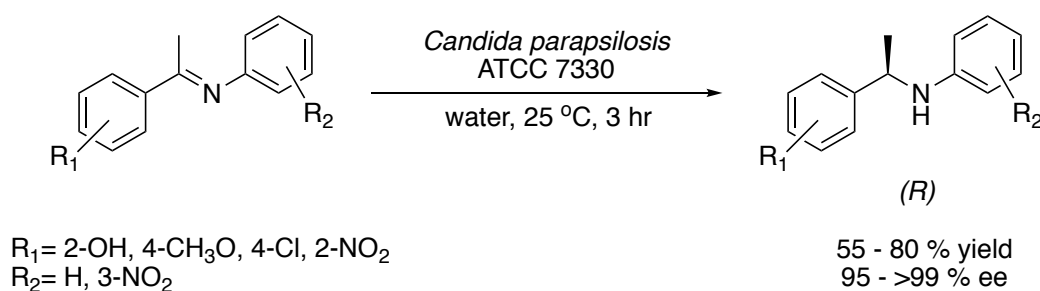
Figure 1.16. Imine reduction using *Candida parapsilosis* ATCC 7330. Modified from Vaijayanthi *et al.* (2008).[53]

Li *et al*. demonstrated the use of a dynamic combinatorial screen as a versatile approach for the discovery of imine reductase activity.[61] They used whole cells of *Acetobacterium woodii,* an anaerobic bacterium which reduces C=C double bonds as part of a respiratory process, to reduce aldimines, formed *in situ* from the corresponding amines and aldehydes. The products were obtained in low quantities, and the enzymes responsible for this reaction were not identified.

Enzymes from *Pseudomonas putida* ATCC 12633[55] and *Pseudomonas syringe* pv. tomato[56] were also observed to possess imine reductase activity towards Δ^1-piperidine-2-carboxylate and Δ^1-pyrroline-2-carboxylate, producing the corresponding *(S)*-amines in the presence of NADPH as the cofactor (Figure 1.16). These *Pseudomonas* enzymes have been classed as NADPH-dependent oxidoreductases belonging to a new family of malate / lactate dehydrogenases (MDH / LDH). The family retains no sequence homology to conventional MDH / LDHs, and the main difference was observed in the NADPH-binding site[62,63] therefore displaying

different activities.[64-66] However, yields and optical purities of the corresponding amines were not reported.
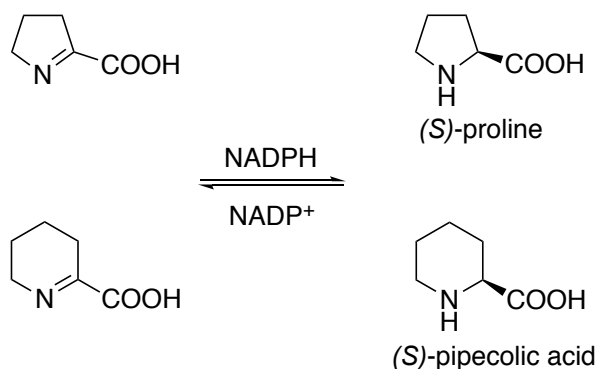
Figure 1.17. Imine reduction using *Pseudomonas* strains.[56]

Streptomyces sp. was another strain reported to possess imine reductase activity by Mitsukura *et al*. in 2010, and has been extensively studied ever since.[57] Five *Streptomyces* sp. based strains were reported to display asymmetric imine reduction activity with 2-methyl-1-pyrroline as substrate (Figure 1.18). *Streptomyces* sp. GF3587 produced the corresponding *(R)*-enantiomer with an optical purity of 99 % ee, while *Streptomyces* sp. GF3546 produced the *(S)*-enantiomer, with 81 % ee.
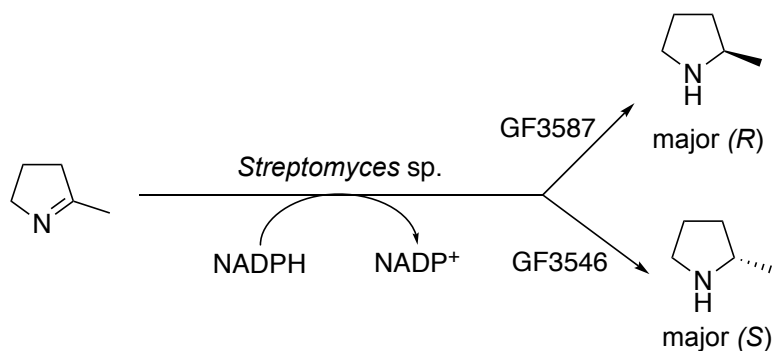
Figure 1.18. Imine reduction using *Streptomyces* strains.[57]

1.1.3.2 Imine reductases and their applications

Following the successful results described above with the *Streptomyces* strains, the same research group purified and characterised the corresponding enzymes responsible for the imine reduction activity, which were found to be NADPH-dependent.[67] The *(R)*-imine reductase (*(R)*-IRED) from *Streptomyces* sp. GF3587 was

only active with 2-methyl-1-pyrroline,[67] whereas the *(S)*-imine reductase (*(S)*-IRED) *Streptomyces* sp. GF3546 displayed a broader substrate specificity (Figure 1.19a).[52]

Turner and collaborators extended this investigation into *(S)*-IRED from *Streptomyces* sp. GF3546, reporting the acceptance of six and seven membered cyclic imines as substrates.[68] However, reported k_{cat} values (maximum number of substrate molecules converted to product per enzyme molecule per second) were relatively low (10^{-1}-10^{-3} s^{-1}). In addition, when incorporated into an *E.coli* whole cell biocatalyst supplemented with glucose to aid cofactor recycling, this *(S)*-IRED was shown to enantioselectively catalyse the reduction of a range of substituted dihydroisoquinolines and 1-substituted dihydro-β-carbolines with excellent ee values (>98 %, Figure 1.19b).[68]

Another example of a tailor-made whole cell catalyst was designed more recently using imine reductase from *Streptomyces viridochromogenes,* alongside glucose dehydrogenase from *Bacillus subtilis,* for *in situ* cofactor regeneration. The system was incorporated and expressed in *E.coli,* and was shown to effectively reduce the model substrate 1-methyl-3,4-dihydroisoquinoline at high substrate concentrations (100 mM) with high conversion and excellent enantioselectivity (>99 % ee). This was a promising result towards any future whole-cell enantioselective imine reduction processes.

Grogan and co-workers reported a protein homologous to the *Streptomyces* sp. GF3587 *(R)*-IRED, named Q1EQE0 from *Streptomyces kanamyceticus.*[58] This enzyme showed *(R)*-selective imine reduction activity towards the monocyclic imine, 2-methyl-1-pyrroline as well as towards some dihydroisoquinoline derivatives such as 3,4-dihydroisoquinoline, including an iminium ion (Figure 1.19c).[58] This was also the first structurally characterised IRED.

Following from the successful isolation and application of IRED from *Streptomyces* strains, efforts have multiplied to find new members of this enzyme family using bioinformatics tools. At present, with the aid of recently established Imine Reductase Engineering Database ([www.ired.biocatnet.de)](www.ired.biocatnet.de) more than 30 IREDs have been

a) Substrate range of (S)-IRED from *Streptomyces* sp. GF3546

92-99 % ee
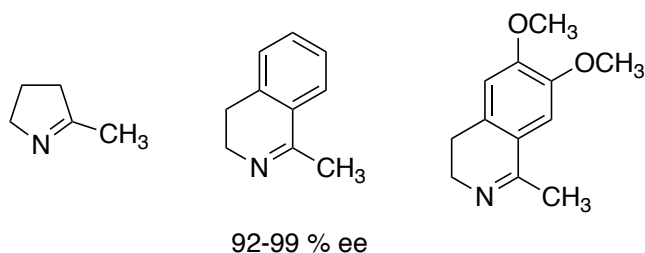
b) Imine reduction performed using (S)-IRED *Streptomyces* sp. GF3546 in whole cells
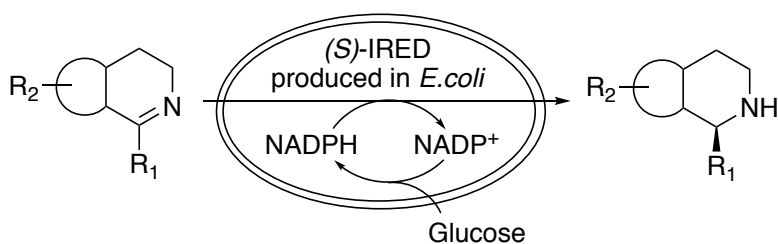
c) Substrate range of Q1EQE0 from *Streptomyces kanamyceticus*
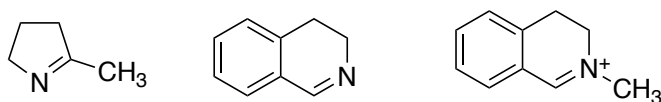
Figure 1.19. Substrate range and application scope of IREDs from *Streptomyces* strains.[52,58,68]

identified for enantioselective reductions of various cyclic imines. They are split into two superfamilies, *(R)*-IRED and *(S)*-IRED, based upon their stereopreference. Some examples of IREDs from different organisms, identified by screening of the IRED database, are briefly discussed next.

The substrate spectrum was expanded with the discovery of the *(S)*-IRED from *Amycolatopsis orientalis* (*Ao*IRED), which could reduce 5-, 6- and 7-membered monocyclic imines, in addition to isoquinolines and a few iminium ion substrates (Figure 1.20a).[69] Lenz *et. al.* reported the identification and isolation of *(S)*-IRED from *Panenibacillus elgii* (*Pe*IRED) and of the *(R)*-IRED from *Streptosporangium roseum* DSM 43021 (*Sr*IRED),[70] which were specific for their substrates: *Pe*IRED displayed a specific activity of 0.24 U / mg with 3,4-dihydroisoquinoline**,** whereas *Sr*IRED displayed a specific activity of 2.58 U / mg with 2-methyl-1-pyrroline (Figure 1.20b). These results confirmed the relatively low activities seen with the previously discussed IREDs

(0.1-3 U / mg), as well as the lower activities of *(S)*-IREDs compared to their *(R)*-IRED counterparts.

On the other hand, Li *et. al.* report *(S)*-IRED identified from *Stackebrandtia nassauensis* (*Sn*IRED),[71] which performed the reduction of 1-methyl-3,4-dihydroisoquinoline with a catalytic activity that was 25- to 1400-fold greater compared to previous IREDs. A range of dihydroisoquinolines containing relatively bulky substituents at the 1 position were reduced with moderate to excellent enantioselectivities (up to 99 % ee), depending on the α-carbon substituent (Figure 1.20c).[71]

1.1.3.3   Characterisation and mechanism of IREDs

All IREDs characterised so far are NADPH-dependent and do not contain catalytic metal ions. The majority of the IREDs discovered are of bacterial origin. Their size and complexity ranges from 21 kDa observed for small monomeric proteins to 370 kDa for the large homodecamers. They are diverse in their structure and no restricted fold for imine reductase activity has been identified. Nevertheless, the majority of IREDs share the same overall architecture: they are homodimeric proteins with one molecule of NADPH bound to each subunit. Their natural function is unknown, and their large active site suggests accommodation of larger natural substrates than the small hydrophobic imines investigated so far. This is supported by the low catalytic activities observed with these substrates.

Analysis of the IRED sequences identified two specific regions, consisting of a highly conserved co-factor binding site and a specific active site motif, relating to a primarily hydrophobic substrate-binding cleft.[72] The conservation analysis also revealed two clusters, depending on the catalytic protic residues. Generally, *(R)*-IREDs are observed in the larger cluster, possessing a conserved aspartate, while known *(S)*-IREDs are members of the smaller cluster, with a conserved tyrosine. These residues are responsible for catalysis, as demonstrated by loss of activity when mutated to alanine. However, the discovery of non-protic residues Asn and Phe in this position have also shown to be active IREDs.[69,73]

R = CH$_3$, C$_6$H$_5$, pFC$_6$H$_5$, p-OC$_7$H$_8$ R = CH$_3$, p-OC$_7$H$_8$

H$_3$CO

H$_3$CO

R = H or CH$_3$

CH$_3$

R$_1$ = CH$_3$ or C$_7$H$_7$,
R$_2$ = H or F

R$_1$ = CH$_3$ or C$_6$H$_{11}$, R$_2$ = H or OCH$_3$

b)

(R)-SrIRED

NADPH

S.A. = 0.24 U / mg

(S)-PeIRED

NADPH

S.A. = 2.58 U / mg

c)

SnIRED

NADPH

R = CH$_3$, C$_2$H$_5$, n-C$_3$H$_7$,
i-C$_3$H$_7$, C$_6$H$_{11}$, C$_6$H$_5$

up to 81 % yield
up to >99 % ee
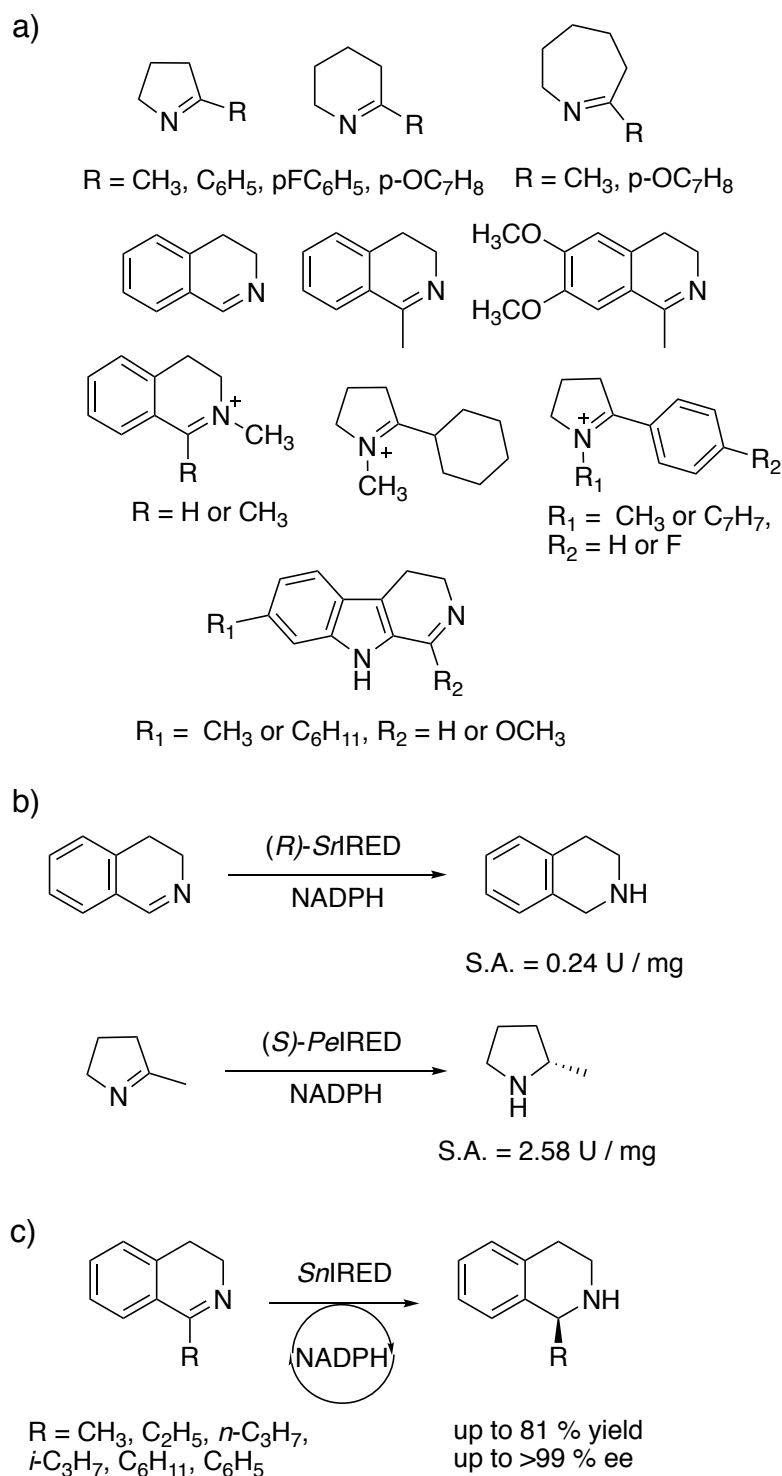
Figure 1.20. Substrate scope of asymmetric imine reduction with different IREDs identified by screening of the IRED database. a) *Ao*IRED b) *Pe*IRED and *Sr*IRED c) *Sn*IRED highlighting activities and enantioselectivities.

The IRED mechanism and the type and role of the catalytic residues are still under debate. The basis of the mechanism[74] involves the enzymes ability to bind both the cofactor and substrate in a suitable coordination for hydride transfer, and the

presence of an active site residue with a role in proton transfer. It is unclear which of hydride or proton transfer occurs first, and two approaches have been highlighted: 1) formation of an iminium ion through protonation of the imine, followed by hydride transfer forming the nascent amine; or 2) concerted transfer of hydride and proton. These mechanisms are similar to the bifunctional and ionic mechanisms described in Section *1.1.2.2* with the synthetic catalysts, except that in the case of the IREDs hydride delivery is not mediated by a metal.

The first structurally characterised IRED was reported by Grogan and co-workers and was the *(R)*-selective Q1EQE0 from *Streptomyces kanamyceticus*.[58] Three reductases that were structurally similar to this IRED were identified from the analysis: dihydrofolate reductase (DHFR) and Irp3 from *Yersinia enterocolitica*, both exhibiting imine reduction activity towards their natural substrates, and hydroxyisobutyrate dehydrogenase (HiBDH), which was a ketoreductase identified by searching similar structures *via* the DALI server.[75] DHFR is believed to transfer a proton from a water molecule to the imine substrate, thus forming an iminium ion, which is reduced to an amine *via* hydride transfer.[76] On the other hand, Irp3 is believed to first transfer the hydride and then the proton, from either a His or Tyr residue. Hydride transfer prior to protonation seems unlikely due to the high basicity of the resulting amide intermediate. In HiBDH, Lys165 in the active sites provides the proton to the nascent hydroxyl group. Superimposition of the Q1EQE0 structure with HiBDH identified Asp187 at the place of the lysine. Genetic modification of this residue to asparagine and alanine resulted in a loss of activity. From this, the suggested IRED mechanism involved imine protonation by Asp187, whose pKa is most likely lowered by the hydrophobic residues Leu191 and Leu137. The resulting iminium ion is stabilised by the predominately negatively charged active site (Figure 1.21).[58] In support of this mechanism, recent theoretical activation energies calculated by Lenz *et. al.* suggested that the protonation of imines occurred prior to hydride transfer, as the iminium ions were demonstrated to be more reactive than the corresponding imines.[74]
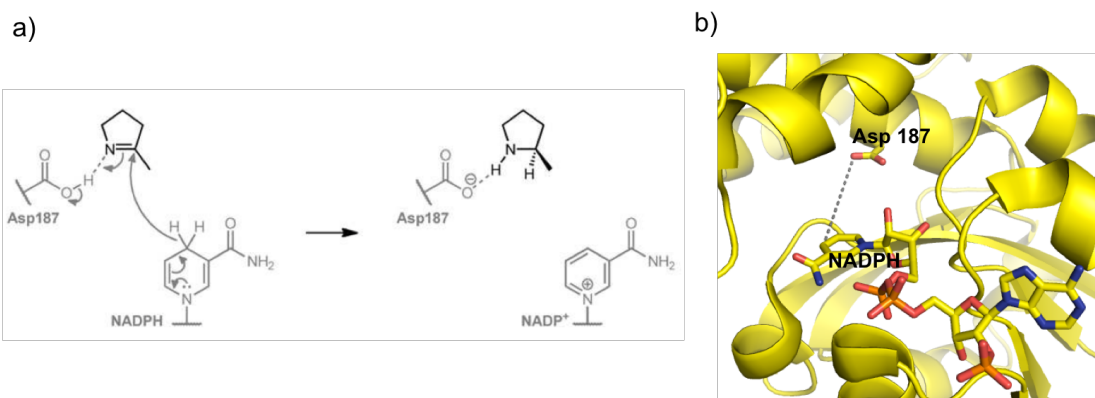
Figure 1.21. a) Suggested mechanism of Q1EQE0 IRED. Modified from Schrittwieser *et al.* (2015);[77]
b) Active site of Q1EQE0, with the suggested catalytic residue Asp187 highlighted as yellow sticks.

The *Ao*IRED structure co-crystallised with NADPH and the corresponding amine product 1-methyl-1,2,3,4-tetrahydrosioquinoline was also reported (Figure 1.22), providing the first insights into the possible substrate-binding site and interaction with active site residues. The binding position of the *(R)*-amine product shows the nitrogen atom within a 4.4 Å distance of the active site Tyr179 residue, and the chiral carbon within 3.5 Å of the C4 atom of NADPH, which delivers the hydride.
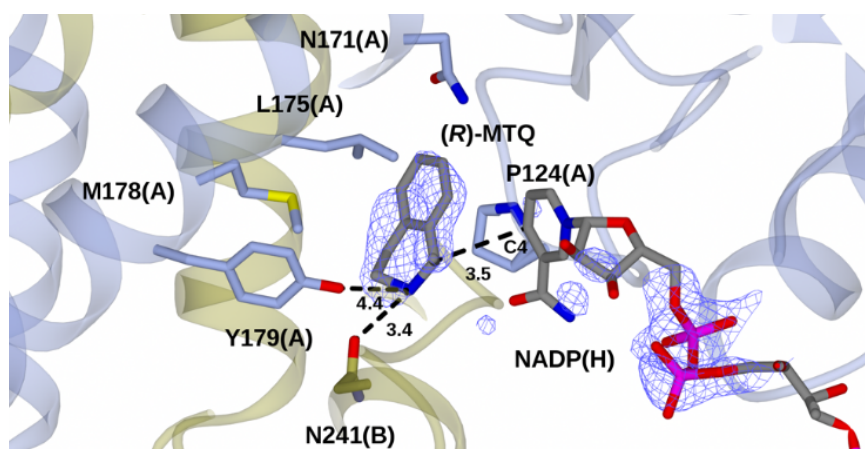
Figure 1.22. Structure of *Amycolatopsis orientalis*, AoIRED co-crystallised with model substrate 1-methyl-1,2,3,4-tetrahydrosioquinoline and NADPH. Reproduced from Aleku *et al.* (2016)[69] **(A)** and **(B)** identifying the different protein monomers.

Lenz *et al.* also showed *Pe*IRED and *Sr*IRED activity towards the reduction of the carbonyl bond in 2,2,2-trifluoroacetophenone.[74] This demonstrated for the first time IRED reaction promiscuity towards the reduction of carbonyls and raised an interesting question: can this expansion of activity be mimicked in carbonyl reductases (alcohol dehydrogenases, ADHs)? These enzymes (ADH) are well-studied and

characterised, encompassing a broad range of substrates, with the majority employing the cheaper NADH cofactor.

1.2 Alcohol dehydrogenases

1.2.1 Background and classification

Alcohol dehydrogenases [ADHs, *EC 1.1.1.1*] are a group of enzymes belonging to the oxidoreductase family.[78] They catalyse the reversible oxidation of alcohols to the corresponding aldehydes or ketones, with the concomitant reduction of the coenzyme nicotinamide adenine (phosphate) NAD(P)$^+$ cofactor *via* hydride transfer (Figure 1.23).
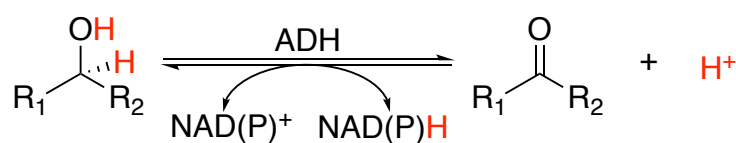
Figure 1.23. Reactions catalysed by alcohol dehydrogenase (ADH).

ADHs are present in many organisms, including humans, animals, plants, yeasts and bacteria. In the mammalian organisms, they facilitate the breakdown of alcohols, which are toxic to the body if left untreated. Whereas in plants, yeast and bacteria, the reverse reaction occurs, producing the alcohol, as part of the fermentation process. ADHs selectively transform a broad range of substrates including hemi-acetals, primary, secondary and cyclic alcohols.[78]

Alcohol dehydrogenases can be split into three classes depending on their structure and amino acid chain length.

- Long chain dehydrogenase / reductases (LDR), approx. 700 amino acids, such as *Zymomonas mobilis* ADH;
- Medium chain dehydrogenase / reductase (MDR), approx. 350-375 amino acids, such as horse liver ADH and yeast ADH;
- Short chain dehydrogenase / reductase (SDR) approx. 250 amino acids, such as *Drosophila* ADH.

Many alcohol dehydrogenases contain a zinc ion in their active site, however some were described to contain iron (*Saccharomyces cerevisiae* ADH),[79] magnesium

(*Thermus thermophilus*) or nickel (*Oenococcus oeni*).[80] SDRs, such as the ADH from *Drosophila*, contain no metal ions.[81]

1.2.1.1 Medium chain dehydrogenase / reductase

Zinc-containing MDRs constitute a large part of the alcohol dehydrogenase family and have been studied extensively. These alcohol dehydrogenases exist either as dimers (mammalian ADHs) or tetramers (bacterial ADHs) of subunits, as represented by the two most explored enzymes of this group: ADH from horse liver (HLADH) and from yeast.[82] MDRs consist of a chain of approximately 350 amino acids per monomer, weighing approximately 40 kDa. The monomer is divided into two domains: a coenzyme-binding domain and a catalytic domain, which are separated by a long deep cleft in the protein structure (Figure 1.24a).[83]

The coenzyme binding domain binds either NAD^+ or $NADP^+$, or their reduced forms, depending on the enzyme and its sequence. In most cases the catalytic domain contains two zinc ions, one which is responsible for the catalysis and one that is structural. The catalytic zinc is coordinated in an approximate tetrahedral conformation to three protein ligands, usually one histidine and two cysteines (Figure 1.24b). The fourth ligand is usually a water molecule. The structural zinc interacts with four protein ligands, all of which are cysteines in all structurally characterised ADHs so far.[84]
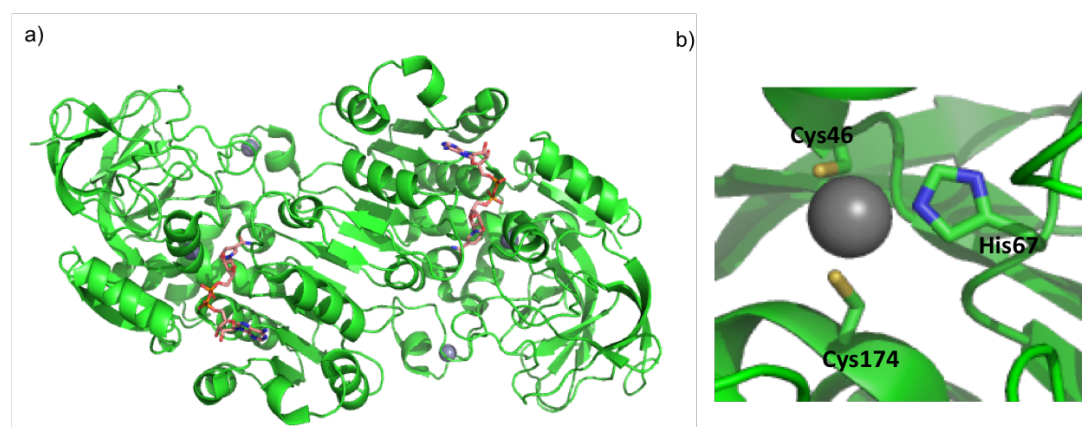
Figure 1.24. a) Dimeric HLADH structure, co-crystallised with NADH (orange sticks), zinc ions (grey spheres); b) close view of the HLADH active site showing the amino acids (green sticks) bound to the catalytic zinc (grey sphere). (PDB ID 4XD2).

A review of the 3D structures of MDRs shows that the catalytic domain varies slightly throughout the entire alcohol dehydrogenase family.[82] For example, the spacing between the metal binding ligands can vary, and a more significant variation is observed with the third ligand. In most NADP(H)-dependent dehydrogenases the third ligand is found to be an aspartic acid while in polyol dehydrogenases, this is replaced by a glutamic acid.[84] In a few cases the coordination by the forth ligand is a glutamic acid rather than a water molecule.[84,85] Only two structurally described ADHs lack the structural zinc, and they come from the thermophiles *Thermoanaerobacter brockii* and *Thermoanaerobacter ethanolicus.*[86]

1.2.1.2   Short chain dehydrogenases / reductases

Short chain reductases (SDRs) are distinct from the MDRs due to their lack of metal ion and shorter chain length.[87] This enzyme family includes representatives from all domains of life, from primitive bacteria to higher eukaryotes.[88] The most studied SDR is *Drosophila* ADH coming from an insect species. The chain length of SDRs varies between 250 and 300 amino acids, and, like MDRs, they also have a cofactor-binding site and a substrate-binding site. The substrate binding cleft determines substrate selectivity, however across the family there is a considerable variation in the structure of this site, leading to variation in their substrate scope. On the other hand, active site residues are similar, and consist of a highly conserved tyrosine in close proximity to Lys, Ser and Asn residues, presenting an active tri- / tet- rad capable of performing acid/base catalysis.[89] This mechanism is in contrast to the MDR substrate activation by zinc(II) (disscussed later).

1.2.2   Mechanism of zinc-dependent alcohol dehydrogenases

HLADH was generally used as the model for the enzymatic mechanism, which was suggested based on crystallography, kinetic and spectroscopic studies. The hydride transfer reaction can occur reversibly between the carbon bound to the alcohol / carbonyl functionality of the substrate and the pyridinium ring of NAD^+ in its reduced / oxidised form. In the oxidation direction, two hydrogen atoms are removed from the alcohol one of which is released as a proton and the other transferred as a hydride to NAD^+, reducing it to NADH.

The NAD^{+} binds to the coenzyme binding site transforming the enzyme into an active species, as a result of a conformational change in the enzyme structure, during which the nicotinamide ring moves deeper into the active site and the substrate binding pocket is formed (Figure 1.25). Substrate binding occurs by coordination of the oxygen to the catalytic zinc acting as a Lewis acid, and displacement of a water molecule. In the oxidative direction, the zinc draws electrons from the oxygen and facilitates proton release, aided by hydrogen bonding with the enzyme. The proton from the alcohol function is involved in H-bonding with residue Ser48. As shown in Figure 1.26, this proton is removed *via* a proton relay system between the alcohol, the 2'-hydroxyl group of the nicotinamide ribose, and residues Ser48 and His51.[83]
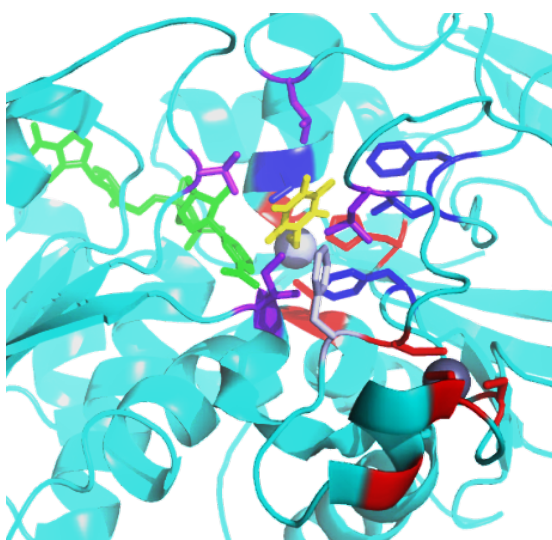
Figure 1.25. Structure of HLADH monomer co-crystallised with pentafluorobenzyl bromide. Catalytic and structural zinc ions are represented in grey, cofactor NAD^{+} in green and pentafluorobenzyl bromide in yellow, representing the substrate. The metal binding residues are highlighted in red and the substrate pocket residues are highlighted in dark blue, purple and grey. Modelled on HLADH (PDB 1HLD).

After deprotonation of the alcohol and formation of the negatively charged alkoxide ion, a hydride is transferred from the alcohol to the C4 position on the nicotinamide ring, consequently forming the corresponding carbonyl and NADH. The carbonyl is released, followed by release of NADH. NADH binding to the enzyme is stronger than NAD^{+} binding, and the NADH release is classed as the rate determining step in the alcohol oxidation.[90] In the reverse reaction of carbonyl reduction, coordination of the oxygen to the catalytic zinc(II) increases the electrophilicity on the α-carbon and

facilitates the hydride transfer from the NADH. This is then followed by proton relay from a water molecule to the carbonyl, resulting in the corresponding alcohol.
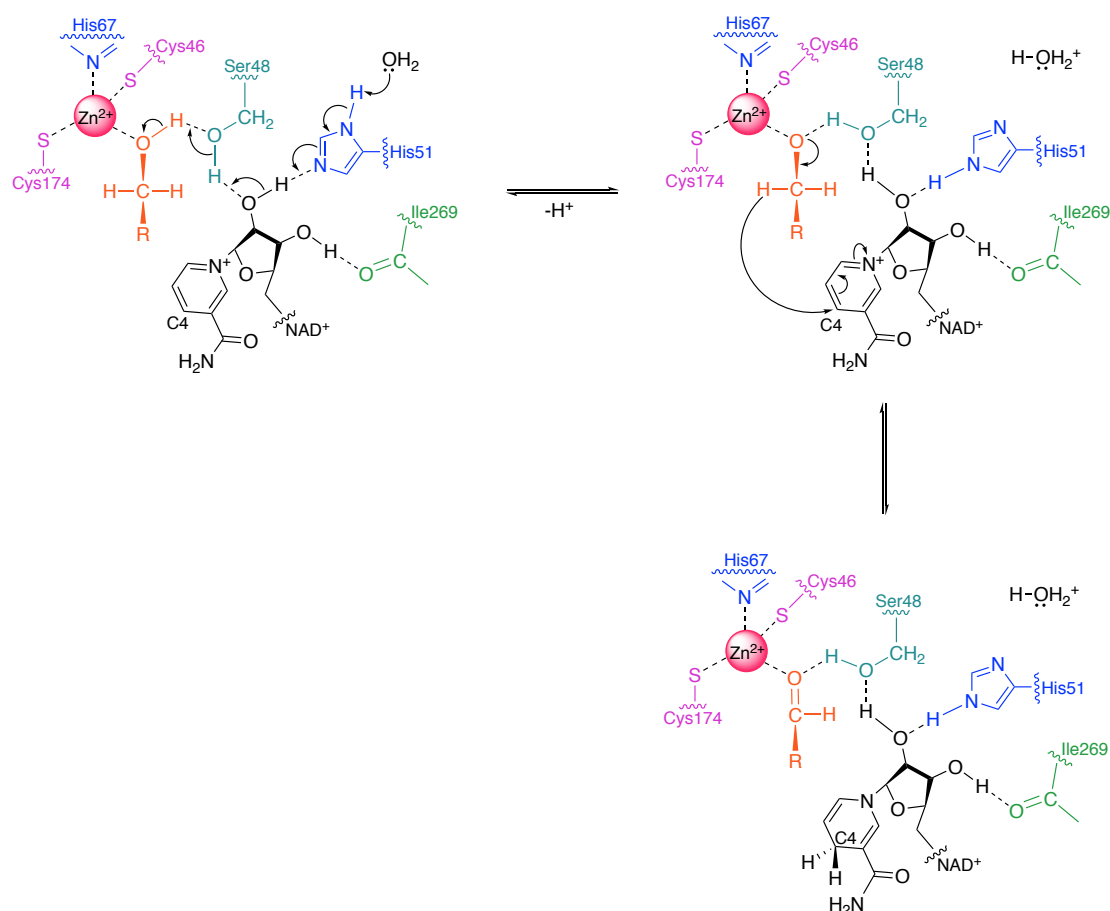
Figure 1.26. Proposed HLADH mechanism illustrating the proton relay system. Modified from Eklund *et al.* (1982)[91] and Choonseok *et al.* (2013).[92]

Whilst this mechanism is generally accepted for HLADH, certain authors suggested a different mechanism for some bacterial ADHs, such as the thermostable TbADH from *Thermoanaerobacter brockii.*[86] Based on data obtained by X-ray absorption, circular dichroism (CD), fluorescence spectroscopy, structural analysis and modelling studies of the ternary complex TbADH-NADP$^+$-DMSO (as ketone mimic), the zinc ion was suggested to be pentacoordinated during hydride transfer, with the water molecule acting as the fifth ligand, instead of being displaced by the substrate.[93] The absence of a proton relay system was also suggested in the TbADH mechanism, and was supported by the lack of hydrogen bonds between Ser37 and His42 (corresponding to residues Ser48 and His51 in HLADH) to the 2'-hydroxyl group of the nicotinamide ribose, observed from the crystal structure.

Depending on the ADH hydride transfer takes place from NAD(P)H to the *re*-face of the ketone producing the *(S)*-alcohol (referred to as Prelog's rule); or to the *si*-face, delivering the *(R)*-alcohol (following the anti-Prelog's rule). In addition to the stereospecific approach of the substrate, the hydride transfer to / from NAD(P)H is also stereospecific: some dehydrogenases specifically transfer the pro-*R* hydrogen, while other transfer the pro-*S* hydrogen at position 4 of the NAD(P)H nicotinamide ring. A number of reasons have been proposed for this stereospecificity.[94] From a structural standpoint, to accommodate both the nicotinamide ring and the substrate in the pocket, the enzyme binds the cofactor in a particular conformation, in which the amide group is away from the pocket. For example, HLADH exclusively follows Prelog's rule, resulting in a predictable stereochemical outcome for the substrate in which the pro-*R* hydride is transferred from the NADH coenzyme to the *re*-face of the carbonyl group resulting in the *(S)*-alcohol (Figure 1.27).
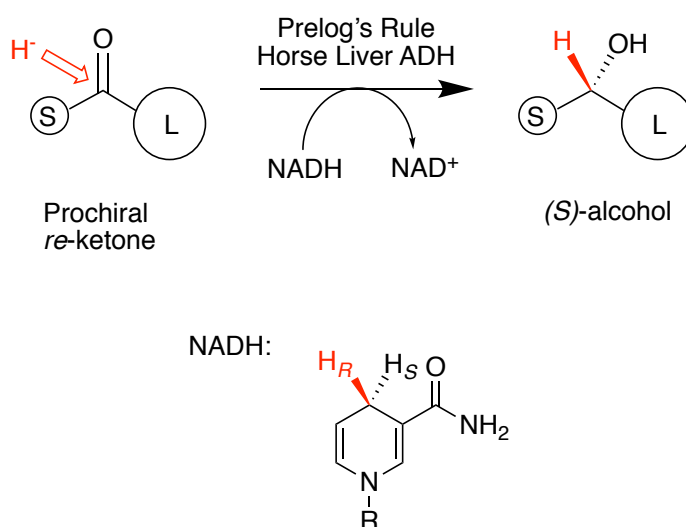
Figure 1.27. HLADH following Prelog's rule, resulting in the corresponding *(S)*-alcohol. The *si*-face of the ketone is shown, as well as the pro-*R* and pro-*S* hydride in NADH.

1.2.3 Applications of selected zinc-dependent alcohol dehydrogenases

There is considerable interest in the use of ADHs in the food, pharmaceutical, and fine chemicals industries for the production of aldehydes, ketones, and particularly chiral alcohols. After hydrolases, ADHs are the most widespread enzymes in organic synthesis.[95] A range of ADHs are commercially available, and taken together they have

a broad substrate range, including aldehydes, acyclic, bicyclic, aromatic and unsaturated ketones, as well as diketones and oxo-esters (Figure 1.28).[96]
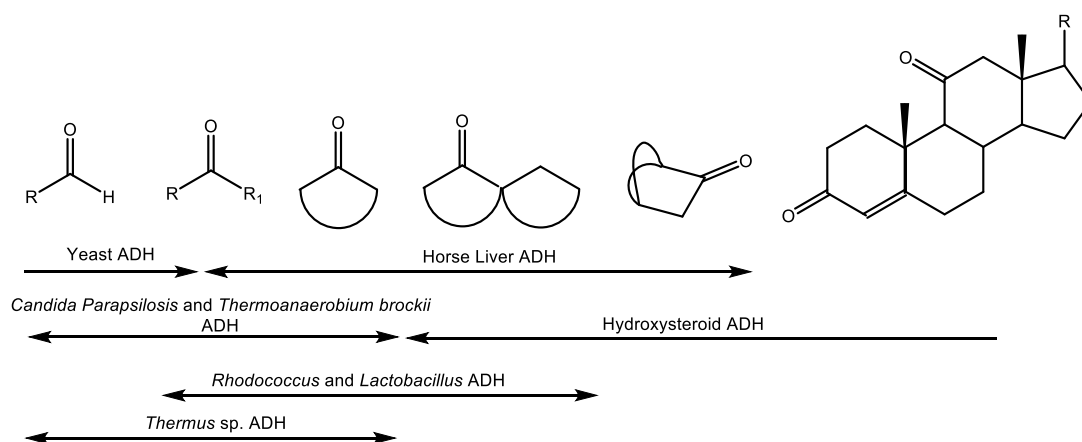
Figure 1.28. Illustration of the substrate range of a range of common ADHs. Modified from Faber (2011).[96]

Horse liver ADH reduces a wide range of substrates with good to excellent enantio- and regio-selectivities, including cyclic and bicyclic ketones of medium size (4-9 membered), diketones and organometallic compounds[97,98] (Figure 1.29a-b). Molecules larger than decalines (>10 membered bicyclic rings) are not as readily accepted as substrates.[99] While *O*- and *S*- containing heterocyclic ketones are well tolerated by HLADH, the presence of amines (for example in *N*-heterocyclic ketones) inhibits the reaction, presumably due to the strong binding of the nitrogen to the catalytic zinc.[100] HLADH also catalyses the oxidation of racemic primary and secondary alcohols, and is particularly useful for the oxidation of polyols and diols to ultimately yield chiral lactones (Figure 1.29c).[101]

On the other hand, acyclic ketones and secondary alcohols are not good substrates for HLADH. Other commercial enzymes such as TbADH are used as catalysts for the oxidation / reduction of these substrates. Interest in TbADH for biocatalysis is due to its high thermostability (up to 85 $^{\circ}$C) and high tolerance for organic solvents.[102] It is particularly effective for the oxidation of medium chain aliphatic secondary alcohols and the reduction of the corresponding acyclic ketones with excellent selectivities.[103] High optical purities have been observed for ω-haloalkyl-, methyl- or trifluoromethyl ketones with heterocyclic substituents,[104,105] whereas α,β-unsaturated ketones and ketones with both substituents larger than an ethyl group are not accepted as

substrates.[96] TbADH has also been employed in the synthesis of bioactive compounds.[106]

a) Desymmetrisation of prochiral diketones

>98 % ee
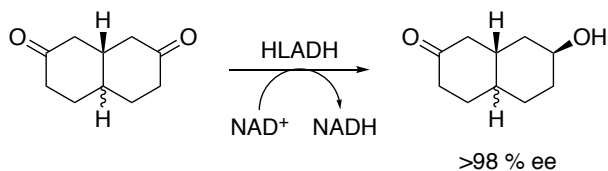
b) Enantioselective reduction of chiral organometallic moieties (eg. 1-formyl-2-methyl(benzene)tricarbonylchromium)

racemic aldehyde

(1R)-alcohol
>99 % ee

(1S)-aldehyde
>99 % ee
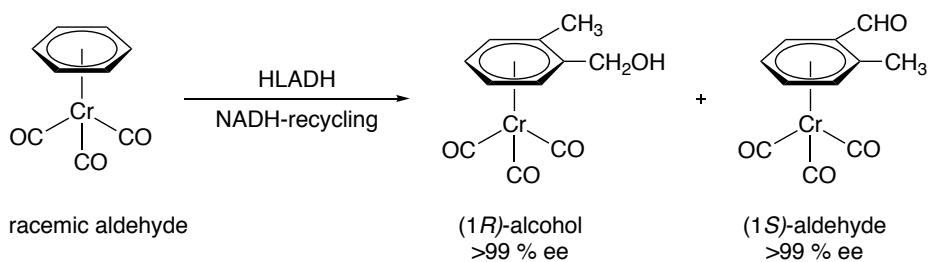
c) Enzymatic production of lactones from primary or secondary alcohols

64-90 %
>97 % ee
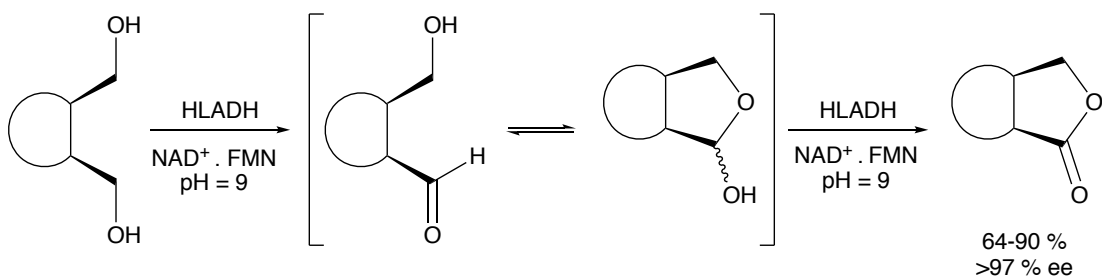
Figure 1.29. Examples of reduction and oxidation reactions performed with HLADH.[96,98,101]

Interestingly, TbADH exhibits a substrate size-induced reversal of enantioselectivity: when the substrate is small, *i.e.* methyl ethyl, methyl isopropyl or methyl cyclopropyl ketones, reduction follows the anti-Prelog rule with the hydride attacking the *si*-face of the carbonyl resulting in the corresponding *(R)*-alcohol. However, when the ketones are larger in size, TbADH follows Prelog's rule with the hydride attacking the *re*-face of the carbonyl resulting in the *(S)*-alcohol. Some examples of substrates and their alcohol configuration are shown in Figure 1.30.[96]
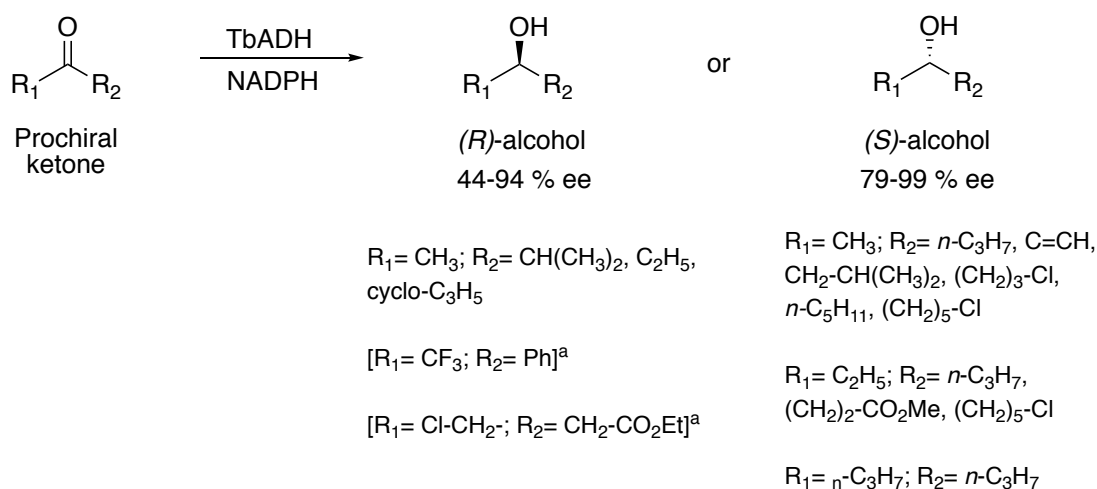
Figure 1.30. Enantioselectivity for TbADH on selected substrates; [a]**switch of the ketone reduction catalysed by TbADH.** Modified from Keinan *et al.* (1986).[106]

As demonstrated with TbADH, the application of robust biocatalysts, in terms of heat and solvent tolerability commonly displayed by thermostable enzymes, is desired in many industrial processes. Whilst mesophilic ADHs such as HLADH have found application in biotransformations, these enzymes have been shown to undergo conformational changes affecting their activity under thermal stress.[107] On the other hand, the substrate scope of TbADH is limited compared to, for example, HLADH. A zinc-dependent thermostable enzyme from *Thermus* sp. ATN1 raised considerable interest, due to its large substrate scope, thermal and organic solvent tolerance, as well as compatibility with inorganic rhodium-based catalysts for cofactor regeneration.[108,109]

1.2.4 Alcohol dehydrogenase from Thermus sp. ATN1 (TADH)

Zinc-dependent ADH from *Thermus* sp. ATN1 was initially reported in 2001[110] and was shown to be highly thermostable (up to 90 °C).[108] The enzyme was expressed and purified from *E. coli* and displayed a broad substrate range, including alcohols (primary, secondary and cyclic), aldehydes and ketones (acyclic and cyclic), with a preference for primary alcohols and their corresponding aldehydes. Excellent activities towards cyclohexanone and its derivatives (Figure 1.31) have also been observed.[109] TADH exclusively follows Prelog's rule, catalysing the formation of *(S)*-alcohols.

a) Oxidative substrate scope:

1-butanol
142 %

1-octanol
57 %

2-pentanol
84 %

3-methylbutanol
133%

cyclohexanol
100 %

benzylalcohol
47 %

4-ethylcyclohexanol   3-methylphenethyl alcohol   decahydro-2-naphthol
60 %   64 %   37 %
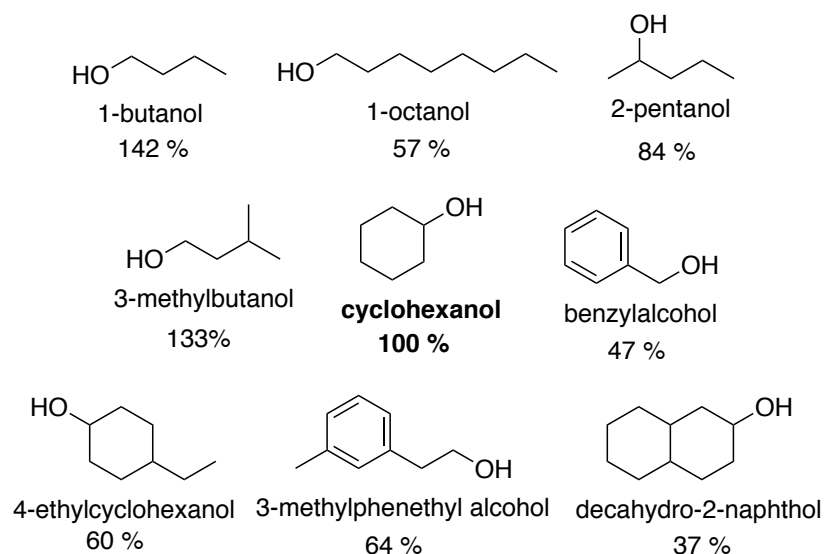
b) Reductive substrate scope:

benzaldehyde
154 %

butyraldehyde
359%

cyclohexanone   2-methylcyclohexanone   (rac)-3-methylcyclohexanone
100 %   46 %   163 %

4-methylcyclohexanone   4-ethylcyclohexanone   2-Decalone
25 %   22 %   28 %
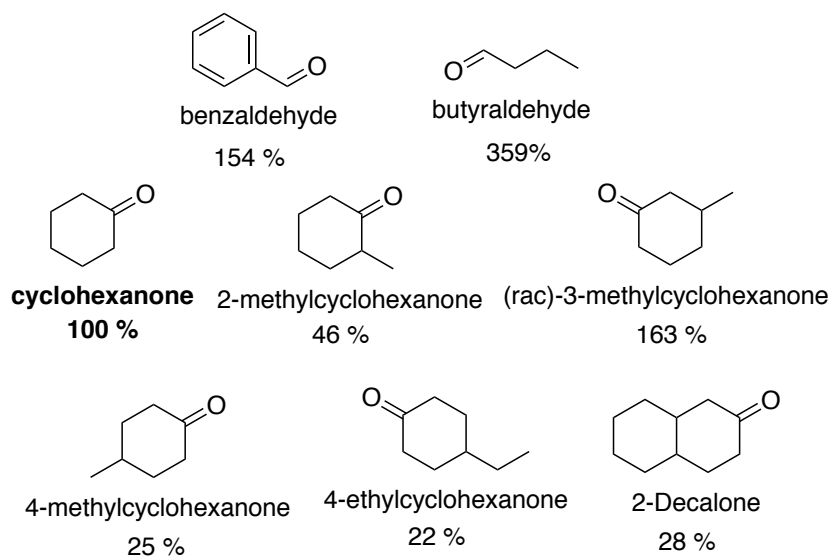
Figure 1.31. Substrate scope of TADH as reported by Höllrigl *et. al.* (2008).[109] a) In the oxidative direction displaying the relative activity as a percentage of cyclohexanol (100 %, 20.8 U / mg); b) In the reductive direction displaying the relative activity as a percentage of cyclohexanone (100 %, 15.1 U / mg).

TADH was also shown to exhibit tolerance towards water-miscible and immiscible organic solvents. Octane and hexane (50 % v / v) were shown to act as substrate / product sinks in two phase systems, while acetone could be used both as sacrificial substrate in regeneration systems, or as a solubiliser to increase substrate availability.[109]

Hollmann and co-workers studied the interaction between TADH and the $[Cp^*Rh(bpy)(H_2O)]^{2+}$ catalyst, which can be used for cofactor regeneration.[111] They found that TADH could bind up to 4 equivalents of the catalyst without detectable decrease in catalytic activity and stability, whilst higher molar ratios led to inactivation of the enzyme.

The crystal structure of TADH was recently solved (PDB ID 4CPD), and showed the occurrence of the catalytic and structural zinc-binding sites. Similar to other bacterial ADHs, such as TbADH, the catalytic zinc is bound in a tetrahedral coordination to Cys38, His59 and Asp152, as well as a water molecule as the fourth ligand. While the structural zinc ion is bound by four cysteines at positions 89, 92, 95 and 103. TADH is a homotetrameric structure (subunits A-D), each monomer containing 347 residues, which can also be observed as two dimers due to the close association of A with B and C with D. There are numerous interactions between subunits, along with a high number of prolines and condensed surface loops in its structure, which are all features attributed to increased thermostability, as is seen with TADH displaying activity in temperatures up to 90 $^{\circ}$C and in some organic solvents.[109]

1.2.5   Use of NADH mimics with alcohol dehydrogenases

To avoid the use of expensive cofactors in biocatalysis, cofactor regeneration systems have been developed.[112-114] In a different approach, mimics of the nicotinamide cofactors have been synthesised, and their use was demonstrated with certain NAD(P)H-dependent reductases.

Fish and co-workers reported the use of 1-benzylnicotinamide **9r** and of β-nicotinamide-5'-ribose methyl phosphate **10r** (Figure 1.32) instead of NADH during reduction of ketones by HLADH.[115] These structures led to high enantioselectivities and conversions of the selected ketone substrates, in combination with HLADH and a chemical regeneration system based on a rhodium-bipyridine complex and sodium formate .
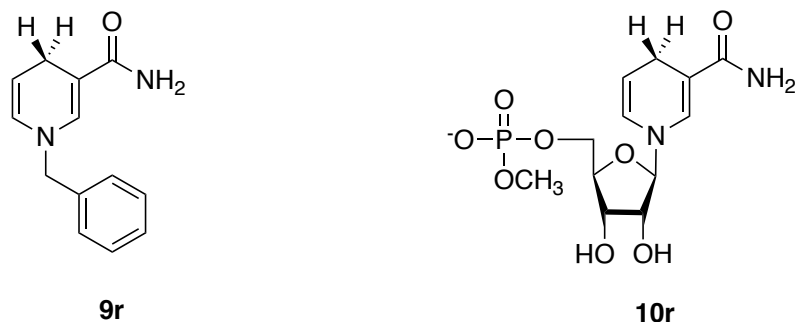
Figure 1.32. Use of NADH mimics for the HLADH-catalysed reduction of ketones. **9r** and **10r** refer to the reduced for of NAD⁺ mimics **9** and **10** discussed in section *4.4.2.*

The results obtained with the NADH mimics were similar to the results with the natural cofactor. Thus, the authors suggested that the binding of the mimics to ADH, resulting in production of the desired chiral alcohol, was similar even in the absence of the adenosine, pyrophosphate or ribose functions of NADH. Any doubts that activity was due to residual binding and recycling of NADH were dismissed in a recent report, displaying thoroughly performed controls,[116] showing that only racemic alcohol was detected in the absence of reduced analogues **9r** and **10r**.

Hollmann and co-workers also used compound **9r** and its derivatives as synthetic nicotinamide cofactors for enoate reductases, which depend on both FMN and NADH.[116]

1.2.6   Exchange of zinc for other metals in alcohol dehydrogenases

Successful metal exchange was reported for two metal-dependent ADHs: HLADH and TbADH. Metals other than Zn were used as spectroscopic probes instead of the spectroscopically "invisible" Zn(II) ion, as well as to investigate their influence on the kinetics of the catalytic mechanism. The catalytic zinc(II) ion of HLADH was replaced with a series of first row transition metals, and the resulting properties of the enzyme were examined. These metals include Co(II),[117] Ni(II),[118] Cu(I) and (II),[119] Fe(II),[120] Mn,[121] as well as a second row transition metal, Cd(II). Bogin *et al.* reported the effects of exchanging the zinc ion for V(III), Mn(II), Co(II), Cu(II) and Cd(II) on the TbADH structure and enzymatic properties.[122]

X-ray crystallographic studies of HLADH variants substituted with Co, Ni and Cd showed that the overall active site and protein structure were essentially preserved,

maintaining a tetrahedral, or in the case of the cadmium(II) ion, a distorted tetrahedral geometry with the binding ligands, Cys46, His67, Cys174 and a water molecule.[123] Some of the original catalytic activity was also maintained when ethanol was used as substrate. Substrate binding and activation investigations with *trans*-4-(*N,N*-dimethylamino)cinnamaldehyde (DACA) revealed that both the dissociation rate of DACA and the hydride transfer rate constant were correlated with the expected Lewis acidities of investigated metals, in the order Co(II) > Ni(II) ≥ Zn(II) >> Cd(II). This indicated that the different catalytic behaviours observed were a reflection of the different chemical properties of the metal ion introduced at the active site, emphasising its importance on the kinetics of catalysis.

In support of the above conclusion, replacement of the zinc ion in TbADH with Mn(II) and Co(II) resulted in enhanced activity (245 % and 130 % of the initial activity, respectively), whilst replacement with Cd(II), Cu(II) and V(III) resulted in reduced activity (20 % for Cd and <5 % of the initial activity for Cu and V). These results were explained by the Lewis acidity of the metals in the tetrahedral coordination.[124] To further understand the increase in native activity, the authors investigated the local structure and electronics at the catalytic cobalt site using X-ray absorption (XAS) and quantum chemical calculations. The data provided was consistent with an octahedral coordination at the metal active site in Co-TbADH, with the two additional ligands believed to be water molecules. Using DMSO as a substrate model, it was found that the coordination number remained as six when the substrate analogue was bound, with a small variation in the bond lengths between the zinc site with bound and unbound substrate (Figure 1.33). This change in bond length may result in a slight conformational change upon substrate binding, resulting in a more favourable position for catalysis. It was suggested that the higher coordination number was directly correlated with the higher reactivity seen with Co-TbADH. This hypothesis could also explain the increased activity seen with Mn-TbADH, as manganese tends to coordinate octahedrally in proteins.
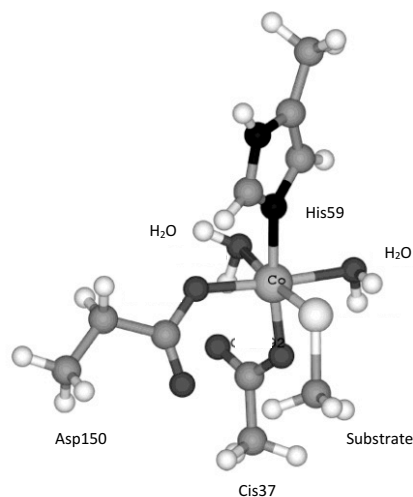
Figure 1.33. Hypothesised geometry of the catalytic metal site in Co-TbADH. Reproduced from Kleifield *et al.* (2004).[124]

Furthermore, the same group also suggested oxidation to Co^{3+} due to the accumulation of additional positive charge from the octahedral coordination at the catalytic site DMSO was found to induce a distinct change in the catalytic zinc charge in native TbADH, which correlated to the formation of a pentacoordinated intermediate during catalysis. Whereas in Co-TbADH, DMSO binding did not cause such changes,[93] suggesting it remained in an octahedral coordination throughout catalysis, displacing one of the ligands rather than adding as an extra ligand, as observed with Zn-TbADH. It has been proposed by this group that the additional positive charge found with cobalt substitution stabilised the catalytic transition state and consequently lowered the barrier for catalysis.[117,125]

1.3 Enzyme engineering for promiscuous reactivity

1.3.1 Background

Enzymes are of great interest for applications in industrial chemical transformations, due to their high selectivity and efficiency under mild reaction conditions. However, they are usually limited to their natural substrates, or variations of these. Promiscuous reactivities are rare, in which transformations that are completely different from the native reactivity are catalysed by enzymes.[126] Protein engineering methods can be applied to expand the reactivity scope of existing biocatalysts.

Some enzymes naturally display reaction promiscuity. For example, *Candida antarctica* lipase B (CALB) has been observed to catalyse an array of transformations, in addition to its native hydrolysis and transacylation reactions. These additional reactivities include aldol additions, conjugate additions, epoxidations, Mannich reactions and Markovnikov additions which proceed through different transition state geometries and reaction mechanisms.

In contrast to altering the reactions conditions to coax reaction promiscuity, a lot of effort has gone into the re-design of enzymes to induce new or promiscuous activities. This was accelerated by the tremendous advances in molecular biology, bioinformatics, computational modelling and protein engineering observed in the past two decades. Genetic modification at enzymatic active sites can be performed by rational design or directed evolution, to allow acceptance of new substrates and consequently new reactivities. For example, replacement of an active site alanine with a histidine in human glutathione transferase (hGST A1-1, *EC 2.5.1.18*) transformed a transferase into a hydrolase.[127,128]

The approach highlighted above relies on an existing protein scaffold, suitable for the re-design exclusively by genetic modifications. A different method involves a semi-synthetic enzyme design, by attachment of a synthetic transition metal catalyst into a protein scaffold, affording novel reactivities. These hybrid catalysts are known as artificial metalloenzymes.

1.3.2 Artificial metalloenzymes

1.3.2.1 General features

The creation of artificial metalloenzymes (AMs) has emerged in the past decade as a hybrid of homogeneous and enzymatic catalytic approaches,[129-131] encompassing advantages of the traditional methods thus, merging "the best of both worlds."[132] They rely on the incorporation of a catalytic metal complex into a macromolecular host, such as a protein.[129] The protein host acts as a chiral scaffold and is therefore responsible for inducing high enantioselectivity and for allowing the reaction to be carried out in aqueous solution. The metal catalyst determines the reactivity and reaction scope, allowing performance of non-natural reactions in a protein host.

Another benefit is the ease of modification of these artificial metalloenzymes by chemical (spacers, ligands, etc.) or genetic means (rational design or directed evolution) approaches, thus allowing the AMs to be rapidly optimised for a particular reaction.

One of the first artificial metalloenzymes was developed by Whitesides and Wilson in the late 1970s.[133] They performed asymmetric hydrogenation of alkenes with a hybrid catalyst based on a biotinylated rhodium complex incorporated into avidin (Figure 1.34).
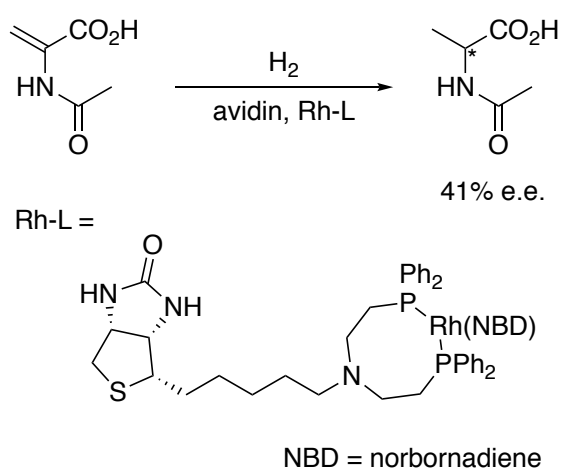
Figure 1.34 Asymmetric hydrogenation of functionalised alkenes using Whitesides biotin-avidin system.[133]

Whilst organic cofactors have been introduced into protein scaffolds as catalysts,[134] the introduction of metal complexes has proved to be the most successful. This is due to the reactivities associated with transition metals, which can be honed with change in oxidation states, ligands, geometrical structures or change in metal ion. However, this approach is limited by the number and location of binding sites available to bind a metal complex inside a protein. Nevertheless, it is possible to create artificial binding sites, using chemical or genetic protein modifications to introduce non-natural amino acids or completely artificial ligands at desired positions.[135-138]

Metal catalysts can be attached to the protein *via* three different modes of anchoring: dative, covalent or non-covalent (supramolecular). Dative anchoring is the direct coordination of the metal to amino acid side chains, and usually implies the existence
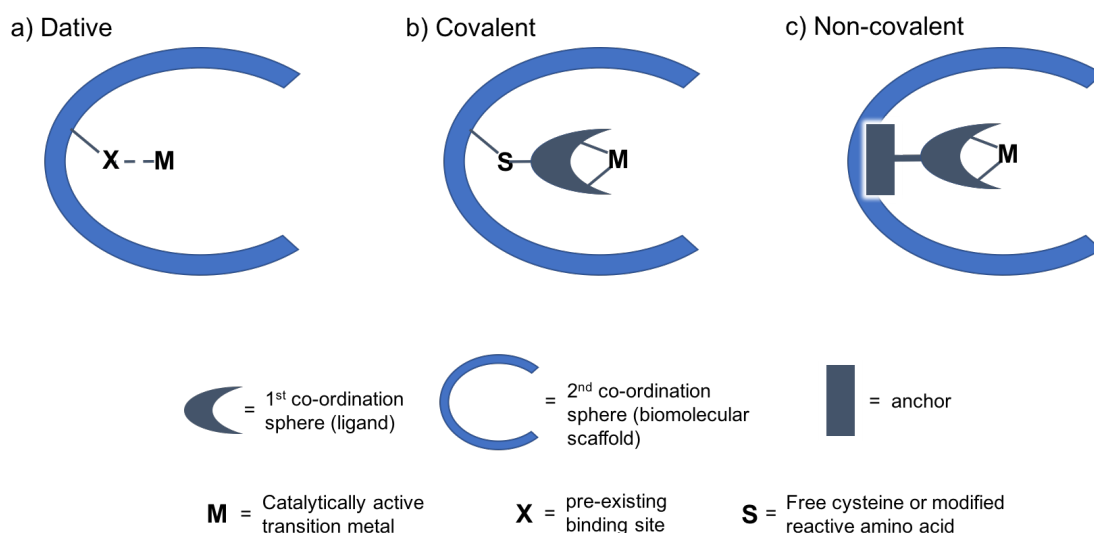
Figure 1.35. General design of artificial metalloenzymes illustrating the different anchoring strategies.[129] a) dative, b) covalent and c) non-covalent.

of a defined binding site within the protein scaffold.[129] This strategy usually consists in the removal of the catalytic active metal from an existing metalloenzyme and replacing it with a different metal ion, in order to enhance current activity or to introduce a new reactivity (see section *1.4.2.2*). Covalent anchoring involves the covalent binding of a catalytic complex to a uniquely reactive amino acid, such as a cysteine, within the protein host. For example, Kamer and co-workers developed a highly efficient method for selective-cysteine bioconjugation of phosphine ligands for attachment of a rhodium phosphine complex.[139] The non-covalent or supramolecular approach consists of the binding of the metal complex to the protein *via* hydrogen bonding, hydrophobic or electrostatic interactions. An exciting example of this is the incorporation of metalloporphyrins containing the non-native Ir metal into heme-dependent proteins, leading to the catalysis of carbene insertions into C-H bonds.[140] Another supramolecular approach consists in linking a completely synthetic metal complex to a cofactor with affinity for the protein host. The biotin-streptavidin system is one of the most successful examples of this strategy.[141-143]

1.3.2.2   Introduction of non-native metals in existing metal-binding sites

Substitution of an existing metal by a non-native one has been shown to change the reactivity of metalloenzymes. One of the earliest examples was provided by Kaiser in 1976, who reported the oxidation of ascorbic acid using a Cu(II) substituted

carboxypeptidase A (Cu^{2+}-CPA).[144,145] In 2002, Bakker *et al*. reported the oxidation of thioanisole with hydrogen peroxide, employing a thermolysin variant in which zinc was replaced with much larger anions (molybdate, selenate or tungstate).[146] However, it wasn't until 2006 that metal-substituted artificial metalloenzymes were developed to perform enantioselective reactions. The groups of Kazlauskas[147] and Soumillion[148] both reported the replacement of the native zinc with manganese in carbonic anhydrase, a metalloenzyme which catalyses the hydration of carbon dioxide to bicarbonate. The substitution for manganese transformed this enzyme into an enantioselective peroxidase, displaying a similar or enhanced enantioselectivity for the epoxidation of styrenes and olefins in comparison with natural peroxidases.

Kazlauskas and co-workers also reported the successful exchange of the active site zinc ion in human carbonic anhydrase (hCA) for a rhodium. The exchange was performed by dialysis with a zinc chelator, 2,6-pyridinedicarboxylate (dipicolinic acid), resulting in apo-hCA with 5-10 % remaining active site zinc, followed by subsequent dialysis against a rhodium salt, to give the Rh-hCA enzyme. In a first report, the authors used [Rh(COD)$_2$]BF$_4$, which was reported to avoid protein precipitation, and obtained hCA containing a 6.5-fold excess of Rh.[149] Both chemical and genetic modifications were used to remove the binding of Rh to surface histidines and greatly reduced the amount of additional bound rhodium to 2.3 and 1.8, respectively. These rhodium carbonic anhydrase complexes showed selectively reduced *cis*-stilbene over *trans*-stilbene. In a subsequent report, the same authors reported an improved Rh-hCA variant, with only 0.4 extra Rh equivalents, when [Rh(CO)$_2$(acac)] was used as metal precursor.[150] The majority of the rhodium was bound by three histidines at the active site, assuming a tetrahedral geometry, with a water molecule as the fourth ligand. This Rh(I)-hCA adduct catalysed the regioselective hydroformylation of styrene, with up to 8.4-fold selectivity for linear over branched product (Figure 1.36).

More recently, the groups of Hartwig[150] and Piazzetta[151] also reported their studies on the incorporation of iridium and of rhodium into human carbonic anhydrase, and its applications. Hartwig reported the characterisation of organometallic fragments bound to hCA, following treatment of the apo enzyme lacking three surface histidines with [Rh(NBD)$_2$]BF$_4$, [Rh(CO)$_2$(acac)] and [Ir(CO)$_2$(acac)]. NMR, IR, UV-Vis and EXAFS
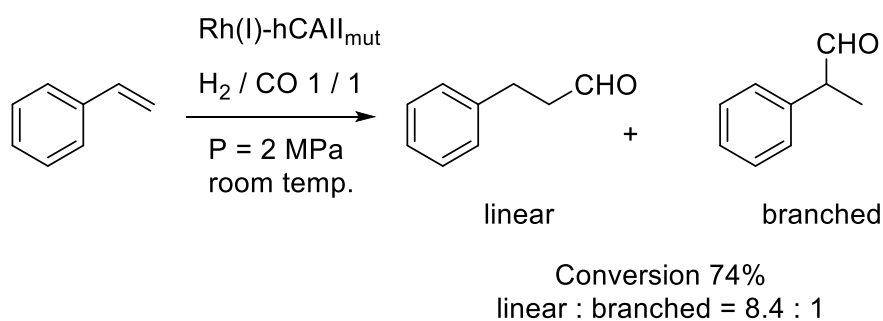
Figure 1.36. Regioselective hydroformylation of styrene catalysed by a human carbonic anhydrase II mutant, incorporating Rh(I) catalyst.

spectroscopy were used to characterise the discrete organometallic fragments at the metal-binding site, and it was suggested that these fragments were not responsible for catalysis. On the other hand, theoretical calculations reported by Piazzetta *et al.* suggested that Rh(I) bound at the active site of hCAII could catalyse the direct hydrogenation of CO_2 to formic acid.

1.3.2.3 *Artificial metalloenzymes for enantioselective imine reduction*

The best hybrid catalytic systems reported so far for the reduction of imines come from the group of Ward and co-workers. They initially reported on biotin-streptavidin catalysts containing Noyori-type complexes for ketone transfer hydrogenation.[141,152,153] These were later demonstrated to be effective for the enantioselective reduction
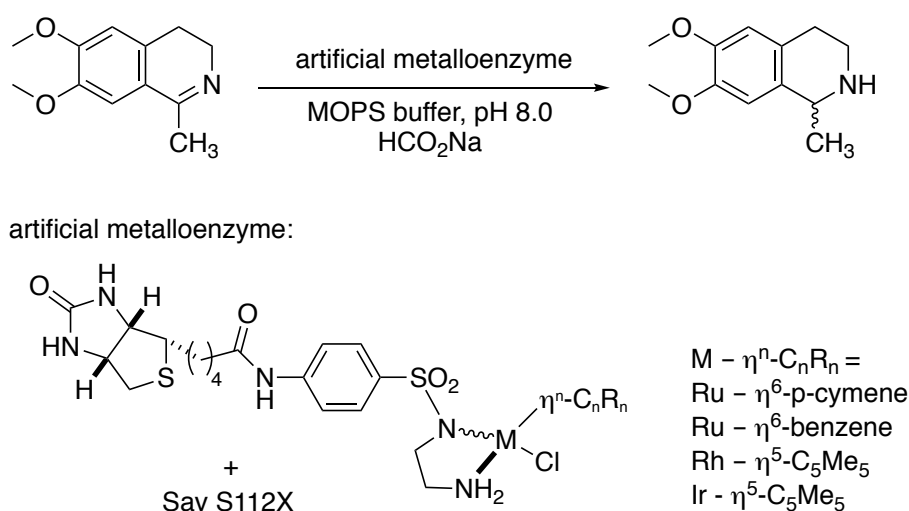
Figure 1.37. Artificial metalloenzyme based on biotin-streptavidin technology for imine reduction. Modified from Duerrenberger *et al.* (2011).[154]

of imines.[154] The group identified that a biotinylated iridium piano stool complex [(η^5-Cp*)Ir(Biot-p-L)Cl] incorporated into different mutants of streptavidin at the 112 position produced both the *(R)-* and *(S)-* enantiomers of salsolidine (Figure 1.37), with high ee's (98 % and 78 %, respectively), employing formate as the hydrogen source.

This reaction was optimised by two different approaches. The first consisted of the introduction of an appropriately positioned histidine, which was used to reinforce the anchoring of the iridium metal complex within the active site *via* a dative bond as shown in Figure 1.38.[142] Secondly, they investigated the genetic optimisation of this system, with introduction of lipophilic amino acids around the active site, resulting in an 8-fold increase in catalytic efficiency compared with the wild type artificial imine reductase.
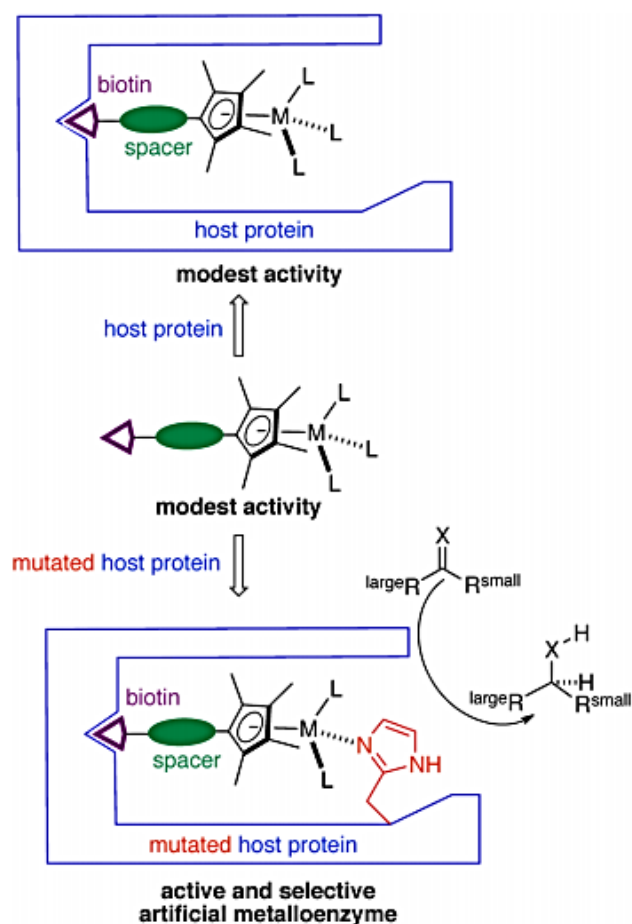
Figure 1.38. Dual anchoring strategy based on biotinylated piano stool catalysts incorporated into streptavidin. Reproduced from Zimbron *et al.* (2013).[142]

Ward and co-workers also investigated the use of human carbonic anhydrase II (hCA II) in combination with iridium piano- tool complexes for imine reduction. In this case, aryl sulphonamide inhibitors, known to bind with high affinity to hCA II, were used as anchors for the metal catalysts (Figure 1.39). These presented lower turnover numbers in contrast to the streptavidin systems. Nonetheless, incorporation of the iridium complex into the hCA II provided a significant improvement in catalytic activity and selectivity (up to 68 %) in comparison to the free catalysts, in which only racemic mixtures were available.[155]
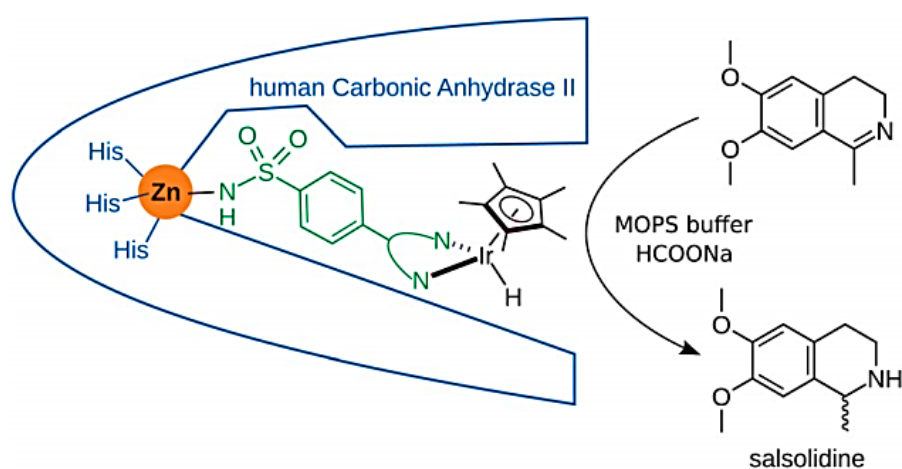
Figure 1.39. Artificial imine transfer hydrogenase based on aryl-sulfonamide functionalised Ir-complexes incorporated into human carbonic anhydrase II. Reproduced from Monnard *et al.* (2013).[155]

Chapter 2 Aim and objectives

The literature review highlighted the importance of the enantioselective reduction of carbon-nitrogen double bonds, as an efficient route to chiral secondary amines. The need for more sustainable methods led to successful recent discoveries, and a number of imine reductases were developed as efficient biocatalysts for this transformation. However, their activities are still low, and the substrate scope is limited.

Given the chemical similarity between ketone and imine substrates and their enzymatic reduction mechanisms, it is surprising that no ADHs have been shown to catalyse the reduction of imines. Several reasons can be identified for this. Imine substrates or amine products might inhibit ADHs, as a result of the strong binding between nitrogen and the catalytic zinc. Imine size and shape may also be an issue, due to the extra substituent bound to the nitrogen atom. Finally, imine instability in aqueous media may result in hydrolysis of the substrate being faster than the reduction.

In contrast to IREDs, ADHs have a broader substrate range, many of them employ the cheaper cofactor NADH, and thermostable enzymes have been discovered, which also show organic solvent tolerance. Therefore, they represent good starting points for engineering of reaction promiscuity towards imine reduction.

The overall aim of this thesis is to engineer a thermostable ADH in order to introduce imine reductase activity, by exploring different modes of substrate activation. The first approach consists of mimicking the active site of current IREDs, by introducing a protic residue in place of the catalytic zinc. The second approach is to chemically modify the zinc-binding site, by incorporating a Rh(I) ion in place of the active site zinc(II) in an effort to replicate the imine activation mechanism of chemical catalysts. The third strategy is to introduce a synthetic catalyst into the TADH active site, by anchoring it to a NADH mimic, previously reported to occupy the NADH-binding site in horse liver ADH. For each of these approaches, the objectives are outlined below.

1) **Genetic engineering of the TADH active site for imine reduction**

This objective involves replication of the IRED active site within an ADH, by replacement of the catalytic zinc ion with an aprotic residue situated within range of substrate interaction. First, the choice of the thermostable TADH from *Thermus* sp. will be justified, and reliable methods for its expression in *E. coli*, purification and enzymatic assay will be developed, based on literature reports. The interaction of TADH with imines will be characterised, and this will be performed by experimental (inhibition studies) and computational (docking) methods. Based on the comparison between ADH and IRED active sites, mutants devoid of catalytic zinc and containing a protic residue will be designed, produced and tested for IRED activity.

2) **Replacement of the catalytic zinc with rhodium in TADH**

This objective involves the development of a method to perform the replacement of the catalytic zinc(II) of TADH with another metal. To achieve this, studies into removal of the catalytic zinc will be performed, to create the apo-TADH. Reinsertion of zinc(II) will be studied, to assess whether the enzyme can be reconstituted with full activity and metal content. Following this, reinsertion of other metals, such as Co(II) and Rh(I) will be tested: the first is aimed at comparing zinc exchange in TADH with other published ADHs, while the second is aimed at introducing imine reduction activity, in a fashion similar to synthetic transition metal catalysts.

3) **Synthesis of an artificial metal-binding site for TADH**

The third objective involves the incorporation into TADH of a metal-containing catalyst capable of imine reduction, anchored to a NAD^+ analogue with affinity for the enzyme. To achieve this, a transition metal catalyst will be designed and synthesised, and its imine reduction activity will be tested in the presence and in the absence of the enzyme. The interaction of the nicotinamide-functionalised complex with TADH will be studied by inhibition kinetics.

Chapter 3 Materials and Methods

3.1 Materials

All chemical reagents unless otherwise stated were purchased as analytical grade from Sigma Aldrich. *E.coli* BL21(DE3) and BL21(DE3)pLysS competent cells and Overnight Express™ Autoinduction System 2 were purchased from Novagen. The kits for protein concentration assays: Detergent compatible (*DC)* assay and Bicinchoninic acid (BCA) assay kit were purchased from Bio-Rad Laboratories Inc. and Pierce respectively (UK). NAD$^+$, NADH and 4-chloronicotinic acid were purchased from Apollo Scientific Ltd (UK). HiTrap Q Sepharose High Performance (5mL), HiLoad Superdex 200 and disposable PD-10 desalting columns were from GE Healthcare. 4-Bromonicotinic acid was purchased from Key Organics Ltd. (UK). Water was purified using the Milli-Q® Reference Water Purification System from Merck.

The pASZ2 plasmid, harbouring the TADH gene on a derivative of the pET11a vector was a kind donation from Dr. Frank Hollmann, Department of Biotechnology, Delft University of Technology (Netherlands) and its construction was previously described.[108] To confirm its integrity, sequencing was performed by Eurofins MWG Operon (Germany), results shown in Appendix 1.

3.2 Instruments

Sterilisation of all media and flasks was performed using a Prestige Classic 2100 benchtop autoclave (Medstore Medical) at an operating temperature and pressure of 121 $^{\circ}$C and 20 psi.

New Brunswick Scientific Innova 40 Incubator Shakers (Eppendorf), Centrifuge 5810R (Eppendorf), Avanti J-26 XP Centrifuge (Beckman Coulter) and One Shot Cell Disruptor (Constant Systems Ltd.) were used in protein expression.

Protein chromatography was performed using an AKTA Fast Protein Liquid Chromatography system (GE Healthcare) and monitored by absorbance at 280 nm.

Enzymatic activity was measured using UV mini-1240 UV-VIS spectrophotometer (Shimadzu).

ICP-MS data was acquired on an iCAP-Q equipped with CCTED (collision cell technology with energy discrimination, Thermo-Fisher Scientific), with the help of Dr. Scott Young at the University of Nottingham, Sutton Bonington Campus.

NMR spectra were recorded at 298 K using a Bruker AV(III)400, AV400, DPX400 (400 MHz ^{1}H frequency, 100 MHz ^{13}C frequency) or DPX300 instrument (300 MHz ^{1}H frequency, 75 MHz ^{13}C frequency). Chemical shifts are quoted in parts per million (ppm), referenced to the residual deuterated solvent quoted in text as internal standard. Coupling constants J are quoted in Hz. Multiplicity of each signal is designated with the following abbreviations: s, singlet; d, doublet; t, triplet; q, quartet; m, multiplet; app, apparent; br, broad. In the ^{13}C spectra, signals corresponding to C, CH, CH_2 and CH_3 were assigned from DEPT experiments. Mass spectra were recorded on a Bruker MicroTOF 61 mass spectrometer using electrospray ionisation (ESI).

3.3   Computational techniques

Protein sequences for IREDs and ADHs were obtained from the RCSB Protein Data Bank and were compared via sequence alignment performed using the Clustal Omega programme (http://www.ebi.ac.uk/Tools/msa/clustalo/). All protein 3D structures were extracted from the RCSB Protein Data Bank (http://www.rcsb.org).

The proteins used were:

TADH from *Thermus* sp. ATN1, *EC 1.1.1.1*, PDB ID 4CPD, (2.70 Å).

IREDs: Q1EQE0 from *Streptomyces kanamyceticus, EC 1.5.1*, PDB ID 3ZHB, (2.73 Å); from *Streptomyces* sp. GF3546 PDB ID 4OQY, (1.90 Å); and BcSIRED from *Bacillus cereus* BAG3X2, *EC 1.5.1.3*, PDB ID 4D3D, (1.71 Å).

Superimposition of the structures was executed using LigAlign, treating the cofactors NADH and NADPH as ligands. Automated docking of organic substrates within TADH was performed using AutoDock Vina.[156] Imines were prepared using Chemdraw 3D and BIOVINA Discovery Visualiser. The appropriate pdbqt files for the dimeric model of TADH and the ligands were prepared by using Autodock tools. The active site of TADH was contained in a grid size of 28 Å × 34 Å × 26 Å with 1 Å spacing, centred

around the catalytic centre at positions 23.44 $\mathring{A}$ × 12.69 $\mathring{A}$ × 106.06 $\mathring{A}$ (corresponding to x, y, z), which was generated using AutoGrid in the Autodock Tools interface. Substrates were flexibly docked, while the protein receptor was kept rigid performed by VINA. Results were visualised using Autodock Vina and Pymol.

3.4 Expression, purification and characterisation of TADH

3.4.1 General methods

Media components were sterilised by autoclaving (121 °C, 20 min, 20 psi), or where stated in the text by filtration (0.2 μm filter), and mixed when cooled. Media solutions were prepared in deionised water (dH$_2$O) and stored at room temperature unless otherwise stated. Where solid medium was required, agar (Melford; 15 g / L) was added to the medium prior to autoclaving. Antibiotics were prepared as a 1000 times concentrate of the working concentration: chloramphenicol solutions (34 mg / mL) were prepared in ethanol (100 %) and carbenicillin (50 mg / mL) was prepared in water, filter sterilised and stored at -20 °C.

E. coli BL21(DE3) or BL21(DE3) pLysS cells were transformed with the pASZ2 plasmid according to the manufacturer's protocol. Unless otherwise stated, transformed *E.coli* strains were generally cultured in lysogeny broth (LB), which contained LB granulated medium (25 g / L, referring to a mixture of 10 g / L NaCl, 10 g/ L tryptone and 5 g / L yeast extract), supplemented with 1 % (w / v) glucose. When cells were BL21(DE3) pLysS, growth and expression media contained carbenicillin (50 μg / mL) and chloramphenicol (34 μg / mL). When cells were BL21(DE3), the antibiotic was carbenicillin (50 μg / mL). All cultivations were performed in Erlenmeyer flasks, with nominal volumes five times the culture volume, unless when 1 L expression was performed, when the total volume of the flask was double (2 L). Strains were routinely stored as glycerol stocks at -80 °C. Glycerol stocks were prepared by picking a single colony of the strain and culturing it overnight in LB supplemented with the appropriate antibiotic (100 mL).

The pH of the buffers was adjusted after supplementation with the desired additive, and was performed once the solution reached the desired temperature (4 $^{\circ}$C, 25 $^{\circ}$C or 60 $^{\circ}$C).

3.4.2 Protein expression

An overnight pre-culture was prepared by inoculating LB medium (10 mL) with glycerol stocks (20 µL) and incubating overnight at 30 $^{\circ}$C. Overnight cultures were used to inoculate fresh LB medium (100 mL) to an OD_{660} of 0.1-0.2 and the cultures incubated at 30 $^{\circ}$C, 160 rpm until OD_{660} ˜1.0. This second pre-culture was used to inoculate the expression culture (1 L), which was grown at 30 $^{\circ}$C, 160 rpm to an OD_{660} = 0.6-0.8. Expression was induced with isopropyl β-D-1-thiogalactopyranoside (IPTG) (final concentration generally 0.4 mM, otherwise the concentration stated in the text) and cells were grown overnight at 30 $^{\circ}$C, 160 rpm to an OD_{660} of ˜4-5. Cells were harvested by centrifugation (8500 rpm, 4 $^{\circ}$C, 20 min) and stored at -80 $^{\circ}$C.

When auto-induction medium was used, a pre-culture (20 mL) previously grown in LB medium to an OD_{660} 0.5-0.6 from a cryostock was used to inoculate Overnight Express™ Autoinductive System 2 medium (200 mL) containing carbenicillin (50 µg / mL), to an OD_{660} 0.1. The culture was grown at 37 $^{\circ}$C, 300 rpm for 24 hours. Cells were harvested by centrifugation (8500 rpm, 4 $^{\circ}$C, 20 min) and stored at -80 $^{\circ}$C.

3.4.3 Protein purification

The harvested cell pellet was resuspended in 20 mM Tris buffer (pH 7.5), benzonase nuclease (0.1 µL / mL) was added, and the cells were lysed by two passages through the One Shot Cell Disrupter (25 kpsi). The resulting sample was centrifuged (12000 rpm, 4 $^{\circ}$C, 20 min) and the supernatant was heated at the desired temperature (75 or 80 $^{\circ}$C) for the specified time (15 or 20 min), to precipitate most of the cell proteins. The sample was centrifuged (12000 rpm, 4 $^{\circ}$C, 20 min) and the supernatant containing TADH was aliquoted and stored at -20 $^{\circ}$C or subjected for further purification by either anion exchange chromatography (AEX) or size exclusion chromatography (SEC).

AEX was performed using a HiTrap Q Sepharose High Performance column (5 mL). The column was equilibrated with 20 mM Tris buffer pH 7.5, the sample was loaded

(1-5 mg / mL, up to 10 mL) and the protein was eluted with 20 mM Tris buffer, pH 7.5 using a linear gradient from 0 to 1 M NaCl.

SEC was performed using a HiLoad Superdex 200 column, which was equilibrated with 20 mM Tris buffer pH 7.5, the sample was loaded (1-5 mg / mL, 3-5 mL) and the protein was eluted with 20 mM Tris buffer, pH 7.5.

Fractions containing pure protein (SDS-PAGE) were pooled together, concentrated by ultrafiltration using Vivaspin 6 (10 kDa MWCO) centrifugal concentrator, (Sartorius Stedim Biotech), subjected to protein analysis and stored at -20 ^{o}C until further use.

3.4.4   Protein concentration

The protein content of the expressed TADH was determined by the Bradford assay (Pierce). For all Bradford assays a standard curve of bovine serum albumin (BSA) was constructed using known concentrations of BSA (0.2-1.5 or 2 mg / mL), and formation of adducts determined at 595 nm. All assays performed in triplicate.

A typical calibration curve is shown below for the Bradford assay.
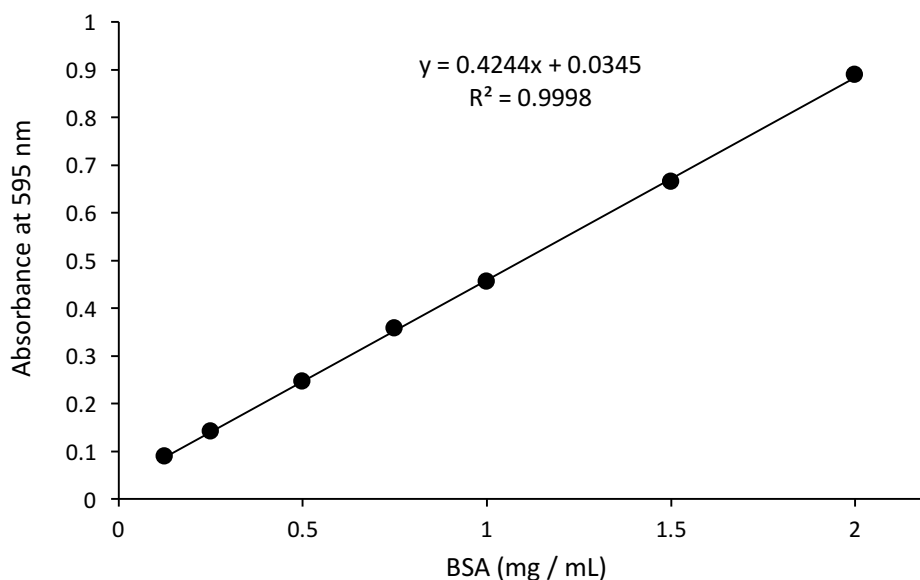
Figure 3.1. Calibration curve for the Bradford assay

A typical calculation of the protein concentration of a sample is given below.

Sample: 5x dilution

Sample absorbance: $A_{595} = 0.24$ (within calibration range)

Calibration equation: $A_{595} = 0.4244$ x conc. (mg / mL) + 0.0345

$$0.24 = 0.4244 \text{ x conc. (mg / mL)} + 0.0345$$

$$\text{conc. (mg / mL)} = (0.24 - 0.0345) / 0.4244$$

$$= 0.484 \text{ mg / mL}$$

Thus, non-diluted sample concentration = 0.484 x 5

$$= \textbf{2.4 mg / mL}$$

3.4.5   SDS-PAGE analysis

SDS-PAGE was used to analyse protein expression and purity. Cell samples for analysis were taken pre-induction and at intervals stated in the text post-induction. The OD_{660} of the sample was measured and samples (1 mL) were harvested by centrifugation (13400 rpm, 2 min). The supernatant was discarded and the cell pellets were frozen (-20 ^{o}C) until required. Cell pellets were resuspended to an OD_{660} of 0.2 in BugBuster lysis buffer (Novagen). BugBuster lysis buffer was supplemented with benzonase nuclease (0.1 μL / mL). Cell suspensions were incubated with gentle shaking (room temperature, 15 min) and the cell debris removed by centrifugation (13400 rpm, 10 min). Supernatant (20 μL) was transferred to a fresh tube containing sample buffer (20 μL) and the remaining supernatant discarded. The cell debris was resuspended in potassium phosphate buffer pH 7.0 (50 μL) and samples (20 μL) transferred to a fresh tube containing sample buffer (20 μL). Sample buffer contained Laemmli buffer (Bio-Rad) and 5 % (v / v) β-mercaptoethanol (β-ME). Samples were heated (105 ^{o}C, 5 min) and stored on ice until required.

Running buffer was Tris / Glycine / SDS (2.5 mM Tris, 19.2 mM glycine, 0.01 % SDS, pH 8.3) (Bio-Rad). Gels were loaded with denatured protein (15 μL) along with PageRuler Prestained Protein Ladder (5 μL), used as a marker and run at 150 volts for 50 min.

Gels used 12 % Mini-PROTEAN® TGX™ Precast Protein Gels, 12-well, 20 μl. (Bio-rad) Staining of gels was performed with EzBlue Stain (Bio-Rad).

3.4.6 Standard enzymatic assays

3.4.6.1 Oxidation assays

The enzymatic activity of TADH was routinely assayed with substrates 1-butanol or cyclohexanol. The following standard procedure is outlined with 1-butanol. Any variations in enzyme assay parameters are highlighted in the Results.

The reagents and cell compartment of the spectrometer were kept at 60°C prior to assay. The following reagents were added to a 1 mL cuvette: 1-butanol (100 mM), enzyme (10 μL, 3 μg) and up to 1 mL 50 mM Glycine-NaOH buffer, pH 9.0, and the absorbance was set to zero. The reaction was initiated by addition of NAD^+ (1 mM), followed by mixing of the reagents with a 1 mL pipette, in the cell compartment (at 60 °C). The increase of absorbance at 340 nm, (due to the formation of NADH) was monitored. For all enzymatic assays the specific activity was calculated from the initial linear rate of reaction (up to the initial 300 s). For all enzymatic assays, a control reaction was performed replacing the enzyme with 50 mM Glycine-NaOH buffer, pH 9.0 (10 μL) following NADH absorbance at 340 nm, no increase in absorbance was observed. A typical example of NADH absorbance increase during an oxidative enzymatic assay is shown below in Figure 3.2.
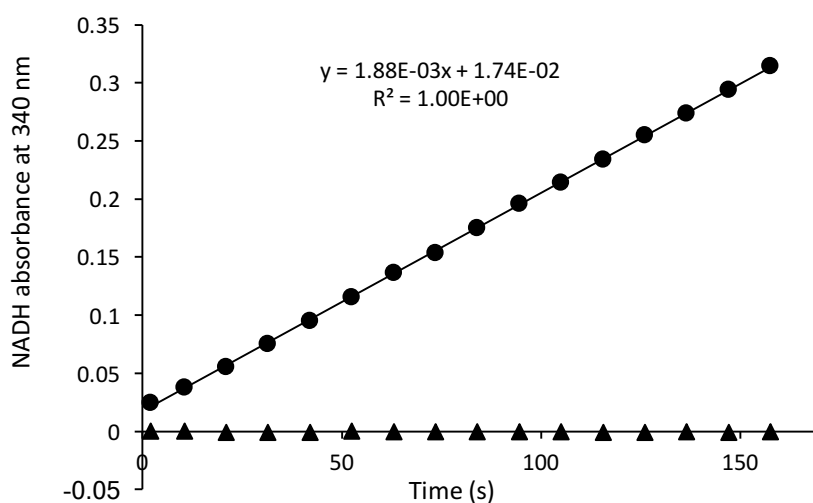
Figure 3.2. Initial rate of reaction for an enzymatic assay in the oxidative direction monitoring NADH absorbance at 340 nm with 1-butanol as the substrate: (▲) control; (●) 100 mM 1-butanol.

The absorbance readings for the initial rate of reaction were converted to NADH concentration (Figure 3.3) (mol / L) using the Beer-Lambert law: $A = \varepsilon lc$, where A = absorbance at 340 nm; ε = extinction coefficient (L / (mol.cm); l = path length (cm) and c = concentration (mol / L). The extinction coefficient for NADH is 6220 L / (mol.cm) and the path length was 1 cm. The concentration of NADH was plotted against time (seconds) and a line of best fit assigned. The equation of the line of best fit was then used to calculate the enzymatic activity (µmol / min) of the sample assayed.
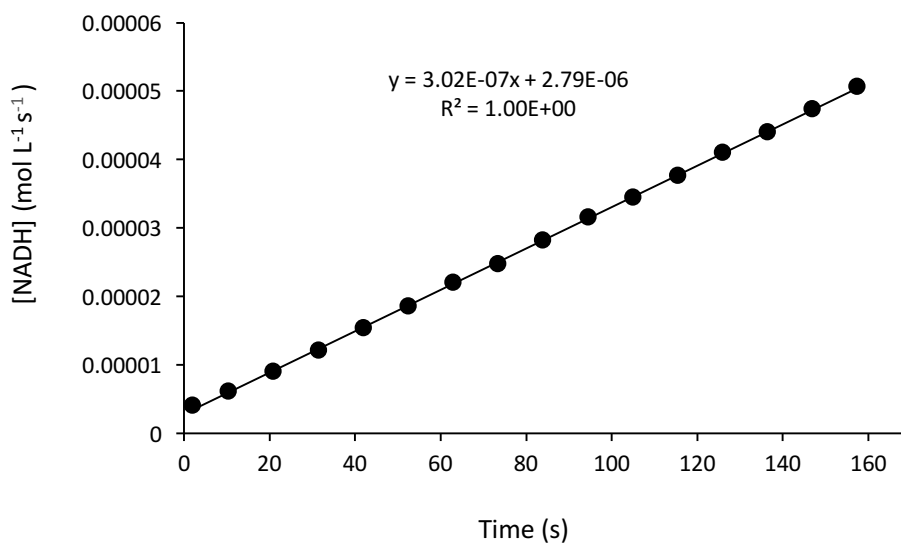
Figure 3.3. Initial rate of reaction of an enzymatic assay in the oxidative direction plotted as NADH concentration against time.

In the example shown, the best fit line equation is $\mathbf{y} = 3.02 \times 10^{-7}\,\mathbf{x} + 2.79 \times 10^{-6}$, where the gradient of the line (3.02×10^{-7}) is the initial rate:

$v_0 = \Delta[\text{NADH}] / \Delta\text{time}$ in mol $L^{-1} s^{-1}$.

Enzymatic activity, EA (µmol . $mL^{-1}.min^{-1}$) = $v_o \times 10^6 \times 10^{-3} \times 60 = v_0 \times 60\,000$

Following from the previous example the enzymatic activity is calculated as:

EA = $3.02 \times 10^{-7} \times 60\,000 = 0.01812$ µmol . mL^{-1} . min^{-1} = 18.1 µM / min

The specific activity (µmol min^{-1} mg^{-1} or U mg^{-1}) was calculated from the enzymatic activity (µmol mL^{-1} min^{-1}) for the volume of the reaction (1 mL) divided by the total

mass of protein in the sample (mg). From the previous example the total mass of TADH added was 0.003 mg, the specific activity was calculated as:

SA = (0.01812 x 1) / 0.003 = **6.0 U / mg**

3.4.6.2   Reduction assays

The enzymatic activity of TADH was routinely assayed with substrates butyraldehyde or cyclohexanone. The following standard procedure is outlined with butyraldehyde. Any variations in enzyme assay parameters are highlighted in the Results.

The reagents and cell compartment of the spectrometer were kept at 60 °C prior to assay. The following reagents were added to a 1 mL cuvette: butyraldehyde (20 mM), enzyme (10 µL, 1 µg) and up to 1 mL 50 mM Bis-Tris buffer, pH 6.0, and the absorbance was set to zero. The reaction was initiated by addition of NADH (0.1 mM), followed by mixing of the reagents with a 1 mL pipette, in the cell compartment (at 60 °C). The decrease of absorbance at 340 nm, (due to the consumption of NADH) was monitored. For all enzymatic assays the specific activity was calculated from the initial linear rate of reaction (up to the initial 300 s). For all enzymatic assays, a control reaction was performed replacing the enzyme with 50 mM Bis-Tris buffer, pH 6.0 (10 µL) following NADH absorbance at 340 nm, no decrease in absorbance was observed.

3.4.7   Enzyme kinetics and inhibition studies with different organic substrates

Enzymatic assays were performed in both the reductive and oxidative directions for both native activity and imine reductase activity. Wild-type and other TADH variants enzymes were prepared to a concentration of 0.2 mg / mL in 20 mM Tris pH 7.5. NADH was prepared to a concentration of 10 mM in milliQ water. NAD^+ was prepared to a concentration of 50 mM in milliQ water. Imine (2-methyl-1-pyrroline **1**, 2,3-dihydroisoquinoline **2**) and ketone (cyclohexanone) stock solutions were prepared in a concentration of 1 M in acetonitrile (or other organic solvent as specified in text). Amine (2-methylpyrrolidine **3**, 1,2,3,4 tetrahydroisoquinoline **4**) and alcohol (cyclohexanol) stock solutions were prepared at a concentration of 5 M in acetonitrile (or other relevant solvent, as specified in text). To vary solvent concentrations in the assay, the concentration of the substrate stock in organic solvent was varied.

Reduction: The following reagents were added to a 1 mL cuvette; NADH (10 µL, final conc. 0.1mM), substrate (20 µL, final conc 20 mM), enzyme (100 µL, final conc. 0.02 mg/mL) and 50 mM Bis-Tris buffer, pH 6.0 (to 1 mL). The reaction was initiated by addition of NADH followed by mixing of the reagents with a 1 mL pipette, in the cell compartment (at 60 ^{o}C). The decrease of absorbance at 340 nm, (due to the consumption of NADH) was monitored. A control assay was performed, replacing the enzyme with 50 mM Bis-Tris buffer, pH 6.0 (100 µL), no decrease in NADH absorbance was observed.

Oxidation: The following reagents were added to a 1 mL cuvette; NAD$^+$ (20 µL , 1 mM), substrate (20 µL, 100 mM), enzyme (100 µL, final conc. 0.02 mg/mL) and 50 mM Glycine-NaOH buffer, pH 9.0 (to 1 mL). The reaction was initiated by addition of NAD$^+$ followed by mixing of the reagents with a 1 mL pipette, in the cell compartment (at 60 ^{o}C). The increase of absorbance at 340 nm, (due to the formation of NADH) was monitored. A control assay was performed, replacing the enzyme with 50 mM Glycine-NaOH buffer, pH 9.0 (10 µL), no increase in NADH absorbance was observed.

The procedures described above were repeated for the Michaelis-Menten kinetics, except that the concentration of the substrate was varied, to reach the following concentrations in the assay:

Cyclohexanol: 0.5, 1, 1.5, 2, 3, 5, 7.5 and 10 mM

Cyclohexanone: 1, 2.5, 7.5, 15, 25 and 50 mM

The procedures described for Michaelis-Menten kinetics were repeated for inhibition kinetics with imine and amines, except that inhibitor was added in each kinetics series, in the following concentrations:

2-methyl-1-pyrroline **1** in the oxidation assay: 10 mM, 25 mM, 50 mM

2-methyl-pyrrolidine **2** in the reduction assay: 1 mM, 5 mM, 10 mM

For each inhibition study the resulting values were used to plot a Lineweaver-Burk graph in Excel and GraphPad Prism 8 was used to plot the Michaelis-Menten kinetics and to determine the kinetic constants.

The procedures described above were repeated for inhibition kinetics with the nicotinamide ligand **21a** (0.1 mM and 0.25 mM) and Ir-complex **24a** (0.05 mM and 0.1 mM). The parameters of the enzymatic assays are outlined in section *3.9.1* and *3.9.2.*

3.5   Preparation and characterisation of TADH mutants

All TADH single and double mutants were prepared using the QuikChange Lightning Site-Directed Mutagenesis Kit (Agilent), and their DNA sequences confirmed by sequencing performed by Eurofins Genomics. Primers were designed using the QuikChange® Primer Design Program (Agilent) and purchased from Integrated DNA Technologies. Primer sequences for each mutation can be found in Appendix 2.

PCR was performed on a Mastercycler® personal (Eppendorf) under the following conditions: 1 cycle at 95 $^{\circ}$C for 2 min followed by 18 cycles of 95 $^{\circ}$C for 20 s, 60 $^{\circ}$C for 10 s and 68 $^{\circ}$C for 30 s, finishing with a cycle at 68 $^{\circ}$C for 5 min.

Following successful mutagenesis, the mutated plasmids were then transformed into BL21(DE3) cells and glycerol stock prepared and stored at -80 $^{\circ}$C. Each of the mutants was then grown as described in section *3.4.*2. (LB media, 37 $^{\circ}$C, 200 rpm) and expression induced at 30 $^{\circ}$C OD_{600} ~0.8 with IPTG to a final conc. 0.4mM. Purification was performed by heat treatment (80 $^{\circ}$C, 20 min) and a sample taken for SDS-PAGE analysis, protein concentration and activity assays. Expression cultures were performed in 250 mL expression volumes for single mutants and 50 mL volumes for double mutants.

3.5.1   *Enzymatic assays of mutants*

All mutants were investigated for both native activity and imine reductase activity in both oxidative and reductive directions as outlined in section 3.4.6., using substrates 1-butanol, 2-methylpyrrolidine **3** and 1,2,3,4-tetrahydroisoquinoline **4** in the oxidation

assays and butyraldehyde, 2-methylpyrroline **1** and 3,4-dihydroisoquinoline **2** in the reduction assays**.**

Oxidation: Stock solutions of amines, **3** and **4** were prepared in ACN to a final concentration of 5 M.

Table 3.1. Enzyme parameters for oxidative assays outlined below.[a]

	Stock conc.	Vol (μL) added control	Vol (μL) added	Final conc.
Glycine-NaOH pH 9.0	50 mM	860	860	-
Enzyme	0.2 mg / mL	100	100	0.02 mg / mL
Substrate[b]	5 M in ACN	20	20	100 mM
ACN	-	20	0	2 %
NAD^{+}	50 mM	0	20	1 mM

[a] Assays run at 340 nm, 60 ^{o}C for 5 min; [b] 1-butanol was added to a final conc. of 100 mM with no addition of organic solvents.

Reduction: Stock solutions of imine **1** and **2** were prepared in ACN to a final concentration of 1 M.

Table 3.2. Enzyme parameters for reductive assays outlined below.[a]

	Stock conc.	Vol (μL) added control	Vol (μL) added	Final conc.
Bis-Tris pH 6.0	50 mM	Up to 1 mL	Up to 1 mL	-
Enzyme	0.2 mg / mL	10 or 100	10 or 100	0.002 or 0.02mg / mL
Substrate[b]	1 M in ACN	20	20	20 mM
ACN	-	20	0	2 %
NAD^{+}	10 mM	0	10	1 mM

[a] Assays run at 340 nm, 60 ^{o}C for 5 min; [b] butyraldehyde was added to a final conc. of 20 mM with no addition of organic solvents.

Controls performed without NADH showed that both 3,4-dihydroisoquinoline **2** and the corresponding amine **4** have an absorbance at 340 nm, therefore the absorbance was set to zero before addition of NAD(H) to begin the reactions.

3.6 Replacement of zinc with other metals

3.6.1 Equipment

Dialysis tubing (Sigma-Aldrich) (molecular cut-off = 14 kDa) was treated for the removal of traces of glycerol, sulphides and heavy metals. Dialysis tubing was washed in distilled water with shaking for 3-4 hours. This was followed by treatment with 0.3 % w / v sodium sulphide solution at 80 $^{\circ}$C for 1 minute and washing with hot water at 60 $^{\circ}$C for 2 minutes. Acidification with 0.2 % v / v sulphuric acid solution was then performed, rinsing with hot water to remove the acid. Finally, the tubing was added to a 1 mM EDTA + 2 % w / v sodium bicarbonate solution with gentle shaking for 4 hours followed by extensive rinsing with Chelex100® treated milliQ. The treated dialysis tubing was then stored in Chelex100® treated 20 % ethanol solution at 4 $^{\circ}$C, until ready for use. Prior to dialysis, the tubing was soaked and washed extensively with MilliQ-H_2O. All buffers were treated with Chelex100® (0.01 g of Chelex100® for every 1 g of buffer salt) and the resulting solution stirred at room temperature for one hour. The Chelex100® was removed from solution with Buchner filtration. All glassware used in dialysis were treated with 3 x 30 % nitric acid washes following by extensive rinsing with milliQ-H_2O.

3.6.2 General procedures

Each dialysis step was carried out at 4 $^{\circ}$C unless otherwise stated, against three changes of buffer (100-500 volumes), with 3 hours between first two buffer changes and overnight for the final buffer change. Sample solutions of TADH (1-5 mg / mL, 0.8-3 mL) were prepared and loaded into the pre-soaked dialysis tubing. The sample solutions were dialysed against initial buffer containing chelators for zinc removal. After this, chelators were removed by dialysis against one round of initial buffer (3 h) followed by two rounds of final buffer (3 h and overnight), to yield apo-TADH. The apo-TADH solutions were dialysed against final buffer containing metal ions (up to 1 mM, M^{n+}) for 12 hours (no buffer change used for this step). Excess M^{n+} was removed by

dialysis against final buffer. Protein concentration, purity and enzymatic activity assays were performed on initial TADH, apo-TADH after chelator removal and metal-TADH after removal of the excess metal salt.

Apo-TADH after chelator removal, M^{n+}-TADH after removal of excess M^{n+} and control samples were centrifuged, unless stated otherwise (12,000 rpm, 4 $^{\circ}$C, 2 min) and any protein pellets removed before sample analysis. Apo-, M^{n+}-TADH and control samples (250 - 500 μL) were analysed by ICP-MS, as detailed in section *3.6.10.*

A control sample was performed for each dialysis: this was a TADH sample which was kept at the sample temperature and the same conditions as the final M^{n+}-TADH, excluding any chelator or metal addition to the buffers, for the entire length of the dialysis investigation, before protein and metal analysis was performed.

The following buffer and chelators were used:

Initial buffers: 50 mM sodium acetate buffer pH 5.5; 20 or 50 mM MES buffer pH 6.0 or 6.5; 20 mM Tris buffer pH 6.5

Chelators: 5-20 mM dipicolinic acid (DA); 5-20 mM 1,10-phenanthroline (OPA); 5-20 mM ethylenediaminetetraacetic acid (EDTA) or a combination thereof

Final buffers: 20 mM MES pH 6.5, 20 mM Tris pH 6.5 or 7.5

Metals: Zinc(II) acetate dihydrate, cobalt(II) acetate tetrahydrate or Dicarbonyl(acetylacetonato) rhodium(I).

3.6.3 Preliminary chelator investigations

Six samples of TADH (6.5 mg / mL, 500 μL) were dialysed using midi dialysis tubing (up to 800 μL total volume) against 500 volumes of buffer. Initial buffers: 50 mM sodium acetate pH 5.5 containing dipicolinic acid (5 and 1 5mM), 1,10-phenanthroline (5 and 15 mM) or ethylenediaminetetraacetic acid (5 and 15 mM); Final buffer: 20 mM MES pH 6.5; Metal salts: Zinc(II) acetate dihydrate (20 μM).

3.6.4 Impact of pH on zinc removal

TADH samples (1.3 mg / mL. 2.5 mL) were dialysed in dialysis tubing (2.5 mL) against 100 volumes of buffer. Initial buffers: 50 mM sodium acetate buffer pH 5.5, 20 mM MES pH 6.5 containing 1,10-phenanthroline (5 mM), dipicolinic acid (15 mM) and a combination of 1,10-phenanthroline (5 mM) an dipicolinic acid (20 mM); Final buffer: 20 mM MES pH 6.5, 20 mM Tris pH 7.5; Metal salts: Zinc(II) acetate dihydrate (20 µM).

3.6.5 Impact of chelator combinations on zinc removal

TADH samples (1.3 mg / mL, 3 mL) were dialysed in dialysis tubing against 100 volumes of buffer. Initial buffers: (20 mM) MES pH 6.0 or pH 6.5 containing 1,10-phenanthroline (10 mM) and a combination of 1,10-phenanthroline (10 mM) and EDTA (20 mM); Final buffer: 20 mM MES pH 6.5 or Tris pH 7.5; Metal salts: Zinc(II) acetate dihydrate (20 µM).

3.6.6 Impact of temperature on zinc removal

TADH (1.3 mg / mL 900 uL) samples were dialysed in dialysis tubing against 150 volumes of buffer. Initial buffers: 20mM Tris pH 6.5 containing a combination of 1,10-phenanthroline (10 mM) and EDTA (20 mM); Final buffer: 20 mM Tris pH 7.5; Metal salts: Zinc(II) acetate dihydrate (20 µM); Temperature throughout dialysis: 4 ^{o}C, room temp and 60 ^{o}C.

3.6.7 Cobalt insertion

TADH (0.5 mg / mL, 0.5 mL) was dialysed in dialysis tubing against 100 volumes of buffer. For cobalt reinsertion, the 'apo-TADH' created with treatment of 20 mM Tris pH 6.5, 4 ^{o}C containing combination of OPA (10 mM) and EDTA (20 mM) was then dialysed against 20 mM Tris pH 7.5 containing cobalt(II) acetate tetrahydrate (1 mM).

3.6.8 Metal exchange using purified secTADH

3.6.8.1 Dialysis procedure

TADH (0.60 and 0.88 mg / mL, 2.5 mL) samples were dialysed in dialysis tubing against 150 volumes of buffer. An initial buffer exchange step was performed by dialysis

against 20 mM MES pH 6.0 for 2 h. Dialysis for creation of Rh-TADH was performed in degassed buffers under nitrogen during introduction of rhodium.

<u>Initial buffers:</u> 20 mM MES pH 6.0 containing (10 mM) 1,10-phenanthroline or a combination of 1,10-phenanthroline (10 mM) and EDTA (20mM); <u>Final buffer:</u> 20 mM MES pH 6.5 (degassed for Rh insertion); <u>Metal salts:</u> Zinc(II) acetate dihydrate (20 µM) or $Rh(acac)(CO)_2$ (20 µM); <u>Temperature throughout dialysis:</u> 4 ^{o}C.

3.6.8.2   Gel filtration procedure

Sephadex G-25 PD-10 columns (2.5 mL sample volume) were equilibrated with the appropriate buffer (20 mM MES pH 6.0 or 20 mM MES pH 6.5) before each protein loading. The same buffers were used for all washes and buffer exchanges. Sample concentration was performed after each buffer exchange. Buffer was initially exchanged from 20 mM Tris pH 7.5 to 20 mM MES pH 6.0. This was followed by direct treatment of secTADH with chelating agents (10 mM OPA or 10 mM OPA & 20 mM EDTA) in 20 mM MES pH 6.0, stirring at 4 ^{o}C for 2 h. This sample was then subjected to a buffer wash with 20mM MES pH 6.0 and buffer exchange into 20mM MES pH 6.5 for creation of apo-TADH. Zn-TADH and Rh-TADH were prepared via direct addition of apo-TADH to a solution of 20 mM MES pH 6.5 containing 20 µM zinc acetate stirring at 4 ^{o}C for 2 h, or a degassed solution of 20 mM MES pH 6.5 containing of 20 µM $Rh(acac)(CO)_2$, respectively. Samples were stirred at 4 ^{o}C under nitrogen for 2 h. This was followed by 2 x column wash with 20 mM MES pH 6.5 to yield the final Zn-TADH and Rh-TADH samples.

The control was kept at 4 ^{o}C throughout and underwent 2 x buffer exchanges into 20 mM MES pH 6.0 and 20 mM MES pH 6.5. 1 mL samples of control apo-TADH and Zn- / Rh-TADH were submitted for analysis.

3.6.9   Imine reductase activity

The following reagents were added to a 1 mL cuvette: NADH (0.1 mM), 2-methyl-1-pyrroline (20 mM), enzyme (4 µg and 20 µg) and up to 1 mL 50 mM Bis-Tris buffer containing 2 % v / v ACN, pH 6.0. The reaction was initiated by addition of NADH

followed by mixing of the reagents with a 1 mL pipette, in the cell compartment (at 60 $^{\circ}$C). Absorbance at 340 nm was monitored.

3.6.10 ICP-MS analysis for metal content

Metal content was analysed in TADH samples *via* multi element analysis by Inductively Coupled Plasma Mass Spectrometry (ICP-MS). TADH samples were centrifuged (12,000 rpm, 4 $^{\circ}$C, 2 min) and any insoluble pellet removed to ensure the sample was homogeneous. Samples (0.5 mL, with >20 ppb metal content) were submitted for ICP-MS analysis. The samples were diluted to a 1 in 20 dilution with a solvent containing a non-ionic surfactant in 1 % nitric acid and then analysed for metal content. Results are reported as gravimetric concentrations (μg / L or mg / L) taking into account the 1 in 20 dilution so the each value represents the metal concentration for the protein concentration of the 0.5 mL sample. To evaluate the metal : protein ratio in the sample submitted, the protein concentration was first determined (using Bradford assay as outlined in section *3.4.4*).

The digestion procedure used by the ICP-MS lab was compared with the literature, where harsher conditions for digestion are usually reported (incubation of samples with 6 M HNO_3 at 110 $^{\circ}$C, 6 h; MilliQ-H2O was added to the samples for a 1 in 15 dilution), and the differences were very small (Table 3.3).[117]

Table 3.3. Comparison of ICP-MS sample procedures.

Sample	Zn : TADH[a] ratio	Zn : TADH[b] ratio
htTADH	0.73	0.74
secTADH	0.67	0.64
secC38A-TADH	0.33	0.38
secD152A-TADH	0.39	0.36

[a] ICP-MS lab prepared samples; [b] Acid digestion prepared samples

3.7 Synthesis of nicotinamide NHC functionalised iridium complexes

3.7.1 General methods

Commercially available reagents were used throughout, without purification unless otherwise stated. All aqueous solutions were prepared using deionised water. Analytical thin layer chromatography was carried out on aluminium backed plates coated with Merck Kieselgel 60 GF254 and visualised under UV light at 254 and / or 360 nm. Chemical staining was also routinely used, with aqueous basic potassium permanganate. Flash chromatography was carried out using Davisil silica 60 Å, with the eluent specified.

All compounds presented below were synthesised to a high degree of purity, (see Appendix 9 for ^{1}H and ^{13}C NMR spectra of compounds.)

3.7.2 Step 1 - Preparation of 4- and 5- halide substituted nicotinamide precursors

5- and 4-Chloro-*N*,*N*-diisopropylnicotinamide were prepared from 5-bromonicotinic acid or 4-chloronicotinic acid, respectively, according to a previously reported procedure.[157]

General procedure:

Thionyl chloride (10 equivalents) was added dropwise at room temperature under N_2 to the solid corresponding nicotinic acid (1 equivalent). The resulting suspension was refluxed for 2 h and the volatiles were removed *in vacuo*. The crude acid chloride was dissolved in anhydrous CH_2Cl_2 (8 mL) and the solution was added slowly at 0 °C to a solution of diisopropylamine (100 equivalents) in CH_2Cl_2 (8 mL). Stirring was continued overnight. Aqueous K_2CO_3 (2.0 M, 20 mL) was added and the aqueous layer was extracted with CH_2Cl_2 (3 x 15 mL). The combined organic extract was dried using $MgSO_4$, concentrated *in vacuo* and the crude product was purified by flash column chromatography on silica gel.

5-Bromo-*N*,*N*-diisopropylnicotinamide, 16a:[157]
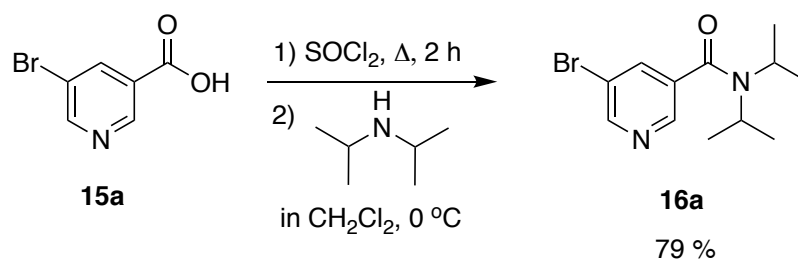
The procedure described above was used with 5-bromonicotinic acid (1.0 g, 4.95 mmol), thionyl chloride (7.2 mL, 99.0 mmol) and diisopropylamine (1.5 mL, 10.9 mmol). Elution with petroleum ether / EtOAc (70 / 30) afforded fine white crystals (1.12 g, 3.93 mmol, 79 % yield).

^{1}H NMR (300 MHz, (CD$_3$)$_2$CO-d_6, 298 K): δ_H (ppm) 8.69 (d, *J* = 2.3 Hz, 1H, pyridyl-*H*), 8.51 (d, *J* = 1.8 Hz, 1H, pyridyl-*H*), 7.94 (t, *J* = 2.0 Hz, 1H, pyridyl-*H*), 3.73 (s, br, 2H, diisopropylamine-NC*H*), 1.35 (s, br, 12H, diisopropylamine-C*H*$_3$).

^{13}C NMR (100 MHz, (CD$_3$)$_2$CO-d_6, 298 K): δ_C (ppm) 151.3 (pyridyl-*C*H), 145.7 (pyridyl-*C*H), 137.4 (pyridyl-*C*), 136.6 (pyridyl-*C*H), 121.1(pyridyl-*C*), 20.7 (4 x diisopropylamine-*C*H$_3$).

ESI$^+$-MS: 285.1 ([M+H]$^+$, 36.9 %), 307.0 ([M+Na]$^+$, 98.2 %).

4-Chloro-*N*,*N*-diisopropylnicotinamide, 16b:
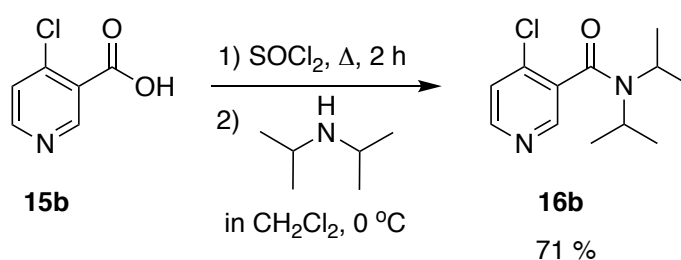
The procedure described above was used with 4-chloronicotinic acid (1.0 g, 6.35 mmol), thionyl chloride (9.2 mL, 127 mmol) and diisopropylamine (2.0 mL, 14.0 mmol). Elution with Petroleum Ether / EtOAc (70 / 30) afforded fine white crystals (1.08 g, 4.50 mmol, 71 % yield).

^{1}H NMR (300 MHz, (CD$_3$)$_2$CO-d_6, 298 K): δ_H (ppm) 8.53 (d, J = 5.4 Hz, 1H, pyridyl-H), 8.48 (d, J = 0.6 Hz, 1H, pyridyl-H), 7.94 (dd, J = 5.4, 0.6 Hz, 1H, pyridyl-H), 3.56-3.71 (s, br, 2H, diisopropylamine-NCH), 1.55 (d, J = 2.6 Hz, 3H, diisopropylamine-CH_3), 1.52 (d, J = 2.6 Hz, 3H, diisopropylamine-CH_3), 1.24 (d, J = 6.7 Hz, 3H, diisopropylamine-CH_3), 1.16 (d, J = 6.7 Hz, 3H, diisopropylamine-CH_3).

^{13}C NMR (100 MHz, (CD$_3$)$_2$CO-d_6, 298 K): δ_C (ppm) 153.3 (C=O), 151.3 (pyridyl-CH), 148.3 (pyridyl-CH), 140.1 (pyridyl-C), 136.2 (pyridyl-C), 125.4 (pyridyl-CH), 46.9, 52.1 (diisopropylamine-NCH), 20.9, 20.9, 20.8, 20.5 (diisopropylamine-CH$_3$).

ESI$^+$-MS: 241.1 ([M+H]$^+$, 94.1%), 263.1 ([M+Na]$^+$, 100%), 503.2 ([2M+Na]$^+$, 53.1%).

3.7.3 Step 2 - Preparation of imidazole-substituted nicotinamide derivatives by Ullmann coupling

The following compounds were prepared according to a procedure adapted from the literature.[158]

General procedure:

All manipulations were carried out using standard Schlenk techniques. The corresponding starting material (1 equivalent), imidazole (1.6 equivalents), cesium carbonate (2.0 equivalents) and copper(I) iodide (0.2 equivalents) were mixed in deoxygenated dimethylformamide (8 mL) and heated to 115-120 ^{o}C under dinitrogen for 24 h. After this time, the DMF was removed *in vacuo* and the crude product purified by flash column chromatography on silicagel.

5-(1 *H*-Imidazol-1-yl)-*N,N*-diisopropylnicotinamide, 17a:[158]

16a   Cul, CsCO$_3$, in DMF, 110-120 ^{o}C, 24 h   17a

68 %
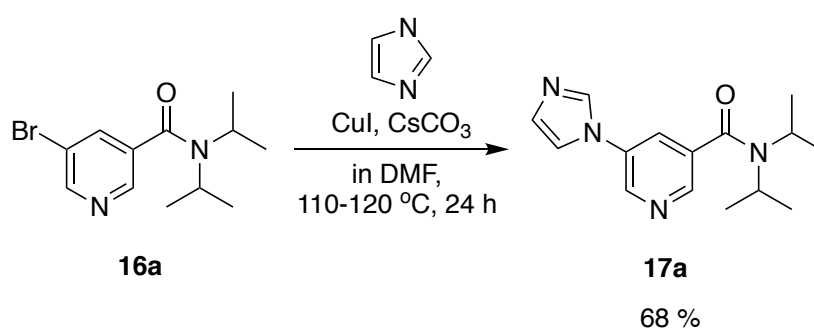
The procedure described above was used with 5-bromo-*N*,*N*-diisopropylnicotinamide (500 mg, 1.75 mmol), imidazole (192 mg, 2.81 mmol), cesium carbonate (1144 mg, 3.51 mmol) and copper(I) iodide (67 mg, 0.35 mmol). Elution with CH_2Cl_2 / MeOH (95 / 5) afforded the product (323 mg, 1.19 mmol, 68 % yield).

^{1}H NMR (300 MHz, (CD$_3$)$_2$CO-d_6, 298 K): δ_H (ppm) 8.93 (d, *J* = 2.6 Hz, 1H, pyridyl-*H*), 8.51 (d, *J* = 1.8 Hz, 1H, pyridyl-*H*), 8.22 (m, 1H, imidazolyl-*H*), 8.00 (dd, *J* = 2.6, 1.8 Hz, 1H, pyridyl-*H*), 7.73 (t, *J* = 1.4 Hz, 1H, imidazolyl-*H*), 7.16 (dd, *J* = 1.4, 0.9 Hz 1H, imidazolyl-*H*), 3.77 (s, br, 2H, diisopropylamine-NC*H*), 1.37 (s, br, 12H, diisopropylamine-C*H₃*).

^{13}C NMR (100 MHz, (CD$_3$)$_2$CO-d_6, 298K): δ_C (ppm) 167.4 (C=O), 145.5 (pyridyl-*C*H), 142.6 (pyridyl-*C*H), 136.6 (imidazolyl-N-*C*-N), 136.5 (pyridyl-*C*), 134.7 (pyridyl-*C*), 131.6 (imidazolyl-*C*H), 126.0 (pyridyl-*C*H), 118.7 (imidazolyl-*C*H), 20.5 (4 x diisopropylamine-*C*H₃).

ESI[+]-MS: 273.2 ([M+H]$^+$, 100 %), 295.2 ([M+Na]$^+$, 12.7 %), 567.3 ([2M+Na]$^+$, 43 %).

4-(1*H*-Imidazol-1-yl)-*N*,*N*-diisopropylnicotinamide 17b:
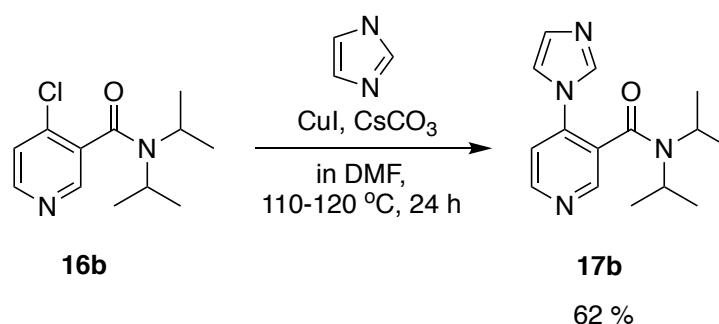
The procedure described above was used with 4-chloro-*N*,*N*-diisopropylnicotinamide (150 mg, 0.62 mmol), imidazole (58 mg, 0.85 mmol), cesium carbonate (344 mg, 1.06 mmol) and copper(I) iodide (20 mg, 0.11 mmol). Elution with CH_2Cl_2 / MeOH (95 / 5) gave the product (104 mg, 0.38 mmol, 62 % yield).

^{1}H NMR (300 MHz, (CD$_3$)$_2$CO-d_6, 298 K): δ_H (ppm) 8.72 (d, *J* = 5.4 Hz, 1H, pyridyl-*H*), 8.60 (s, 1H, pyridyl-*H*), 8.02 (s, br, 1H, imidazolyl-*H*), 7.59 (s, 1H, pyridyl-*H*), 7.57 (s, 1H, imidazolyl-*H*), 7.18 (s, br 1H, imidazolyl-*H*), 3.40-3.59 (m, 2H, diisopropylamine-

NC*H*), 1.52, (d, *J* = 6.8 Hz, 3H, diisopropylamine-C*H₃*), 1.42, (d, *J* = 6.8 Hz, 3H, diisopropylamine-C*H₃*), 1.05, (d, *J* = 6.8 Hz, 3H, diisopropylamine-C*H₃*), 0.61 (d, *J* = 6.7 Hz, 3H, diisopropylamine-C*H₃*).

^{13}C NMR (100 MHz, (CD₃)₂CO-*d₆*, 298 K): δ_C (ppm) 166.2 (C=O), 151.9 (pyridyl-*C*H), 149.6 (pyridyl-*C*H), 140.6 (imidazolyl-*C*H), 131.4 (imidazolyl-*C*H), 129.2 (imidazolyl-*C*H), 118.7 (pyridyl-*C*H), 51.9, 46.7, (diisopropylamine-N*C*H), 20.8, 20.6, 20.0, 19.9 (diisopropylamine-*C*H₃).

ESI[+]-MS: 273.2 ([M+H][+], 100 %), 295.2 ([M+Na][+], 41.7 %), 567.3 ([2M+Na][+], 9.5 %).

5-(1*H*-Imidazol-1-yl)nicotinamide, 20a:

19a   CuI, CsCO₃   **20a**

in DMF, 110-120 °C, 24 h

78 %
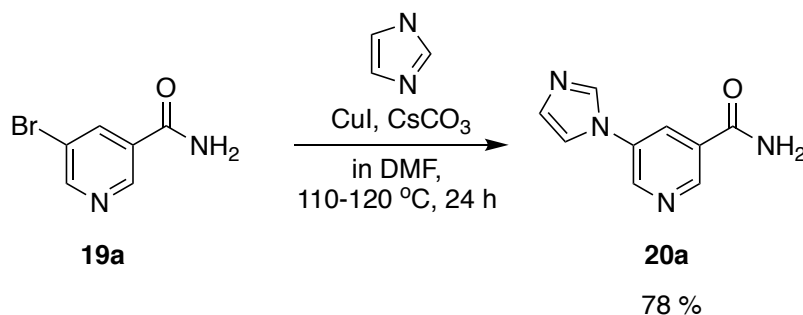
The procedure described above was used with 5-bromonicotinamide (500 mg, 2.49 mmol), imidazole (271 mg, 3.98 mmol), cesium carbonate (1621 mg, 4.97 mmol) and copper(I) iodide (95 mg, 0.50 mmol). Elution with CH₂Cl₂ / MeOH (80 / 20) gave the product (366 mg, 1.94 mmol, 78 % yield).

^{1}H NMR (400 MHz, CD₃OD-*d₄*, 298 K): δ_H (ppm) 9.04 (d, *J* = 1.9 Hz, 1H, pyridyl-*H*), 9.02 (d, *J* = 2.4 Hz, 1H, pyridyl-*H*), 8.49 (dd, *J* = 2.5, 1.9 Hz, 1H, pyridyl-*H*), 8.32 (s, br, 1H, imidazolyl-*H*), 7.74 (s, br, 1H, imidazolyl-*H*), 7.24 (s, br, 1H, imidazolyl-*H*).

^{13}C NMR (100 MHz, CD₃OD-*d₄*, 298 K): δ_C (ppm) 168.7 (*C*=O) , 148.3 (pyridyl-*C*H), 145.7 (pyridyl-*C*H), 135.3 (pyridyl-*C*), 132.2 (pyridyl-*C*), 131.0 (imidazolyl-*C*H), 129.4 (pyridyl-*C*H), 119.7 (imidazolyl-*C*H).

ESI[+]-MS: 189.1 ([M+H][+], 100 %).

4-(1*H*-Imidazol-1-yl)nicotinic acid, 23:
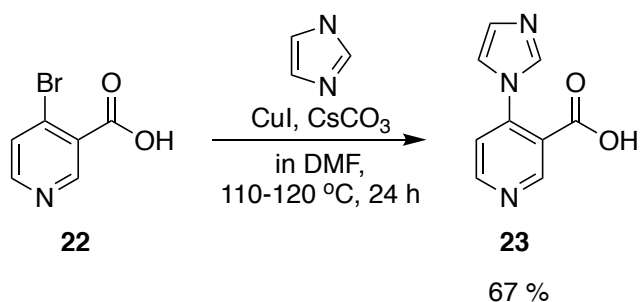
The procedure described above was used with 4-bromonicotinic acid (500 mg, 2.48 mmol), imidazole (2.5 eqv., 421 mg, 6.19 mmol), cesium carbonate (3.1 eqv., 2520 mg, 7.73 mmol) and copper(I) iodide (0.3 eqv., 147 mg, 0.77 mmol). Elution with CH_2Cl_2 / MeOH / Et_3N (85 / 10 / 5) and washing with DCM gave the final product (315 mg, 1.67 mmol, 67 % yield).

^{1}H NMR (300 MHz, $(CD_3)_2SO$-d_6, 298 K): δ_H (ppm) 9.01 (d, *J* = 0.6 Hz, 1H, pyridyl-*H*), 8.83 (d, *J* = 5.4 Hz, 1H, pyridyl-*H*), 8.01 (t, *J* = 1.1 Hz, 1H, imidazolyl-*H*), 7.59 (dd, *J* = 5.4, 0.6 Hz, 1H, pyridyl-*H*), 7.51 (t, *J* = 1.4 Hz, 1H, imidazolyl-*H*), 7.11 (d, *J* = 1.2 Hz, 1H, imidazolyl-*H*).

^{13}C NMR (100 MHz, $(CD_3)_2SO$-d_6, 298 K): δ_C (ppm) 165.7 (C=O), 153.4 (pyridyl-*C*H), 151.5 (pyridyl-*C*H), 142.6 (pyridyl-*C*), 137.4 (imidazolyl-*C*H), 129.2 (imidazolyl-*C*H), 123.0 (pyridyl-*C*), 120.5 (imidazolyl-*C*H), 120.2 (pyridyl-*C*H).

ESI$^+$-MS: 190.1 ([M+H]$^+$, 100 %), 212.0 ([M+Na]$^+$, 37.2 %).

3.7.4 Step 3 – Preparation of benzylated imidazole substituted nicotinamide derivatives

General procedure:

To a solution of imidazoyl starting material (1 equivalent) in ACN (5 mL) was added dropwise benzyl bromide (4 equivalents). The resulting reaction mixture was stirred at room temp. overnight followed by heating to 40 °C for a further 24 h, after which time a precipitate was observed. The solution was allowed to cool and diethyl ether

(10 mL) was added to further precipitate the final product. After filtering, the product was washed with diethyl ether (3 × 10 mL), to afford the bromide salt.

1-benzyl-3-(*N*-benzylimidazol-1-yl)-5-(diisopropylcarbamoyl)pyridinium bromide, 18a:
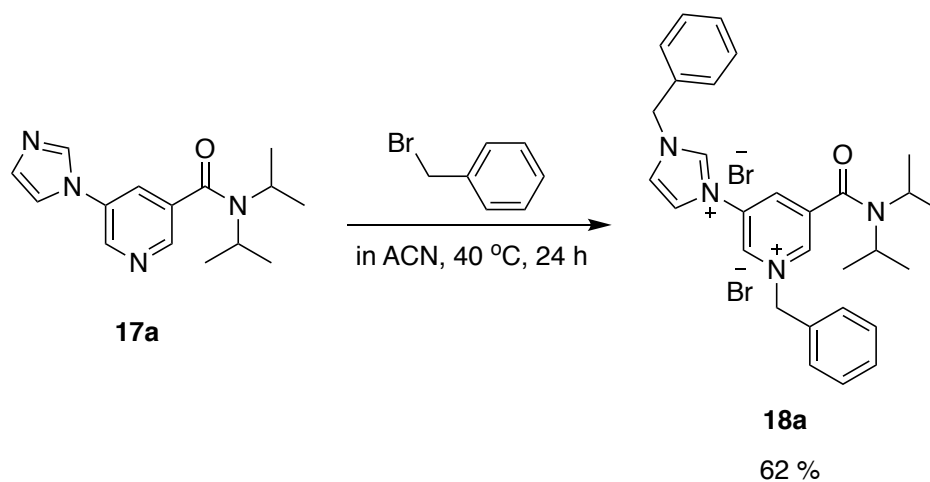
17a

in ACN, 40 °C, 24 h

18a

62 %

The procedure described above was used with 5-(1 *H*-imidazol-1-yl)-*N,N*-diisopropylnicotinamide (200 mg, 0.73 mmol) and benzyl bromide (0.35 mL, 2.93 mmol) affording the product (274 mg, 0.45 mmol, 62 % yield).

^{1}H NMR (300 MHz, CD$_3$OD-d_4, 298 K): δ_H (ppm) 9.96 (dd, *J* = 2.2, 1.2 Hz, 1H, pyridyl-*H*), 9.40 (t, *J* = 1.4 Hz, 1H, pyridyl-*H*), 9.09 ((t, *J* = 1.7 Hz, 1H, pyridyl-*H*), 8.36 (d, *J* = 2.2 Hz, 1H, imidazolyl-*H*), 7.99 (d, *J* = 2.2 Hz , 1H, imidazolyl-*H*), 7.65 – 7.69 (m, 2H, benzyl-*H*), 7.56 – 7.60 (m, 2H, benzyl-*H*), 7.45 – 7.51 (m, 6H, benzyl-*H*), 6.03 (s, 2H, benzyl-C*H$_2$*), 5.62 (s, 2H, benzyl-C*H$_2$*), 3.78 (s, br, 2H, diisopropylamine-NC*H*), 1.53 (s, br, 6H, diisopropylamine-C*H$_3$*), 1.20 (s, br, 6H, diisopropylamine-C*H$_3$*).

^{13}C NMR (100 MHz, CD$_3$OD-d_4, 298 K): δ_H (ppm) 138.1 (pyridyl-*C*H), 134.2 (pyridyl-*C*), 131.4, 130.8, 130.7, 130.6, 130.2 (2 x benzyl-*C*), 125.1, 123.8 (benzyl-*C*H$_2$), 67.1, 55.2 (2 x diisopropylamine-N*C*H).

ESI$^+$-MS: 485.3 ([M^{2+}+MeO$^-$]$^+$, 92 %), 486.3 ([M^{2+}+MeOH]$^{2+}$, 32.7 %).

1-benzyl-4-(*N*-benzylimidazol-1-yl)-3-(diisopropylcarbamoyl)pyridinium bromide, 18b

17b

in ACN, 40 °C, 24 h

18b

30 %
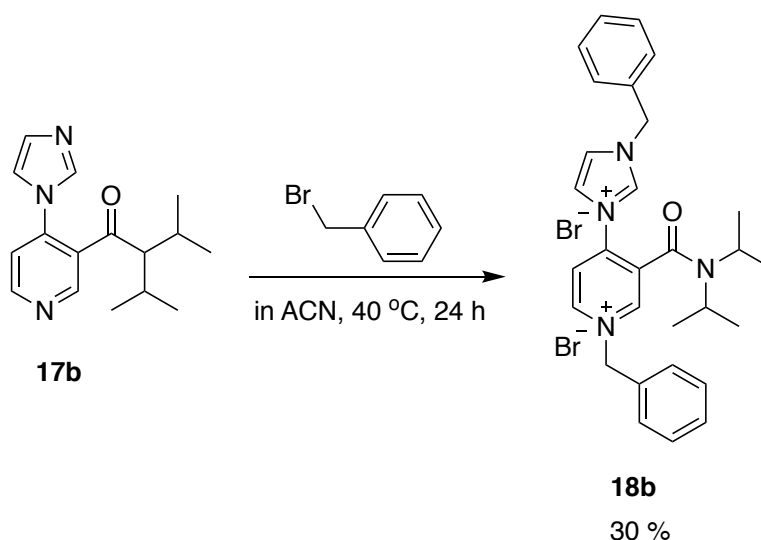
The procedure described above was used with 4-(1 *H*-imidazol-1-yl)-*N*,*N*-diisopropylnicotinamide (46.5 mg, 0.17 mmol) and benzyl bromide (81 μL, 0.68 mmol) affording the product, (31 mg, 0.05 mmol, 30 % yield).

^{1}H NMR (300 MHz, CD$_3$OD-*d$_4$*, 298 K): δ_H (ppm) 9.84 (s, 1H, imidazolyl-*H*), 9.63 (s, 1H, pyridyl-*H*), 9.47 (d, *J* = 6.5 Hz, 1H, pyridyl-*H*), 8.65 (d, *J* = 6.5 Hz, 1H, pyridyl-*H*), 8.09 (s, 1H, imidazolyl-*H*), 8.05 (s, 1H, imidazolyl-*H*), 7.62 − 7.65 (m, 2H, benzyl-*H*), 7.54 − 7.58 (m, 2H, benzyl-*H*), 7.49 − 7.51 (m, 3H, benzyl-*H*), 7.45 − 7.47 (m, 3H, benzyl-*H*), 6.03 (s, 2H, benzyl-C*H$_2$*), 5.64 (s, 2H, benzyl-C*H$_2$*), 3.53 − 3.71 (m, 2H, diisopropylamine-NC*H*), 1.49, (d, *J* = 6.8 Hz, 3H, diisopropylamine-C*H$_3$*), 1.22, (d, *J* = 6.8 Hz, 3H, diisopropylamine-C*H$_3$*), 1.09, (d, *J* = 6.8 Hz, 3H, diisopropylamine-C*H$_3$*), 0.72 (d, *J* = 6.7 Hz, 3H, diisopropylamine-C*H$_3$*).

^{13}C NMR (100 MHz, CD$_3$OD-*d$_4$*, 298 K): δ_H (ppm) 131.4, 130.9, 130.8, 130.6, 130.5, 130.3 (2 x benzyl-*C*), 128.0, 125.0 (benzyl-C*H$_2$*), 55.3 (2 x diisopropylamine-N*C*H), 20.2 (4 x diisopropylamine-*C*H$_3$).

1-benzyl-3-(*N*-benzylimidazol-1-yl)-5-carbamoylpyridinium bromide, 21a:

20a

in ACN, 40 °C, 24 h

21a

87 %
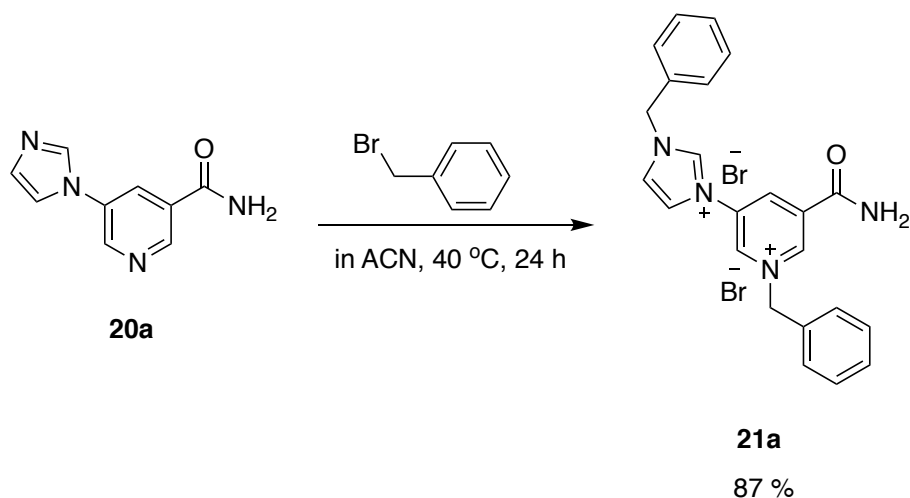
The procedure described above was used with 5-(1*H*-imidazol-1-yl)nicotinamide (250 mg, 1.33 mmol) and benzyl bromide (0.63 mL, 5.31 mmol) affording the product, (982 mg, 1.85 mmol, 87 % yield).

^{1}H NMR (400 MHz, CD$_3$OD-d_4, 298 K): δ_H (ppm) 10.07 (t, *J* = 1.7 Hz, 1H, pyridyl-*H*), 10.05 (dd, *J* = 2.1, 1.2 Hz, 1H, pyridyl-*H*), 9.68 (t, *J* = 1.3 Hz, 1H, imidazolyl-*H*), 9.51 (dd, *J* = 2.0, 1.6 Hz, 1H, pyridyl-*H*), 8.40 (t, *J* = 2.0 Hz, 1H, imidazolyl-*H*), 8.01 (t, *J* = 1.9 Hz , 1H, imidazolyl-*H*), 7.68 – 7.70 (m, 2H, benzyl-*H*), 7.58 – 7.61 (m, 2H, benzyl-*H*), 7.49 – 7.51 (m, 6H, benzyl-*H*), 6.08 (s, br, 2H, benzyl-C*H*$_2$), 5.64 (s, br, 2H, benzyl-C*H*$_2$).

^{13}C NMR (100 MHz, CD$_3$OD-d_4, 298 K): δ_C (ppm) 163.6 (*C*=O), 146.4 (imidazolyl-N-*C*H-N), 143.1 (pyridyl-*C*H), 139.6 (pyridyl-*C*H), 136.9 (pyridyl-*C*), 136.4 (pyridyl-*C*), 134.2 (benzyl-*C*), 133.4 (benzyl-*C*), 131.4, 130.8, 130.7, 130.6, 130.3 (2 x benzyl-*C*), 125.2 (imidazolyl-*C*H), 123.7 (imidazolyl-*C*H), 67.1 (benzyl-C*H*$_2$), 55.2 (benzyl-C*H*$_2$).

ESI$^+$-MS: 401.2 ([M^{2+}+ MeO$^-$]$^+$, 100 %), 369.2 ([M^{2+}- H$^+$]$^+$, 23 %), 279.1 ([M$^+$- PhCH$_2$]$^+$, 11 %).

3.7.5 Step 4 – Preparation of iridium NHC functionalised complex via metalation

The following procedure was adapted from the reported procedure by Crabtree[159] using 1-benzyl-3-(*N*-benzylimidazol-1-yl)-5-carbamoylpyridinium bromide, **21a** as the NHC and [IrCp*Cl$_2$]$_2$ as the metal precursor.

21a

24a
28 %
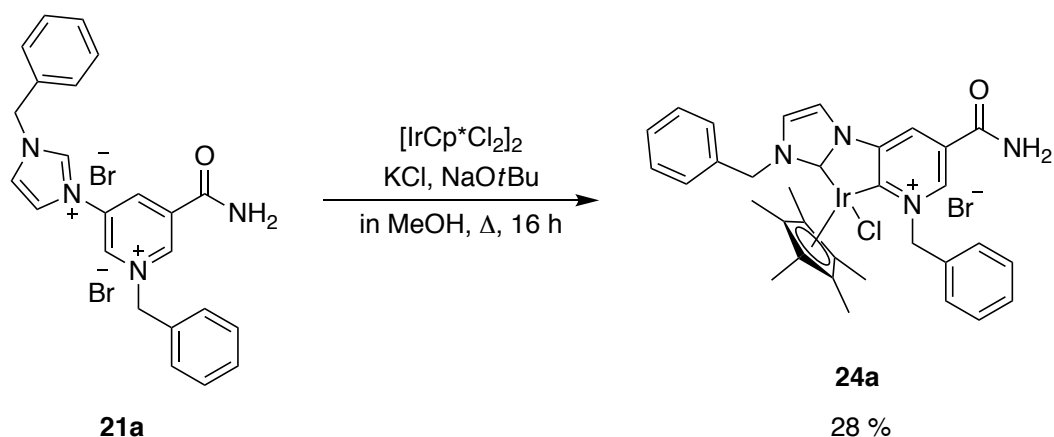
All manipulations were carried out under standard Schlenk techniques. A mixture of **21a** (75 mg, 0.14 mmol), potassium chloride (71 mg, 0.95 mmol), sodium *tert*-butoxide (14 mg, 0.14 mmol) and pentamethylcyclopentadienyl iridium dichloride dimer (56 mg, 0.07 mmol) was stirred in degassed MeOH (1.5 mL) at reflux for 16 h. The suspension was filtered through celite and dried under vaccum. This solid was then purified by chromatography on silicagel using CH_2Cl_2 / MeOH (90 / 10) to afford the product (31 mg, 0.04 mmol, 28 % yield).

^{1}H NMR (400 MHz, CD$_3$OD-d_4, 298K): δ_H (ppm) 9.09 (d, J = 1.5 Hz, 1H, pyridyl-H), 8.55 (d, J = 1.5 Hz, 1H, pyridyl-H), 8.05 (d, J = 2.4 Hz, 1H, imidazolyl-H), 7.50 – 7.55 (m, 4H, benzyl-H), 7.44 – 7.47 (m, 3H, benzyl-H), 7.35 – 7.37 (m, 3H, benzyl-H), 7.19 (d, J = 2.3 Hz, 1H, imidazolyl-H), 5.70 (d, J = 2.3 Hz, 2H, benzyl-CH_2), 5.50 (dd, J = 25.7, 13.7 Hz, 2H, benzyl-CH_2), 1.81 (s, 15H, Cp*-CH_3). NMR shows some impurities at low chemical shift.

^{13}C NMR (100 MHz, CD$_3$OD-d_4, 298K): δ_C (ppm) 175.5 (*C*=O) , 170.7 (pyridyl-*C*-Ir), 167.6 (imidazolyl-*C*-Ir), 151.8 (pyridyl-*C*), 144.0 (pyridyl-*C*), 139.9 (pyridyl-*C*H), 136.5 (benzyl-*C*), 134.9 (benzyl-*C*), 130.8, 130.6, 130.5, 130.0, 129.8, (2 x benzyl-*C*H), 124.4 (imidazolyl-*C*H), 123.7 (pyridyl-*C*H), 118.5 (imidazolyl-*C*H), 97.0 (Cp*-*C*-*C*) , 64.5 (benzyl-CH_2), 55.5 (benzyl-CH_2), 9.6 (Cp*-CH_3).

ESI$^+$-MS: 732.2 ([NHC$^+$(IrCp*Cl)]$^+$ 6.3%).

3.8 Catalysis experiments with Ir complex 24a

3.8.1 *Catalysis of transfer hydrogenation in organic solvent*

All solutions were thoroughly degassed and all manipulations were carried out under standard Schlenk techniques. The following reactions were performed according to the reported procedure by Zhu.[25]

General Procedure

The desired substrate, acetophenone, 2-methyl-1-pyrroline or 2,3-dihydroisoquinoline, (0.15 mmol), NaOtBu (1.4 mg, 0.015 mmol) and iridium complex (1.2 mg, 0.0015 mmol) were added to a N_2 purged vial. This was followed by dry iPrOH (0.5 mL), the reaction mixture was then refluxed under nitrogen for 24 h. The resulting solution was dried under vacuum, redissolved in CDCl$_3$ and analysed by NMR. ^{1}H NMR analysis of the crude product showed substrate and product as the major compounds, and no side products could be identified. Therefore, conversion was calculated assuming the alcohol / amine as the only products, based on the integration of specific signals in the ^{1}H-NMR spectra as highlighted below.

For the transfer hydrogenation of acetophenone to 1-phenylethanol, conversion was calculated by integration of the methyl signals at 2.61 and 1.50 ppm, respectively see Appendix 10.

> Acetophenone: ^{1}H NMR (300 MHz, CDCl$_3$-d, 298K): δ_H (ppm) 7.95 – 7.99 (m, 2H, benzyl-H x 2), 7.54 – 7.60 (m, 1H, benzyl-H), 7.44 – 7.50 (m, 2H, benzyl-H x 2), 2.61 (s, 3H, -COCH_3).

> 1-phenylethanol: ^{1}H NMR (300 MHz, CDCl$_3$-d, 298K): δ_H (ppm) 7.32 – 7.40 (m, 3H, benzyl-H x 3), 7.25 – 7.30 (m, 2H, benzyl-H), 4.91 (q, J = 6.5 Hz, 1H, -CHOHCH$_3$), 1.50 (dd, J = 6.4, 0.5 Hz, 3H, -CHOHCH_3).

For the transfer hydrogenation of 3,4-dihydroquinoline **2** to 1,2,3,4-tetrahydroisoquinoline **4**, conversion was calculated by integration of the signals at 3.74 and 3.10 ppm, respectively (see Appendix 10).

.

3,4-dihydroisoquinoline: ^{1}H NMR (400 MHz, CDCl$_3$-d, 298K): δ_H (ppm) 8.30 (s, 1H, phenyl-CHN), 7.36 – 7.30 (m, 1H, phenyl-H), 7.24 – 7.28 (m, 2H, phenyl-H x 2), 7.12 – 7.14 (d, J = 7.4 Hz, 1H, phenyl-H), 3.74 (m, 2H, pyridyl-CH_2N), 2.73 (m, 2H, pyridyl-CH_2).

1,2,3,4-tetrahydroisoquinoline: ^{1}H NMR (400 MHz, CDCl$_3$-d, 298K): δ_H (ppm) 7.03 – 7.11 (m, 3H, phenyl-H x 3), 6.96 – 7.99 (m, 1H, phenyl-H), 3.98 (s, 2H, phenyl-CH_2N), 3.10 (t, J = 6.0 Hz, 2H, CH_2NH), 2.77 (t, J = 6.0 Hz, 2H, CH_2 -phenyl).

3.8.2   Catalysis of transfer hydrogenation in buffer at high substrate concentrations

All solutions were thoroughly degassed and all manipulations were carried out under standard Schlenk techniques. The following reactions were prepared and performed according to and adapted from the reported procedure by Ward.[154]

General Procedure

The reaction buffer was prepared by mixing 3-(N-morpholino)propane sulfonic acid (MOPS, final conc. 1.2 M) and sodium formate (final conc. 3M) in milliQ water. The pH was adjusted to pH 8.0 with NaOH. Substrate stock solutions were prepared by solubilising the desired substrate (acetophenone, 2-methyl-1-pyrroline and 2,3-dihydroisoquinoline) in DMF to a final concentration of 7.5 M. The iridium complex was dissolved in DMF to a final concentration of 0.1 M.

Substrate (20 μL, final conc. 0.3 M) and iridium complex (15 μL, final conc. 0.003 M) were added to a N$_2$ purged vial containing reaction buffer (0.5 mL). The reaction mixture was then heated to 55 ^{o}C under nitrogen for 24 h. After this time, milliQ water (1 mL) was added to the reaction mixture along with 20 % NaOH (0.1 mL) to those vials containing an imine substrate and extracted with CHCl$_3$ (4 x 3 mL). The organic phase was then dried over MgSO$_4$, solvent removed under vacuum and the crude residue was analysed by NMR.

For the transfer hydrogenation of acetophenone to 1-phenylethanol, conversion was calculated as above, by integration of the methyl signals at 2.61 and 1.50 ppm, respectively.

For the transfer hydrogenation of 3,4-dihydroisoquinoline **2** in aqueous media, the NMR showed presence of amine only, and no sign of degradation.

3.8.3 Catalysis of transfer hydrogenation at low substrate concentrations and in the presence of TADH

General procedure

The reaction buffer was prepared by mixing 3-(*N*-morpholino)propane sulfonic acid (MOPS, final conc. 0.4 M) and sodium formate (final conc. 1M) in milliQ water. The pH was adjusted to 8.0 with NaOH. Substrate stock solutions were prepared by solubilising the desired substrate (acetophenone, 2-methyl-1-pyrroline and 2,3-dihydroisoquinoline) in ACN to a final concentration of 50 mM. The iridium complex was dissolved in degassed milliQ water containing ACN (5 % v / v) to a final concentration of 1.25 mM. TADH stock solution was prepared to a final concentration of 0.25 mM in 20 mM Tris pH 7.5. NADH was dissolved in milliQ water to a final concentration of 0.25 M to prepare a NADH stock solution.

Substrate (50 µL, final conc. 2.5 mM), iridium complex (20 µL, final conc. 25 µM) TADH (100 µL, final conc. 25 µM) and NADH (10 µL), final conc. 2.5 mM) were added to a N_2 purged vial containing reaction buffer (820 µL). The reaction mixture was then heated to 55 ^{o}C under nitrogen for 24 h. After this time, milliQ water (1 mL) was added to the reaction mixture along with 20 % NaOH (0.1 mL) to those vials containing an imine substrate and extracted with $CHCl_3$ (4 x 3 mL). The organic phase was then dried over $MgSO_4$, solvent removed under vacuum and the crude residue was analysed by NMR. Controls were also performed following the above procedure, either without TADH (replaced by 100 µL of Tris buffer) or without NADH (replaced with 10 µL milliQ water).

3.9   Inhibition studies with ligand 21a and Ir-complex 24a

3.9.1   *Ligand (21a) inhibition studies*

The reaction buffer was prepared by dissolving Bis-Tris salts in milliQ water for a final concentration of 50 mM. The pH was adjusted to 6.0 with HCl. The substrate stock was prepared by dissolving cyclohexanone in milliQ water to a final concentration of 500 mM. The ligand was dissolved in DMSO to a final concentration of 5 and 12.5 mM. TADH stock solution was prepared to a final concentration of 0.25 mM in 20mM Tris pH 7.5. NADH stock solutions were prepared by dissolving NADH in milliQ water at final concentrations of 12.5, 5, 3.75, 2.5, 1.25 and 0.5 mM to prepare a NADH stock solution.

Stock solutions of ligand **21a** (20 μL, final conc. 0.1 or 0.25 mM), TADH (10 μL, 5.6 μg) and NADH (20 μL, final conc. 0.25, 0.1, 0.075, 0.05, 0.025, 0.01 mM) were added to 50 mM Bis-Tris pH 6.0 buffer (910 μL) and heated to 60 $^{\circ}$C for 2 min. The reaction was started with the addition of NADH and mixing. NADH absorbance was measured at 340 nm over 250 seconds.

Table 3.4. Enzyme assay parameters for inhibition studies with Ligand 21a

	Stock conc.	V (μL) for control	V (μL) for 21a	Final conc.
Bis-Tris pH 6.0	50 mM	910	910	~50 mM
Enzyme	0.56 mg / mL	10	10	0.0056 mg / mL
Substrate	500 mM	40	40	20 mM
DMSO	-	20	0	2 %
Ligand **21a**	0, 5, 12.5 mM	0	20	0, 0.1, 0.25 mM
NADH	12.5, 5, 3.75, 2.5, 1.25, 0.5 mM	20	20	0.25, 0.1, 0.075, 0.05, 0.025, 0.01 mM

3.9.2 Ir complex (24a) inhibition studies

The reaction buffer was prepared by dissolving Bis-Tris salts in milliQ water for a final concentration of 50 mM. The pH was adjusted to 6.0 with HCl. The substrate stock was prepared by dissolving cyclohexanone in milliQ water to a final concentration of 500 mM. The Ir catalyst was dissolved in ACN to final concentrations of 2.5 and 5 mM. TADH stock solution was prepared to a final concentration of 0.25 mM in 20mM Tris pH 7.5. NADH stock solutions were prepared by dissolving NADH in milliQ water at final concentrations of 12.5, 5, 3.75, 2.5, 1.25 and 0.5 mM to prepare a NADH stock solution.

Stock solutions of Ir-complex **24a** (20 μL, final conc. 0.05 or 0.1 mM), TADH (10 μL, 5.6 μg) and NADH (20μL, final conc. 0.25, 0.1, 0.075, 0.05, 0.025, 0.01 mM) were added to 50 mM Bis-Tris pH 6.0 buffer (880 μL) and heated to 60 °C for 2 min. The reaction was started with the addition of NADH and mixing. NADH absorbance was measured at 340 nm over 250 seconds.

Table 3.5. Enzyme assay parameters for inhibition studies with Ir complex 24a

	Stock conc.	V (μL) for control	V (μL) for 24a	Final conc.
Bis-Tris pH 6.0	50 mM	880	880	~50 mM
Enzyme	0.56 mg / mL	10	10	0.0056 mg / mL
cyclohexanone	500 mM	40	40	20 mM
ACN	-	50	30	5%
Ir complex **24a**	0, 2.5, 5 mM	0	20	0, 0.05, 0.1 mM
NADH	12.5, 5, 3.75, 2.5, 1.25, 0.5 mM	20	20	0.25, 0.1, 0.075, 0.05, 0.025, 0.01 mM

Chapter 4 Results and Discussion

4.1 Selection and characterisation of a suitable ADH to engineer imine reductase activity
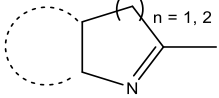
4.1.1 Introduction and highlights

The enzymatic reduction of carbonyls is performed by well-described alcohol dehydrogenases (see section 1.2). On the other hand, the enzymatic reduction of imines, which differ from carbonyls only by replacement of the oxygen with a substituted nitrogen, was rarely encountered in nature until recently; when the class of imine reductases (IREDs) was discovered and characterised. Similar to ADHs, IREDs depend on a nicotinamide cofactor, which transfers the hydride to the carbon-nitrogen double bond. Therefore, it was hypothesised that ADHs would make suitable starting points for the engineering of enzymes with promiscuous reactivities, towards the transfer of hydrides to other carbon-heteroatom bonds than carbonyls.

Since the beginning of this thesis, the knowledge and application of IREDs to biotransformations have increased very rapidly. However, there are still challenges associated with IRED application to organic synthesis. In comparison, ADHs are better understood and characterised, which makes them very desirable starting points to engineer new activity. Some of the main advantages of ADHs compared with IREDs, in terms of application scope, are highlighted in Table 4.1.

The use of ADHs to reduce imines might circumvent some of the IRED issues, such as their NADPH dependence, their relatively low catalytic efficiency and their relatively narrow substrate specificity towards cyclic imines. The aim of this section is to identify and characterise a suitable ADH to be used as a starting point for the development of IRED activity.

Table 4.1. Comparison of key traits of ADHs and IREDs highlighting the advantages of ADHs.

	ADH	IRED
Cofactor dependence	NADH and NADPH	Mostly NADPH
Thermostability	Several thermostable ADHs characterised	No thermostable IRED characterised so far
Solvent tolerance	Several solvent tolerant ADHs characterised	No solvent tolerant IREDs characterised so far
Substrate scope	Wide substrate range with different structural architecture	Preferred cyclic imines
Structural characterisation	Several crystal structures	Three crystal structures

<u>Highlights</u>

- Thermostable ADH from *Thermus* sp. ATN1 (TADH) was identified as a starting point for the engineering of promiscuity towards imine reduction.

- Literature protocols for the expression and purification of TADH from *E. coli* were adapted, to yield good amounts of relatively pure protein for further studies.

- The kinetic parameters of the purified TADH were similar to the ones reported in the literature, although the specific activity was consistently lower.

- The zinc content in the TADH purified by heat treatment was lower than expected. Purification by size exclusion chromatography led to a protein : zinc molar ratio of 1 : 1.6, closer to the expected result.

4.1.2 Selection of TADH from Thermus sp. ATN1 as starting point for enzyme engineering

At the beginning of this project, few imine reductases were known and characterised. Since then, an imine reductase database was created using bioinformatics tools, and

several of these putative IRED sequences were cloned and characterised. Sequence alignments of IREDs with either Zn-dependent (medium-chain) or non-Zn dependent (short-chain) ADHs resulted in no sequence similarity between these enzymes (below 20 %), suggesting no evolutionary relationship between the ADH and IRED scaffolds.

In the absence of sequence similarity, the criteria listed in Table 4.1 above were used to select a suitable ADH for the engineering of imine reductase activity. A range of ADHs previously highlighted as potential biocatalysts for stereoselective reductions[160] were initially selected as possible candidates, outlined in Table 4.2. A list of desired criteria was created to assist in the selection of the best ADH scaffold for introduction of imine reductase activity:

- *Stability*. Thermostable ADHs were preferred, which are usually tolerant to both high temperatures and organic solvents. Organic solvent use was thought to prevent hydrolysis of the imine substrate, and to contribute to solubilisation of hydrophobic substrates.
- *Broad substrate range*. Compared to their carbonyl precursors, imines possess an extra substituent at the nitrogen atoms. An enzyme with a promiscuous substrate spectrum was hypothesised to have increased chances to accept non-native imines.
- *NADH dependence*. Use of NADH as cofactor was preferred, since it is more available and cheaper than NADPH.
- *Available crystal structure*. Well characterised ADHs allow for better understanding of the structure and mechanistic functions, affording informed decisions on protein engineering.
- *E. coli expression system*. Recombinant expression in *E.coli* and easy purification were desirable for quick and easy production of the enzyme.

Table 4.2. Comparison of desired criteria of potential ADHs for introduction of imine reductase activity.[a]

	HLADH	ADH-A	TbADH	TADH	TeSADH	PpADH	AdhA
Thermostability	✗	✓	✓	✓	✓	✓	✓
High solvent stability	✗	✓	✓	✓	✓	✓	✓
Broad substrate range	~	✗	✗	✓	✓	✗	~
NADH dependent	✓	✓	✗	✓	✗	✓	✗
Available crystal structure	✓	✓	✓	✓	✗	✗	✗
***E. coli* expression system**	✓	✓	✓	✓	✓	✓	✓

[a] HLADH: from horse liver, ADH-A from *Rhodococcus* rubber, TbADH from *Thermoanaerobacter brockii*, TADH from *Thermus* sp. ATN1, TeSADH from *Thermoanaerobacter ethanolicus*, PpADH from *Paracoccus pantotrophus*, AdhA from *Pyrococcus furiosus*.[161]

One of the most studied ADHs is HLADH from horse liver. This NADH-dependent mesophilic enzyme accepts predominantly primary alcohols and aldehydes as substrates, although reduction of ketones was also described. HLADH was also reported to show some organic solvent tolerance. The limited substrate scope, thermal stability and organic solvent tolerance of HLADH reduce its applicability to organic transformations. In addition, recombinant production of HLADH from *E. coli* requires purification procedures that are not straightforward. Production of a His-tagged version of HLADH has been reported, however tentatives to reproducibly purify this construct were not trivial (Mattias Basle, unpublished data).

On the other hand, several ADHs with tolerance towards organic solvents and / or possessing thermostability have been published. Amongst these, the best

characterised are Zn-dependent ADHs from *Rhodococcus ruber* DSM 44541 (ADH-A),[162] *Thermoanaerobacter brockii* (TbADH),[122] *Thermus* sp. ATN1 (TADH),[163] *Thermoanaerobacter ethanolicus* (TeSADH):[164] as well as non metal-dependent ADHs from *Paracoccus pantotrophus* DSM 11072 (PpADH)[165] and *Pyrococcus furiosus* (AdhA).[161] Crystal structures have also been published for the Zn-dependent enzymes excluding TeSADH; no crystal structures have been reported for either of the non-metal dependent ADHs, thus they were ruled out. Half of these enzymes, including TbADH are NADPH-dependent and were therefore not considered for this study. Thus, leaving ADH-A from *Rhodococcus ruber* and TADH from *Thermus* sp., both NADH-dependent thermostable enzymes as potential candidates. ADH-A is reported to withstand high solvents concentrations, for example acetone (up to 50 % v / v) and 2-propanol (80 % v / v).[166] TADH is reported to retain activity in a range of solvents for example, acetone (10 % v / v) and octane (50 % v / v).[109] However, ADH-A has a much narrower substrate range when compared to TADH, primarily catalysing medium chain secondary alcohols and their corresponding ketones, whilst TADH has a broad ketone substrate range including primary, secondary and cyclic alcohols. Furthermore, TADH has been used in the presence of chemical catalysts and in electroenzymatic setups for cofactor recycling and was reported to be recombinantly expressed in *E. coli* and purified by heat.[108,167] A comparison of TADH with HLADH shows very similar features in catalysis and in the substrate binding pocket (Figure 4.1) except that an aspartate residue (Asp152) in TADH replaces Cys174 in HLADH. Therefore, it was hypothesised that TADH would represent a suitable starting point for active site engineering.

One potential issue with the use of the TADH enzyme is the presence of five cysteine residues in its sequence (see Appendix 1). As mentioned previously, one cysteine is involved in the binding of the catalytic zinc(II) ion located in the active site, the remaining four are bound to a second zinc(II) ion at a structural site. It is these four neighboring cysteines which could cause problems, if oxidised, forming disulphide bonds with one another which can drastically change the conformation of the enzyme and increase the chance of misfolding. Nonetheless, investigations proceeded as it was assumed these cysteines, present in all structurally characterised ADHs containing

a structural zinc,[84] would not be easily accessible for oxidation due to their location embedded within the protein structure and strong binding to the structural zinc ion.
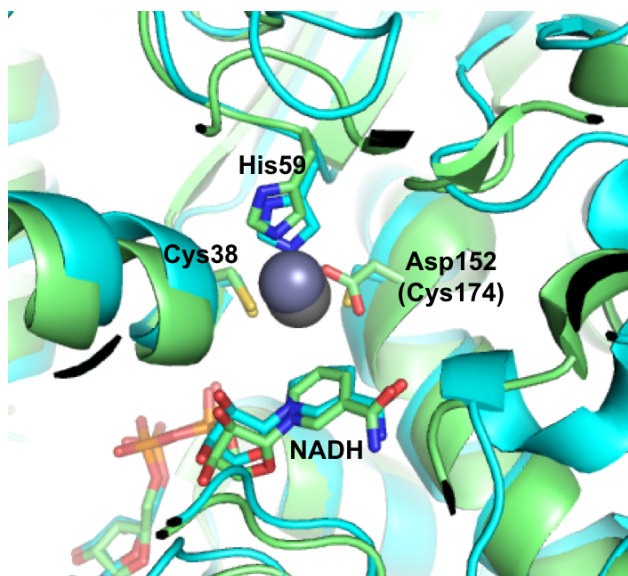
Figure 4.1. Alignment of TADH (PDB 4CPD, green) and HLADH (PDB 4XD2, cyan) active sites, highlighting Zn-binding amino acids and the NADH cofactor. Amino acid numbering is from TADH. Cys174 replaces Asp152 in TADH.

4.1.3 Expression of TADH in E. coli

The gene for TADH was obtained from Prof. Frank Hollmann from TU Delft, and was already cloned into the pASZ2 plasmid, previously reported. This plasmid carried the TADH gene cloned between the EcoRI and BamHI restriction sites of pET11aEco (a derivative of pET11a, Novagene, carrying an additional EcoRI site between the NdeI site and the ribosome binding site of pET11a). Gene sequencing confirmed that no mutations were present in the material received from the collaborators, and the gene sequence is presented in Appendix 1. The plasmid was transformed into chemically competent *E. coli* BL21(DE3) pLysS, and successful transformants were grown at 37 °C and used for the expression of TADH in LB medium with IPTG induction at 30 °C.

Expression of TADH was analysed by SDS-PAGE of the soluble and insoluble protein extracts of the expression cultures, at different times after induction with IPTG. Visual inspection of the SDS-PAGE showed a protein band at 37 kDa, which was not observed in the cells before induction (Figure 4.2a, lane 1 *vs.* 2-7). The first attempt using the adapted published protocol resulted in mostly insoluble TADH (Figure 4.2a lanes 8-9).
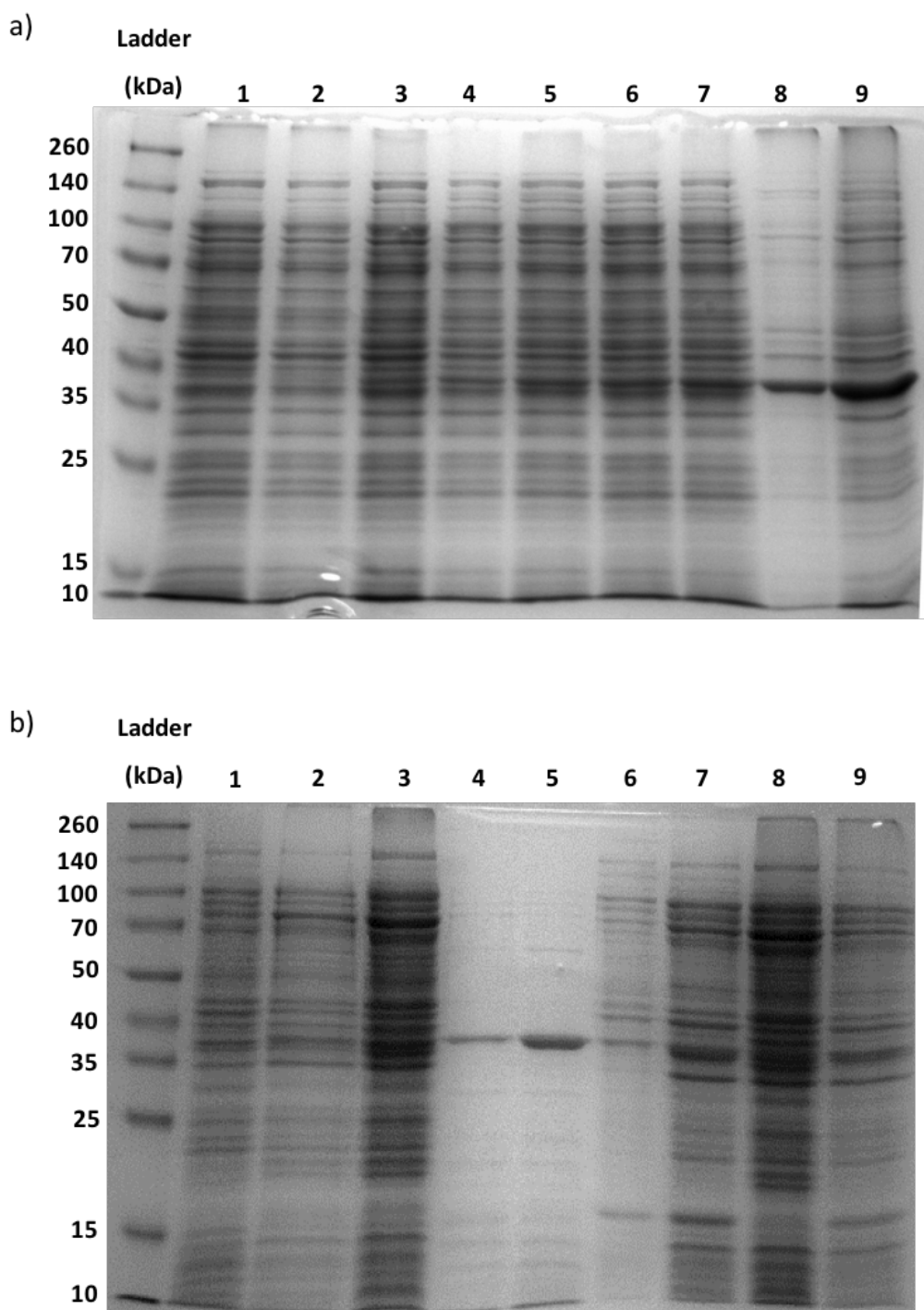
Figure 4.2. TADH expression time course at different growth temperatures: a) 37 ^{o}C, b) 30 ^{o}C

E. coli BL21(DE3) pLysS pASZ2 was grown in LB supplemented with carbenicillin. Protein expression was induced at OD_{600} of ~0.7 by the addition of sterile IPTG (1 mM final concentration). The cultures were incubated for the specified time and temperature, and 1 mL samples were harvested by centrifugation. Samples were lysed using Bugbuster lysis reagent and the protein content analysed by SDS-PAGE. **a)** growth at 37 ^{o}C, expression at 30 ^{o}C. **1-7**: soluble cell fractions after **1:** 0 h, **2**: 1 h, **3**: 2 h, **4**: 3 h, **5**: 4 h, **6**: 5 h, **7**: 22 h; **8**: insoluble fraction 3 h, **9**: insoluble fraction 22 h; **b)** growth at 30 ^{o}C, expression at 30 ^{o}C, heat treatment 80 ^{o}C 15 min. **1**: soluble fraction 0 h, **2-3**: soluble fractions 18 h, **4**: soluble fraction 0 h after heat treatment, **5-6**: soluble fraction 18 h after heat treatment, **7 & 9**: insoluble fraction 18 h after heat treatment. **8**: insoluble fraction 0 h after heat treatment.

To optimise expression, the growth temperature was reduced to 30 $^{\circ}$C, which resulted in a reduced amount of insoluble protein, although the amount of soluble TADH was not increased (Figure 4.2b).

The effect of IPTG concentration on TADH expression was also investigated, as Winograd *et al.* showed that reduction of IPTG increased protein solubility, preventing the formation of inclusion bodies.[168] A slight increase in both soluble and insoluble protein concentration was observed by SDS-PAGE, when IPTG was lowered from 1 mM to 0.4 mM final concentration during induction (Figure 4.3a-b, lanes 3-4 & 7-8). Expression also occurred in the absence of IPTG, as shown by SDS-PAGE of both soluble and insoluble fractions (Figure 4.3a-b, lane 6). This might be due to the two operons (*lac* operon and T7 promoter) present in the pASZ2 plasmid, resulting inexpression that is harder to control. Addition of 1 % glucose to the growth medium did not prevent expression before induction. When expression was performed in auto-inductive Terrific Broth (TB) medium, without addition of IPTG, little expression of the desired protein was observed (Figure 4.3a-b, lane 9).

In addition, after induction with IPTG, it was noted that the expression culture had unexpectedly high OD_{600}, (5-7), which could not be related to the appearance of the sample. When samples were examined under the microscope, large clumps of dead cells were observed, which may relate to the higher than expected OD_{600} values. Cell death was observed after induction with IPTG at 1 mM, as well as during expression using the auto-induction TB medium, whilst no cell death was observed before IPTG induction, nor during induction with IPTG at 0.4 mM.

Literature reports do not mention the amount of insoluble protein formed during expression. Growth of cells to a final OD_{600} of 9 was reported using 1 mM IPTG induction, which was not reproduced in this work. A subsequent literature report by the same group used a different methodology, based on expression using an auto-induction medium yielding high amounts of protein. Again, this was not reproduced in this work, using TB auto-induction medium.
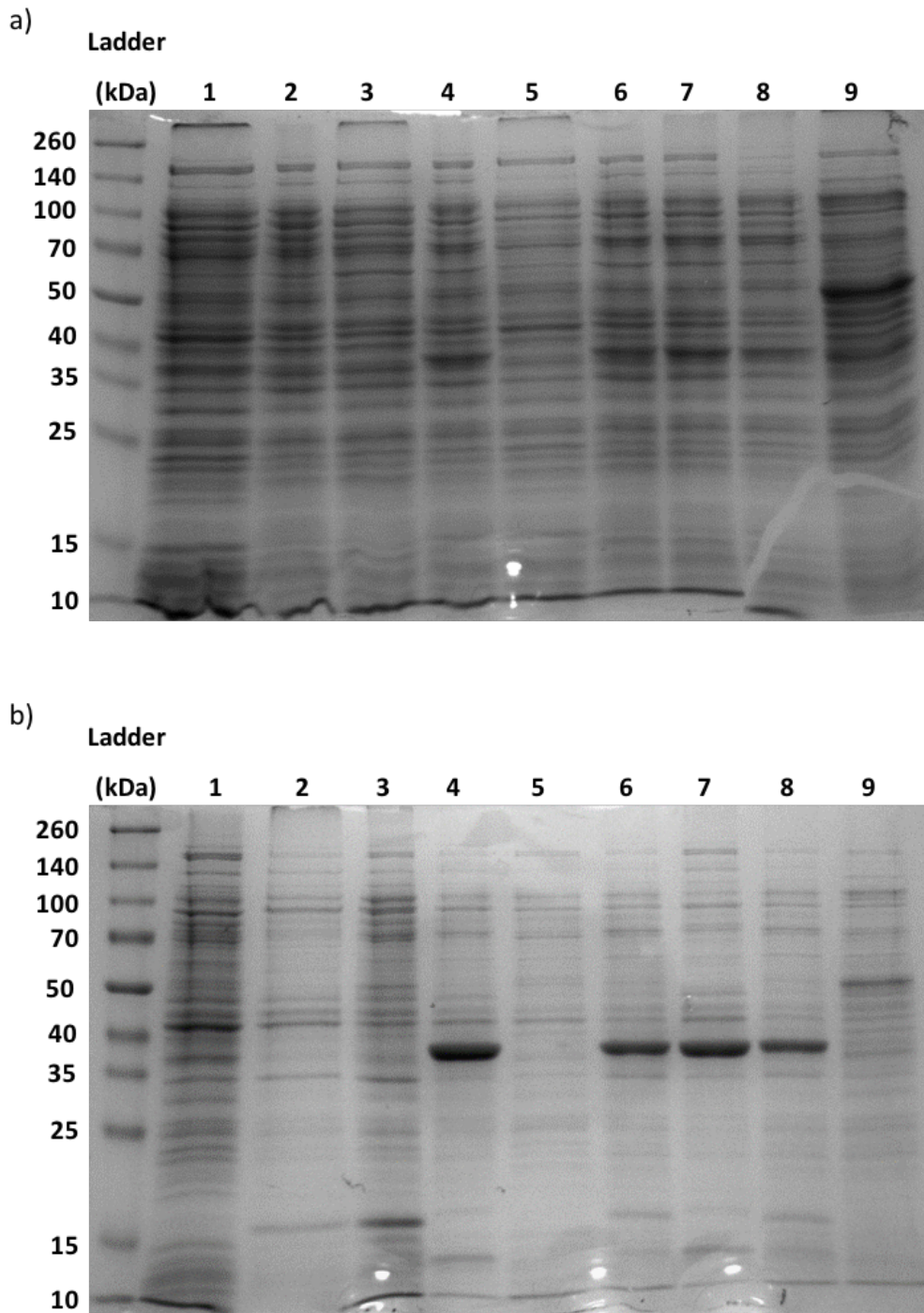
Figure 4.3. TADH expression time course in LB media with different concentrations of IPTG at the point of induction compared to auto-induction TB media : a) soluble protein fractions, b) insoluble protein fractions.

E. coli BL21(DE3) pLysS pASZ2 was grown in LB / TB supplemented with carbenicillin. Protein expression was induced in LB at OD_{600} of 0.6-0.7 by the addition of sterile IPTG (0.4 mM or 1 mM final concentration). The cultures were incubated for the specified time at 30 ^{o}C, and 1 mL samples were harvested by centrifugation. Samples were lysed using Bugbuster lysis reagent and the protein content analysed by SDS-PAGE. a) soluble fractions. **1**: 0 h in LB, **2**: 5 h in LB, no IPTG, **3**: 5 h in LB after induction with 0.4 mM IPTG, **4**: 5 h in LB after induction with 1 mM IPTG, **5**: 7 h expression in Auto induction TB media, **6**: 20 h in LB, no IPTG, **7**: 20 h in LB after induction with 0.4 mM IPTG, **8**: 20 h in LB after induction with 1 mM IPTG, **9**: 23 h expression in Auto induction TB media.

The expression studies presented here suggested the following optimal conditions for expression: cell growth and expression at 30 ^{o}C, in LB medium supplemented with 1 % (w / v) glucose to repress basal expression,[169] and induction with IPTG at 0.4 mM final concentration, when the cells reached an OD$_{600}$ of 0.6 - 0.7. Further investigations showed no difference in protein concentration or enzymatic activity when a freshly transformed colony was used, compared to a 25 % cryostock, and both these methods were used for expression in the following work.

4.1.4 Purification of TADH

The first published work with TADH suggested a heat step purification at 80 ^{o}C for 15 min, whilst in a subsequent publication, the heat step was at 75 ^{o}C for 20 min, followed by anion exchange chromatography (AEX). This was found to increase the purity and specific activity of TADH. The most recent paper, published during the course of this work and describing the TADH crystal structure, reports purification by heat treatment at 80 ^{o}C for 20 min, followed by size exclusion chromatography. Therefore, the effect of the purification on the specific activity and on the purity of TADH was investigated. The purity was evaluated by visual inspection of the SDS-PAGE, whilst the specific activity was determined in the oxidative direction at 60 ^{o}C, using 1-butanol as the substrate.

Initial attempts to purify TADH were performed following the best conditions reported at the time of study, which were by heating the soluble cell extract at 75 ^{o}C for 20 min, followed by centrifugation of the precipitated proteins. SDS-PAGE analysis of the soluble fraction after centrifugation showed a high degree of purity, with removal of most proteins from the soluble cell extract, except for the desired heat-stable TADH (Figure 4.4a, lanes 1-2). A good specific activity (1.3 U / mg) was determined for the heat-purified (75 ^{o}C 20 min) TADH , although this was lower than the reported 4.7 U / mg (80 ^{o}C, 15 min).[108] Following the literature report, a subsequent AEX chromatography step was performed after heating, using a HiTrap Q Sepharose High Performance column, resulting in further purification, as confirmed by an increased specific activity to 1.6 U / mg, and by fainter protein impurity bands observed by SDS-PAGE (Figure 4.4a, lane 3). However, this increase in specific activity (25 %) was lower

than the reported one, which increased by 33 % after AEX treatment using a Sepabeads® EB-QA405 column, (from 15.0 to 20.6 U / mg reported for substrate cyclohexanol). This was most probably due to heat loss during the enzymatic activity assay: when a sealed heating block was used during the assay, an increased specific activity to 6.0 U / mg was obtained for 1-butanol.
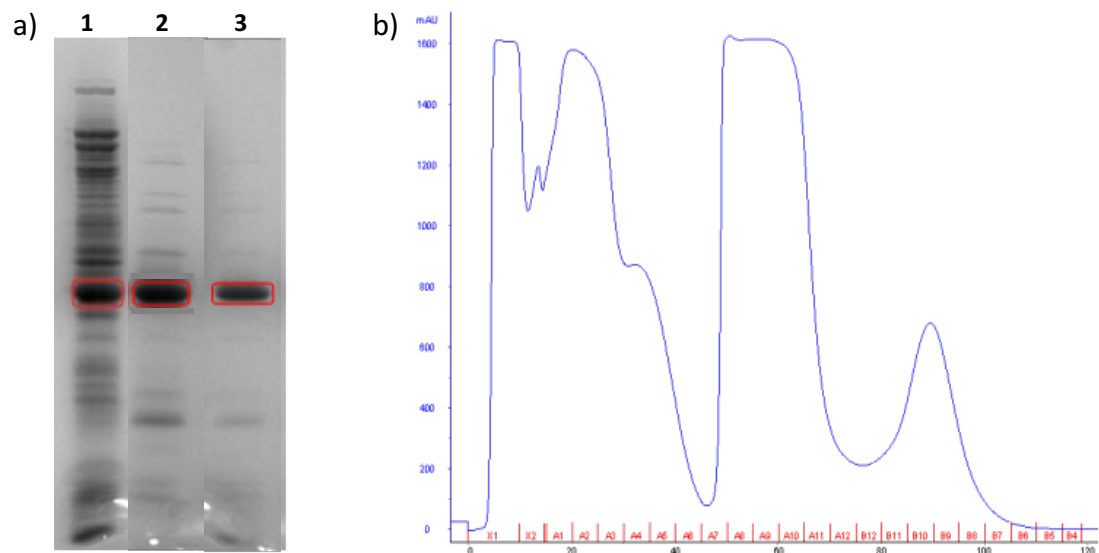
Figure 4.4. Purification of TADH by heat treatment and ion exchange. a) SDS-PAGE analysis of TADH purification. **1**: soluble cell extract, obtained after cell lysis and centrifugation of cell debris, **2**: soluble cell extract after heating at 75 ^{o}C for 20 min and centrifugation of the insoluble proteins, **3**: combined fractions after AEX purification; b) AEX chromatogram displaying the UV trace at 280 nm in blue.

Different temperatures and heating times were evaluated for the heat purification step, due to the variations in the reported methods for heat purification and to the lower than expected specific activities obtained during initial purification attempts. It was observed that variations in both the temperature and the time of heating resulted in different specific activities. Hollmann and co-workers reported an increase in specific activity when the purification temperature increased, perhaps due to increased folding and formation of the quaternary structure. This phenomenon has previously been observed with thermostable proteins expressed in *E. coli*. Similar results were observed in this study (Table 4.3) and the optimal heat purification conditions were selected as 80 ^{o}C for 20 min. When the enzyme was expressed in TB auto-induction medium, the specific activity was lower than after LB expression, thus confirming the choice of this expression system as the optimal one.

After the heat treatment at 80 °C for 20 min, two different chromatography steps were compared, to assess whether TADH specific activity could be increased: anion exchange (AEX) and size exclusion chromatography (SEC).

Table 4.3. Effect of temperature and time of heating on the specific activity of TADH.

Entry	Temperature (°C)	Time (min)	Specific activity (U / mg)[a]
1	75	15	1.2 ± 0.10
2	75	20	1.3 ± 0.21
3	80	20	2.2 ± 0.16
4[b]	80	20	1.6 ± 0.10

[a] TADH was expressed in LB medium, following induction with 0.4 mM IPTG. Specific activity was determined in the oxidative direction at 60 °C, using 1-butanol (100 mM) as a substrate, NAD^+ (1 mM) as cofactor, in 50 mM Glycine-NaOH buffer pH 9.0. [b] TADH was expressed in overnight express autoinduction medium. Where error bars are specified, specific activities were determined in triplicate, by purifying and analysing three different batches from the same cell pellet.

Only a slight increase in activity was observed when an additional chromatography step was applied (Table 4.4) although both chromatograms showed the removal of impurities absorbing at 280 nm, with the SEC purified sample displaying the highest purity. Unexpectedly, the largest peak obtained during SEC purification was not representative of active TADH and did not show any presence of proteins when assessed by Bradford assay, despite its high absorbance at 280 nm.

Table 4.4. Specific activity of TADH purified by different methods.

Entry	Purification conditions	Specific activity (U / mg)
1	80 °C for 20 min	2.1
2	80 °C for 20 min & AEX	2.3
3	80 °C for 20 min & SEC	2.2

Fractions 18-19 highlighted in Figure 4.5 showed faint protein bands of similar size to TADH when analysed by SDS-PAGE, but exhibited no activity.
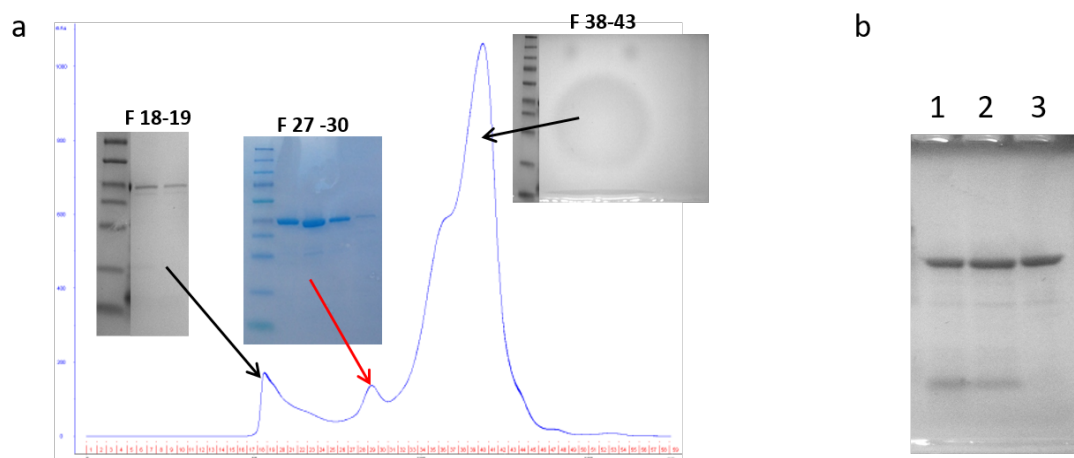
Figure 4.5. Comparison of TADH chromatography purification methods. a) Chromatogram of TADH purification by size exclusion chromatography. The chromatogram shows the UV trace at 280 nm, alongside the SDS-PAGE analysis of the collected fractions; b) SDS-PAGE comparison of TADH samples obtained by three different purification methods: **1**: heat; **2**: heat & AEX; **3**: heat & SEC.

4.1.5 Determination of TADH zinc content

The zinc content of purified TADH was analysed by inductively coupled plasma mass spectrometry (ICP-MS) and then compared to protein concentration determined by Bradford assay, to calculate the ratio of TADH to zinc. TADH is a homotetrameric structure, with each monomer containing two zinc ions: the catalytic zinc(II) found in the active site, and the structural zinc(II). Thus, the expected TADH : zinc ratio is 1 : 2.

Analysis of the heat-purified TADH resulted in a lower than expected Zn content, with a slightly higher Zn ratio observed after the heat step at a higher temperature for a longer time. This confirms that the higher purification temperature might promote better folding of the protein during purification. Further AEX purification did not increase the Zn : protein ratio, but SEC purification resulted in an increased Zn content, and suggested SEC as the optimal purification method (Table 4.5). Nonetheless, purification by SEC was not performed throughout the thesis, because the results above were obtained after initial TADH engineering experiments were performed. For much of the following studies in Section 4.3, only heat purification was used, which yielded high purity. The different purification methods used will be highlighted throughout.

Table 4.5. Zinc content of TADH purified by different methods.

Entry	Purification conditions	TADH : Zinc ratio[a]
1	75 °C for 15 min	1.0 : 0.5 - 0.7
2	80 °C for 20 min	1.0 : 0.9 - 1.2
3	80 °C for 20 min & AEX	1.0 : 1.2
4	80 °C for 20 min & SEC	1.0 : 1.5 - 2.1

[a] Expected TADH : Zinc ratio = 1.0 : 2.0; where ranges are observed zinc content analysis was performed on different batches of TADH purified under the same conditions.

The differences in Zn content depending on the purification method were assumed to be due to zinc-devoid inactive protein, which was removed throughout purification. From SDS-PAGE analysis, which showed high purity of all samples, it seemed that the majority of this inactive protein was inactive TADH, perhaps due to misfolding of this thermostable protein expressed in a mesophilic organism. The ranges of Zn contents observed for samples purified in similar manner are the result of Zn content analysis of various enzyme batches.

4.1.6 Determination of TADH kinetic parameters at steady state

Kinetic parameters of TADH were determined according to methods published in the literature, using cyclohexanol and cyclohexanone as substrates. Specific activities determined for cyclohexanol and cyclohexanone were 9.9 ± 0.2 and 15.9 ± 0.4 U / mg, compared to previously reported (20.6 U / mg for cyclohexanol after AEX purification). The differences might come from slight changes in the enzymatic assay setup. Steady state kinetic parameters also differed slightly from the reported values, highlighting the difficulty to reproduce TADH as characterised in the literature (Table 4.6). For cyclohexanone reduction, the low solubility of the substrate hindered the collection of a complete set of data to accurately determine V_{max}.

Table 4.6. Kinetic constants observed for cyclohexanol and cyclohexanone as compared to the reported constants found in the literature.

	Kinetic constants	Reported Value[109]	Achieved Value
Oxidation[a]	V_{max} (U / mg)	20.78 ± 0.55	16.0 ± 0.37
	K_M (mM)	2.09 ± 0.26	1.5 ± 0.11
Reduction[b]	V_{max} (U / mg)	15.14 ± 0.2	7.3 ± 0.11
	K_M (mM)	3.68 ± 0.26	8.2 ± 0.37

[a] Oxidation was performed at 60 ^{o}C, using TADH (3 μg), cyclohexanol (0.5, 1, 1.5, 2, 3, 5, 7.5 and 10 mM) as substrate, NAD$^+$ (1 mM) as cofactor, in 50 mM Glycine-NaOH buffer pH 9.0; Michaelis-Menten plot is presented in **Appendix 3**. [b] Reduction was performed at 60 ^{o}C, using TADH (1 μg), cyclohexanone (1, 2.5, 7.5 15, 25 and 50 mM) as substrate, NADH (0.1 mM) as cofactor, in 50 mM Bis-Tris buffer pH 6.0; Michaelis-Menten plot is presented in **Appendix 4**.

4.1.7 Conclusions

Some issues were observed with reproducing the TADH preparation as reported in the literature. This included reproduction of the high degree cell growth and subsequent protein expression observed in the literature with a final OD_{600} of 9 whereas a final OD_{600} between 3 and 5 where generally achieved in the work reported here. Initially, heat loss during the activity assays was observed to be an issue with reproduction of the reported specific activities (e.g. for 1-butanol 2.2 U /mg compared to the literature 4.7 U / mg). However, when this was resolved the specific activities were similar (6.0 U /mg) to those reported in the literature for the heat-treated samples. Further purification by chromatography methods however did not reproduce the increased activity observed in the literature, with only minor increases in activity observed. SDS-PAGE analysis did show the removal of impurities. Finally, a lower than expected zinc content was observed to be an issue depending on the purification method. The literature however does not report quantitative metal analysis for comparison it is assumed at two zinc ions per monomer of TADH.

Nonetheless, an efficient method for the expression, purification and characterization of TADH was developed, involving *E. coli* growth at 30 ^{o}C, induction with 0.4 mM IPTG

at 30 $^{\circ}$C, heat purification at 80 $^{\circ}$C for 20 min, followed by size exclusion chromatography. The resulting TADH showed specific activity of 6.0 U / mg towards 1-butanol and 11.8 U / mg towards cyclohexanol, steady state kinetic parameters similar to the ones reported in the literature, and a Zn content which was lower than the expected 1 : 2 ratio (protein : Zn). This was probably due to unfolded inactive TADH.

4.2 Genetic engineering of the active site of TADH for promiscuity towards imine reduction

4.2.1 Introduction and highlights

From a chemical point of view, reduction of ketones and of imines is similar, and is effected by similar catalysts. However, ADHs have no cross-reactivity towards imines, whilst IREDs do not reduce ketones. The aim of this section is to gain understanding of the specificity of ADHs / IREDs towards ketones / imines, respectively. In particular, to understand why there is no cross-reactivity, and to assess whether cross-reactivity can be introduced by genetic engineering of the active site.

The main features of the TADH reductive mechanism, which follows the mechanism of all medium-chain (Zn-dependent) ADHs, involve carbonyl activation by the catalytic Zn(II) acting as Lewis acid, to promote hydride transfer from the NAD(P)H cofactor, situated within 4-5 Å from one another (Figure 4.6). This is followed by protonation of the nascent hydroxyl by Ser40 (TADH numbering), *via* a proton relay system. Metal-devoid short-chain reductases activate the substrate *via* an acidic active site residue (Brønsted acid), which generally employ a tyrosine as part of a hydrogen bond network tetrad with serine-lysine-asparagine. Similar to short-chain reductases, IREDs activate imines by an aspartate or a tyrosine side-chain situated within a short distance (5-8 Å) from the C4 of NADPH (Figure 4.6).

Whilst the inability of IREDs to reduce ketones was systematically tested, the lack of activity of ADHs for imine reduction was less explored. Kroutil's group showed some activity ADHs towards oximes, but reduction occurred at the nitrogen, rather than at the carbon atom, and the resulting aldimine spontaneously hydrolysed.[170]

Several hypotheses were made to explain the specificity of ADHs / IREDs for their respective substrates. In the case of IREDs, the acidic Asp / Tyr residue might not be strong enough to activate the ketone. Indeed, the pKa of this acidic residue in short-chain ADHs is modulated by involvement in a tetrad, which enables the proton relay, whilst IREDs do not generally possess this hydrogen network. In the case of Zn-dependent ADHs, one hypothesis for lack of imine reduction activity was the inhibition by the imine substrate or by the amine product, as a result of strong binding between

the nitrogen-containing functionality and the catalytic zinc. Additionally, depending on the extra substituent bound to the nitrogen atom, the imines might not fit in the substrate-binding pocket or have the correct orientation within the active site for proton transfer. In particular, the cyclic imines that are generally used to avoid substrate hydrolysis in water might not fit in the same position as their linear ketone counterparts.
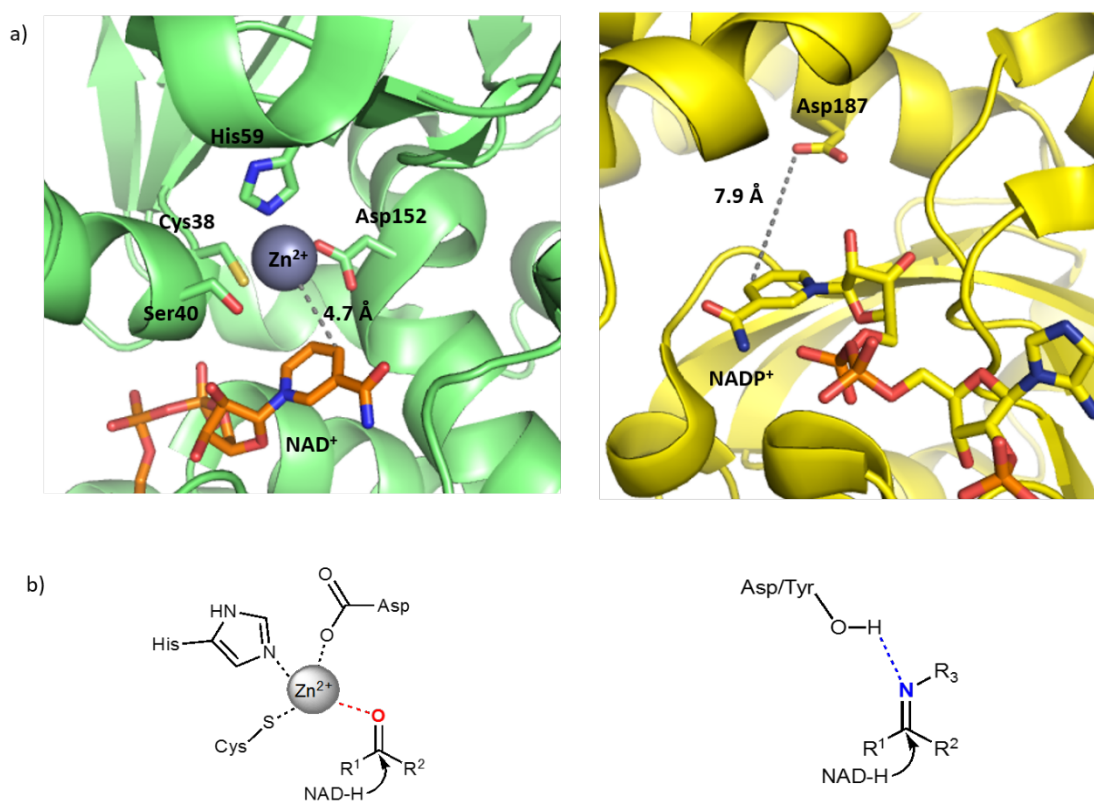
Figure 4.6. Comparison of the active sites of ADH and IRED. a) Left: active site of TADH (PDB 4CPD), highlighting the Zn^{2+}-binding amino acids; right: active site of IRED Q1EQE0 (PDB 3ZH8), highlighting the acidic catalytic residue Asp187; b) Left: ketone activation *via* catalytic zinc ion within the TADH active site; right: imine activation *via* H-bonding within the IRED active site.

The aim of this thesis was to design catalytic promiscuity, by extending the substrate specificity of ADHs from ketones to imines. To do this, an important issue explored in this section was whether imines could bind into the hydrophobic substrate pocket in the correct orientation for hydride transfer. Activity assays with relevant ketones, inhibition assays and docking studies were used to gain understanding of the interaction of imines with ADHs. Following an active site structural comparison of TADH with IREDs, several mutations were designed to introduce acidic residues in the TADH active site, in an attempt to reproduce IRED catalytic features.

Highlights

- TADH was demonstrated to maintain activity towards 2-pentanone and 2-ethylbenzaldehyde, albeit this was much reduced compared to cyclohexanone. These carbonyl substrates were similar in size to the corresponding precursors of cyclic imines, thus suggesting that imine substrates could also fit into the TADH binding pocket.

- TADH activity was inhibited by the presence of imines and amines. Inhibition kinetics showed that 2-methyl-1-pyrroline (a common imine substrate) and its reduced amine product acted as mixed inhibitors of TADH.

- Docking of imines in the presence and in the absence of cofactor and of ketone substrate suggested that both the substrate-binding pocket and the cofactor-binding pocket could accommodate imines and amines.

- TADH mutants devoid of catalytic zinc and possessing a protic residue in proximity of the docked imine nitrogen were designed and produced, but they lacked imine reduction activity.

4.2.2 TADH activity with bulky aldehydes / ketones

Two cyclic imines and their reduced amine products were chosen as possible substrates for TADH, as they were shown to be stable under aqueous conditions, and were good substrates for IREDs: 2-methyl-1-pyrroline **1** and 3,4-dihydroisoquinoline **2**. TADH showed no activity in either reduction or oxidation directions when these imines and their respective amines were used as substrates.

1	**2**	**3**	**4**
2-methyl-1-pyrroline	3,4-dihydroisoquinoline	2-methylpyrrolidine	1,2,3,4-tetrahydroisoquinoline
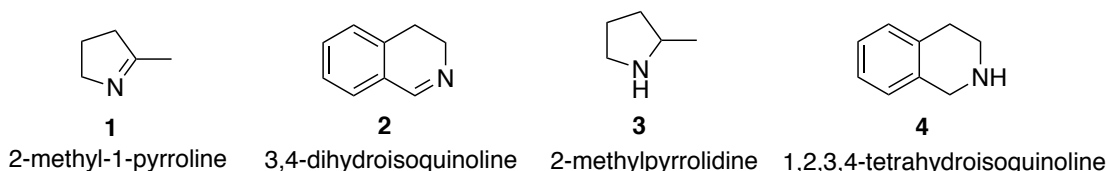
Figure 4.7. Imine and amine compounds used in this study to assess interaction with TADH.

To assess whether the lack of activity was due to the inability of these substrate architectures to fit into the catalytic pocket, investigations into the activity of TADH with a selected bulky aldehyde and ketone were performed. Selected substrates were 2-pentanone **5** and 2-ethylbenzaldehyde **6**, as well as their corresponding alcohols.

They were selected because of their similar structure to imines **1** and **2**, where the C=N bond was replaced by a C=O bond. TADH has been shown in the literature to accept a wide spectrum of substrates, including 2-pentanone and benzaldehyde;[109] yet, activity with 2-ethylbenzaldehyde **6** was not reported.

5

pentan-2-one

6

2-ethylbenzaldehyde

7

pentan-2-ol

8

(2-ethylphenyl)methanol
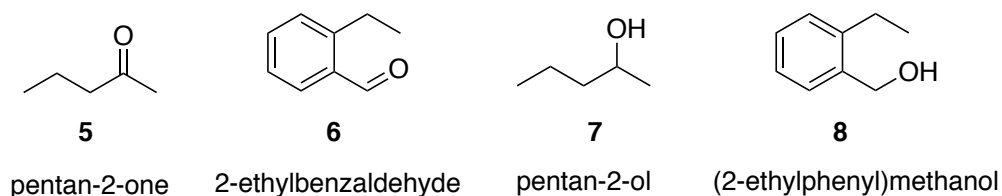
Figure 4.8. Carbonyl and alcohol compounds used in this study to assess activity with TADH.

Before activity of TADH with selected substrates could be determined, a suitable solvent had to be found, to allow substrate solubilisation. This was particularly important in the case of the bulky aldehyde **6.** The activity of TADH was assessed using a range of solvents, at the minimal concentrations necessary to solubilise both carbonyl and alcohol substrates.

4.2.2.1   Solvent effect on TADH activity

Literature reported that TADH maintained activity in a range of water-miscible and water-immiscible solvents up to 10 % (v / v) and 50 % (v / v), respectively.[109] In this study, the effect of acetonitrile (ACN), dimethylformamide (DMF) and dimethyl sulfoxide (DMSO) on TADH activity was investigated at different concentrations.

Initial assays were performed using 1-butanol as the standard substrate in the oxidative direction, using 10 % v / v solvent, to ensure solubilisation of the substrates in subsequent assays. DMSO was observed to maintain the highest percentage of TADH activity, which was 47 % compared to no solvent addition, whilst ACN and DMF inhibited the activity, to approximately 35 % and 39 % residual activity, respectively (Figure 4.9 and Table 4.7, entries 1-4). This is in contrast with reported results showing higher inhibitory effects, with residual activities of 10 % for DMF and 20 % for DMSO at 10 % v / v, obtained for the oxidation of cyclohexanol.[109] When the substrate was changed for cyclohexanol, using 5 % ACN, the relative specific activity was 86 % (Table 4.7, entry 6).
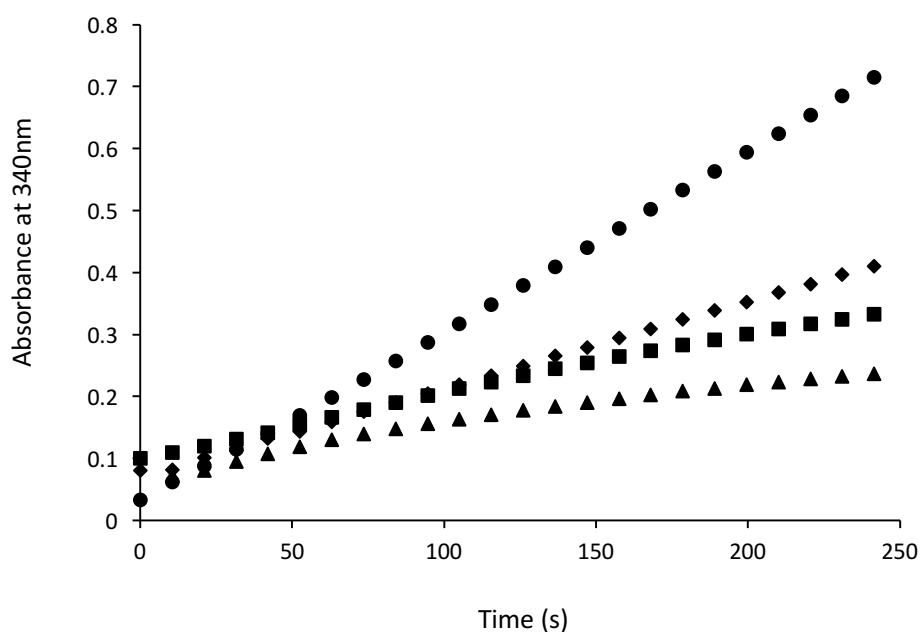
Figure 4.9. Effect of selected solvents on the 1-butanol oxidation by TADH. Enzymatic activity was determined in the oxidative direction at 60 $^{\circ}$C, using 1-butanol (100 mM) as substrate, NAD^{+} (1 mM) as cofactor, in 50 mM Glycine-NAOH buffer pH 9 containing the following solvents: (●) 10 % v / v dH$_2$O, (▲) 10 % v / v ACN, (■) 10 % v / v DMF, (♦) 10 % v / v DMSO. The reported absorbances are averages of triplicate assays, and error bars (approx. 10 % error, less than 2 % error for 10 % v / v dH$_2$O) were omitted for clarity.

Table 4.7. Specific activities of TADH in the presence of water-miscible solvents.

Entry	Substrate	Solvent	Solvent (% v / v)	Specific activity (U / mg)[a]	Relative specific activity (%)[b]
1	1-butanol	H$_2$O	10	6.06 ± 0.10	100
2	1-butanol	ACN	10	2.14 ± 0.21	35
3	1-butanol	DMF	10	2.34 ± 0.26	39
4	1-butanol	DMSO	10	2.87 ± 0.29	47
5	Cyclohexanol	H$_2$O	5	9.88 ± 0.20	100
6	Cyclohexanol	ACN	5	8.46 ± 0.73	86

[a] Specific activities were determined from the slope of the activity plot in Figure 4.9 calculated in the first 250 seconds; [b] Relative Specific activities were calculated by comparison to entries 1 and 5, where dH$_2$O was added instead of organic solvent.

In the reductive direction, ACN was illustrated to have the least effect on TADH activity, with 58 % of the specific TADH activity maintained, compared to no solvent addition (Figure 4.10 and Table 4.8). DMSO and DMF had a larger inhibitory effect, with 42 % and 15 %, respectively, of remaining specific activity, even at 2 % (v / v) concentration in the mixture. This could be explained by the inhibitor behaviour reported with DMF and DMSO,[171] which can act as a substrate analogue for the carbonyls.[172,93] Further increase of ACN concentration to 5 % (v / v) resulted in 31 % residual activity. (Table 4.8, entry 5). Following these results, ACN was selected as the solvent of choice to assess activity of TADH with the selected carbonyls. Considering both substrate solubility requirements and the effects on relative activity, 5 % (v / v) ACN was used in the oxidative assays, whereas for the reductive assays a decreased 2 % (v / v) ACN was employed.
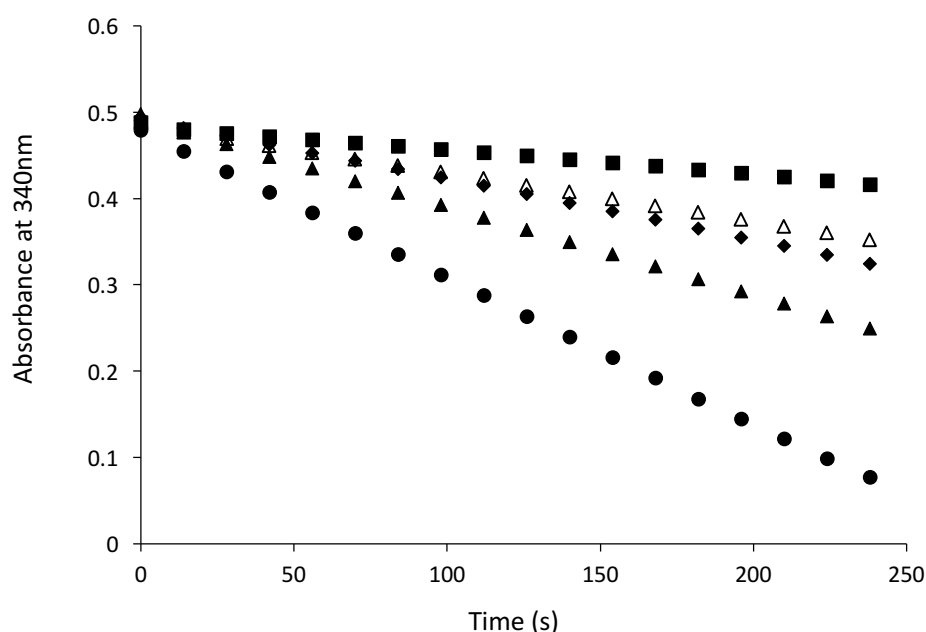
Figure 4.10. Effect of selected solvents on the cyclohexanone reduction by TADH. Enzymatic activity was determined in the reductive direction at 60 $^{\circ}$C, cyclohexanone (20 mM) as substrate, NADH (0.1 mM) as cofactor, in 50 mM Bis-Tris buffer pH 6.0 containing the following solvents: ($\bullet$) 5 % v / v dH$_2$O, ($\triangle$) 5 % v / v ACN, ($\blacktriangle$) 2 % v / v ACN, ($\blacksquare$) 2 % v / v DMF, ($\blacklozenge$) 2 % v / v DMSO. The reported absorbances are averages of triplicate assays, and error bars (less than 3 % error, 8 % error observed for 2 % v / v DMF) were omitted for clarity.

Table 4.8 - Specific activities of TADH with cyclohexanone in the presence of water-miscible solvents.

Entry	Solvent	Solvent ratio (% v / v)	Specific activity (U / mg)[a]	Relative specific activity (%)[b]
1	H_2O	5	15.9 ± 0.37	100
2	ACN	2	9.19 ± 0.21	58
3	DMF	2	2.40 ± 0.19	15
4	DMSO	2	6.59 ± 0.21	42
5	ACN	5	5.00 ± 0.10	31

[a] Specific activities were determined from the slope of the activity plot in Figure 4.10, calculated in the first 250 seconds; [b] Relative Specific activities were calculated by comparison to entry 1, where dH_2O was added instead of organic solvent.

4.2.2.2 TADH activity with substrates 5-8

The activities of TADH for the oxidation of substrates **7** and **8** was assayed using 5 % ACN which was shown to have little (>15 %) effect on the oxidation reaction, and resulted in 45 % and 1 % remaining activity, respectively, when compared to the activity obtained with cyclohexanol under the same conditions (Table 4.9, entries 1-3). Similarly, reduction of **5** and **6** yielded 5 % and 4 % relative activity compared to cyclohexanone, respectively (Table 4.9, entries 4-6). Previous literature reported relative specific activities of 85 % and 6 % for 2-pentanol oxidation and 2-pentanone reduction, respectively, but these results were obtained in the absence of added organic solvent.

The use of 2-ethylbenzaldehyde **6** has not yet been reported as a substrate for TADH, however an increase of relative specific activity was reported with benzylaldehyde (154 % compared to cyclohexanone). The explanation for the low activities might be the presence of the bulky ethyl group in the 2 position, which might sterically interfere in the active site. This effect was previously observed with 2-methylcyclohexanone (46 % residual activity) and 2-decalone (28 %). The decrease in activity with 2-pentanone and 2-pentanol was probably due to the addition of 5 % v / v ACN.

Table 4.9. Specific activities of TADH with selected bulky alcohols and the corresponding ketone / aldehyde, relative to cyclohexan –ol / -one.

Entry	Substrate	Specific activity (U / mg)[a]	Relative specific activity (%)[b]
1	cyclohexanol	11.5 ± 0.55	100
2	2-pentanol	5.13 ± 0.19	45
3	2-ethylbenzyl alcohol	0.12 ± 0.007	1
4	cyclohexanone	9.19 ± 0.21	100
5	2-pentanone	0.46 ± 0.004	5
6	2-ethylbenzaldehyde	0.35 ± 0.26	4

[a] Specific activities were determined from the slope calculated in the first 250 seconds of enzymatic activity plots: in the oxidative direction at 60 ^{o}C, substrate (100 mM), NAD^+ (1 mM) in 50 mM Gylcine-NaOH buffer pH 9.0 containing 5 % (v / v) ACN; in the reductive direction at 60 ^{o}C, substrate (20 mM), NADH (0.1 mM) in 50 mM Bis-Tris buffer pH 6.0 containing 2 % (v / v) ACN. [b] Relative Specific activities were calculated by comparison to cyclohexanol in entries 1-3 and cyclohexanone in entries 4-6, where dH_2O was added instead of solvent.

The results presented above showed that TADH could accept bulky aldehyde / ketone substrates, albeit with much reduced activity compared to cyclohexanone. Therefore, it was hypothesised that the cyclic imine substrates **1** and **2** could, in principle, fit into the TADH binding pocket and act as substrates for imine reduction.

4.2.3   Inhibition of TADH by imine and amine compounds

While the results presented above showed that structures similar to **5** and **6** could fit into the TADH binding pocket, no activity was observed in either reduction or oxidation directions when the corresponding imines (**1** and **2**) or the respective amines (**3** and **4**) were used as substrates. To further confirm whether these compounds could access the substrate-binding pocket, their inhibitory effect on the reduction of cyclohexanone and on the oxidation of cyclohexanol was investigated.

4.2.3.1 Preliminary inhibition experiments

Imines were added to cyclohexanone reduction activity assays, in equal concentrations to the substrate (20 mM). The results showed that 3,4-dihydroisoquinoline **2** completely inhibited cyclohexanone reduction, while 2-methyl-1-pyrroline **1** only slightly decreased the activity (Figure 4.11). When the concentration of **1** was increased to 50 mM, an increased inhibition was observed. This result suggested that the five-membered ring might be too small and perhaps not hydrophobic enough to strongly bind to the substrate pocket with the same affinity as the cyclohexanone substrate.
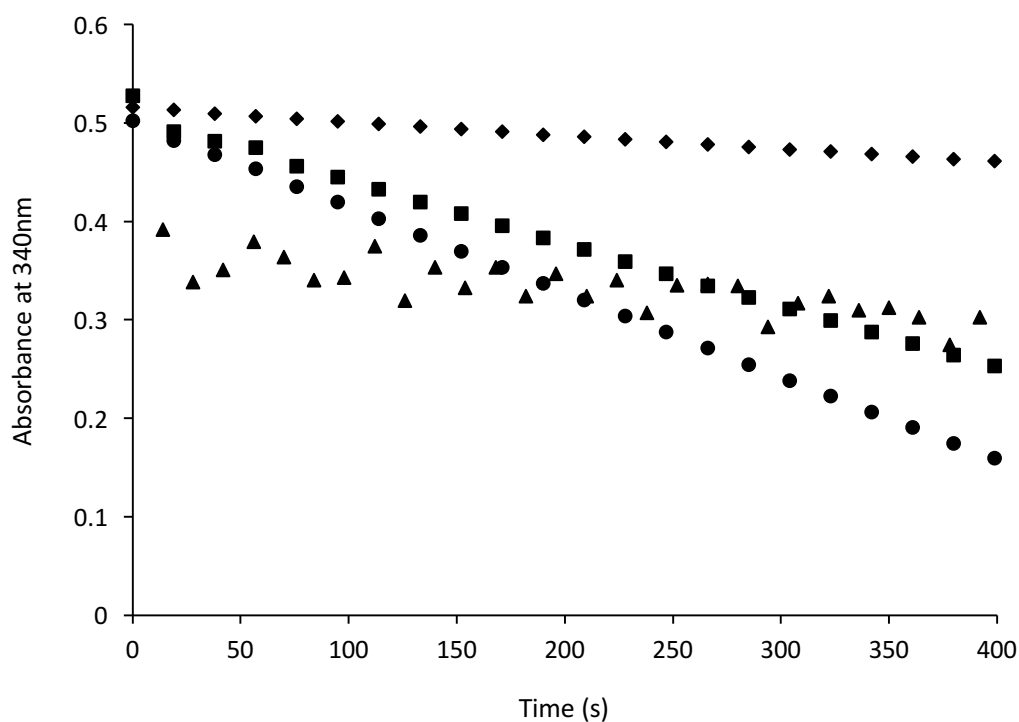
Figure 4.11. Inhibitory effect of imines 1 and 2 on cyclohexanone reduction. NADH absorbance was monitored at 340 nm in the reductive direction at 60 ^{o}C, cyclohexanone (20 mM) as substrate, NADH (0.1 mM) as cofactor, in 50mM Bis-Tris buffer pH 6.0 containing 2 % v / v ACN with: (●) control - No imine, (▲) 20 mM 3,4-dihydroisoquinoline, **2** (■) 20 mM 2-methyl-1-pyrroline, **1** (◆) 50 mM 2-methyl-1-pyrroline, **1**. The reported absorbances are averages of triplicate assays, and error bars (less than 2 % error for control and 20 mM, **1** whereas 50 mM **1** and 20 mM **2** had a higher error percentage 8 % of and 15 % error, respectively) were omitted for clarity.

On the other hand, when amines **3** and **4** were added to cyclohexanol oxidation activity assays, complete inhibition was observed with both amines (Figure 4.12). Even when the concentration of **3** was decreased to a fifth of the substrate concentration (20 mM *vs.* 100 mM), activity was not observed. This suggested that competitive

inhibition by this amine was less likely, as a very strong binding of the amine compound to the TADH active site seemed to occur.
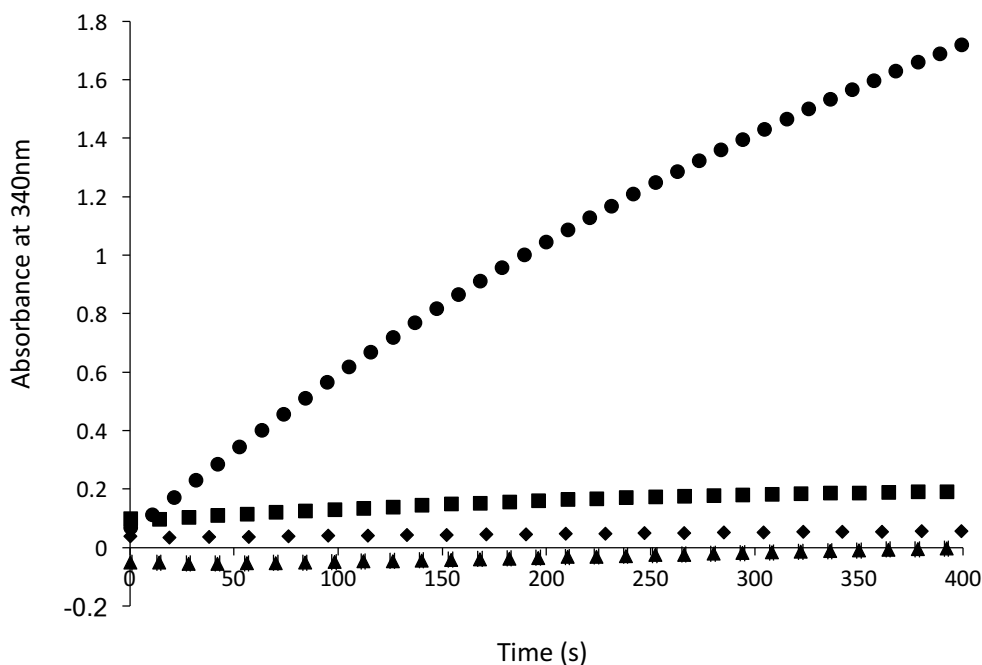
Figure 4.12. Inhibitory effect of amines 3 and 4 on cyclohexanol oxidation. NADH absorbance was monitored at 340 nm in the oxidative direction at 60 $^{\circ}$C, cyclohexanol (100 mM) as substrate, NAD$^+$ (1 mM) as cofactor, in 50 mM Glycine-NaOH buffer pH 9.0 containing 5 % v / v ACN with: (●) control - No amine, (▲) 100 mM 1,2,3,4-tetraisoquinoline, **4** (■) 100 mM 2-methylpyrrolidine, **3** (◆) 20 mM 2-methylpyrrolidine, **3**. The reported absorbances are averages of triplicate assays, and error bars (less than 2 % error) were omitted for clarity.

Overall, these results suggested that imines and their reduced amine counterparts could act as inhibitors of TADH. Imine **1** showed a dependence of the inhibition on its concentration, whilst imine **2** and both amines showed complete inhibition under the conditions tested. To gain a better understanding of the type of inhibition, kinetic studies were performed, in the presence of different concentrations of 2-methyl-1-pyrroline **1** and 2-methyl-1-pyrrolidine **3** as inhibitors. These inhibitors were chosen because the corresponding imine showed a variation in the inhibitory effect at concentrations similar to the substrate, rather than the complete inhibition observed with **2** and **4** at low concentrations.

4.2.3.2 Determination of kinetic constants of inhibition with imine and amine inhibitors

Michaelis-Menten kinetics was determined for cyclohexanone reduction in the presence of 10 mM, 25 mM and 50 mM of **1**, and the results are presented as Lineweaver-Burk plots (Figure 4.13, see Appendix 5 for Michaelis-Menten plots).
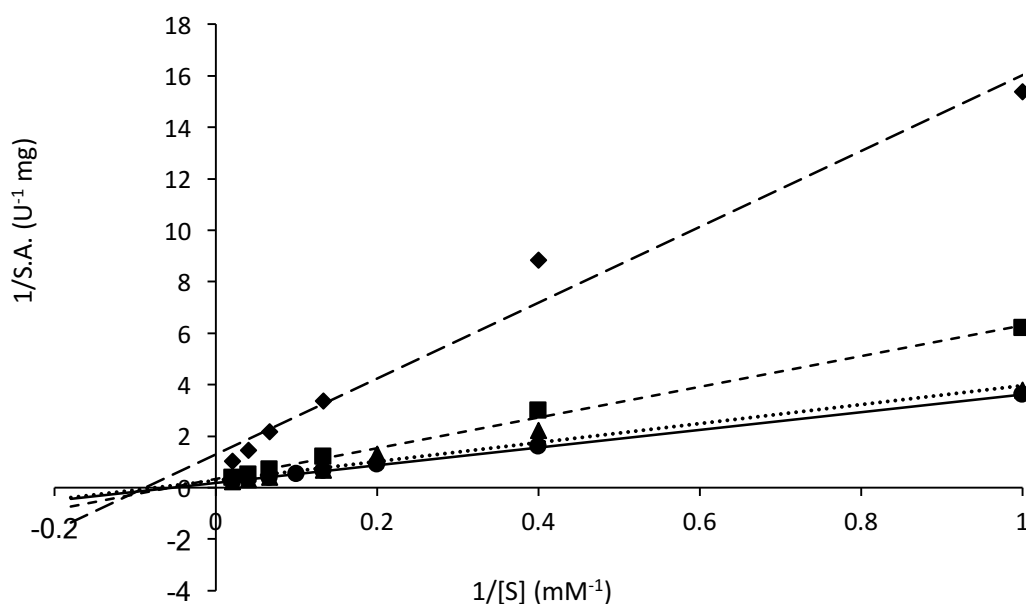
Figure 4.13. Lineweaver-Burk plot illustrating the inhibitory effect of 2-methyl-1-pyrroline (1) on cyclohexanone reduction. Specific activities were calculated from the enzymatic activities determined in the reductive direction at 60 $^{\circ}$C, using TADH (1 μg), cyclohexanone (1, 2.5, 5, 7.5, 10, 15, 25, 50 mM) as substrate, NADH (0.1 mM) as cofactor, in 50 mM Bis-Tris buffer pH 6.0 containing 2 % v / v ACN with 2-methyl-1-pyrroline, **1** as inhibitor at concentration: (●) 0 mM , (▲) 10 mM, (■) 25 mM, (◆) 50mM. The data shown represents averages of triplicate assays (error bars are presented in the Michaelis-Menten plot in **Appendix 5**.)

Enzyme activity (V_{max}) was found to decrease with increasing inhibitor concentration, whereas K_M seemed to slightly increase (Table 4.10). These results suggest a mixed inhibition, in which the inhibitor can bind to both the free enzyme and to the enzyme-substrate complex, at a site which is different from the substrate-binding site. The increase in K_M suggests that the binding of the free enzyme is preferred. The decrease in V_{max} suggests that the enzyme becomes inactive upon inhibitor binding. For example, the inhibitor might bind to the active site Zn, but without occupying the substrate-binding pocket. Binding at the place of the nicotinamide ring cannot be excluded. In the absence of structural information on inhibitor binding, these hypotheses cannot be confirmed.

Table 4.10. Kinetic constants determined for cyclohexanone in the presence of different concentrations of 2-methyl-1-pyrroline (1) as inhibitor.

Inhibitor concentration (mM)	V_{max} (U / mg)	K_M (mM)
0	6.87 ± 0.27	25.06 ± 1.57
10	6.73 ± 0.40	27.69 ± 3.37
25	4.40 ± 0.22	30.09 ± 2.90
50	1.79 ± 0.21	39.91 ± 8.24

Reduction assays were performed at 60 ^{o}C, using TADH (1 μg), cyclohexanone (1, 2.5, 7.5 15, 25 and 50 mM) as substrate, NADH (0.1 mM) as cofactor, and 2-methyl-1-pyrroline **1** as inhibitor, in 50 mM Bis-Tris buffer pH 6.0 containing 2 % v / v ACN. Michaelis-Menten plot is presented in Appendix 5.

Preliminary investigations outlined in Figure 4.11 and Figure 4.12 suggested that the amine **3** had different inhibition characteristics compared to its imine counterpart. For example, it took as little as a fifth of amine concentration compared to substrate to inhibit TADH activity, which might be the result of strong binding of the amine to the catalytic zinc, as a consequence of the more nucleophilic character of the amine nitrogen compared to the imine. To investigate this further, Michaelis-Menten kinetics was determined for cyclohexanone reduction in the presence of 1 mM, 5 mM and 10 mM of **3**, and the results are presented as Lineweaver-Burk plots (Figure 4.14, see Appendix 6 for Michaelis-Menten plots).

The analysis of the results again suggests that 2-methyl-1-pyrrolidine **3** acted as a mixed inhibitor. Enzyme activity (V_{max}) was found to decrease with increasing inhibitor concentration, whereas this time K_M seemed to slightly decrease (Table 4.11). In this case, the slight decrease in K_M suggests an increase in the apparent affinity of the enzyme for the substrate, meaning that the inhibitor favours the binding of the enzyme-substrate complex. Again, the decrease in V_{max} suggests that the enzyme becomes inactive upon inhibitor binding, and this might be due to binding of the amine to the catalytic zinc, alongside the substrate.
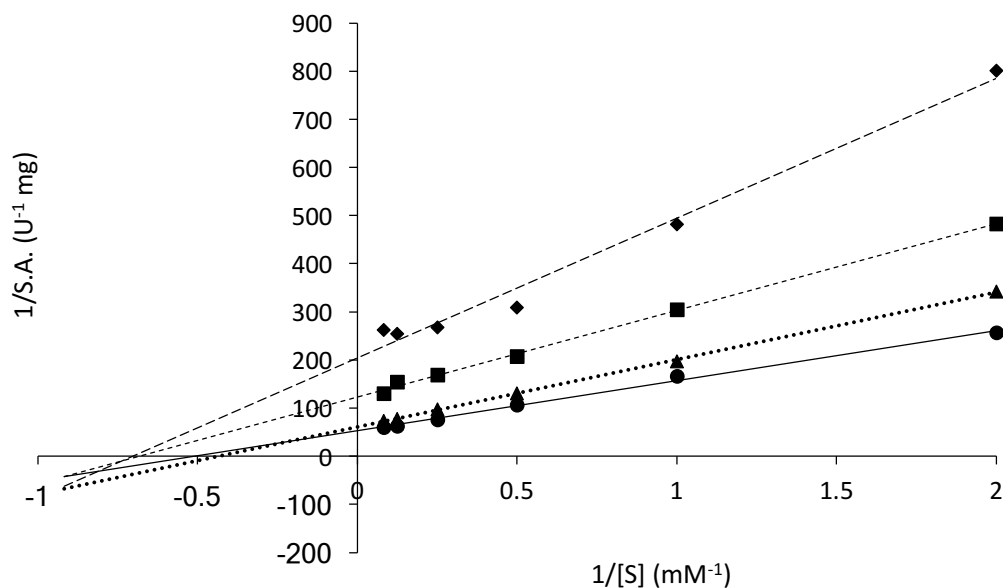
Figure 4.14. Lineweaver-Burk plot illustrating the inhibitory effect of 2-methylpyrrolidine (3) on cyclohexanol oxidation. Specific activities were calculated from the enzymatic activities determined in the oxidative direction at 60 °C, using TADH (3 μg), cyclohexanol (0.5, 1, 2, 4, 8, 12 mM) as substrate, NAD^+ (1 mM) as cofactor, in 50 mM Glycine-NaOH buffer pH 9.0 containing 5 % v / v ACN with 2-methylpyrrolidine, **3** as inhibitor at concentration: (●) 0 mM , (▲) 1 mM, (■) 5 mM, (◆) 10 mM.

The results of the inhibition studies confirmed binding of the imine and amine compounds to TADH, followed by inactivation of the enzyme.

Table 4.11. Kinetic constants determined for cyclohexanol in the presence of different concentrations of 2-methylpyrrolidine (3) as inhibitor.

Inhibitor concentration (mM)	V_{max} (U / mg)	K_M (mM)
0	6.60 ± 0.10	2.16 ± 0.10
1	5.45 ± 0.05	2.27 ± 0.05
5	2.73 ± 0.24	1.50 ± 0.46
10	1.74 ± 0.12	1.47 ± 0.35

Oxidation assays were performed at 60 °C, using TADH (3 μg) cyclohexanol (0.5, 1, 2, 4, 8, 12 mM) as substrate, NAD^+ (1 mM) as cofactor, and 2-methyl-1-pyrrolidine **3** as inhibitor, in 50 mM Glycine-NaOH buffer pH 9.0 containing 5 % ACN; Michaelis-Menten plot is presented in Appendix 6.

They also suggested that inhibitor binding to TADH occurs at a different site from the substrate (mixed inhibition was observed). Although binding of the inhibitors to the

catalytic Zn(II) seems plausible, the inhibition mechanism cannot be determined at this stage. To gain further insight into the interaction of imines and amines with the active site of TADH, and in the absence of structural information of inhibitors bound to the enzyme, docking studies were performed starting from the published TADH crystal structure.

4.2.4 Docking of imines into the TADH catalytic site

Small organic molecules can be easily docked into enzyme hydrophobic pockets using Autodock Vina.[156] During this docking method, the protein scaffold is maintained rigid, whilst rotatable bonds can be defined within the small organic molecule using the Autodock Vina software. This methodology gives a good indication whether an organic compound can fit into a particular binding pocket, and can also provide an insight into which orientation of the ligand would provide better binding.

The crystal structure of TADH (PDB 4CPD), containing the NADH cofactor, was used for the docking. First, to assess whether the docking methodology developed here was suitable, the 1-phenylacetone substrate was docked inside the protein scaffold, following the parameters previously outlined by Man *et al*.[163] Figure 4.15 shows a very similar substrate orientation was obtained, thus confirming that the docking procedure used here was suitable for further application to other organic compounds.
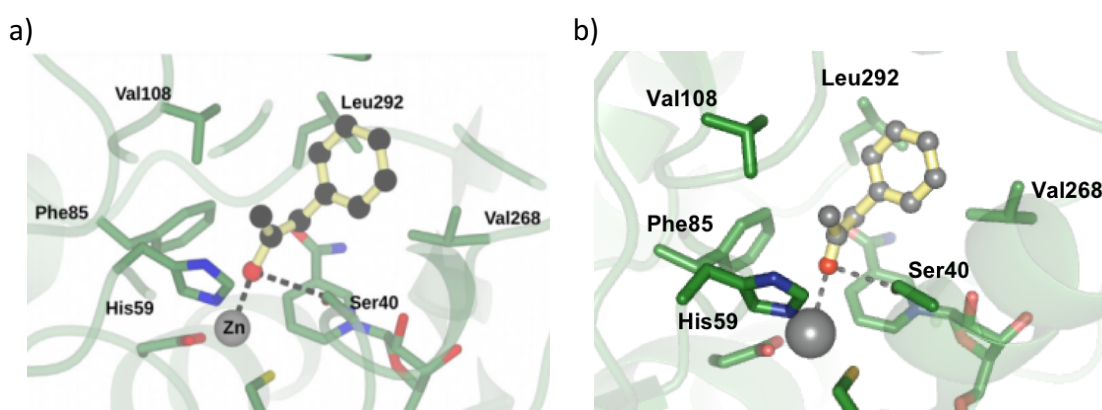
Figure 4.15. Model of 1-phenylacetone docked within the TADH active site using Autodock Vina. 1-Phenylacetone represented in ball and stick format (carbon atoms shown in grey and bonds yellow); distances of the carbonyl oxygen to the catalytic zinc ion and serine 40 residue are highlighted with dashed lines (grey, illustrating distances of 2.8 Å and 2.9 Å respectively); a) Model taken from Man *et al*.;[163] b) Reproduction of model a) within this study.

Using a similar procedure, imines **1** and **2** were successfully docked into the hydrophobic substrate pocket of TADH with the bound cofactor (Figure 4.16). The best poses (lowest binding energies) were obtained when the imines occupied the substrate-binding pocket, in similar orientations to the ketone substrate (Figure 4.15). The unsaturated carbon atom was positioned within an approximate 4.0-4.5 Å distance from the nicotinamide C4, and within 3 Å distance from the Ser40 hydroxyl group (Figure 4.16) and these distances were almost identical to those observed for 2-phenylacetone (Figure 4.15) which were 4.3 and 2.9 Å, respectively. These results were intriguing, given that inhibition studies suggested binding of the inhibitor at a site which is different from the substrate. Further docking studies were performed, where the substrate-binding pocket was occupied with the previously docked 1-phenylacetone. Whilst these docking studies cannot be used to analyse any complex equilibria taking place in the advent of reversible inhibition, they do suggest plausible binding orientations of the inhibitor in the active site.
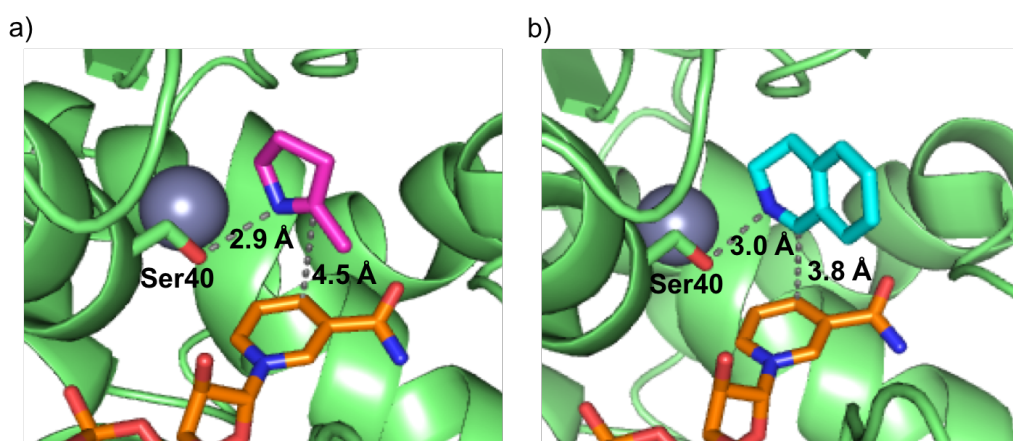
Figure 4.16. TADH (PDB 4CPD) active site with model imine substrates 2-methyl-1-pyrroline (1) and 3,4-dihydroisoquinoline (2) docked using Autodock vina. Distances to Ser40 and C4 of NADH (orange sticks) shown via dashed lines (grey) a) 2-methyl-1-pyrroline (pink sticks) b) 3,4-dihydroisoquinoline (cyan sticks).

Docking in the presence of the model ketone showed the lowest energy imine binding orientations to occur at different positions in the substrate-binding pocket (Figure 4.17). This seemed plausible, due to the large hydrophobic pocket present in TADH. In these conformations, interaction of the imine with zinc was not observed.
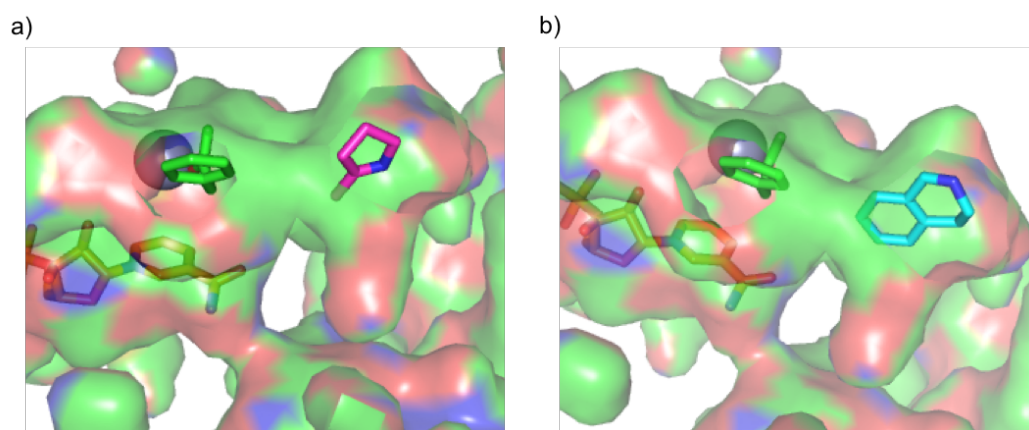
Figure 4.17. TADH (PDB 4CPD) active site (surface) with model imine inhibitors 2-methyl-1-pyrroline (1) and 3,4-dihydroisoquinoline (3) docked in the presence of substrate 1-phenylacetone (green sticks). a) 2-methyl-1-pyrroline (pink sticks); b) 3,4-dihydroisoquinoline (cyan sticks). Cofactor shown in orange sticks and catalytic zinc ion as a grey sphere.

These results can be used to provide an explanation for the experimental results observed previously: binding of the imines at a secondary hydrophobic binding site, which might prevent the reaction from occurring.

A third docking was performed, where imines **1** and **2** were docked in the TADH structure, from which the NADH cofactor was manually removed. Binding at the cofactor binding-site would explain the decreased activity observed during the inhibition studies, and could also influence substrate binding, thus explaining the variation in K_M. Imine **1** docked outside the nicotinamide-binding pocket within a 5.0 Å radius and the correct orientation towards the catalytic zinc, thus suggesting that interference with cofactor binding does not occur. On the other hand, imine **2** occupied the nicotinamide space, therefore suggesting that interference with cofactor binding is a plausible route for inhibition in this case (Figure 4.18).

The combined results from docking and inhibition studies suggested that the binding of imines and amines was possible in the proximity of the substrate-binding site. However, the activation mechanism that gives activity with ketones and alcohols is not suitable for the activation of imines and amines. "Poisoning" of the catalytic zinc by imine / amine binding could not be overruled. Thus, a different substrate activation must be envisaged, if imines are to act as TADH substrates. Inspired by the recently published IRED catalytic mechanism, it was decided to engineer the TADH catalytic site and to replace the Zn activation by an activation based on an acidic residue.
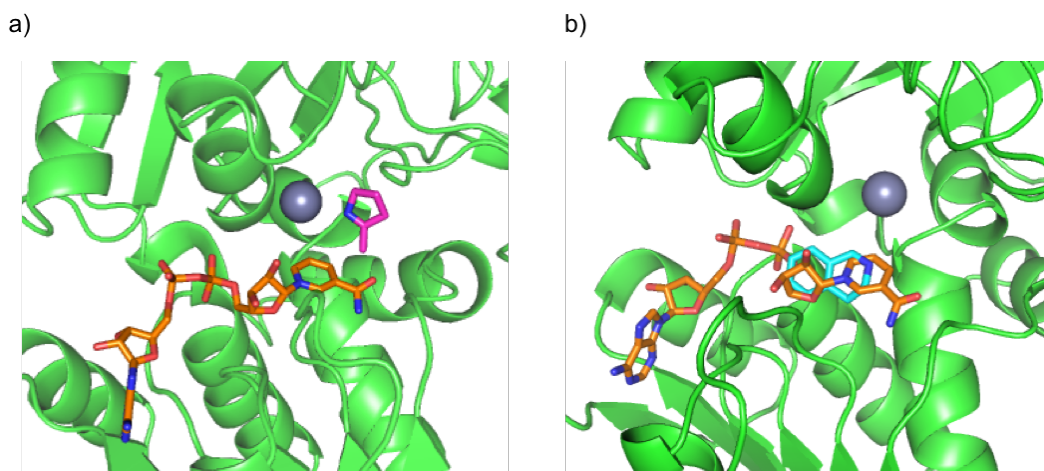
Figure 4.18. TADH (PDB 4CPD) active site with model imine inhibitors 2-methyl-1-pyrroline (1) and 3,4-dihydroisoquinoline (3) docked in the absence of NADH cofactor. a) 2-methyl-1-pyrroline (pink sticks) b) 3,4-dihydroisoquinoline (cyan sticks). The superimposed cofactor structure is shown in orange sticks.

4.2.5 Design of an IRED activation mechanism within TADH

Inspection of recently published *(R)*- and the *(S)*-IRED crystal structures showed that the distance between the hydride delivery site, *i.e.* the C4 of the nicotinamide ring and the H-bond donor functionality of the enzyme (Asp or Tyr oxygen atom) was 5-8 Å (Figure 4.19) In TADH, the distance between the C4 of NADH and the activating Zn atom in TADH is 4.7 Å, while between the C4 and the Ser40 oxygen atom, responsible for the proton relay, is 4.6 Å. It was hypothesised that proton donor residues (Brønsted acids) could be introduced as "activators" at the place of the Zn Lewis acid in TADH, provided they would be in a range suitable for activation of the carbon-heteroatom bond. In order to attempt reproduction of the IRED activation mechanism in TADH, residues that were at a suitable distance from the C4 hydride delivery point in TADH were identified, and suitable mutations were designed, to introduce H-bond donor residues at these positions.

In order to compare their arrangement around the hydride delivery site, the TADH and IRED crystal structures were aligned based on the cofactors, using the ligand-based active site alignment tool in PyMol, LigAlign.[173] This tool allowed the alignment of the bound cofactors, treated as rigid ligands, and comparison of the interactions in the two active sites, such as the position of the substrate-activating functionality and of the substrate-binding pocket, relative to the bound cofactor.
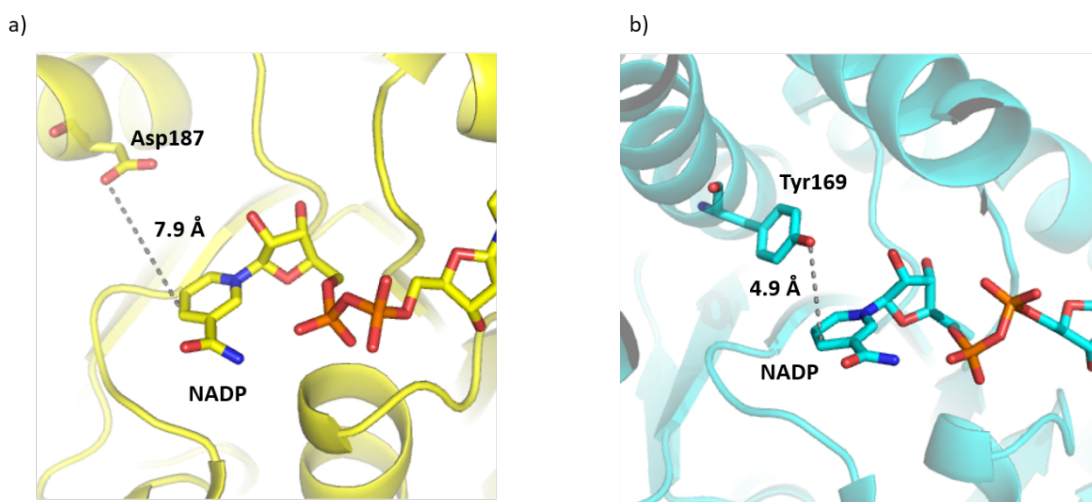
Figure 4.19. Active sites of (*R*)- and (*S*)-IRED crystal structures. The distance between the substrate activation site (protic residue) and the hydride delivery site, C4 of NADPH, is highlighted (grey dashed line). a) *(R)*-selective Q2EQE0 from *Streptomyces kanamyceticus* (PDB 3ZHB, yellow cartoon); b) *(S)*-selective IRED from *Streptomyces* sp. GF3546 strain (PDB 4OQY, cyan cartoon).

The two *(S)*-selective IREDs for which crystal structures were available at the time of this work (PDB 4OQY and PDB 4D3F) gave very similar results, thus only one is presented here.
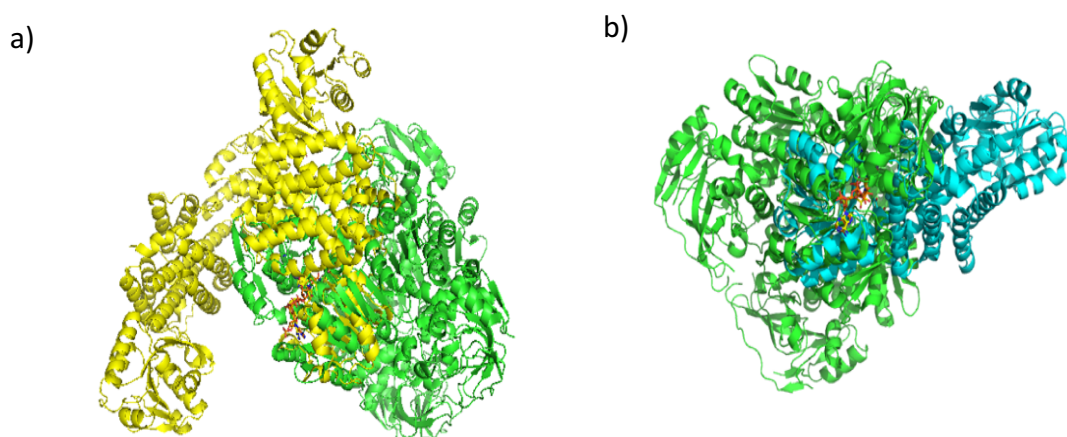
Figure 4.20. Superimposed crystal structures of IRED and TADH using LigAlign. TADH (PDB 4CPD) is shown as green cartoon. a) *(R)*-selective IRED Q2EQE0 (yellow cartoon, PDB 3ZHB); b) *(S)*-selective IRED from *Streptomyces* GF3546 (cyan cartoon, PDB 4OQY).

Inspection of the superimposed structures (Figure 4.20) showed little resemblance between the quaternary arrangements of the two enzymes. This outcome was expected, due to the small sequence identity (<20 %) showed by the alignment of the respective sequences. Upon closer inspection of the NADH / NADPH alignment, whilst the majority of the co-factor ligands align, the opposite face of the nicotinamide ring

is presented in the IRED active site, i.e. the pro-*S* hydride is offered to the imine whereas in TADH the pro-*R* is offered to the ketone (Figure 4.21). As a result of this when aligned, the substrate pockets are presented opposite one another, making it difficult to compare a position within TADH for introduction of a protic residue similar to that found in IREDs.
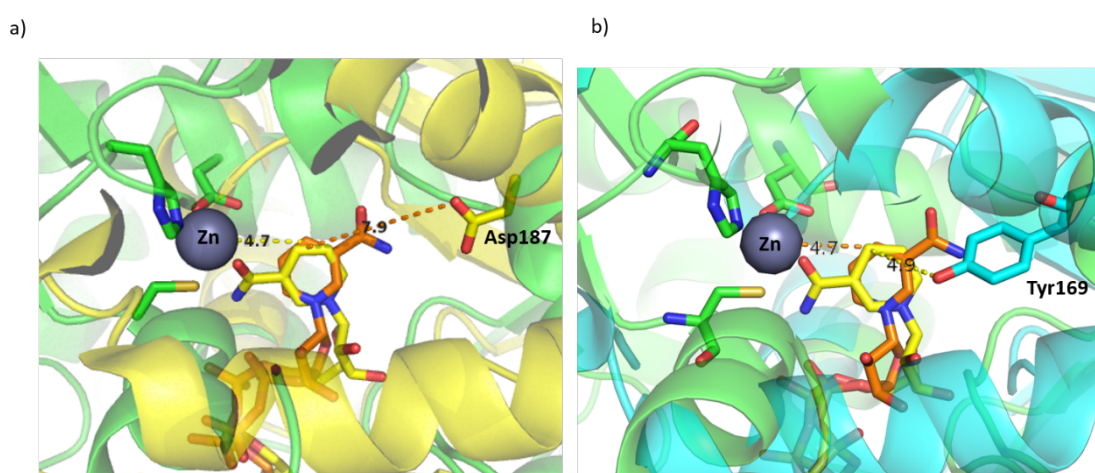
Figure 4.21. Close view of the active sites of TADH (green cartoon), superimposed with (*R*)- and (*S*)-IREDs using LigAlign. The distance (Å) between the substrate-activating functionality (Zn ion or protic residue) and the hydride delivery site (C4 of NAD(P)H) is highlighted for both TADH and IRED. The Zn ion is represented as grey sphere, and the TADH-bound NADH is represented as orange sticks. a) *(R)*-selective IRED Q2EQE0 (yellow cartoon, PDB 3ZHB), with the distance shown between Asp187 (yellow sticks) and the C4 of NADPH (yellow sticks); b) *(S)*-selective IRED from *Streptomyces* GF3546 (cyan cartoon, PDB 4OQY), with the distance shown between Tyr169 (cyan sticks) and the C4 of NADPH (yellow sticks).

Sixteen residues within a radius of 8 Å from the C4 of the TADH-bound NADH cofactor were highlighted: Cys38, Ser40, His59, Phe85, His86, Asp152, Ile153, Ser155, Thr156, Val180, Val266, Gly267, Val268, Leu292, Ala293 and Val295 (Figure 4.22) Out of these, certain residues (Ile153, Ser155, Thr156, Val180, Val266, Gly267, Ala293 and Val295) were present on the opposite side of NADH from the substrate, and therefore not available for interaction during catalysis. Further visual inspection showed that Leu292 was in close proximity to the amide functional group of NADH, and could therefore interfere with cofactor binding. In His86, the distance from the NADH C4 to the N-H available for hydrogen binding was 9.4 Å, and was considered too far from interaction. Therefore, these positions were considered not suitable for introducing substrate activating functionalities.
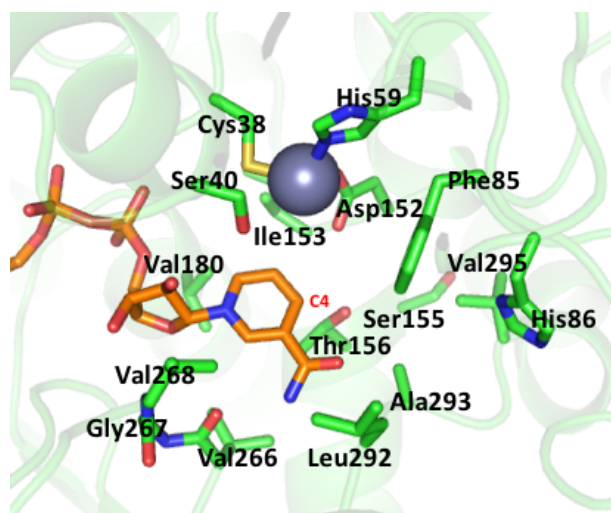
Figure 4.22. TADH active site highlighting the residues (green sticks) within 8.0 Å of the C4 position of NADH (orange sticks).

Six possible sites remained available for mutagenesis: Cys38, Ser40, His59, Phe85, Asp152 and Val268 (Figure 4.23a). In addition, a seventh residue, Val108, was identified by Man *et al.* to be involved in the formation of the immediate cavity around the substrate.[163] Although 0.6 Å further away from the C4 NADH than the selected 8.0 Å range, model docking with 1-phenylacetone displays the distance between the substrate and point of activation as 5.3 Å. Thus, this residue was also selected (Figure 4.23b). In addition to this, the furthest residue of the seven selected was Val268 identified at 6.5 Å from the model substrate and the shortest distance was observed with Ser40 at 2.9 Å highlighted in Figure 4.23b). The remaining residues all resided within a 5.0 Å distance.

The amino acids highlighted above were selected for mutagenesis to both tyrosine (pKa 10.5) and aspartic acid (pKa 3.9), which are the two main functionalities responsible for substrate activation in IREDs. Before creating the desired mutant library, the catalytic zinc ion had to be completely removed, in order to avoid its interference with the imine substrate, resulting in inhibition of the reaction. All three amino acids from the zinc binding site were present in the above selection for mutagenesis into a proton donor, and their mutation was likely to result in less affinity for zinc. However, to ensure complete zinc removal, the three binding residues were separately mutated to alanine, which was previously shown to prevent zinc binding in ADH.
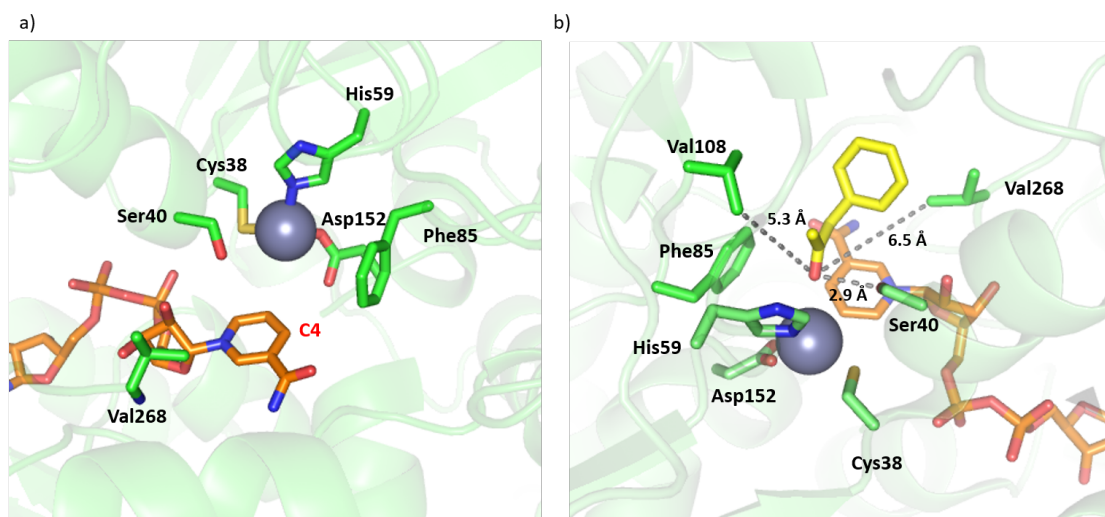
Figure 4.23. TADH active site highlighting residues (green sticks) selected for mutagenesis studies. Catalytic zinc ion represented with a grey sphere and NADH with orange sticks; a) Six remaining residues highlighted as possible candidates for mutagenesis. b) Model substrate, 1-Phenylacetone (yellow sticks) docked into TADH active site using Autodock Vina. The distances of the closest and farthest away of the six residues to the oxygen of the ketone is highlighted with grey dashed lines. A seventh residue, Val108 has also been highlighted for mutagenesis with the distance to the ketone illustrated by a grey dashed line.

TADH with the selected imines **1** and **2** modelled in the zinc free active site is illustrated in Figure 4.24. The removal of catalytic zinc also ensures the imine substrates have access to the zinc binding residues once mutated, as these are promising candidates for introduction of protic residues due to their positions within the active site.
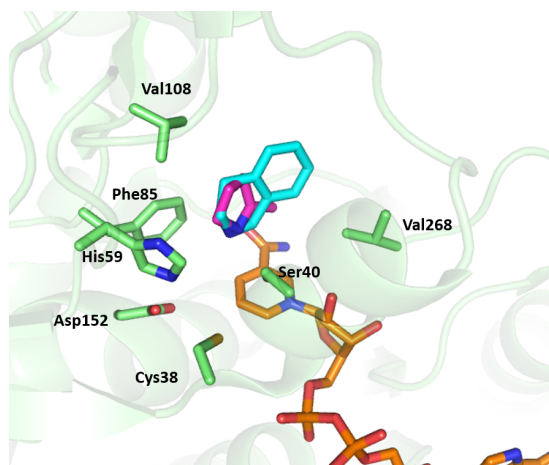
Figure 4.24. Model of TADH 'zinc free' active with 2-methyl-1-pyrroline (pink sticks) and 3,4-dihydroisoquinoline (cyan sticks) docked using Autodock vina. The selected residues to undergo mutagenesis are represented with green sticks and NADH in orange sticks.

4.2.6 Active site engineering of TADH

4.2.6.1 Mutagenesis of the metal-binding amino acids

The three single mutants of TADH (C38A, H59A and D152A) were created by site-directed mutagenesis. They were expressed and purified from 250 mL expression

cultures using the previously developed procedure for the preparation of wild-type (WT) TADH. The presence of zinc in the active site was investigated by enzymatic activity assays using 1-butanol as the substrate. Given the catalytic role of the zinc in substrate activation, it was hypothesised that any loss in activity could be correlated to a loss in catalytic zinc ion.

SDS-PAGE and protein concentration analyses of the heat-purified TADH mutants from soluble cell extract showed that the zinc-devoid mutants were expressed in lower yields than the wild-type TADH (Figure 4.25 and Table 4.12). This result may be due to less protein being folded as soluble protein in the absence of zinc.
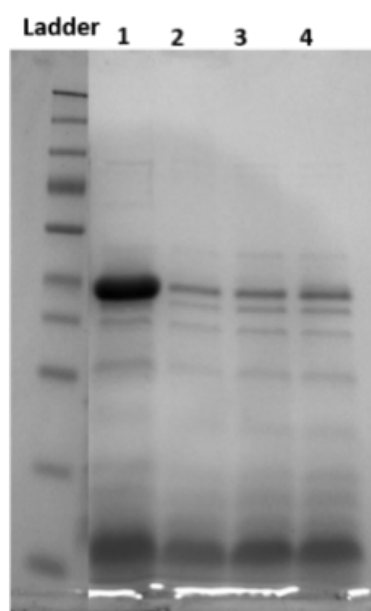
Figure 4.25. SDS-PAGE of heat-purified TADH and single mutants. 1: WT TADH; 2: C38A, 3: H59A, 4: D152A.

The specific activity of all alanine mutants decreased from 4.6 U / mg in WT TADH to ~0.06 U / mg (<1 %), supporting the fact that the catalytic zinc was no longer bound (Table 4.12). The C38A mutant was selected for further single point mutagenesis for introduction of the desired protic residue Asp / Tyr. This was due to the slightly higher expression concentrations compared to the other two mutants.

Table 4.12 - Enzyme content and activity following expression of TADH WT and mutants.[a]

Entry	TADH Sample	Protein Content (mg)	Specific activity (U / mg)	Relative Specific Activity (%)
1	WT	5.95	4.64	100
2	D152A	2.38	0.06	1
3	H59A	2.31	0.06	1
4	C38A	2.75	0.05	1

[a] WT and mutant TADH was expressed in 250 mL cultures in LB medium, following induction with 0.4 mM IPTG, as described in Section 3.1. The protein was purified by heating at 80 ^{o}C for 20 min. Protein content of the soluble fraction was determined by Bradford assay, after heat-purification and centrifugation. Specific activity was determined in the oxidative direction at 60 ^{o}C, using 1-butanol (100 mM) as a substrate, NAD^{+} (1 mM) as cofactor, in 50 mM Glycine-NaOH buffer pH 9.0. Relative specific activity is given compared to WT TADH.

4.2.6.2 Preparation and assay of the designed mutants

The residues selected for changing to tyrosine and aspartate were Ser40, His59, Phe85, Asp152, Val108 and Val268. All corresponding variants were designed to contain the initial single mutation C38A for zinc removal. Given that aspartic acid is already present at position 152, this resulted in 11 double mutants and one single mutant as TADH variants. To introduce both tyrosine and aspartic acid at position 38, two double mutants were created from the single mutated D152A protein. The 13 new mutants were created by site-directed mutagenesis. They were expressed and purified alongside the three single mutants C38A, H59A and D152A, from 50 mL expression cultures using the previously developed procedure for the preparation of wild-type (WT) TADH. As previously observed for the single mutants, all mutants containing the acidic residues were expressed in yields that were 25-75 % lower compared to the wild-type.

The expression levels were considered sufficient for the purpose of this investigation, and were not optimised further.
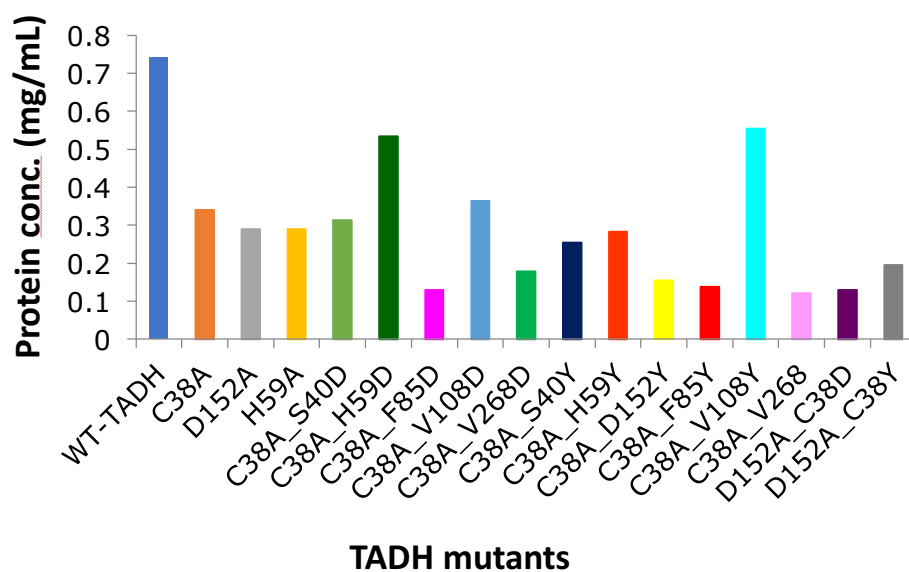
Figure 4.26. Expression yields of mutant and wild-type TADH presented as protein concentration (mg/mL) in lysis buffer 8 mL.

Each of the 16 mutants were investigated for IRED activity in the reduction and oxidation directions using 2-methyl-1-pyrroline **1** and 3,4-dihydroisoquinoline **2**, and their corresponding amines as substrates. No activity was observed for any of the mutants. Their activity was also assayed using cyclohexanone, but again unsuccessfully, the mutations resulted in a loss of native activity. The presence of a hydrogen donor at the place of zinc in the active site was not sufficient to promote catalysis. This might be due to inappropriate positioning of the H-donor residue for the H-bond to form, or to a non-suitable pKa of the H-donor, necessary to activate the substrate.

Furthermore, it is extremely difficult to predict the orientation of the mutated amino acids within the active site, and how or if this orientation will affect the structure and activity of the enzyme, despite visual or predictive aids. Investigations into the pKa and ionisation of the key residues are required, before a definitive suggestion as to why these mutants lack imine reductase activity can be put forward. Since a complete lack of activity was observed in all mutants, no further effort was invested in this approach.

4.2.7 Conclusions

A robust method was developed, which allowed TADH activity assay with bulky insoluble substrates, in the presence of acetonitrile as water-miscible co-solvent. The presence of the acetonitrile reduced TADH activity to 30-60 % of the initial activity, depending on the reaction and on the co-solvent concentration. In order to assess the ability of TADH to accept the common 5-membered or 6-membered cyclic imine architecture into the substrate-binding pocket, the activity of TADH was determined with two carbonyl substrates, 2-pentanone and 2-ethylbenzaldehyde, and with their corresponding reduced alcohols. These substrates were chosen because their structures were similar to the ones of common cyclic imine substrates used with IREDs. TADH showed activity with both these substrate architectures, albeit a greatly reduced activity was observed with 2-ethylbenzaldehyde (4 % remaining activity compared to cyclohexanone), and less than half remaining activity with 2-pentanol (compared to cyclohexanol). Nonetheless, these results demonstrated that architectures similar to the cyclic imine substrates could fit into the active site.

Two cyclic imines and their reduced amine counterparts were tested as inhibitors of TADH in the reductive and oxidative directions, respectively. TADH activity was completely inhibited by both 3,4-dihydroisoquinoline **2** and its corresponding amine **4**, when used in the same concentration as the substrate. Inhibition kinetics were determined with the 5-membered imine **1** and the reduced amine **3,** and showed that both these compounds behaved as mixed inhibitors of TADH. This result suggested that imine and amine inhibitors occupy a different location from the substrate-binding site, but their binding prevents the reaction to occur. For example, as illustrated with the docking studies they might bind at the place of NADH, and / or bind elsewhere in the substrate pocket. The amine compound was shown to have inhibitory effect at lower concentrations compared to the imine, thus suggesting a possible interaction with the catalytic zinc.

The combined inhibition and docking results suggested that imines could in principle be accepted into the TADH active site, but that possible binding elsewhere in the active site might prevent their turnover.

Mutations in the active site were designed to remove the catalytic zinc, and to introduce protic residues aspartate or tyrosine in the proximity of the carbon-nitrogen bond. A total of 14 TADH variants were created with these features, in which Zn was removed by mutation of zinc-binding Cys38 to alanine. Removal of zinc was confirmed by lack of activity towards alcohol oxidation. The TADH variants containing Asp or Tyr at positions 38, 40, 59, 85, 108, 152 and 268 were successfully expressed and purified. No activity was observed for either imine reduction or amine oxidation. Despite the mechanistic similarity of ketone and imine reduction and structural resemblance of the carbonyl and imine bond, it seems the differences in their chemical properties dictate their reactivity. For example, the reduction potential of an imine is less negative than that of a carbonyl group and thus imines have a higher tendency towards reduction. This in conjugation with the relative pKa values of imines (~24) and ketones (~20) and their reduced counterparts amines (~35) and alcohols (~17) may explain, alongside the high basicity of the nitrogen within imines / amines, why IREDs use Brønsted rather than Lewis acid activation. Another point to note, is that while imines and ketones can react in a similar fashion, for example, under nucleophilic attack the conditions under which they react differ. Imines usually require a stronger nucleophile or more forceful conditions due to the differences in electronegativity of oxygen and nitrogen, the double bond in imines is less polarised and thus less electrophilic. Considering this along with the results present within, it was hypothesised that the active site of TADH was not suited for the redesign of catalytic promiscuity by site-directed genetic engineering. An alternative approach was to take advantage of the existing metal-binding site, by using it as a way to introduce a non-native metal centre, more suited to the reduction of imines.

4.3 Replacement of the catalytic zinc with rhodium in TADH

4.3.1 Introduction and highlights

In addition to the recent discoveries of natural IREDs, efforts also yielded the creation of artificial metalloenzymes capable of imine reduction *via* the incorporation of non-native, chemical complexes within protein scaffolds.[174,175] This approach relied on building *artificial* metal binding sites, by using a linker to connect the metal-binding ligand to the protein (see Section *1.3.2.3*). The flexibility of the linker-ligand construct resulted in less control over the exact positioning of the metal. An alternative approach consists in the direct metal incorporation within *native* binding sites, in which amino acids form the first coordination sphere of the metal and ensure its precise localisation.[176] This method generally exploits the catalytic properties of an existing metalloenzyme, such as its substrate-binding site, and changes its reactivity by introducing non-native metals at the place of existing catalytic metal ions. Using this method, Kazlauskas and co-workers prepared rhodium(I)-containing carbonic anhydrases for the hydrogenation of olefins and hydroformylation of styrene and reduction of CO_2.[149,177] An artificial metalloenzyme for imine reduction has yet to be created *via* this approach and our attempts are investigated in this section.

In the previous section, TADH was shown to accept imines in the active site, and it was hypothesised that their inhibitory effect was due to binding to the catalytic zinc. However, replacement of the zinc (Lewis acid) with a Brønsted acid failed to produce an IRED. The aim within this chapter is to replace the catalytic zinc ion in TADH with a metal ion known to activate imines when part of synthetic catalysts, and to investigate its effect on the activity. Literature precedents exist, where dihydropyridine derivatives were used to reduce imines. The starting point of the work presented here was a report showing hydride transfer from a Hantzsch ester to an imine substrate, activated by a rhodium catalyst (Figure 4.27).[47]
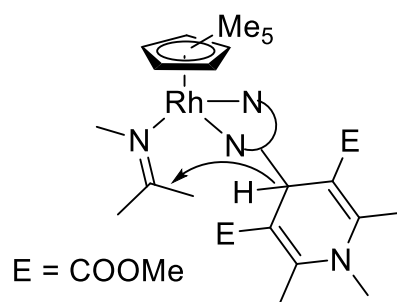
Figure 4.27. Imine reduction by a bioinspired rhodium catalyst tethered to a Hantzsch ester. The imine is activated by binding to rhodium, whilst hydride is delivered by the tethered dihydropyridine.

Previous studies reported that zinc can be replaced by other metals in ADHs (see Section *1.2.6*). Crystallographic studies of Co-, Ni- and Cd-HLADH showed that the overall protein structure and the active site tetrahedral geometry were essentially preserved. Substrate binding and hydride transfer rates were shown to be positively correlated with the Lewis acidities of the metals.[123,178] In TbADH, studies of the Co-substituted enzyme indicated an octahedral coordination of the metal, with the two additional ligands believed to be water molecules.[124] The higher coordination number was suggested to be responsible for the increased activity observed with this enzyme. Taken together, these investigations illustrate the connection between metal charge, Lewis acid strength, coordination geometry and metalloenzyme catalysis, and indicate that metals with different coordination geometries can be accommodated into the ADH binding site and can modulate its catalytic behaviour. It should be noted that none of the reconstituted ADHs mentioned above were investigated for novel reactivities. Moreover, no examples were published, where late transition metals such as Ru, Rh, Ir were introduced within ADH.

Additionally, encouraging reports were published, where rhodium(I) was used to replace zinc(II) in human carbonic anhydrase (see Section *1.3.2.2*).[149,177] Zinc(II) removal was performed by dialysis against a chelating agent, such as 2,6-pyridinedicarboxylate, and rhodium was inserted into the resulting apo enzyme by dialysis against a Rh(I) salt. Unspecific binding of rhodium to surface histidines was observed, and diminished when the histidines were mutated or chemically inactivated. This work demonstrated the exciting possibilities to introduce catalytic

promiscuity in metalloenzymes, by exchanging native with non-biological metals, which are not readily available to enzymes in nature.

This section outlines the attempts to replace the catalytic zinc ion in TADH with rhodium, in an effort to introduce imine reductase activity into TADH. Several samples of TADH were used throughout this work, which were prepared using the various purification methods described in Chapter 4.1. Initially, heat-treated (80 $^\circ$C for 20 min) samples of TADH (htTADH) were considered from SDS-PAGE to be relatively pure to perform zinc replacement and subsequent analysis. The low zinc content obtained by ICP-MS suggested that further purification was necessary, to remove any protein that might not contain zinc and thus might not be properly folded. Size exclusion chromatography was used as the purification method[163] and the resulting secTADH displayed an increased zinc occupancy confirmed by ICP-MS, despite only a small increase in specific activity compared to htTADH (Table 4.13, All work presented in sections *4.3.2* to *4.3.4* was performed with htTADH, while in sections *4.3.5* and *4.3.6*, secTADH was employed.)

Table 4.13. TADH samples used in Chapter 4.3 for metal exchange investigations.

Sample[a]	TADH : Zn molar ratio[b]
htTADH	1.0 : 0.5 - 0.9
secTADH	1.0 : 1.5 - 2.1

[a] htTADH was purified by heat treatment only (80 $^\circ$C for 20 min), secTADH was purified by heat treatment and size exclusion chromatography; [b] The ranges of TADH : Zn molar ratio are given based on the results of different ICP-MS analyses of different samples. The expected TADH : Zn molar ratio is 1.0 : 2.0. TADH samples were expressed and purified as described in Chapter 4.1.

Despite the low zinc(II) content for htTADH these samples were subjected to preliminary zinc removal investigations. The low zinc(II) content was not an issue as the initial criteria for success was recovery of native activity, after zinc removal (loss of activity.) As the recovery of activity is only possible as a result of reinsertion of zinc(II) at the active site (responsible for catalysis). Enzymatic activity assays were employed in the analysis.

- Dialysis of TADH against a mixture of 1,10-phenanthroline (OPA, 10 mM) and EDTA (20 mM) at pH 6.0 or 6.5 and at 4 $^{\circ}$C resulted in almost complete removal of the specific activity, and a partial loss of zinc up to 50 %. These results were consistent with removal of the catalytic zinc, to create apo-TADH.

- Reinsertion of zinc into apo-TADH was successfully achieved by dialysis against a Zn-containing buffer, as demonstrated by the recovery of the specific activity and of the zinc(II) content. However, replicates yielded variable results, and a considerable amount of protein was lost.

- Successful insertion of cobalt(II) into apo-TADH yielded Co-TADH, with 82 % of the initial specific activity and with a cobalt occupancy lower than expected (65 %).

- Insertion of Rh^{+}(acac) into apo-TADH resulted in a protein containing 2.6-fold excess of Rh, probably due to unspecific binding. The protein was shown to retain activity, but it cannot be contributed solely to Rh binding as residual zinc was also inserted. No imine reduction activity could be obtained by this method.

4.3.2 *Preliminary chelator investigations*

Despite metal exchange having not previously been performed with TADH, methods were developed for metal exchange in both HLADH[1,16] and TbADH[6,9] and included removal of zinc with 1,10-phenanthroline (OPA), 2,6-pyridinedicarboxylate or dipicolinic acid (DA), ethylenediaminetetraacetic acid (EDTA) and/or mixtures of these chelators in a range of concentrations, up to 20 mM. The main method reported for metal exchange was dialysis and thus has been chosen for investigations of zinc removal and metal reinsertion in TADH, as shown in Figure 4.28.

The main challenge of this work is the presence of both a catalytic and a structural zinc in the protein structure. The removal of catalytic zinc only would result in exactly 50 % zinc loss, which was the target for apo-TADH. Given the similarities between the TbADH and TADH catalytic zinc-binding sites, it was hypothesised that complete removal of catalytic zinc in TADH was possible using similar methods to TbADH.[122,124]
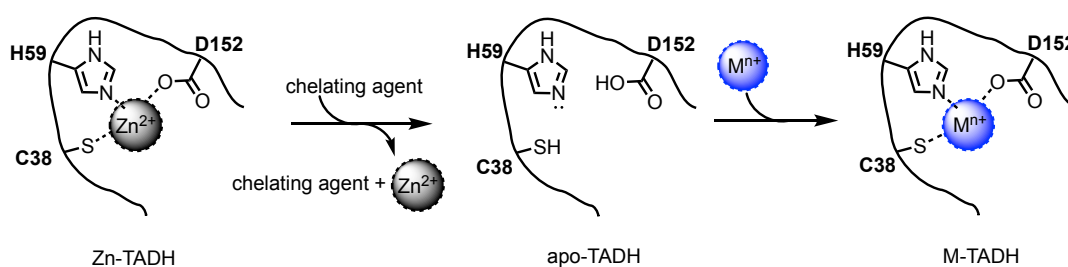
Figure 4.28. General outline of the dialysis method for zinc removal and metal re-insertion in TADH.

Additionally, a previous report showed that in the absence of structural zinc, a disulphide bond could maintain the protein structure in the ADH from the hyperthermophilic *Aeropyrum pernix*.[179] Previous studies with HLADH suggested that the catalytic zinc was fast exchanging, whilst the structural zinc was more inert.[117] The tetrahedral coordination of the structural zinc was thought to hinder the approach of the chelating ligand. On the other hand, most studies with HLADH were performed on a crystallised form of the enzyme, which was though to favour specific removal of the catalytic zinc.[117,120]

In the case of the TADH studies reported here, a crystallised form of the enzyme was not available, and all studies were performed in solution. Therefore, the hypothesis was that successful removal of all catalytic zinc would result in complete loss of catalytic activity, and a loss of ≥50 % of the initial amount of zinc.

The three chelating agents identified from the literature were investigated at concentrations 5 mM and 15 mM for the removal of zinc and creation of apo-TADH. The removal was performed in mini dialysis tubes (800 µL), using a concentrated sample of TADH (6.5 mg / ml; 175 µM), which was dialysed against 50 mM sodium acetate buffer at pH 5.5, containing the chosen chelator in the chosen concentration, as described in the experimental section. After three rounds of dialysis, the sample was purified from excess chelators by dialysis against 20 mM MES buffer at pH 6.5. Removal of zinc was assayed by determining the specific enzymatic activity in the oxidative direction with 1-butanol as substrate. Additionally, the protein : zinc molar ratio was estimated from protein concentration (determined by the Bradford assay) and zinc concentration (determined by ICP-MS).

To assess the ability of apo-TADH to re-form a metal-containing active site, zinc was added to apo-TADH by dialysis against Zn^{2+}-containing MES buffer (20 mM, pH 6.5, containing 20 μM Zn^{2+}), to reconstitute Zn-TADH. After removal of excess zinc, the specific activity and the zinc content of the resulting protein were assayed as described above. A control experiment was performed, to assess the stability of TADH under prolonged dialysis, including the effect of the dialysis in the absence of the chelators on zinc removal. The control showed 22 % loss in protein concentration, 0 % loss in Zn content and 14 % loss in activity, compared to the non-dialysed sample, suggesting that the impact of dialysis on TADH was not a major issue.

The analysis of the apo-TADH samples showed that four dialysis conditions resulted in relevant loss of activity (>30 %), and that the maximum activity loss was 65 %, using 15 mM DA (Table 4.14, entry 7). Treatment with 5 mM OPA decreased both activity and Zn content to ~75 %, although, intriguingly, the result was not reproduced when the OPA concentration was increased to 15 mM (Table 4.14, entries 1 and 3). Similarly, the use of 5 mM EDTA decreased both activity and Zn content to ~55 %, whilst an increase in EDTA concentration was less effective (Table 4.14, entries 9 and 11). Dialysis against 5 mM DA had no effect on the activity, however when the concentration of DA was increased to 15 mM, both specific activity and Zn content were decreased (Table 4.14, entries 5 vs. 7). It is worth noting that Zn removal was not correlated with the percentage of activity loss. For example, if only the catalytic zinc was removed, as initially hypothesised, then a 50 % loss of zinc should result in no activity, whereas 35 % activity was still observed in the case where 15 mM DA was used as chelator. Generally, the zinc content was lower than expected compared to the remaining specific activity, suggesting that perhaps some of the structural zinc was lost.

Examination of the data for zinc reinsertion, showed that activity was fully restored when 5 mM OPA and 15 mM DA were used to prepare the apo-TADH, and the Zn content also increased, equal or above the initial value (Table 4.14, entries 2 and 8). On the other hand, no activity was restored when EDTA was used as chelator, despite zinc content almost doubling for 5 mM EDTA, compared to apo-TADH (Table 4.14,

entry 10). This result suggested that loss in specific activity when EDTA was used was not related to the creation of apo-TADH but rather to a different mechanism for activity removal, such as irreversible binding of EDTA to the active site.

Table 4.14. Preliminary investigations of zinc removal and re-insertion into TADH.[a]

Entry	Chelator conditions	TADH sample	Protein conc. (%)	Specific activity (%)	Zn content (%)[b]
	Control	htTADH	5.1 mg / mL	1.3 U / mg	Protein : Zn 1 : 0.79
1	5 mM OPA	Apo-TADH	40	71	75
2	5 mM OPA	Zn-TADH	75	96	126
3	15 mM OPA	Apo-TADH	33	100	110
4	15 mM OPA	Zn-TADH	92	73	95
5	5 mM DA	Apo-TADH	95	100	116
6	5 mM DA	Zn-TADH	100	89	106
7	15 mM DA	Apo-TADH	100	35	51
8	15 mM DA	Zn-TADH	91	98	96
9	5 mM EDTA	Apo-TADH	100	55	59
10	5 mM EDTA	Zn-TADH	60	58	111
11	15 mM EDTA	Apo-TADH	73	79	73
12	15 mM EDTA	Zn-TADH	83	68	71

[a] Apo-TADH was prepared by dialysing htTADH against 50 mM sodium acetate pH 5.5 containing chelating agents; excess chelators were removed by dialysis against 20 mM MES pH 6.5. Zn-TADH was prepared by dialysing apo-TADH against 20 mM MES pH 6.5 containing 20 µM zinc acetate; excess zinc was removed by dialysis against 20 mM MES pH 6.5. All dialyses were performed at 4 °C. The control sample was htTADH dialysed against 20 mM MES pH 6.5 at 4 °C throughout the experiment (96 h). Experiments were performed in mini dialysis tubes (800 µL), using 250 mL dialysis buffer for a total of 3 samples each. Percentages are given compared to the control. Samples were analysed directly after dialysis; [b] Expected (100 %) zinc occupancy is 1.0 : 2.0 (protein : Zn molar ratio), the control had only 40 % of the expected zinc occupancy.

Protein precipitation was not observed by eye in the mini-dialysis tubes and thus the protein concentration for all of the above samples was determined on the sample as

a whole, which may have been heterogeneous, hence introducing possible error into the results. Little protein loss was observed with EDTA and DA as chelators. On the other hand, significant loss in protein concentration was observed upon OPA treatment, although encouragingly some protein was recovered upon zinc reinsertion.

These results indicated that zinc could be partially removed using 5 mM OPA and 15 mM DA as chelators. The Zn content was lower than expected compared to the remaining specific activity, suggesting that perhaps some of the structural zinc was removed. However, upon zinc reinsertion, both protein content and activity seemed to be reinstated, hence suggesting the possibility to perform a metal exchange. Optimisation of these results were necessary, before inserting a different metal into TADH.

4.3.3 Investigations into factors affecting zinc removal

Initial zinc removal studies were performed at pH 5.5, following literature examples. To optimise preliminary results, different pH, chelator concentrations and combinations, as well as temperature conditions were tested. Zinc reinsertion experiments were systematically performed with all apo-TADH samples, to determine if the enzymes could be reactivated or if loss of activity was a sign of irreversible denaturation.

4.3.3.1 Impact of pH on zinc removal

When the initial promising experiments, using OPA and DA as chelators, were repeated on a larger scale using a more diluted protein sample (1.3 mg / mL), the results obtained for Zn removal and reinsertion were not entirely reproducible (Table 4.15, entries 1-4). In particular, removal of zinc using 15 mM DA resulted in a higher specific activity, but also in significant protein loss, between 50-60 %, which was observed in the dialysis tubing within the first 3 hours. Some protein could be resolubilised upon reinsertion of zinc, but the specific activity did not increase, suggesting that the resolubilised protein was inactive. When a combination of 5 mM OPA and 15 mM DA was used, a greater loss in activity was observed compared to individual chelators (27 % remaining activity, compared to 61 and 74 % for the single chelators), whilst the remaining zinc content was similar (~50 %). However, a great

amount of precipitation was observed, which could not be recovered after zinc reinsertion (Table 4.15, entries 5-6).

It was suspected that protein precipitation was caused by the large pH difference between the initial TADH sample prepared in 20 mM Tris buffer at pH 7.5, and the zinc removal buffer 50 mM sodium acetate at pH 5.5. Therefore, zinc removal was also investigated at pH 6.5. This reduced the loss of protein content dramatically, to 10-20 % loss (Table 4.15, entries 7 and 9). Whilst little reduction in specific activity was observed under these conditions with OPA, the use of DA at pH 6.5 on the larger scale yielded encouraging results, with ~65 % activity loss and ~50 % zinc loss, similar to previous small scale experiments at pH 5.5. The zinc content could be restored upon reinsertion, although no protein resolubilisation was observed (Table 4.15 entry 10). In combination with the fact that only 70 % of activity could be restored, this result may suggest removal of some structural zinc ions, thus causing protein to precipitate beyond the point of repair with zinc insertion.

An additional experiment was performed at pH 6.0, where the concentration of OPA was increased to 10 mM in an attempt to increase the removal of activity. Encouragingly, this resulted in ~80 % loss of activity and ~50 % removal of zinc. The loss in protein under these conditions was close to 50 %, however over half of this was resolubilised at the zinc reinsertion stage (Table 4.16 entries 1-2). Based on literature precedents on Zn removal in TbADH, which showed successful removal using a combination of OPA and EDTA as chelators,[122] this combination of chelators was also assessed, both at pH 6.0 and at pH 6.5. The result was an encouraging almost complete removal of specific activity, correlated with almost halved zinc content (62 % instead of 50 %), with little protein precipitation observed at pH 6.0 (Table 4.16, entries 3-4). At pH 6.5, zinc removal between 38-58 % was observed and specific activity was almost totally removed, once again suggesting removal of catalytic zinc (Table 4.16, entries 5-6). However, large differences were obtained between replicates, suggesting the low reproducibility of these experiments. From these results, it was concluded that protein concentration during removal experiments had a non-negligible effect on the outcome of removal and reinsertion experiments.

Table 4.15. Impact of pH on zinc removal and re-insertion into TADH, using DA and OPA chelators.[a]

Entry	Chelator	TADH sample	pH of dialysis buffer	Protein conc. (%)	Specific activity (%)	Zn content (%)[b]
1	5 mM OPA	Apo-TADH	5.5	20	74	50
2	5 mM OPA	Zn-TADH	6.5	70	69	129
3	15 mM DA	Apo-TADH	5.5	47	61	59
4	15 mM DA	Zn-TADH	6.5	70	61	105
5	5 mM OPA + 15 mM DA	Apo-TADH	5.5	33	27	55
6	5 mM OPA + 15 mM DA	Zn-TADH	6.5	49	51	105
7	5 mM OPA	Apo-TADH	6.5	91	89	63
8	5 mM OPA	Zn-TADH	7.5	94	95	141
9	15 mM DA	Apo-TADH	6.5	82	34	52
10	15 mM DA	Zn-TADH	7.5	75	68	112

[a] Apo-TADH was prepared by dialysing htTADH against 50 mM sodium acetate (pH 5.5) or MES (pH 6.5) containing chelating agents; excess chelators were removed by dialysis against 50 mM MES pH 6.5. Zn-TADH was prepared by dialysing apo-TADH against 50 mM MES (pH.6.5) or Tris (pH 7.5) containing 20 µM zinc acetate; excess zinc was removed by dialysis against 50 mM MES (pH.6.5) or Tris (pH 7.5). All dialyses were performed at 4 °C. The control sample htTADH was at kept at 4 °C throughout the experiment (96 h). The control showed 98 % protein concentration, 62 % specific activity and 100 % zinc compared to the non-dialysed protein at the beginning of the experiment. Experiments were performed on a scale of 2.5 mL sample. Percentages are given compared to the control. Samples were analysed directly after dialysis; [b] Expected zinc occupancy is 1.0 : 2.0 (protein : Zn molar ratio), the control had only 40 % of the expected zinc occupancy.

Additionally, the pH of the buffer seemed to influence the amount of protein precipitation, with the higher pH resulting in more protein being recovered. On the other hand, the pH seemed to have little influence on the removal of zinc: for the samples where the protein was recovered with little loss, similar removal was seen at similar pH conditions (see Table 4.15 entry 3 and Table 4.16 entry 9.)

Table 4.16. Impact of chelator combinations on zinc removal and reinsertion into TADH.[a]

Entry	Chelator	TADH sample	pH of dialysis buffer	Protein conc. (%)	Specific activity (%)	Zn content (%)[b]
1	10 mM OPA	Apo-TADH	6.0	54	19	47
2	10 mM OPA	Zn-TADH	6.5	85	91	113
3	10 mM OPA + 20 mM EDTA	Apo-TADH	6.0	78	2	62
4	10 mM OPA + 20 mM EDTA	Zn-TADH	6.5	80	100	137
5	10 mM OPA + 20 mM EDTA	Apo-TADH	6.5	51-69	3-7	38-58
6[b]	10 mM OPA + 20 mM EDTA	Zn-TADH	7.5	45-62	89-153	163-217

[a] Apo-TADH was prepared by dialysing htTADH against 20 mM MES at the specified pH containing chelating agents; excess chelators were removed by dialysis against 20 mM MES pH 6.5 (as specified at the apo stage). Zn-TADH was prepared by dialysing apo-TADH against 20 mM MES pH 6.5 or Tris pH 7.5 containing 20 µM zinc acetate; excess zinc was removed by dialysis against 20 mM MES pH 6.5 or Tris pH 7.5 as specified. All dialyses were performed at 4 °C. The control sample was htTADH dialysed against chelator-free buffer at the appropriate pH at 4 °C throughout the experiment (96 h). The control showed 95 % protein concentration, 90 % specific activity and 100 % zinc; [b] The control showed 97 % protein concentration, 95 % specific activity and 100 % zinc; compared to the non-dialysed protein at the beginning of the experiment. Experiments were performed on a scale of 3 mL sample. Percentages are given compared to the control. Analyses of protein concentration, specific activity and Zn concentration were performed after centrifugation of the samples; [b] Expected zinc occupancy is 1.0 : 2.0 (protein : Zn molar ratio), the control had only 40 % of the expected zinc occupancy.

To differentiate between protein loss as a result of pH and protein loss due to treatment with chelating agents, occurrence of protein precipitation was visually inspected after dialysis of the protein in buffers at pH 5.5, 6.0 and 6.5. Precipitate was observed after 3 h dialysis in 50 mM sodium acetate buffer at pH 5.5; a slight precipitation was observed after 36 h dialysis in 20 mM MES buffer at pH 6.0; whilst no precipitation was observed after 36 h dialysis in 20 mM MES buffer at pH 6.5. The samples were centrifuged after 36 h and visually assessed considering any visible cell pellets. The sample at pH 6.5 contained a minimal cell pellet, thus further suggesting that removal and reinsertion of zinc should be performed at a pH equal or above 6.5.

To account for any protein precipitate formed during dialysis and to ensure that analyses were performed on soluble protein, which was likely to remain folded, dialysis experiments were repeated with individual chelators at pH 6.5. Instead of directly analysing samples after dialysis, centrifugation was performed and any insoluble pellet was removed. This also meant that no resolubilisation of the protein could be achieved. With 5 mM OPA, some differences were observed compared to the non-centrifuged samples, but they were difficult to explain and might be due to experimental error. Little protein loss was observed upon Zn removal, but activity loss was observed despite no removal of zinc (Table 4.17, entries 1-2). When 15 mM DA was used, the results were similar to the non-centrifuged samples (Table 4.15 entries 3-4). In the following work, samples were centrifuged, to account for protein loss during dialysis.

Table 4.17. Effect of sample centrifugation on zinc removal and re-insertion results.[a]

Entry	Chelator	TADH sample	Protein conc. (%)	Specific activity (%)	Zn content (%)[b]
1	5 mM OPA	Apo-TADH	98	50	100
2	5 mM OPA	Zn-TADH	99	68	118
3	15 mM DA	Apo-TADH	75	49	51
4	15 mM DA	Zn-TADH	48	72	137

[a] Apo-TADH was prepared by dialysing htTADH against 20 mM MES at pH 6.5 containing chelating agents; excess chelators were removed by dialysis against 20 mM MES at pH 6.5. Zn-TADH was prepared by dialysing apo-TADH against 20 mM Tris at pH 7.5 containing 20 μM zinc acetate; excess zinc was removed by dialysis against 20 mM Tris at pH 7.5. All dialyses were performed at 4 °C. The control sample was htTADH dialysed against chelator-free 20 mM MES buffer at pH 6.5 at 4 °C throughout the experiment (96 h). The control showed 63 % protein concentration, 83 % specific activity and 100 % zinc compared to the non-dialysed protein at the beginning of the experiment. Experiments were performed on a scale of 0.9 mL sample. Percentages are given compared to the control. Analyses of protein concentration, specific activity and Zn concentration were performed after centrifugation of the samples; [b] Expected zinc occupancy is 1.0 : 2.0 (protein : Zn molar ratio), the control had only 40 % of the expected zinc occupancy.

The results presented in this section showed that the best conditions to perform the removal of zinc from TADH were achieved at pH 6.0 and 6.5, where protein

precipitation was minimal. When a combination of 10 mM OPA with 20 mM EDTA were used as chelators, almost all specific activity was lost, and ICP-MS indicated loss of about half the zinc content, consistent with removal of catalytic zinc. Similar results were obtained when 10 mM OPA was used, although less activity was lost. Most activity could be restored upon reinsertion, although the Zn content was higher than expected. However, results displayed large errors when replicates were performed.

4.3.3.2 Impact of temperature on zinc removal

All previous dialysis methods were performed at 4 ^{o}C. At this temperature, TADH was hypothesised to be more rigid. It was hypothesised that an increased flexibility might increase zinc removal. TADH is a thermophilic ADH operating at high temperatures (up to 90 ^{o}C), and was therefore deemed to be stable enough to perform dialysis at increased temperatures. The chelator combination of 10 mM OPA and 20 mM EDTA was chosen, because it was shown to successfully remove all activity, which could also be entirely restored upon zinc reinsertion. These conditions were investigated for zinc removal at both room temperature and 60 ^{o}C. Room temperature was chosen for easier handling resulting in operation on a lab bench rather than restricted to the available space in the cold cabinet. 60 ^{o}C was selected as is the temperature at which all TADH enzymatic assays were performed.

Investigations into zinc removal and reinsertion by dialysis at different temperatures showed similar results to the experiments performed at 4 ^{o}C. Protein precipitate still occurred in all cases and little resolubilisation could be seen, in particular at 60 ^{o}C. Similar to previous results at 4 ^{o}C, the zinc concentration obtained after reinsertion was much higher than expected. This could be due to zinc binding at pre-existing available catalytic binding sites within the holo-TADH. However, it was unclear why such binding was not observed with other chelators. To investigate this hypothesis, a control was performed by treating wild type TADH with zinc (20 µM) *via* dialysis at pH 7.5 and 4 ^{o}C for 12 hours, followed by extensive dialysis to remove any excess zinc before enzymatic and metal content analysis. The specific activity and ICP-MS data both showed a 10 % loss after dialysis with zinc, thus demonstrating no binding of zinc

to unspecific binding sites. Another explanation was an experimental error in the assessment of protein concentration, perhaps due to aggregation of the protein.

Table 4.18. Effect of temperature on zinc removal and re-insertion results.[a]

Entry	Temperature conditions	TADH sample	Protein conc. (%)	Specific activity (%)	Zn content (%)[b]
1	Room temperature[c]	Apo-TADH	51-72	5-16	27-74
2	Room temperature[c]	Zn-TADH	62-89	80-188	59-392
3	60 °C	Apo-TADH	29	25	57
4	60 °C	Zn-TADH	32	121	293

[a] Apo-TADH was prepared by dialysing htTADH against 20 mM MES at pH 6.5 containing 10 mM OPA and 20 mM EDTA; excess chelators were removed by dialysis against 20 mM MES at pH 6.5. Zn-TADH was prepared by dialysing apo-TADH against 20 mM Tris at pH 7.5 containing 20 µM zinc acetate; excess zinc was removed by dialysis against 20 mM Tris at pH 7.5. The control sample was htTADH kept at the the desired temperature throughout the experiment (96 h). Experiments were performed on a scale of 1.5 mL sample. Percentages are given compared to the control. Analyses of protein concentration, specific activity and Zn concentration were performed after centrifugation of the samples; [b] Expected zinc occupancy is 1.0 : 2.0 (protein : Zn molar ratio), the control had only 50 % of the expected zinc occupancy; [c] These conditions were repeated with three samples.

4.3.4 Cobalt insertion into apo-TADH

Given the encouraging results obtained with the OPA / EDTA combination in section *4.3.3*, the insertion of a non-native metal into apo-TADH was assessed. Cobalt(II) was chosen as it was a good starting point for metal exchange investigations and has previously been exchanged for the catalytic zinc ion in both HLADH and TbADH.[122,180] The use of cobalt would also give the option to maintain and assess the activity for ketone reduction.

The experiments were performed starting with a heat purified htTADH with 1.2 U / mg specific activity and 24 % of the metal binding sites occupied (protein : zinc ratio 1 : 0.47, instead of 1 : 2, which would represent 100 % occupancy). Apo-TADH was prepared by treatment with 10 mM OPA and 20 mM EDTA, at pH 6.5 and 4 °C, resulting in 3 % residual specific activity and 72 % remaining zinc, compared to the initial sample

(protein : zinc ratio 1 : 0.34), as shown in Table 4.19 and Figure 4.29. Reinsertion of cobalt into the apo-protein by dialysis against a buffer containing 1 mM Co(II) lead to an increase of the specific activity to 0.98 U / mg, which represented 82 % of the specific activity in the original htTADH, before zinc removal (Figure 4.29).
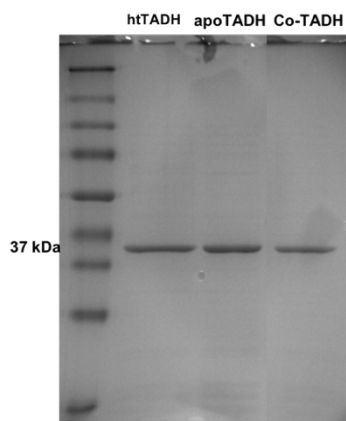
Figure 4.29. SDS-PAGE of protein samples throughout metal exchange. Protein samples purified *via* heat treatment (80 °C, 20 min) and sent for protein concentration analysis. Protein loss at apo stage 14 %; 37 % loss with cobalt addition.

ICP-MS analysis showed an increased cobalt content, as well as a slight increase in zinc, which might come from contamination (Table 4.19). SDS-PAGE shows highly purified protein samples throughout with minor loss at apo stage (~19%) and in total (~37%) at the end of the metal exchange (Figure 4.29).
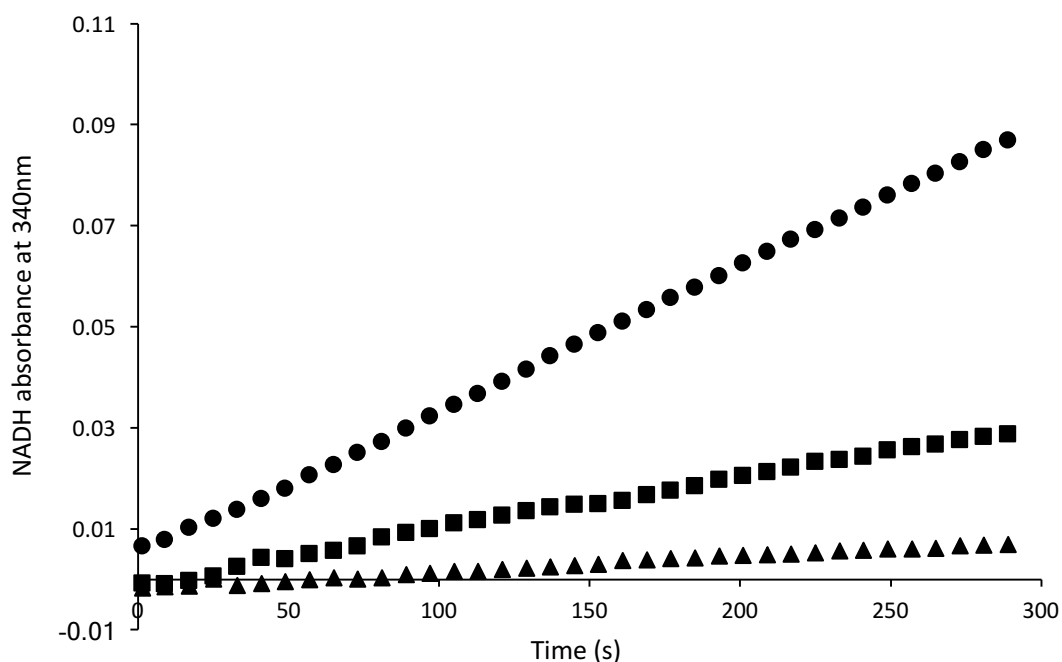
Figure 4.29. Comparison of enzymatic activity assays of htTADH (●), apo-TADH (▲) and Co-TADH (■) with 1-butanol.

Table 4.19. Results of ICP-MS analysis of htTADH, apo-TADH and Co-TADH.

TADH sample	TADH : Zn : Co molar ratio[a]
htTADH	1.0 : 0.47 : 0.01
Apo-TADH	1.0 : 0.34 : 0.00
Co-TADH	1.0 : 0.40 : 0.65

[a] The expected TADH : metal molar ratio is 1.0 : 2.0.

Although the reconstituted protein possessed double the metal content from the original starting sample, it was still almost 50 % less than the expected amount, indicating the presence of inactive protein. However, the recovered 82 % activity was due to the Co(II) binding at the active site, given the lack of activity before Co addition. To ascertain that all cobalt insertion occurred at the active site, wild type htTADH was dialysed against a cobalt(II) solution under the same buffer and temperature conditions as used for the metal exchange procedure. Whilst the specific activity remained the same, the protein : cobalt ratio increased to 1 : 0.29. This data, however was obtained using a different sample of TADH, with an increased zinc content. Whilst the protein : cobalt ratios cannot be directly compared between these two samples, it can be concluded that some unspecific binding of cobalt to TADH might have occurred, implying that only a percentage of the cobalt inserted into the apo-TADH was actually present in the active site.

Table 4.20. Specific activities and cobalt contents of htTADH before and after dialysis against a Co-containing buffer solution.

Sample	Specific activity (U / mg)	TADH : Zn : Co[a] molar ratio
htTADH	1.2	1 : 0.97 : 0.01
htTADH + 1 mM Co^{2+}	1.2	1 : 1.0 : 0.29

[a] Expected TADH : metal ratio = 1.0 : 2.0

In conclusion, successful reinsertion of a non-native metal into TADH was achieved, and activity recovery was obtained. However, all the results presented above, particularly for zinc reinsertion, showed inconsistencies between protein

concentration and metal content, and their correlation with specific activity was difficult to interpret. The work presented so far was performed using TADH samples that were heat purified (htTADH) and showed a reduced (50 %) zinc content to begin with. This may have been a contributing factor to the irreproducible results and the lack of correlation between data. As shown in Chapter 4.1, further purification of TADH by size exclusion chromatography (secTADH) resulted in protein : zinc contents closer to the expected 1.0 : 2.0 ratio. Hence, the next step focused on confirming the Zn removal and reinsertion conditions using secTADH, prior to replacing the catalytic zinc within TADH with rhodium.

4.3.5 Zinc removal and reinsertion into purified secTADH

Removal and reinsertion of zinc into the secTADH purified by size exclusion chromatography were performed using the best conditions determined in Section 4.3.3, using htTADH. Chelators OPA and a combination of OPA and EDTA were used at pH 6.0, which showed most activity and zinc removal. Metal insertion was performed using 20 mM MES buffer at pH 6.5, containing 20 µM Zn.

4.3.5.1 Zinc removal and reinsertion into secTADH by dialysis

Initial experiments followed the same dialysis procedure employed for htTADH. Promisingly, the precipitation issues, previously observed during zinc removal, were not observed in any of the cases with secTADH, and almost all protein was recovered. Treatment of secTADH with 10 mM OPA resulted in 44 % retained activity and 38 % remaining Zn; activity was restored to 72 %, whilst zinc contained was recovered to slightly more than the initial content. When the 10 mM OPA + 20 mM EDTA was used as chelating agent, 74 % of the specific activity was retained, although 50 % of the zinc was lost. Whilst the general trends and the zinc loss were similar to the results obtained with htTADH, the specific activities of the apo-TADH samples obtained from secTADH were much higher than the ones obtained previously.

Table 4.21. Zinc removal and reinsertion into secTADH by dialysis.[a]

Entry	Chelator conditions	TADH sample	Protein conc. (%)	Specific activity (%)	Zn content (%)
	Control[b]	secTADH	0.34 mg / mL	8.3 U / mg	Protein : Zn 1 : 1.6
1	10 mM OPA	Apo-TADH	100	44	38
2	10 mM OPA	Zn-TADH	n.d.	72	113
3	10 mM OPA + 20 mM EDTA	Apo-TADH	94	74	50
4	10 mM OPA + 20 mM EDTA	Zn-TADH	89	96	169
	Control[c]	secTADH	0.58 mg / mL	4.4 U / mg	Protein : Zn 1 : 1.5
5	10 mM OPA + 20 mM EDTA	Apo-TADH	92	1	13
6	10 mM OPA + 20 mM EDTA	Zn-TADH	62	42	93

[a] Apo-TADH was prepared by dialysing secTADH against 20 mM MES pH 6.0 containing chelating agents; excess chelators were removed by dialysis against 20 mM MES pH 6.5. Zn-TADH was prepared by dialysing apo-TADH against 20 mM MES pH 6.5 containing 20 µM zinc acetate; excess zinc was removed by dialysis against 20 mM MES pH 6.5. All dialyses were performed at 4 °C. The control sample was secTADH dialysed against 20 mM MES pH 6.5 at 4 °C throughout the experiment (96 h). [b] The control showed 57 % protein concentration, 91 % specific activity and 94 % zinc compared; [c] The control showed 66 % protein concentration, 76 % specific activity and no loss in zinc content; compared to the non-dialysed protein at the beginning of the experiment. Experiments were performed on a scale of 2.5 mL sample. Percentages are given compared to the control. Analyses of protein concentration, specific activity and Zn concentration were performed after centrifugation of the samples.

To assess reproducibility, zinc removal and reinsertion using the OPA + EDTA mixture was repeated using a newly prepared batch of TADH prepared under the same conditions as highlighted in section 3.4, purifying *via* heat treatment (80 °C, 20 min) and size exclusion chromatography, with slightly different characteristics. This time, the expected almost complete loss of specific activity was observed (1 % residual activity), however much of the zinc seemed to be lost as well, indicating removal of the structural zinc. This was also suggested by only a partial restoration of catalytic activity to 42 %, in contrast to the full activity restoration observed with previous

samples. Despite this assumed removal of a proportion of structural zinc ions, only a minor amount of protein was lost (<10%), and the lost zinc was 93 % recovered after reinsertion.

These results suggested that the dialysis method applied for zinc removal was not reproducible, and might have promoted the removal of structural zinc. The removal of the zinc was never complete, even when specific activity was fully abolished, suggesting that one of the zinc-binding sites were more stable. Throughout this work, based on previous reports, it was hypothesised that the structural zinc was more stable. The results obtained so far showed that the catalytic zinc was at least partially removed and re-inserted using the dialysis method.

On the other hand, the dialysis method was quite lengthy, requiring four days for the metal removal and reinsertion, with loss in protein stability during this time when stored at 4 °C. Protein precipitate was observed in the control with a total protein loss of 35-45 %, while the loss in activity over this period was 10-25 %. Thus, metal exchange of TADH was investigated by direct contact with the chelator, followed by removal of the excess using gel filtration.

4.3.5.2. Zinc removal and reinsertion into secTADH by gel filtration

The use of gel filtration for removal and reinsertion of zinc is a much shorter process and can be performed in 6-8 hours. Prior examples of chromatography use for metal exchange were published by Maret *et al.* for cobalt substitution in HLADH.[117] Additionally, others have also reported Rh insertion into apo carbonic anhydrase by direct treatment with the metal salt, followed by gel filtration. This procedure was adapted to TADH.

In brief, a sample of TADH in 20 mM MES buffer at pH 6.0 was treated directly with the chelating agent with stirring for 2 hours, before excess chelator was removed by gel filtration using PD-10 desalting columns, as described by the manufacturer (see Materials and Methods section 3.1). Excess zinc was then added to apo-TADH and the mixture was stirred for 2 hours again before exchange into fresh buffer 20 mM MES pH 6.5 by gel filtration, resulting in Zn-TADH. A control was performed with buffer

exchange into 20 mM MES pH 6.0 at the beginning of the experiment, followed by a second buffer exchange into 20 mM pH 6.5 at the end of the experiment, whilst stored at 4 °C in between. The control showed no significant protein loss, however less than 50 % activity was recovered.

Table 4.22. Zinc removal and reinsertion into secTADH by gel filtration.[a]

Entry	Chelator conditions	TADH sample	Protein conc. (%)	Specific activity (%)	Zn content (%)
	Control	secTADH	2.1 mg / mL	3.2 U / mg	Protein : Zn 1 : 1.5
1	10 mM OPA	Apo-TADH	66	22	73
2	10 mM OPA	Zn-TADH	75	21	120
3	10 mM OPA + 20 mM EDTA	Apo-TADH	61	47	20
4	10 mM OPA + 20 mM EDTA	Zn-TADH	82	21	7

[a] Apo-TADH was prepared by stirring secTADH in 20 mM MES pH 6.0 containing chelating agents for 2 h, followed by 2 x buffer exchange using Sephadex G-25 PD-10 columns; Zn-TADH was prepared by stirring secTADH in 20 mM MES pH 6.5 containing 20 µM zinc acetate for 2 h, followed by 2 x buffer exchange using Sephadex G-25 PD-10 column. The control sample was secTADH that underwent 1 x buffer exchange using PD-10 against 20 mM MES pH 6.0, and a second buffer exchange using PD-10 against 20 mM MES pH 6.5. The control showed 100 % protein concentration, 43 % specific activity and zinc content not checked, compared to the non-dialysed protein at the beginning of the experiment. Experiments were performed on a scale of 2.5 mL sample. Percentages are given compared to the control.

This method resulted in significant protein loss occurring upon treatment with chelators. Moreover, whilst protein activity was lost, as expected, upon removal of zinc, the reinsertion was less successful, and no activity was recovered. When OPA was used, some zinc appeared to be reinserted which, corroborated with the lack of activity, suggested the removal of structural zinc using this method. When the OPA + EDTA mixture was used, most of the zinc was lost and was not reinserted, again suggesting that direct contact with these chelators removed a significant proportion of catalytic zinc, and that the protein could not be reactivated by direct contact with the zinc. It was hypothesised, at this stage, that these conditions were too harsh and denatured the protein.

Despite some encouraging results obtained using dialysis against specific chelators, and zinc or cobalt reinsertion, a robust method for the creation of apo-TADH has yet to be developed. For HLADH, Maret *et al.* reported selective removal of the catalytic zinc ions with 10 mM DA and a partially crystallised HLADH in a solution of *tert*-butanol (25% v/v) in TES buffer.[117] Equilibrium dialysis at pH 5.5 against a Co(II)-containing buffer was also reported.[16] Selective removal of the catalytic zinc in HLADH seems to be more successful in this crystallised form of HLADH, where the structural zinc ions are less accessible to the chelator. Conditions for the crystallisation of TADH were published during the course of this thesis by Man *et al.,*[18] and employed 0.1 M Bis-Tris buffer pH 6.5 containing 1 M sodium chloride and 1.5 M ammonium sulphate. Moving forward, further attempts at the creation of apo-TADH could be made, with a crystallised solution of TADH and a range of selected chelators. A column chromatography method was also employed by Maret *et al.*, in which the zinc was replaced by cobalt on a gel filtration (Sephadex G-25) column pre-equilibrated with a Co(II)-containing buffer, thus avoiding direct chelator treatment. The exchange was performed at 55 ^{o}C during 8 h. The increase in temperature was shown to favour the exchange of catalytic zinc over the structural one, presumably by inducing more flexibility in the tertiary structure. It is possible that this method could be applied to TADH, as inspection of the structure suggests that the structural binding site resides closer to the protein surface.

4.3.6 *Rhodium reinsertion into purified secTADH and imine reduction assays*

Given the partial removal of catalytic zinc observed with the above methods, rhodium insertion was attempted using both dialysis and gel filtration. The resulting Rh-TADH was assayed for both ketone and imine reduction.

Rhodium insertion was first attempted by dialysis of the apo-TADH against a 20 μM Rh(I) solution in 20mM MES buffer pH 6.5. Rh(acac)(CO)$_2$ was used as the Rh(I) source as the acetylacetonate group is relatively small to fit within the active site. It is stable in air and fairly water soluble. Nonetheless, the buffer solution was degassed and dialysis performed under nitrogen to prevent any oxidation. Apo-TADH samples were prepared by dialysis against chelators OPA and OPA + EDTA, as described in section

4.3.5. In both cases the activity diminished further upon Rh(I) insertion, from 44 % and 74 % for the apo-TADH samples, to 15 % and 26 % for Rh-TADH, for the OPA and OPA + EDTA treatments, respectively (Table 4.23, entries 1-4). The ICP-MS data not only showed an excess of rhodium binding (rhodium : protein ratios of 6.5 and 24.0), but also, more surprisingly, the reintroduction of zinc after dialysis against the rhodium solution. This result suggested that residual zinc was present in the metal salt. To avoid this issue, the rhodium solution was submitted to treatment with Chelex®100 for removal of residual zinc, and the rhodium reinsertion experiment was repeated.

Table 4.23. Zinc removal and rhodium reinsertion into secTADH by dialysis.[a]

Entry[b]	Chelator	TADH sample	Protein conc. (%)	Specific activity (%)	Zn content (%)	Ratio TADH : Zn : Rh
	Control[c]	secTADH	0.34 mg / mL	8.3 U / mg		1 : 1.6 : 0
1	OPA	Apo-TADH	100	44	38	1 : 0.6 : 0
2	OPA	Rh-TADH	100	15	88	1 : 1.4 : 6.5
3	OPA + EDTA	Apo-TADH	94	74	50	1 : 0.8 : 0
4	OPA + EDTA	Rh-TADH	83	26	156	1 : 2.5 : 24.0
	Control[d]	secTADH	0.58 mg / mL	4.4 U / mg		1 : 1.5 : 0
5	OPA	Apo-TADH	72	6	60	1 : 0.9 : 0
6	OPA	Rh-TADH	82	2	80	1 : 1.2 : 1.7
7	OPA + EDTA	Apo-TADH	92	1	13	1 : 0.2 : 0
8	OPA + EDTA	Rh-TADH	63	32	27	1 : 0.4 : 2.6

[a] Apo-TADH was prepared by dialysing secTADH against 20 mM MES pH 6.0 containing chelating agents; excess chelators were removed by dialysis against 20 mM MES pH 6.5. Rh-TADH was prepared by dialysing apo-TADH against 20 mM MES pH 6.5 containing 20 μM Rh(I)(acac)(CO)$_2$, excess zinc was removed by dialysis against 20 mM MES pH 6.5. All dialyses were performed at 4 °C. The control sample was secTADH dialysed against 20 mM MES pH 6.5 at 4 °C throughout the experiment (96 h). [c] The control showed 57 % protein concentration, 99 % specific activity and 94 % zinc compared; [d] The control showed 66 % protein concentration, 88 % specific activity and no loss in zinc content; compared to the non-dialysed protein at the beginning of the experiment. Experiments were performed on a scale of 2 mL sample. Percentages are given compared to the control. Analyses of protein concentration, specific activity and Zn concentration were performed after centrifugation of the samples; [b] Samples **1-4**: buffers were used as such; samples **5-8**: buffers were treated with Chelex®.

Upon "purification" of the Rh(I)-containing buffer from divalent metal ions such as Zn by treatment with Chelex, rhodium insertion into apo-secTADH formed by treatment with the OPA + EDTA mixture presented a somewhat encouraging result. The zinc content was still observed to increase from 1 : 0.2 to 1 : 0.4 protein : Zn content, which was much less than previously observed (Table 4.23, entry 4 *vs*. 8). The protein : rhodium content was determined to be 1 : 2.6, suggesting the existence of non-specific binding sites within TADH. Some activity was recovered as well, higher than expected from the zinc content. This suggested that some of the activity might be due to the presence of rhodium. It was impossible to ascertain, at this stage, whether the activity was due to the presence of rhodium at the active site, or elsewhere in the protein.

On the contrary, the insertion of rhodium into the apo-TADH prepared by dialysis against OPA did not result in active protein. Again, zinc content was observed to increase in the apo-TADH from 1 : 0.9 to 1 : 1.2 protein : zinc ratio, despite treatment of buffers with Chelex. Rhodium content was also seen to increase to 1 : 1.7 protein : Rh ratio (Table 4.23, entries 5-6). Again, some unspecific binding was observed when rhodium was used.

Finally, rhodium was also reinserted in the apo-TADH samples prepared by gel filtration (Table 4.24). Interestingly, when OPA was used as chelator, the zinc content in the apo-TADH was reduced from 1 : 1.5 in secTADH to 1 : 1.1 in apo-TADH, and was further reduced to 1 : 0.9 in Rh-TADH. On the other hand, Rh content increased to 1 : 0.9, yielding the expected metal content within this protein. Activity also increased compared to apo-TADH, suggesting that the bound Rh was active. However, at this stage it was impossible to ascertain whether the Rh was present at the active site. When OPA + EDTA were used as chelating agents, little Rh binding and little activity were observed. These results were treated with caution, because of the poor results obtained for zinc reinsertion suggesting that this method was not suitable for reconstitution.

Table 4.24. Zinc removal and rhodium reinsertion into secTADH by gel filtration.[a]

Entry	Chelator	TADH sample	Protein conc. (%)	Specific activity (%)	Zn content (%)	Ratio TADH : Zn : Rh
	Control	secTADH	2.1 mg / mL	3.2 U / mg		1 : 1.5 : 0
1	OPA	Apo-TADH	66	22	73	1 : 1.1 : 0
2	OPA	Rh-TADH	91	36	60	1 : 0.9 : 0.9
3	OPA+EDTA	Apo-TADH	61	47	20	1 : 0.3 : 0
4	OPA+EDTA	Rh-TADH	23	8	7	1 : 0.1 : 0.3

[a] Apo-TADH was prepared by stirring secTADH in 20 mM MES pH 6.0 containing chelating agents for 2 h, followed by 2x buffer exchange using Sephadex G-25 PD-10 columns; Rh-TADH was prepared by stirring secTADH in 20 mM MES pH 6.5 containing 20 µM Rh(I)(acac)(CO)$_2$ for 2 h, followed by 2x buffer exchange using Sephadex G-25 PD-10 column. The control sample was secTADH that underwent 1x buffer exchange using PD-10 against 20 mM MES pH 6.0, and a second buffer exchange using PD-10 against 20 mM MES pH 6.5. The control showed 100 % protein concentration, 43 % specific activity and zinc content not checked, compared to the non-dialysed protein at the beginning of the experiment. Experiments were performed on a scale of 2.5 mL sample. Percentages are given compared to the control.

All Rh-TADH samples prepared above were investigated for imine reductase activity with 2-methyl-1-pyrroline **1** as substrate, but no activity was observed. Increase of enzyme concentration, and thus of rhodium, was unsuccessful as well. Without further investigations on the localisation of Rh within TADH, it is difficult to predict how to optimise this result. Before engaging in any further investigations it is important to have a well-defined coordination environment in the Rh-TADH. Given the difficulties to obtain a robust method for the preparation of both apo-TADH and metal-TADH, whether with Zn, Co or Rh, no further work has been performed on developing an artificial metalloenzyme using this route. Other possible ways were envisaged to incorporate rhodium into the TADH scaffold, which are investigated and discussed in detail in Section 4.4.

4.3.7 Conclusions

The removal of the catalytic zinc(II) ion and its re-insertion *via* dialysis were studied using the thermostable TADH. The analysis was complicated by the fact that the proteins contains two zinc ions per monomer: one catalytic, and one structural.

Protein precipitation during zinc removal was minimised by using appropriate buffers. The best conditions for zinc removal were observed at pH 6.0 and 4 °C, with chelating agent OPA (10 mM) or a mixture of OPA + EDTA (10 mM + 20 mM, respectively). These resulted in almost complete loss of specific activity, and partial loss of zinc. Protein loss was also observed during these experiments. Activity, zinc content and protein concentration all increased upon zinc reinsertion by dialysis against a buffer solution containing zinc acetate (20 μM) at pH 6.5 and 4 °C.

Previous literature results suggested that the HLADH structural zinc was more difficult to remove in the presence of chelators,[117] and highlighted its role in maintaining the overall protein structure.[84] The fact that the protein could be recovered upon treatment of apo-TADH with zinc suggested that most of the zinc removed, and thus reinserted, was from the catalytic site. However, protein precipitation and variability of the repeats suggested that this was not a robust method for zinc replacement.

Cobalt(II) was also inserted into apo-TADH and resulted in recovery of the specific activity to 82 % of the initial zinc-containing protein. However, metal content analysis showed that both the zinc and the cobalt content of the protein were lower than expected. This was assumed to be due to the presence of zinc-devoid protein in the initial sample, which also had a lower zinc content than expected. Purification of the TADH sample by size exclusion chromatography increased the zinc content. However, zinc removal and re-insertion experiments into the purified secTADH also led to variable amounts of protein precipitation, and a lack of correlation between activity and amount of remaining zinc.

Binding of Rh(I) to apo-TADH was observed to occur in 2.6-fold molar excess in the best of the studies conditions. Some residual alcohol oxidation was observed possibly due to bound Rh but it is difficult to ascertain. However, no imine reductase activity was observed for the reduction of 2-methylpyrroline. Given the difficulty in developing a robust method for zinc replacement in TADH, a different strategy was adopted, consisting in introducing an artificial binding site into the protein.

4.4 Synthesis of an artificial metal-binding site for TADH

4.4.1 Introduction and highlights

Introduction of a rhodium catalyst by direct and specific binding to the amino acids forming the TADH native metal-binding site was difficult to assess, and could not be applied to imine reduction. A second strategy was adopted, which consisted in designing and synthesising a non-native binding site, to be incorporated into TADH. Two methods have been described for the bioconjugation of a non-native metal-binding site to a protein: direct covalent attachment to a reactive side-chain, *e.g.* cysteine thiol group; and attachment to a molecule with high affinity for the protein, *e.g.* an inhibitor or a cofactor, which can be inserted into a defined binding pocket by supramolecular anchoring. Using this strategy, Ward *et al.* designed biotinylated iridium catalysts, which performed imine reduction upon incorporation into streptavidin using biotin as an anchor.

The aim of this section was to exploit the affinity of the NAD^+ cofactor and of its mimics for ADH, in order to use it as an anchor for the introduction of metal catalysts into TADH. Therefore, the design and synthesis of a metal-containing NAD^+ analogue was performed. The NAD^+ mimic would ensure the positioning of the metal complex within TADH. The metal complex[181] would act as the hydrogen transfer catalyst, in the presence of a stoichiometric hydrogen source, similar to chemical transfer hydrogenation catalysis.

Highlights

- A novel iridium(III) complex, containing a nicotinamide-functionalised *N*-heterocyclic carbene (NHC) ligand, was synthesised and characterised.
- The nicotinamide-functionalised Ir-NHC was shown to be active in the transfer hydrogenation of ketone and imine substrates, both in organic solvents with isopropanol and in buffer with sodium formate as hydride donor.
- Inhibition kinetics and controls in the presence of NADH suggested some interactions of the Ir-catalyst with the protein, but not at the cofactor-binding site

4.4.2 Design of nicotinamide-functionalised metal complexes

Previous work by Fish and co-workers showed that 1-benzylnicotinamide triflate (**9**, Figure 4.30) and β-nicotinamide-5'-ribose methyl phosphate (**10**, Figure 4.30) could perform the enantioselective reduction of ketones inside HLADH, in the presence of a rhodium catalyst and of a hydride donor.[115-116] These nicotinamide derivatives, possessing benzyl or ribose-5'-methylphosphate substituents on the pyridinium ring were demonstrated to yield similar turnover numbers and enantioselectivities to the native cofactor NADH, suggesting that they replaced NADH during catalysis. Control experiments excluded the presence of residual native cofactor performing the catalysis. Therefore, the authors proposed that the pyridinium ring substituents played a role in the binding to the NAD$^+$-binding pocket of HLADH, and in positioning the key nicotinamide motif in proximity of the substrate-binding pocket, where enantioselective hydride transfer takes place.
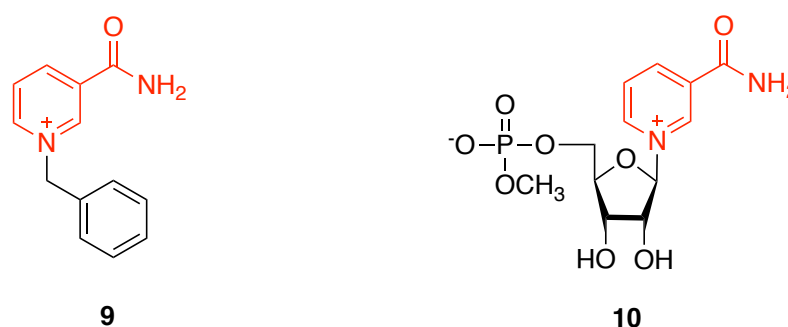

Figure 4.30. NAD$^+$ analogues with the nicotinamide moiety highlighted in red.

The binding of NAD$^+$ mimics to the ADH cofactor site suggested that the pyridinium-substituted nicotinamide ring could act as an anchor, for the attachment and introduction of metal complexes within TADH. TADH and HLADH have a similar cofactor-binding pocket, and it was therefore hypothesised that similar affinity for NAD$^+$ mimics would be observed. The 1-benzylnicotinamide analogue was selected, as it was simple enough to be synthesised. To select a position for the connection of appropriate metal complexes, the ease of nicotinamide modification and the proximity of the metal attachment to the substrate-binding pocket were considered.
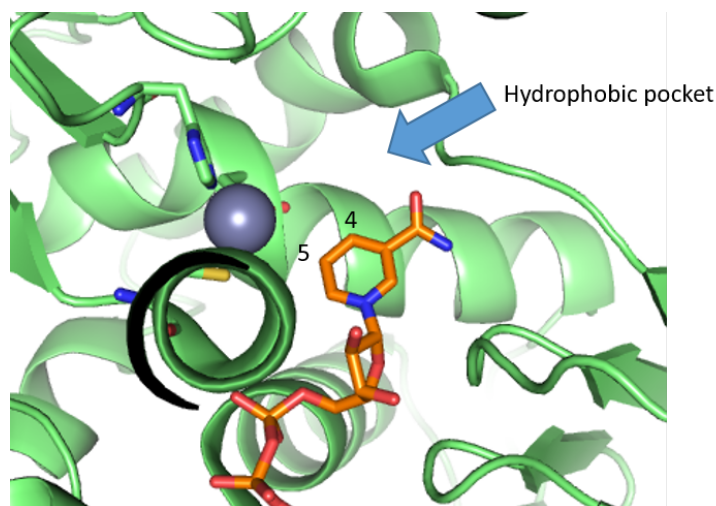
Figure 4.31. Active site of TADH (PDB 4CPD), showing bound NAD$^+$ (orange sticks), the catalytic zinc (grey sphere) and the substrate-binding site.

Figure 4.31 shows the NAD$^+$-binding pocket and the active site in TADH. The orientation of the cofactor is such that position 4 of the nicotinamide ring is positioned towards the substrate-binding pocket, whilst position 5 is oriented towards the active site zinc ion. Assuming that the nicotinamide ring of the NAD$^+$ analogues was similar to that of NAD$^+$ upon TADH binding, these two positions were selected for anchoring of the catalyst, because space was available in their proximity. The general designs chosen for the metal complexes connected to the nicotinamide anchors are presented in Figure 4.32.
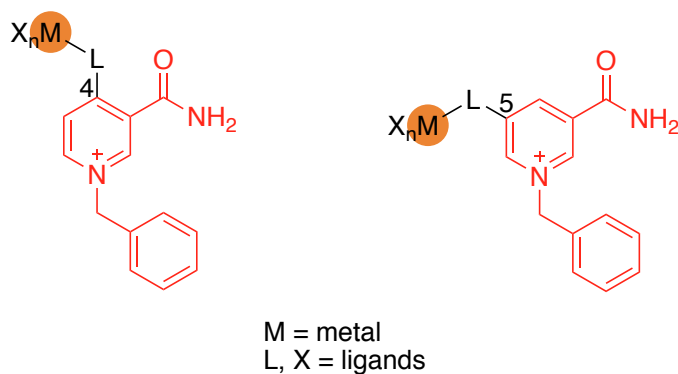
M = metal
L, X = ligands

Figure 4.32. Design of metal complexes connected to nicotinamide mimics, for incorporation into TADH. The benzylnicotinamide anchor is represented in red.

The choice of the metal catalyst was based on reported literature results for imine reduction by transfer hydrogenation.[182,183] The majority of reported catalysts contained iridium, rhodium and ruthenium with a variety of chiral ligands, and the

best conversions were generally obtained with iridium catalysts.[184] Concerning the ligand, small *N*-heterocyclic carbenes (NHCs) were selected, to minimise the space occupied by the metal complex inside the protein. From a synthetic point of view, NHCs can be directly connected to the nicotinamide ring, without the need of a linker (see later), thus enhancing the possibility to position the metal catalyst in close proximity to the nicotinamide ring, and thus to the substrate-binding pocket. Additionally, NHC ligands have the advantage of high thermal stability, and the ability to tune the electronic properties of the metal complex.[185] Rh(III), Ir(I or III)- and Ru(II)-*N*-heterocyclic carbenes were previously demonstrated to perform transfer hydrogenation with imine substrates (Figure 4.33).[186-190] Out of these, iridium catalysts were the most efficient for this transformation.
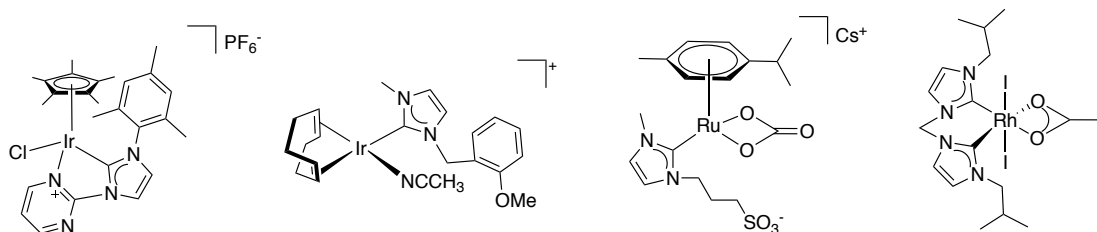
Figure 4.33. Rh, Ru and Ir chemical catalysts capable of performing transfer hydrogenation on imine substrates containing one or more N-heterocyclic carbene.

Additionally, the synthesis and characterisation of a Rh(I)-NHC complex linked to a nicotinamide derivative was recently reported (**12,** Figure 4.34). The report also demonstrated the ability of such complexes to act as hydride ion carriers, by transferring a hydride to the 4 position of the nicotinamide ring.[158] A substituted, tertiary diisopropyl amide was used, due to ease of synthesis and handling, and both the pyridinium ring and the NHC possessed a methyl substitution.
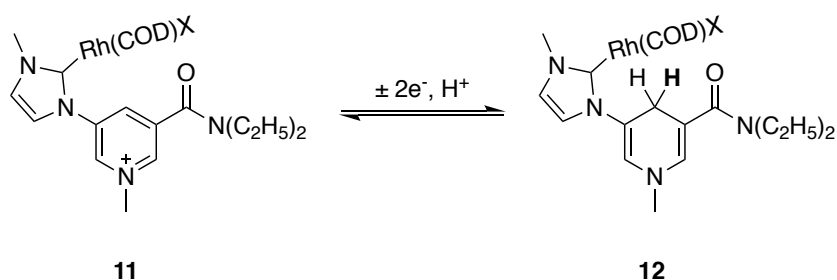
Figure 4.34. Hydride transfer ability of a Rh(I)-NHC complex linked to nicotinamide. Modified from the report of Colbran and co-workers.[158]

In conclusion, following the literature research, four novel structures were proposed to introduce a non-native metal-binding site into TADH (Figure 4.35, **13a** to **14b**). The structural variations included the connection point between the metal-NHC complex and the nicotinamide anchor (position 4 or 5 of the nicotinamide ring), and the type of metal catalyst used for complexation (Ir(I) or Ir(III)).

**13a**   **14a**   **13b**   **14b**
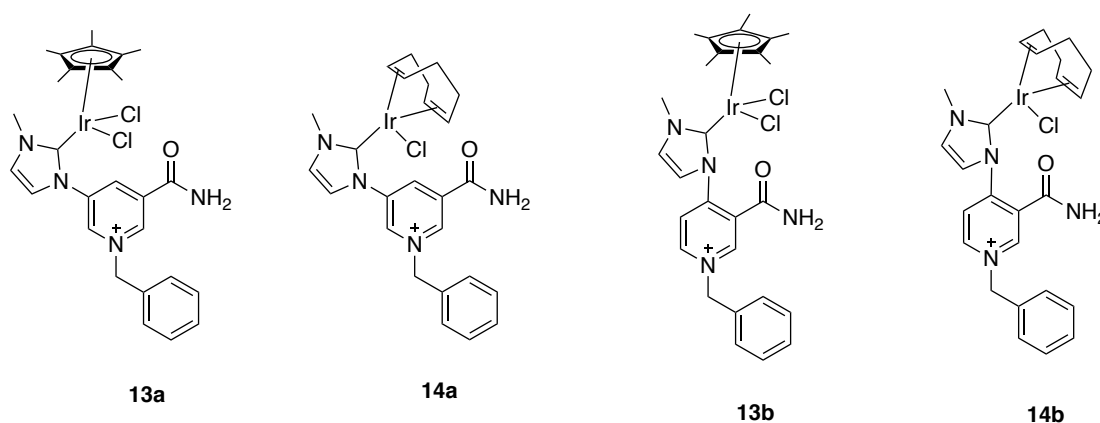
Figure 4.35. Proposed structures of nicotinamide-functionalised Ir-NHC catalysts.

Despite published work suggesting easier handling of the tertiary, diisopropyl-substituted nicotinamide, this substitution was reasoned to add steric bulk to the nicotinamide anchor, and the primary amide was used instead. Moreover, at the difference from the previously published methyl-substituted Rh-NHC **11**, a benzyl group was thought necessary for the recognition of the substituted nicotinamide by ADH. Since the selective *N*-alkylation of the nicotinamide *vs.* the imidazole ring was deemed difficult, benzyl was used both as the pyridinium functionality and as the second substituent of the NHC, despite its increased bulk. Functionalisation of the nicotinamide with a metal-NHC complex at the 4-position has not been previously reported and was therefore investigated. The synthesis of these structures was studied in the following section.

4.4.3 Synthesis of a nicotinamide-functionalised iridium N-heterocyclic carbene complex

The synthesis of the 4- and 5-functionalised benzyl nicotinamide was adapted from the procedure previously published by Colbran and co-workers (Figure 4.36).[158] The reported synthesis[158] relied on an Ullmann coupling reaction between a nicotinamide

halide derivative and imidazole, in the presence of a copper (I) catalyst. Derivatisation with benzyl iodide at both the pyridine and the imidazole nucleophilic nitrogen atoms afforded the corresponding pyridinium and imidazolium functionalities, respectively. Formation of the NHC metal complex from the imidazolium derivatives was relatively straightforward. This synthetic scheme was adapted to the synthesis of ligandss **17a + b** and **18 a + b** (Figure 4.38).
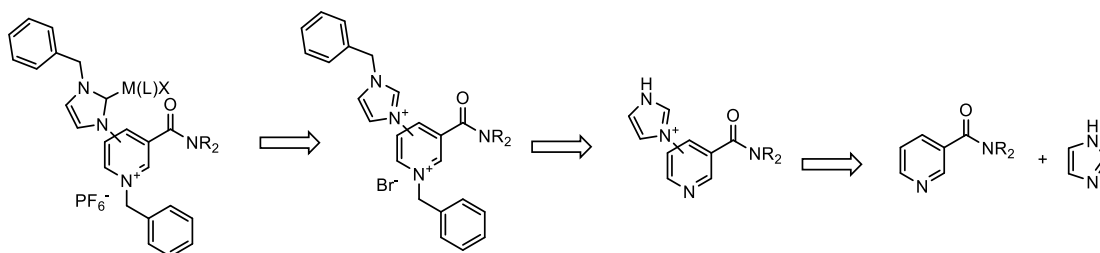
Figure 4.36. Retrosynthetic scheme for the synthesis of nicotinamide derivatives linked to metal-NHC complexes. The synthesis was based on the procedure published by Colbran and co-workers.

Ullmann coupling is a cross-coupling reaction between aryl halides a nucleophile, leading to C-C, C-N and C-O bond formation.[191-196] It is essentially an aromatic nucleophilic substitution, mediated by Cu(I). The generally accepted mechanism involves Cu(I) undergoing oxidative addition, followed by co-ordination to the nucleophile and reductive elimination (Figure 4.37, route A). Mechanisms proposed up until the end of the last century largely suggested the nucleophile to co-ordinate first (Figure 4.37, route B), increasing the electrophilicity on the aromatic and subsequently the susceptibility to oxidative addition. From a recent review on copper-catalysed Ullmann chemistry, it is apparent that the mechanism depends upon the specific substrates and reaction conditions employed.[195]

In the reported synthesis of **12**, the use of a "protected" tertiary nicotinamide avoided the amide group acting as a nucleophile during the coupling.[197,198] Moreover, the authors justified substitution of the primary amide to the tertiary amide by an increased solubility, avoidance of deprotonation due to the excess base, as well as of co-ordination to the copper catalyst. To compare the influence of amide protection on the Ullmann coupling, both the tertiary, diisopropyl nicotinamide and the primary, "free" nicotinamide halide derivatives were used as coupling partners with imidazole.
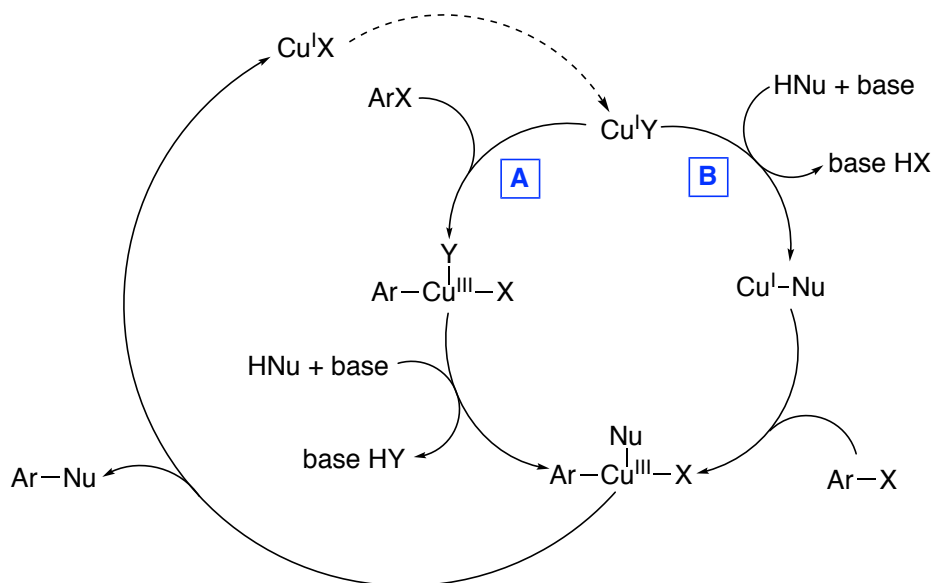
Figure 4.37. Reported catalytic cycles of copper-catalysed Ullmann coupling. Modified from Beletskaya *et al.* (2004).[199]

Substitution of position 4 of the nicotinamide ring by *N*-arylation of the imidazole was not previously published. Only a few examples of *N*-arylation of imidazole using 4-substituted pyridine exist, at high temperatures and long reaction times.[200] Similar to all oxidative additions, the reactivity of the substituted pyridine halides varies in the order I > Br > Cl > F, and both 4-chloro- and 4-bromopyridine were shown to give high yields when coupled to imidazole using Ullmann chemistry (Figure 4.37).[199] Based on these results, both bromo- and chloro-substituted nicotinamide derivatives were tested for the coupling with imidazole. The following two sub-sections describe the syntheses of the metal-NHC complexes linked to tertiary and to primary nicotinamide derivatives, respectively.

4.4.3.1 Synthesis of 4- and 5-imidazolyl-diisopropylnicotinamide ligands

The method published by Colbran and co-workers for the synthesis of a tertiary nicotinamide derivative functionalised with imidazolium at position 5 was reproduced, but using benzyl group substitutions instead of methyl. Additionally, the same method was tested for the synthesis of the 4-substituted nicotinamide derivative (Figure 4.38).

Initially, the tertiary amide **16a** was synthesised according to Marsais from commercially available 5-bromonicotinic acid **15a**, in 79 % yield after purification by silica gel chromatography.[157] Attempts to synthesise 4-bromonicotinamide from

commercial 4-bromonicotinic acid resulted in substitution of the 4-bromide by chloride, during treatment with SOCl$_2$, probably due to the higher reactivity of the 4-position towards nucleophilic substitution. To avoid this issue, 4-chloronicotinic acid **15b** was used as starting material, although it was anticipated that Ullmann coupling would be easier with the Br substituent. Amide synthesis yielded the 4-substituted compound **16b**, in 71 % yield.
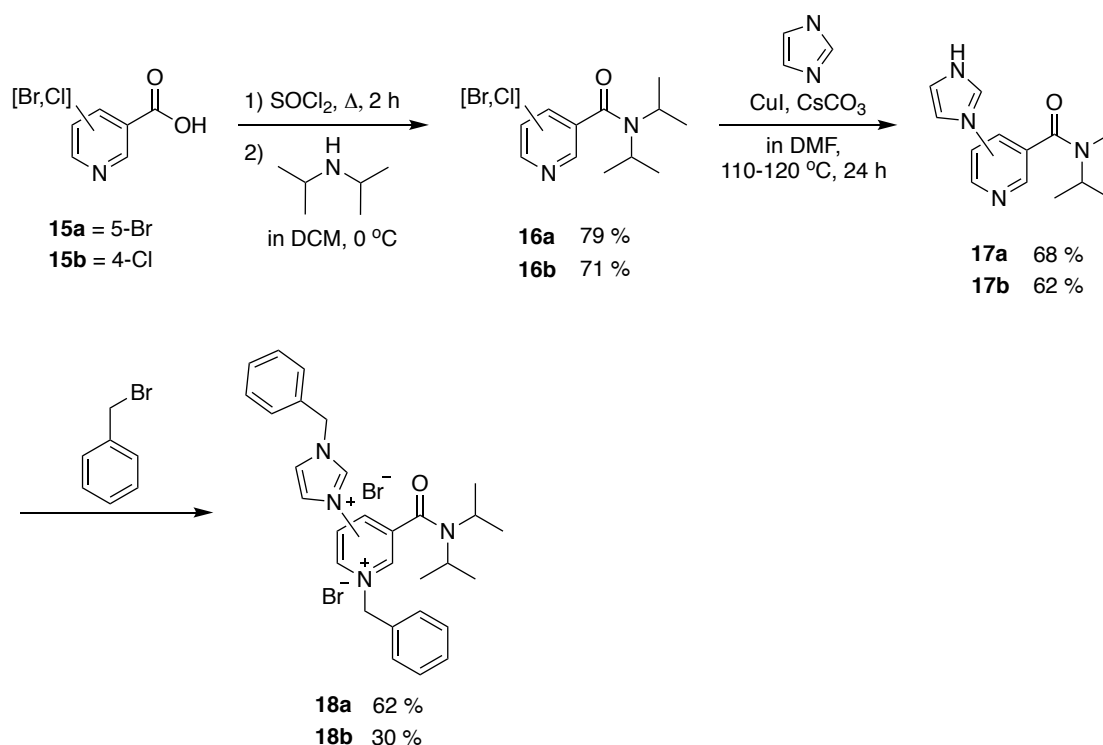
Figure 4.38. Proposed synthesis of 4- and 5-imidazolyl-diisopropylnicotinamide compounds.

Both the 4-chloro and the 5-bromo substituted nicotinamide derivatives were further subjected to Ullmann coupling with imidazole, using Cu(I) catalyst in the presence of caesium carbonate. Products 5-(1*H*-imidazol-1-yl)-*N,N*- diisopropylrnicotinamide **17a** and 4-(1*H*-imidazol-1-yl)-*N,N*-diisopropylnicotinamide **17b** were synthesised successfully in 40 % and 68 % yield, respectively. The yield for the 5-imidazolyl compound **17a** was as expected when compared to the literature (70%).[158] The synthesis of the 4-imidazolyl product **17b** demonstrated that imidazole could successfully be introduced at the 4-position of the diisopropylnicotinamide. However, the lower yield suggested that coupling at the 4-position was challenging.

Benzylation of 4- and 5- imidazolyl coupled products **17a** and **17b** with two equivalents of benzyl bromide resulted in benzyl addition at both the nucleophilic nitrogens of imidazole and pyridine, yielding the double-benzylated products **18a** and **18b** in 30 % and 62 % yield, respectively. These results confirmed the feasibility of introducing an imidazolium substitution at the 4 position of a benzylnicotinamide derivative, starting from a 4-chloro substituted starting material.

4.4.3.2   Synthesis of 4- and 5-imidazolyl-nicotinamide ligands *21a* and *21b*

The synthesis of the 4- and 5-imidazolyl substituted benzylnicotinamide bearing a "free", non-substituted primary amide was attempted following a similar procedure as above. The synthetic scheme is outlined in Figure 4.39.

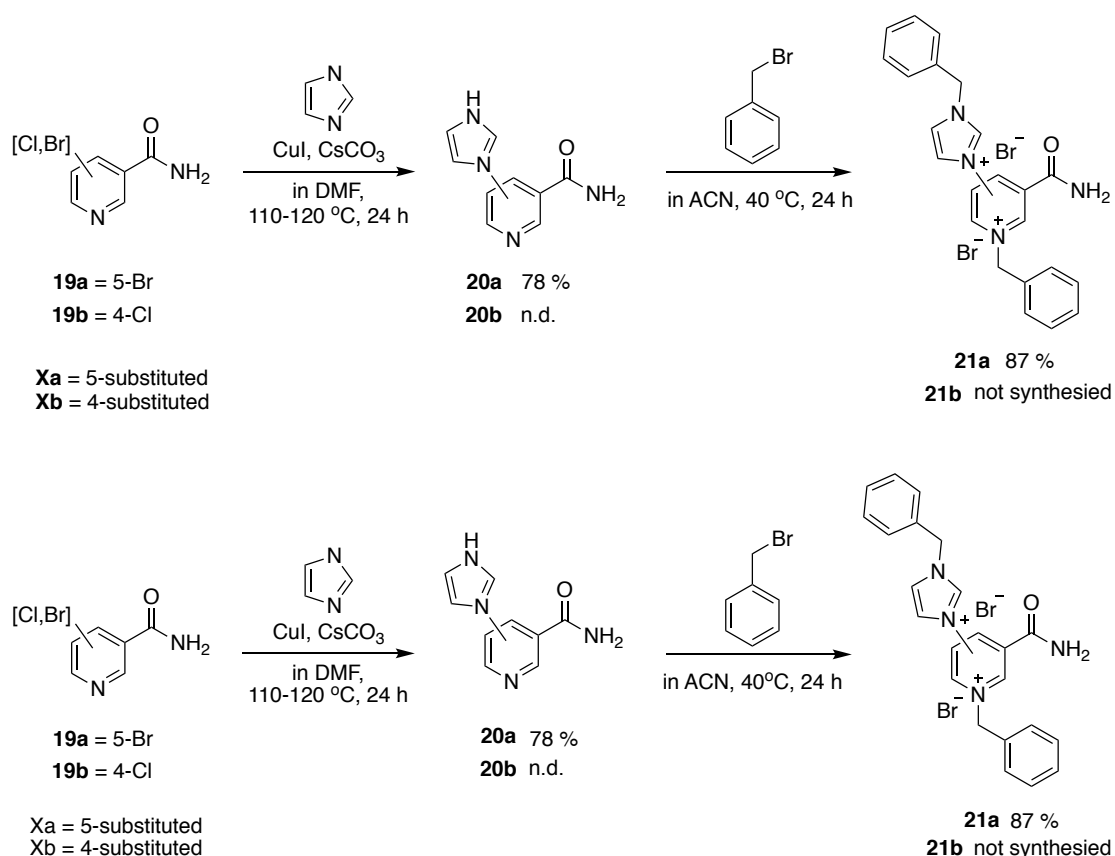**Figure 4.39. Proposed synthesis of 4- and 5-imidazolyl-nicotinamide compounds 21a and 21b.**

5-(1*H*-Imidazol-1-yl)nicotinamide **20a** was successfully synthesised using Colbran's reported procedure and obtained in 78 % yield after purification by silica gel chromatography with DCM / MeOH (80 / 20) as the eluting agent. This demonstrated

the successful use of non-protected 5-bromo substituted nicotinamide as a coupling partner with imidazole under Ullmann reaction conditions. However, the purification of the primary nicotinamide did prove more difficult compared to the corresponding tertiary nicotinamide, due to the occurrence of minor side-products which migrated close together.

On the other hand, the synthesis of 4-(1*H*-imidazol-1-yl)nicotinamide **20b** by imidazole coupling to the 4-chloronicotinamide **19b** was unsuccessful. Several attempts were made to improve this result, including increased reaction time, temperature and reagent equivalents (Table 4.25). However, the outcome remained the same in most cases, *i.e.* unreacted starting materials observed by both TLC and NMR, along with minor side products that could not be isolated. A minor amount of product could be observed by ^{1}H NMR; however, purification by silica gel chromatography proved difficult and the desired product could not be isolated.

Table 4.25. Summary of reaction conditions tested for the Ullmann coupling between 4-chloronicotinamide 19b and imidazole.

Entry	Reaction Conditions [a]	Outcome
1	Imidazole (1.6 eqv.), CsCO$_3$ (2 eqv.), CuI (0.2 eqv.), in DMF at 110-120 ^{o}C, 24 h	Presence of starting material, minor side products and minor amount of desired product
2	Temperature increased to 150 ^{o}C	Degradation and minor side products present.
3	Reaction time increased to 36 h	Same as model reaction
4	Equivalents of reagents increased 1.5 times	Same as model reaction
5	Equivalents of reagents increased 1.5 times, reaction time increased to 36 h	Same as model reaction

[a] Reaction conditions as compared to the model reaction; entry 1.

There were two main differences between the successful and unsuccessful starting materials for the Ullmann coupling: the nicotinamide substitution pattern (4 *vs.* 5-halide) and the nature of the halide. To assess whether the substitution pattern had

an influence on the reaction, the use of 4-bromonicotinamide was envisaged, in order to compare the outcome with the 5-bromonicotinamide use presented above. However, 4-bromonicotinamide was not commercially available and attempts to prepare it from 4-bromonicotinic acid were not straightforward. The reaction with thionyl chloride followed by ammonium hydroxide resulted in very low yields (<25 %) of a non-separable mixture of 4-Br and 4-Cl products, as identified by ^{1}H NMR and mass spectrometry.
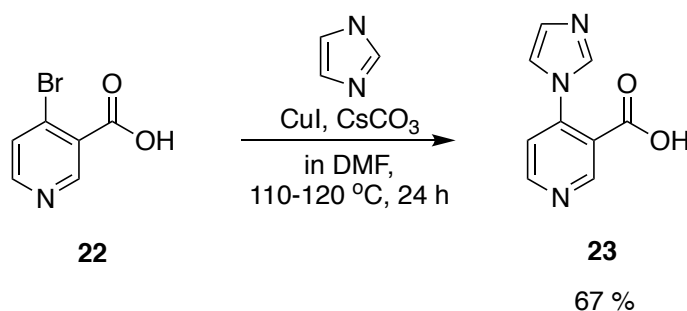

Figure 4.40. Ullmann coupling of imidazole with 4-bromonicotinic acid.

When 4-bromonicotinic acid was directly used as a coupling partner with imidazole, 4-(1*H*-imidazol-1-yl)nicotinic acid **23** was successfully synthesised in 67 % yield after purification by silica gel chromatography (Figure 4.40). Therefore, it was hypothesised that the bromo substitution was required for the reaction to proceed. Aryl chlorides are known to be less reactive substrates than aryl bromides in Ullman coupling reactions. However, oxidative addition of the "protected" 4-chloronicotinamide derivative **17b** to Cu(I) and further coupling to imidazole was successfully demonstrated in the previous section. It was unlikely that the tertiary amide substitution had such a dramatic effect on the reactivity of the aryl halide during oxidative addition.

Considering these results, it was hypothesised that the presence of the primary amide was not compatible with performing the Ullmann coupling at position 4 of the nicotinamide. The primary amide from a second nicotinamide molecule could act as a nucleophile at the place of imidazole; however, this was not observed in the crude NMR. On the other hand, intramolecular coordination of the amide group to the adduct formed from oxidative addition to Cu(I) could occur, thus blocking

coordination of the imidazole coupling partner. When the amide was protected by the bulky diisopropyl groups, this coordination might have been hindered (Figure 4.42).
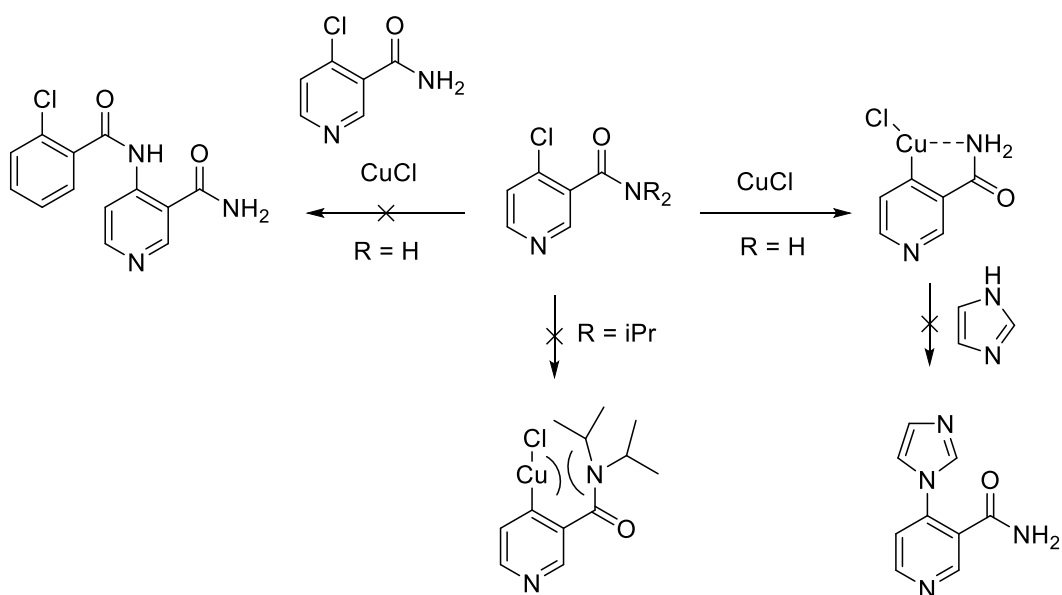

Figure 4.41. Suggested mechanism for the inhibition of Ullman coupling by intramolecular coordination of the Cu adduct to the primary nicotinamide functionality.

Benzylation of the 5-substituted compound **20a** was successfully performed with 4 equivalents of benzyl bromide to yield compound **21a** in 87 %, after precipitation and washing with diethyl ether. Given the difficulty in obtaining the 4-substituted compound **20b**, the synthesis of metal-complexes was only investigated starting from **21a**.

4.4.3.3 Metalation of 5-imidazolyl-nicotinamide ligand *21a*

The synthesis of benzylated NHC complexes of Rh / Ru / Ir is reported in the literature using two different methods.[201,25] The most effective route is the initial formation of the silver carbenoid (Ag(I)-NHC) by reaction with silver oxide, followed by transmetalation with the desired metal complex to achieve the final metal-NHC compound (Figure 4.42).[202] Advantages of this method are the selective binding of Ag(I) to the -N-CH-N- carbon of the imidazolium salt, the lack of additional base required to deprotonate the imidazolium and the broad tolerance for sensitive substituents, avoiding any unwanted side reactions or decomposition of the ligand.[203] An alternative method for NHC formation is the addition of a base to deprotonate the –N-CH-N- carbon.[203,204]
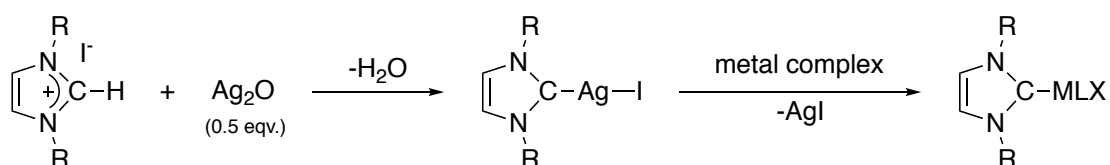
Figure 4.42. General outline for the synthesis of metal-NHC complexes *via* transmetalation with silver (I) oxide

Initial efforts focused on the metalation of ligand **21a** with [Rh(COD)Cl$_2$], in an attempt to reproduce the result previously reported by Colbran and co-workers for the synthesis of nicotinamide-NHC-metal complexes. The method used is outlined in Figure 4.42, with dichloromethane as the solvent. No reaction was observed when the progress of the reaction was monitored by TLC. Addition of the ligand to dichloromethane resulted in a cloudy suspension, suggesting its poor solubility. Before moving forward, the solubilities of the ligand and the metal precursor were assessed in various solvents (Table 4.26) The only solvent observed to fully dissolve both the ligand and Rh(I) complex was dimethylformamide (DMF). However, the reaction did not proceed in DMF. It was then decided to perform a thorough assessment of NHC formation and metalation reaction, using iridium catalysts. The choice of Ir precursors was due to their reported ability to catalyse imine reduction earlier.

Table 4.26. Qualitative solubility assessment of ligand 21a and of metal precursors in selected solvents.[a]

Solvents	Ligand 21a	[Rh(COD)Cl]$_2$
H$_2$O	soluble	not soluble
MeOH	soluble	partially soluble
CH$_2$Cl$_2$	partially soluble	soluble
Acetonitrile	not soluble	soluble
Acetone	not soluble	soluble
DMF	soluble	soluble
DMSO	soluble	not soluble

[a] 5mg of Rh(I) precursor was added to 0.5 mL solvent with stirring and further sonication (2 min) if ppt was observed. Solubility was observed by visual inspection.

Metalation was assessed with both Ir(III) and Ir(I) precursors. $[IrCp^*Cl_2]_2$ was fully soluble in MeOH, whereas $[Ir(COD)Cl]_2$ was only partially soluble, whilst the reverse was observed with CH_2Cl_2 as the solvent. Both the transmetalation with silver oxide and the base treatment and deprotonation were investigated by TLC throughout and NMR analysis of the final adduct, without intermediate isolation of the Ag(I) carbene, and the results are presented in Table 4.27.

Table 4.27. Summary of reaction conditions and outcomes of the metalation attempts of ligand 21a with Ir(I) and Ir(III) precursors.

Entry	Base[a]	Metal complex	Solvent	Outcome
1	Ag_2O	$[IrCp^*Cl_2]_2$	MeOH	No reaction
2	Ag_2O	$[IrCp^*Cl_2]_2$	CH_2Cl_2	No reaction
3	Ag_2O	$[IrCp^*Cl_2]_2$	CH_2Cl_2 / MeOH (5:1)	No reaction
4	Ag_2O	$[Ir(COD)Cl]_2$	MeOH	No reaction
5	Ag_2O	$[Ir(COD)Cl]_2$	CH_2Cl_2	No reaction
6	Ag_2O	$[Ir(COD)Cl]_2$	CH_2Cl_2 / MeOH (5:1)	No reaction
7	Ag_2O	$[Ir(COD)Cl]_2$	CH_2Cl_2 (*in situ*)[b]	No reaction
8	NaOAc	$[IrCp^*Cl_2]_2$	MeOH	Product present
9	*t*BuOAc	$[IrCp^*Cl_2]_2$	MeOH	Product present
10	NaOAc	$[Ir(COD)Cl]_2$	MeOH	No reaction
11	*t*BuOAc	$[Ir(COD)Cl]_2$	MeOH	No reaction

[a] Reaction conditions when Ag_2O was used: Ag_2O (0.5 eqv.), ligand **21a** (1.0 eqv.), metal complex (0.5 eqv.); when base was used: NaOAc/NaO*t*Bu (1.0 eqv.), KCl (6.7 eqv.), ligand **21a** (1.0 eqv.), metal complex (0.5 eqv.): All solvents were degassed. Entries 1-6: Ligand **21a** and Ag_2O added to desired solvent, suspension stirred r.t., 2 h under the exclusion of light. The suspension is then filtered into metal complex containing solvent and stirred at r.t., 12 h, followed by filtration and analysis. [b] The metal complex, ligand and Ag_2O were reacted in situ, entry 7 same process as above without the 1st filtration step, instead the metal complex was added to the reaction mixture after 2 h. Entries 8: Metal complex, base, KCl, ligand **21a** were stirred in MeOH at reflux, 16 h. Suspension then filtered on celite and purified by column chromatography.

No metalation was achieved with the silver oxide method. The poor solubility of the metal precursors in the reaction solvents could explain this. Previous literature suggested silver-induced oxidative degradation of the imidazolium precursor in certain cases,[205] which was also suggested by inspection of the crude ^{1}H NMR of the reaction mixtures containing the Ag(I)-NHC intermediate, and after transmetalation. A complete characterisation of the crude mixtures was difficult to perform, however most analyses showed a large amount of unreacted metal precursor.

On the other hand, the use of either NaOAc or Na*t*OBu for deprotonation were successful for metalation with IrCp*, with the presence of an identical Ir(III)Cp*-ligand complex obtained in both cases, confirmed by NMR and mass spectrometry. No metalation was observed with the [Ir(COD)Cl]$_2$ precursor, probably due to its poor solubility in MeOH. Both the successful IrCp* metalation methods contained impurities and required purification by silica gel chromatography. Isolation was only performed on the reaction mixture from Table 4.27, entry 9, because it contained less impurities. The final product was obtained in 28 % yield after purification.

Analysis of the [Ir(Cp*)**21a**] complex was performed by ^{1}H and ^{13}C NMR and by ESI-MS. Successful formation of the Ir-NHC complex was confirmed by the removal of the imidazolium proton (N-CH-N) at 9.68 ppm, and by the shift of the NHC carbon from 146.4 ppm in the imidazolium ligand, towards 165-170 ppm in the Ir-complex. However, the presence of two ^{13}C signals in the Ir-C region (167.6 and 170.7 ppm) suggested the formation of a second C-Ir bond. Cyclometallation by intramolecular C-H activation has previously been reported for NHC complexes in the presence of a tBuO$^-$ base. Four aromatic C-H positions were available for cyclometalation in the complexation of Ir(Cp*) with **21a**: two of these are on the nicotinamide ring, whilst the other two on the *N*-benzyl functionality of the NHC (Figure 4.43).

Careful inspection of the NMR data suggested that C-H insertion occurred at the nicotinamide ring, as suggested by the removal of one of the corresponding pyridinium protons at 10.1 ppm, as well as by the reduced multiplicity of the remaining protons, from multiplets to doublets. The remaining pyridinium signals shifted upfield, from 10.1 and 9.51, to 9.09 and 8.55, respectively, consistent with an Ir-C bond in the

meta position. This is supported by the fact that the aromatic C-H bond in the *ortho* or *para* position of the protonated nitrogen atom is more activated than the aromatic C-H bond on the benzyl group.
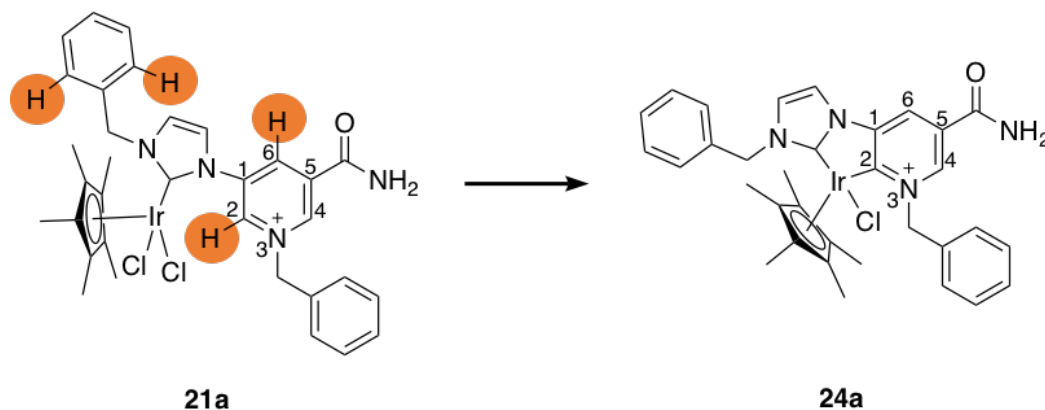
Figure 4.43. C-H activation of Ir-complex 21a

It was difficult to assert unambiguously, from this NMR structure, whether the insertion occurred at position 2 or 6 of the pyridinium ring. However, the ^{13}C signal at position 6 seems to be the same when comparing the ligand and the Ir-complex, suggesting cyclometallation at position 2, thus yielding **24a**. Interestingly, the CH$_2$ protons corresponding to the NHC *N*-benzyl group are diastereotopic, presenting two doublets at 5.53 and 5.47 ppm, consistent with previous work.

Figure 4.44. ^{1}H **NMR analysis of cyclometallated complex** 24a.

In conclusion, an NHC carbene precursor was introduced at the 5-position of benzylnicotinamide, to yield **21a** in reasonable yields. Substitution at the 4-position of benzylnicotinamide proved difficult under the conditions tested. On the other hand, metalation of the 5-substituted ligand **21a** resulted in a new Ir-NHC complex **24a**, which underwent cyclometalation at position 6, it is thought. Whilst this structure was less flexible than the initially d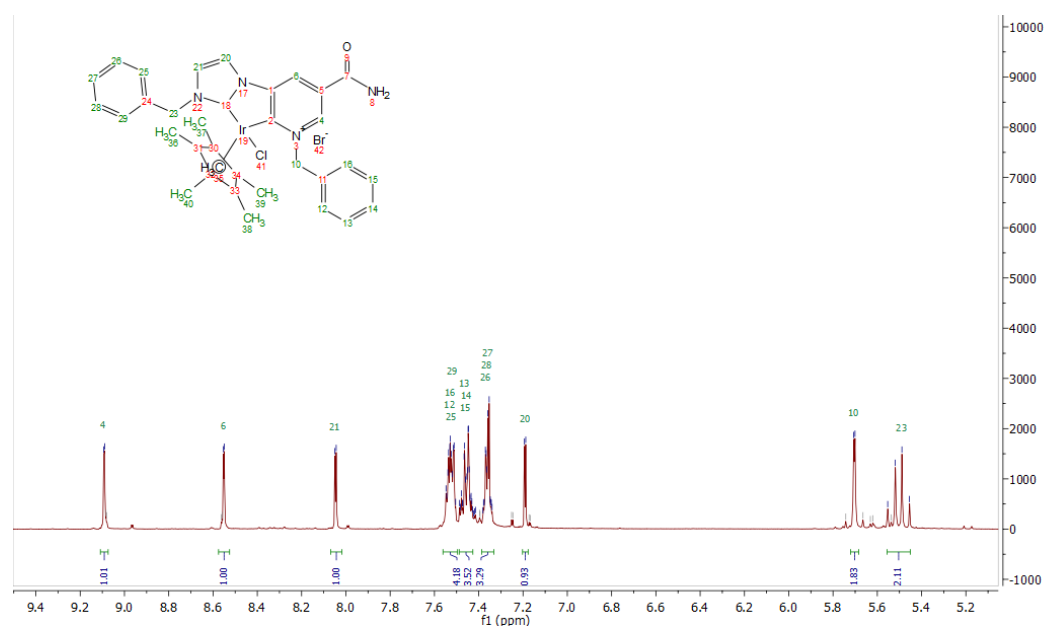esigned complexes, it was decided to investigate its activity towards ketone and imine reduction, in the presence and in the absence of TADH.

4.4.4 Transfer hydrogenation of ketones and of imines by an iridium complex of a nicotinamide-functionalised N-heterocyclic carbene

Preliminary investigations into the ability of **24a** to catalyse ketone and imine reduction were performed under both organic and aqueous transfer hydrogenation conditions. Isopropanol was employed as the solvent and source of hydrogen in the organic reaction, while a buffer solution containing sodium formate provide the hydride in aqueous reactions. Model ketone and imine substrates were acetophenone **25,** 3,4-dihydroisoquinoline **2**, and 2-methyl-1-pyrroline **1**. The conversions were approximated by ^{1}H NMR analysis of the final reaction mixtures as a result of the ratio of integration of the starting material to the product.
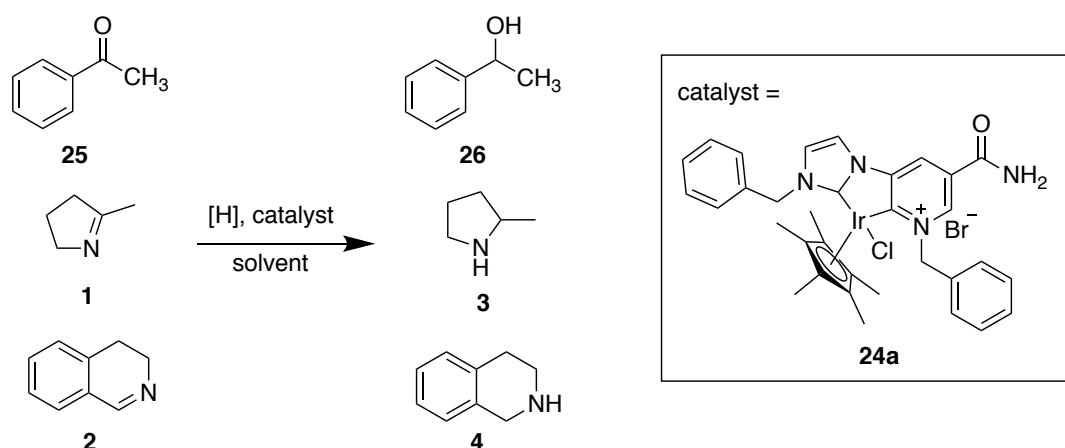
organic conditions: [H] = *i*PrOH / Na*t*OBu; solvent = *i*PrOH
aqueous conditions: [H] = HCOONa; solvent = MOPS buffer containing HCOONa

Figure 4.45. Transfer hydrogenation reactions of acetophenone (25), 2-methyl-1-pyrroline (1) and 2,3-dihydroisoquinoline (2) catalysed by 24a in organic and aqueous media.

4.4.4.1 Transfer hydrogenation of ketones and imines using 24a in organic solvent

Complex **24a** was investigated for the transfer hydrogenation of acetophenone using standard conditions found in literature reports with an isopropanol / Na*t*OBu mixture. The reaction proceeded with 76 % conversion (Table 4.28, entry 1). No side products were observed by ^{1}H NMR. When the substrates and reagents were diluted, to increase compatibility with enzyme presence in subsequent experiments, conversion decreased to 21 % (Table 4.28, entry 2). Transfer hydrogenation of 3,4-dihydroisoquinoline **2** at low concentration yielded a similar conversion of 24 % (Table 4.28, entry 3). On the other hand, no reaction was observed when 2-methyl-1-pyrroline **1** was used. These results demonstrated that the new Ir-NHC complex was active for transfer hydrogenation reactions to ketones and imines. No attempts were made to optimise the conversions. Instead, the activity of the complex in aqueous conditions was tested.

Table 4.28. Transfer hydrogenation of acetophenone (25), 3,4-dihydroisoquinoline (2) and 2-methyl-1-pyyroline (1) with the nicotinamide-functionalised Ir-NHC complex 24a in organic solvent.

Entry	Substrate	Substrate concentration	Conversion (%)[a]
1	acetophenone	3 M	76[b]
2	acetophenone	0.3 M	21
3	3,4-dihydroisoquinoline	0.3 M	24
4	2-methyl-1-pyrroline	0.3 M	0

The reaction was performed at reflux, under N_2 for 24 h containing substrate (0.15 mmol, 300 mM), 10 mol % NaO*t*Bu (0.015 mmol), 1 mol % Ir complex **24a** (0.3 mM, final conc.) in *i*PrOH (0.5 mL). After completion solvent removed and products sent for NMR analysis. [a] Conversions calculated as a percentage of products : oxidised / reduced substrate ratio based upon the integration of specific signals in ^{1}H-NMR. [b] reaction containing substrate (1.5 mmol, 3 M), 10 mol % NaO*t*Bu (0.015 mmol), 1 mol % Ir complex **24a** (3 mM, final conc.) in *i*PrOH (3 mL).

4.4.4.2 Transfer hydrogenation of ketones and imines using 24a in aqueous solvent

Following from the encouraging results observed for hydrogen transfer in organic conditions, complex **24a** was investigated as a catalyst for the same reactions in aqueous conditions. To enhance solubility of both **24a** and the substrates in the aqueous reaction solvent, stock solutions were prepared in DMF, at a final

concentration of the organic solvent in the reaction of 4-7 % (v / v). Under these conditions, reduction of ketone to the corresponding alcohol occurred with a 19 % conversion, similar to the result obtained in organic solvent (Table 4.29, entry 1). Encouragingly, 100 % conversion was observed with imine substrate **2** (Table 4.29, entry 2). On the other hand, no conversion was seen with 2-methyl-1-pyrroline **1**.

Table 4.29. Transfer hydrogenation of acetophenone (25), 3,4-dihydroisoquinoline (2) and 2-methyl-1-pyrroline (1) with the nicotinamide-functionalised Ir-NHC complex 24a in aqueous solvent.

Entry	Substrate	Organic solvent (% v / v)	Conversion (%)[a]
1	acetophenone	4 % DMF	19
2	3,4-dihydroisoquinoline	7 % DMF	100
3	2-methyl-1-pyrroline	4 % DMF	0
4	acetophenone	4 % ACN	0
5	3,4-dihydroisoquinoline	5 % ACN	100
6	2-methyl-1-pyrroline	4 % ACN	0

The reaction was performed at 55 $^\circ$C, under N_2 for 24 h: entries **1-3** containing substrate (0.15 mmol, 300 mM), 1 mol % Ir complex **24a** (0.3 mM, final conc.) in 1.2 M MOPS containing 3 M sodium formate (0.5 mL) and entries **4-6** containing substrate (1.25 μmol, 2.5 mM), 1 mol % Ir complex **24a** (0.0025 mM, final conc.) in 0.4 M MOPS containing 1 M sodium formate (1 mL). After completion products extracted with $CHCl_3$ (4 x 3 mL), dried and sent for NMR analysis. [a] Conversions calculated as a percentage of products : oxidised / reduced substrate ratio based upon the integration of specific signals in ^{1}H-NMR.

The substrate concentrations used for these reactions were too high to be used in the presence of the enzyme, which was objective of this section. Moreover, acetonitrile was highlighted in an earlier section as the solvent with the least effect on TADH activity, in contrast to DMF, which inhibited the reaction. Therefore, a second set of transfer hydrogenation reactions were performed using ACN as the co-solvent to aid substrate solubilisation, and at a substrate concentration >100 times lower compared to the initial experiments. Under these conditions, no conversion was obtained with acetophenone (This was thought to occur because of the low solubility of the ketone substrate in acetonitrile, which resulted in a cloudy reaction mixture throughout. On

the other hand, the imine substrate **2** was observed to undergo full conversion.) It is possible that the difference between the results was due to the higher reactivity of the Ir-catalyst for imine reduction, compared to the ketone counterpart. The result obtained with the imine was most encouraging, as for the purposes of this study, catalyst **24a** was required to react efficiently in mild conditions in order to be used in conjunction with TADH.

*4.4.4.3 Transfer hydrogenation of ketones and imines using **24a** in the presence of TADH*

Next, investigations into hydrogen transfer reactions catalysed by **24a** were performed in the presence of TADH (Table 4.30). Reactions were performed with the addition of ACN (4-5 %) as co-solvent. Again, no reaction was observed with acetophenone **25** or 2-methyl-1-pyrroline **1** as substrates whilst full conversion was observed for the transfer hydrogenation of 3,4-dihydroisoquinoline **2.** This suggested that TADH did not act as an inhibitor of the reaction under these concentrations. This was an interesting result, given that previous reports suggested mutual inactivation between TADH and [Cp*Rh(bipyridine)Cl] catalyst.[111]

Table 4.30. Transfer hydrogenation of acetophenone (25), 3,4-dihydroisoquinoline (2) and 2-methyl-1-pyrroline (1) with the nicotinamide-functionalised Ir-NHC complex 24a in the presence of TADH.

Entry	Substrate	Organic solvent (% v / v)	Conversion (%)[a]
1	acetophenone	4 % ACN	0
2	3,4-dihydroisoquinoline	5 % ACN	100
3	3,4-dihydroisoquinoline	5 % ACN	100[b]
4	2-methyl-1-pyrroline	4 % ACN	0
5	2-methyl-1-pyrroline	4 % ACN	0[b]

The reaction was performed at 55 $^{\circ}$C, under N_2 for 24 h containing substrate (1.25 μmol, 2.5 mM), 1 mol % Ir complex **24a** (0.0025 mM, final conc.) and TADH (0.0025 mM final conc.) in 0.4 M MOPS containing 1 M sodium formate (1 mL). After completion products extracted with $CHCl_3$ (4 x 3mL), dried and sent for NMR analysis. [a] Conversions calculated as a percentage of products : oxidised / reduced substrate ratio based upon the integration of specific signals in ^{1}H-NMR. [b] additionally containing NADH (2.5 mM final conc.)

In conclusion, a novel iridium complex, **24a** was shown to catalyse hydrogen transfer of acetophenone **25** and 3,4-dihydroiisoquinoline **2** under both organic and aqueous conditions. The imine was preferred as a substrate, yielding quantitative conversions even at low substrate concentrations catalyst. However, the 5-membered ring aliphatic imine, 2-methyl-1-pyrroline **1** was not converted. The catalyst was shown to perform effectively in the presence of TADH, however the performance was unaffected in the presence of NADH, suggesting no affinity for the co-factor binding pocket.

To investigate the affinity of the iridium complex for TADH, kinetic studies were performed, where the inhibition of TADH activity was determined with both the Ir-complex **24a** and the corresponding ligand **21a**.

4.4.5 Inhibition studies of TADH by nicotinamide-functionalised ligand and metal complex

Preliminary studies were performed, where Michaelis-Menten kinetics were determined with varying cofactor concentrations in the presence of the metal complex **24a** or of the ligand **21a**, in order to assess whether inhibition occurs. Binding of the modified nicotinamide mimics to the cofactor-binding site would lead to reversible competitive inhibition that would increase K_M, thus lowering the affinity for the cofactor, but would not affect V_{max}. Investigations were performed in the reduction direction with cyclohexanone (500 mM) and NADH (0.5-12.5 mM) as the substrates, and with **21a** or **24a** (0.05-0.25 mM) as inhibitors. A control was also performed in the absence of NADH to confirm **21a** and **24a** had no interfering absorbances at 340 nm.

4.4.5.1 Inhibition studies with nicotinamide-functionalised ligand 21a

Given the poor solubility of ligand **21a**, these experiments were performed with the addition of 2 % DMSO in the reaction mixture, which was required in order to solubilise the ligand. DMSO was reported to act as an inhibitor for HLADH and TbADH. (Section *4.2.2.1*), However the impact of 2 % (v / v) DMSO was relatively low, with 42 % of the activity retained. Michaelis-Menten kinetics was performed in the absence and in the

presence of ligand **21a** as an inhibitor at concentrations of 0.1 mM and 0.25 mM, and the results were used to produce a Lineweaver-Burk (Figure 4.46) and Michaelis-Menten plot (Appendix 7), from which the K_M and V_{max} values were calculated and compared (Table 4.31).
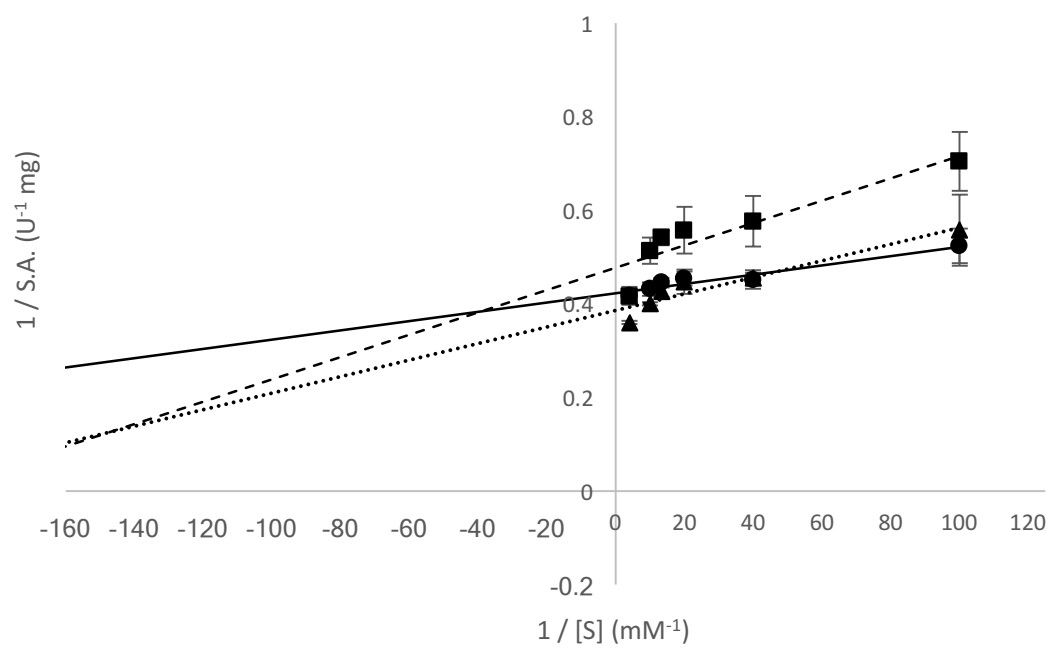
Figure 4.46. Lineweaver-Burk plot illustrating the inhibitory effect of nicotinamide-functionalised ligand 21a in the reductive direction using NADH and cyclohexanone as substrates. Specific activities were determined in the reductive direction at 60 °C, using TADH (5.6 μg), NADH (0.01, 0.025, 0.05, 0.075, 0.1, 0.25 mM) as substrate, cyclohexanone (20 mM) as secondary substrate, in 50 mM Bis-Tris buffer pH 6.0 containing 2 % v/v DMF with nicotinamide-functionalised ligand, **21a** as inhibitor at concentration: (●) 0 mM , (▲) 0.1 mM, (■) 0.25 mM.

The data from Table 4.31 showed irregular trends for these inhibition studies, although relatively low errors were obtained from triplicate experiments, showing that the results were reproducible. The typical trends expected for competitive inhibition were not observed. From the K_M and V_{max} calculated values (Table 4.31), it appeared that V_{max} remained relatively unchanged irrespective of the inhibitor concentration, while K_M was observed to increase as the ligand concentration increased. This hinted towards possible competitive binding of the ligand at the cofactor binding site. To explain the irregular trends observed during the kinetics, it was hypothesised that the low solubility of the ligand in the reaction mixture may have skewed the results.

Table 4.31. Comparison of V_{max} and K_M obtained for NADH in the presence of different concentrations of 21a.

Inhibitor concentration (mM)	V_{max} (μM / min)	K_M (mM)
0	2.36 ± 0.034	0.00232 ± 0.00042
0.1	2.62 ± 0.064	0.00497 ± 0.00093
0.25	2.17 ± 0.078	0.00617 ± 0.0015

Specific activities were determined in the reductive direction at 60 ^{o}C, using TADH (5.6 μg), NADH (0.01, 0.025, 0.05, 0.075, 0.1, 0.25 mM) as substrate, cyclohexanone (20 mM) as secondary substrate, in 50 mM Bis-Tris buffer pH 6.0 containing 2 % v / v DMF with nicotinamide-functionalised ligand, **21a** as inhibitor (0, 0.1, 0.25 mM.) Michaelis-Menten plot is present in Appendix 7.

*4.4.5.2 Inhibition studies with nicotinamide-functionalised Ir-NHC catalyst **24a***

The same inhibition experiments performed with the ligand were repeated in the presence of the Ir-NHC complex **24a**. Inhibition was observed at lower concentrations of the Ir-NHC complex, and experiments were performed at the lower inhibitor concentrations of 0.1 mM and 0.05 mM. The solubility of **24a** in acetonitrile was higher, allowing the use of this solvent in the reaction mixture at 5 % (v / v). The kinetics results were used to produce a Lineweaver-Burk plot (Figure 4.47), and Michaelis-Menten plot (Appendix 8), from which the K_M and V_{max} values were calculated and compared (Table 4.32).

In comparison to the results obtained with ligand **21a**, inhibition studies with the Ir-NHC complex **24a** showed clear and reproducible trends corresponding to mixed inhibition. The K_M was observed to increase, whereas the V_{max} decreased with increasing concentration of Ir-NHC. This type of inhibition suggests binding of the inhibitor at a different site from the cofactor binding site.

The increased K_M suggested that the Ir complex inhibited the binding of the NADH cofactor, because more NADH was required to reach half V_{max}. However, the decreased V_{max} suggested that NADH could not outcompete the inhibitor binding at high concentrations. In contrast to competitive binding, where the inhibitor occupies the substrate-binding pocket and does not allow it to bind, the observed mixed

inhibition suggested that NADH could still bind to the enzyme-inhibitor complex, but the conversion to product was inhibited. This was possibly as a result of the Ir-catalyst binding elsewhere to the enzyme, such as in the proximity of the ketone-binding site.
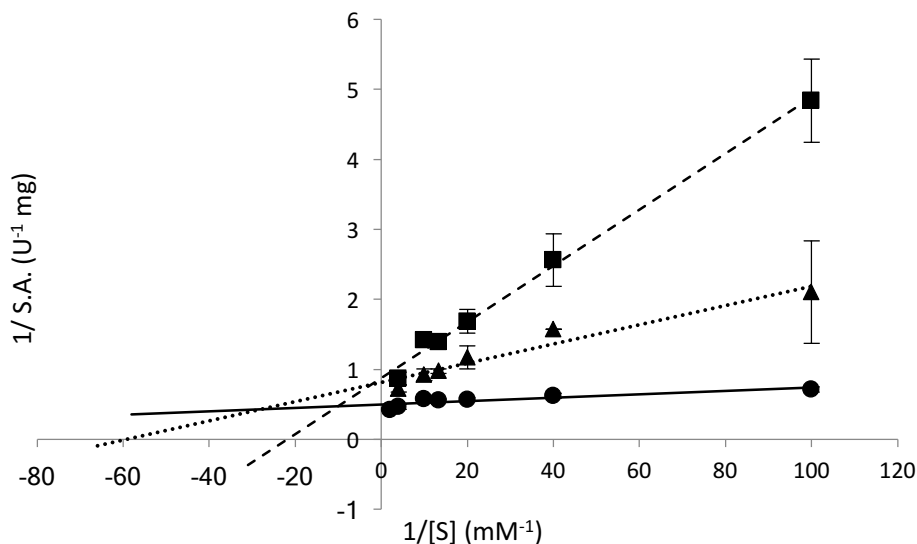
Figure 4.47. Lineweaver-Burk illustrating the inhibitory effect of Ir complex (24a) in the reductive direction using NADH and cyclohexanone as substrates. Specific activities were determined in the reductive direction at 60 $^{\circ}$C, using TADH (5.6 μg), NADH (0.01, 0.025, 0.05, 0.075, 0.1, 0.25 mM) as substrate, cyclohexanone (20 mM) as secondary substrate, in 50 mM Bis-Tris buffer pH 6.0 containing 5 % v/v ACN with Ir complex, **24a** as inhibitor at concentration: ($\bullet$) 0 mM , ($\blacktriangle$) 0.05 mM, ($\blacksquare$) 0.1 mM.

This study showed that both the ligand and Ir catalyst interacted with TADH to decrease its natural activity. However, they also suggested that binding of the nicotinamide-functionalised Ir-NHC complex **24a** does not occur at the NADH binding site.

Table 4.32. Comparison of V_{max} and K_M obtained for NADH in the presence of different concentrations of (24a)

Inhibitor concentration (mM)	V_{max} (μM / min)	K_M (mM)
0	1.98 ± 0.059	0.00484 ± 0.0011
0.05	1.49 ± 0.083	0.0311 ± 0.0059
0.1	1.47 ± 0.11	0.0785 ± 0.013

Specific activities were determined in the reductive direction at 60 $^{\circ}$C, using TADH (5.6 μg), NADH (0.01, 0.025, 0.05, 0.075, 0.1, 0.25 mM) as substrate, cyclohexanone (20 mM) as secondary substrate, in 50 mM Bis-Tris buffer pH 6.0 containing 5 % v / v ACN with Ir complex, **24a** as inhibitor at (0, 0.05, 0.1 mM.); Michaelis-Menten plot is present in Appendix 8.

4.4.5 Conclusions

Two nicotinamide-functionalised *N*-heterocyclic ligand scaffolds were designed as precursors to Ir-complexes to be introduced in TADH. In these scaffolds, benzyl nicotinamide was used as an anchor with affinity for ADH, and connection with the NHC was envisaged at positions 4 and 5 of the nicotinamide ring, to allow orientation of the resulting complex towards the substrate-binding pocket in TADH.

Synthesis of the 5-imidazoyl-functionalised benzylated nicotinamide ring was successfully achieved, and the resulting [(Cp*)Ir(NHC)] complex was formed. Cyclometalation was observed at position 6 of the nicotinamide ring, and the resulting Ir-complex structure was elucidated by NMR and MS studies. On the other hand, the functionalisation at position 4 of the nicotinamide ring with a NHC precursor was unsuccessful, due to the inefficiency of the key Ullmann coupling step. Intramolecular coordination of the non-protected nicotinamide to the Cu catalyst was suggested to be responsible for this result.

The nicotinamide-functionalised [(Cp*)Ir(NHC)] complex was shown to be an active catalyst in the transfer hydrogenation of aryl ketones (acetophenone) and imines (3,4-dihydroisoquinoline). Similar conversions (~20 %) were obtained for the two substrates in organic solvent, using isopropanol as hydride donor. On the other hand, the activity towards the imine substrate was much higher in aqueous buffer, using sodium formate.

Inhibition studies showed that the Ir-catalyst interfered with the enzyme kinetics, acting as a mixed inhibitor for the enzyme when NADH concentration was varied. Whilst the catalyst remained active in the presence of TADH, no decrease in conversion was observed upon NADH addition. Taken together, these results suggested that the nicotinamide-functionalised catalyst did not bind at the cofactor-binding site.

Chapter 5 Conclusions and perspectives

This thesis presents the attempts at both genetic and chemical modification of the active site of a thermostable alcohol dehydrogenase, to introduce reaction promiscuity towards imine reduction. The results obtained allowed an increase in the understanding of how imines interact with the active site of alcohol dehydrogenases. Variants of TADH containing protic residues in the active site were successfully designed. Rh-containing TADH variants were also prepared, however the precise localisation of the Rh at the place of the catalytic zinc was not determined. Imine reduction activity was not identified in any of the modified enzymes, under the conditions employed. In a different approach, a novel iridium(III) complex bearing a nicotinamide anchor was designed for introduction into TADH, and showed imine reduction activity in the presence of the enzyme. However, based on inhibition studies, it was suggested that this complex was not incorporated into the cofactor-binding site of TADH.

Preliminary experiments, outlined in Chapter 4.1, were concerned with the choice of a thermostable protein as a starting point for this work, and with the development of expression and purification methods, based on literature reports. ADH from *Thermus* sp. ATN1 was selected based on its stability and broad substrate range. Some issues were observed with reproducing the TADH preparation as characterised in the literature. Expression of TADH was successfully achieved in *E. coli,* after growth at 30 $^{\circ}$C and induction with 0.4 mM IPTG at 30 $^{\circ}$C. A heat purification step was applied at 80 $^{\circ}$C for 20 min, yielding relatively pure protein, as estimated by SDS-PAGE. The zinc content of this protein was observed to be lower than expected by ICP-MS. Size exclusion purification did not replicate the increased activity observed in the literature, although the zinc content was seen to increase to 1 : 1.6, still lower than the expected 1 : 2 protein : zinc ratio. The resulting TADH showed kinetic parameters similar to the ones reported in the literature.

In Chapter 4.2, the interaction of TADH with two selected cyclic imines, 5-membered ring 2-methyl-1-pyrroline **1** and 6-membered ring 3,4-dihydroisoquinoline **2**, was characterised by inhibition studies and by computational (docking) methods. First,

TADH was observed to maintain activity with the ketone / aldehyde precursors of the two imines. Despite the reduced activities observed with both 2-ethylbenzaldehyde and 2-pentanone (4-5 % remaining activity compared to cyclohexanone), the results demonstrated that architectures similar to the cyclic imine substrates could fit into the active site. Preliminary inhibition studies with imines and their reduced amines illustrated complete inhibition of TADH by the 6-membered structures (**2** and **4**) at concentrations equal to the substrate. Inhibition kinetics with the 5-membered cyclic imine **1** and reduced amine **3** showed mixed inhibition for these compounds, suggesting that inhibitor and substrate-binding sites were different. For example, imines might bind at the place of NADH, and / or at another position within the active site. The amine compound was shown to have inhibitory effect at lower concentrations compared to the imine, thus suggesting a possible interaction with the catalytic zinc.

Furthermore, docking studies of imines **1** and **3** inside cofactor-bound TADH confirmed the possibility of their acceptance in the active site. Their preferred orientation was similar to that of a docked model ketone, within range for both proton and hydride transfer, while the imine nitrogen atom pointed towards the catalytic zinc. In the presence of the ketone, imines docked in a separate cavity, adjacent to the substrate-binding pocket. In the absence of NADH, imine **2** was bound in the cofactor-binding site, whereas imine **1** was bound at the active site, in proximity of zinc. For a better understanding of imine interaction within ADHs, further inhibition studies with NADH as substrate should also be performed, to assess whether imines act as inhibitors of the cofactor-binding. Additionally, a crystal structure with a bound inhibitor would give a clear idea of the interaction of imines and amines with TADH.

Also in chapter 4.2, the active site of TADH was engineered to remove the catalytic zinc, and to introduce a protic acid at various positions, in an effort to replicate the imine reductase active site. While the mutants were successfully expressed and purified, no imine reduction was observed. It was thought that site-directed mutagenesis was not suited for introduction of imine activation, because it could not reconstitute the interplay between parameters that can affect reactivity, such as substrate orientation, active residue pKa and pH of the system. An alternative

approach would be a semi-directed evolution, simultaneously targeting the active site residues. Perhaps a more successful approach would be to target short chain dehydrogenase / reductases as a starting point for engineering, which instead of zinc show the critical presence of a catalytic triad, thus enabling acid / base catalysis. In particular, the presence of this triad hints that not only the acidic residue is important at the correct position for substrate activation, but also the environment around this residue, which promotes proton transfer by modulating the pKa. In support of this, recent studies of IRED mechanism[206,73] have discovered non-protic residues such as alanine, phenylalanine and asparagine in the key position for substrate activation to possess activity.

Investigations into rhodium(I) replacement of the catalytic zinc(II) could not identify a robust and reproducible method, as highlighted in Chapter 4.3. The limiting factor was identified as the zinc removal step, which was complicated by the presence of two zinc ions, one catalytic and one structural. The best conditions for zinc removal were by dialysis against 1,2-phenantroline or a mixture of 1,2-phenantroline and EDTA, at pH 6.0. These resulted in almost complete loss of specific activity, and partial loss of zinc. Protein loss was also observed during these experiments, and might have been due to the instability of the protein in the absence of zinc. Encouragingly, activity, zinc content and protein concentration all increased upon zinc reinsertion by dialysis against a buffer solution containing zinc acetate (20 μM) at pH 6.5 and 4 °C. This suggested that most of the zinc removed, and thus reinserted, was from the catalytic site. Cobalt(II) was inserted into apo-TADH and resulted in recovery of 82 % of the initial activity. Binding of Rh(I) was also observed to occur, however unspecific binding was seen by the presence of excess (2.6-fold) protein, and the binding of Rh at the catalytic site was not confirmed. Some residual alcohol oxidation was observed with the Rh-protein, but no imine reductase activity was observed for the reduction of 2-methyl-1-pyyroline **1**.

To improve these results, metal replacement investigations could be performed on single zinc-containing thermophilic ADHs such as TbADH, which does not possess a structural zinc and where successful zinc removal and metal reinsertion methods have

also been reported. Alternatively, selective removal of the catalytic zinc ions could be further attempted using a crystallised version of TADH, as previously suggested by others for HLADH. Conditions for the crystallisation of TADH were published during the course of this thesis, and could be adapted to this effect.

The design of transition metal complexes bound to an NAD$^+$ mimic was presented in Chapter 4.4, and was based upon the observed ADH recognition of NAD$^+$ analogues.[116] Two nicotinamide-functionalised N-heterocyclic bound Ir complexes were designed for introduction into TADH, differing at the point of attachment between the NHC and nicotinamide ring. Positions 4 and 5 (relative to the nitrogen atom) of the nicotinamide ring were investigated for NHC connection, envisioning that the resulting orientation would present the metal complex towards the substrate-binding pocket in TADH. Synthesis of the 5-imidazoyl-functionalised benzylated nicotinamide ring was successfully achieved, whereas the functionalisation at position 4 of the nicotinamide ring with a NHC precursor was unsuccessful as a result of the inefficiency of Ullmann coupling at this position. This was suggested to be a result of intramolecular coordination of the primary nicotinamide to the Cu catalyst. Future investigations into Ullmann coupling at this position could focus on using an amide protecting group during the coupling, which would complicate the synthesis, but might improve the coupling results.

Complexation of the [Cp*Ir(III)Cl$_2$]$_2$ precursor to the 5-imidazoyl-functionalised benzylated nicotinamide ring was successfully achieved, however low yields were recovered after purification. The isolated compound was observed to undergo cyclometalation, which was suggested to occur at position 6 of the nicotinamide ring. The nicotinamide-functionalised [(Cp*)Ir(NHC)] complex was shown to be an active catalyst in the transfer hydrogenation of aryl ketones (acetophenone) and imines (3,4-dihydroisoquinoline) in both organic and aqueous media. The imine 3,4-dihydroisoquinoline outperformed acetophenone in aqueous conditions. The catalyst was active in the presence of TADH, however the addition of NADH did not show any inhibition, suggesting that the complex was not found in the cofactor-binding pocket. Inhibition studies also showed that the complex was not likely to bind at the cofactor-binding site, although it did act as a mixed inhibitor. Further studies are required to

confirm this lack of interaction. In particular, the enantioselectivity of the reaction should be determined, in order to assess whether TADH has any effect on the catalysis. Additionally, the interaction of the Ir-NHC catalyst with NADH should also be investigated. Hydride transfer from NADH to an Ir(III) cyclometalated complex has previously been reported, and might be responsible for the inhibition results obtained with the Ir-complex.

The affinity of benzyl nicotinamide mimics is currently a subject of debate in the scientific community, with two research groups reporting contradicting results with respect to their activity towards ADHs. Affinity studies should be performed with benzyl nicotinamide and TADH, to ascertain the interaction of this anchor with the enzyme. The use of other pyridinium substituents, such as ribose, might prove beneficial to increase this affinity. The group of Hollmann reported micromolar affinity of substituted nicotinamide for enoate reductases, and these could constitute an alternative starting point to engineer imine reduction promiscuity inside a reductase with a different functionality.

In conclusion, this thesis provided an insight into the chemical and genetic modification of TADH for promiscuity towards imines. Continued efforts in enzyme engineering will provide a better understanding on the IRED activity, to provide a robust and efficient method for the synthesis of chiral secondary amines.

Chapter 6 References

1.   Patel, R. N.; *Biocatalysis in the Pharmaceutical and Biotechnology Industries.* CRC Press LLC: Boca Raton, Florida, 2007, pp 743-755.

2.   Herbert, R. B., *The Biosynthesis of Secondary Metabolites*. 2nd ed.; Chapman and Hall: London, 1989, pp 1-178.

3.   Harvey, A., *Drug Discovery Today* **2008,** *13*, 894-901.

4.   Cassiano, N. M., *Alkaloids: Properties, Applications and Pharmacological Effect:*. Nova Science Publishers, Inc.: New York, 2010, pp 1-185.

5.   Newman, D. J.; Cragg, G. M., *J. Nat. Prod.* **2012,** *75*, 311-335.

6.   Breuer, M.; Ditrich, K.; Habicher, T.; Hauer, B.; Kesseler, M.; Sturmer, R.; Zelinski, T., *Angew. Chem., Int. Ed.* **2004,** *43*, 788-824.

7.   Nugent, T.; El-Shazly, M., *Adv. Synth. Catal.* **2010,** *352*, 753-819.

8.   Constable, D.; Dunn, P. J.; Hayler, J. D.; Humphrey, G. R.; Leazer, J. L.; Linderman, R. J.; Lorenz, K.; Manley, J.; Pearlman, B. A. *et al.*, *Green Chem.* **2007,** *9*, 411-420.

9.   Levi, A.; Modena, G.; Scorrano, G., *J. Chem. Soc., Chem. Commun.* **1975**, 6-7.

10. James, B., *Catal. Today* **1997,** *37*, 209-221.

11. Bakos, J.; Orosz, A.; Heil, B.; Laghmari, M.; Lhoste, P.; Sinou, D., *J. Chem. Soc., Chem. Commun* **1991**, 1684-1685.

12. Fleury-Bregeot, N.; De La Fuente, V.; Castillon, S.; Claver, C., *ChemCatChem* **2010,** *2*, 1346-1371.

13. Blaser, H.; Buser, H.; Jalett, H.; Pugin, B.; Spindler, F., *Synlett* **1999**, 867-868.

14. Wang, C.; Villa-Marcos, B.; Xiao, J., *Chem. Commun.* **2011,** *47*, 9773-9785.

15. Fujii, A.; Hashiguchi, S.; Uematsu, N.; Ikariya, T.; Noyori, R., *J. Am. Chem. Soc.* **1996,** *118*, 2521-2522.

16. Hashiguchi, S.; Fujii, A.; Takehara, J.; Ikariya, T.; Noyori, R., *J. Am. Chem. Soc.* **1995,** *117*, 7562-7563.

17. Li, L.*;* Wu, J. S.; Wang, F.; Liao, J.; Zhang, H.; Lian, C. X.; Zhu, J.; Deng, J. G., *Green Chem.* **2007,** *9*, 23-25.

18. Haack, K. J.; Hashiguchi, S.; Fujii, A.; Ikariya, T.; Noyori, R., *Angew. Chem., Int. Ed.* **1997,** *36*, 285-288.

19.   Yamakawa, M.; Ito, H.; Noyori, R., *J. Am. Chem. Soc.* **2000,** *122*, 1466-1478.

20.   Uematsu, N.; Fujii, A.; Hashiguchi, S.; Ikariya, T.; Noyori, R., *J. Am. Chem. Soc.* **1996,** *118*, 4916-4917.

21.   Koike, T.; Ikariya, T., *Adv. Synth. Catal.* **2004,** *346*, 37-41.

22.   Wills, M., *Top. Curr. Chem.* **2016,** *374,* 1-36.

23.   Diez-Gonzalez, S.; Marion, N.; Nolan, S., *Chem. Rev.* **2009,** *109*, 3612-3676.

24.   Gulcemal, S.; Gokce, A.; Cetinkaya, B., *Inorg. Chem.* **2013,** *52*, 10601-10609.

25.   Zhu, X.; Cai, L.; Wang, C.; Wang, Y.; Guo, X.; Hou, X., *J. Mol. Catal. A: Chem.* **2014,** *393*, 134-141.

26.   Noyori, R.; Hashiguchi, S., *Acc. Chem. Res.* **1997,** *30*, 97-102.

27.   Noyori, R.; Yamakawa, M.; Hashiguchi, S., *J. Org. Chem.* **2001,** *66*, 7931-7944.

28.   Prokopchuk, D. E.; Morris, R. H., *Organometallics* **2012,** *31*, 7375-7385.

29.   Prokopchuk, D. E.; Sonnenberg, J. F.; Meyer, N.; Zimmer-De Iuliis, M.; Lough, A. J.; Morris, R. H., *Organometallics* **2012,** *31*, 3056-3064.

30.   Ikariya, T.; Murata, K.; Noyori, R., *Org. Biomol. Chem.* **2006,** *4*, 393-406.

31.   Joseph, S. M.; Samec, J. S.; Bäckvall, J. E.; Andersson, P. G.; Brandt, P., *Chem. Soc. Rev.* **2006,** *35*, 237-248.

32.   Bullock, R. M., *Chem. Eur. J.* **2004,** *10*, 2366-2374.

33.   Wang, C.; Li, C.; Wu, X.; Pettman, A.; Xiao, J., *Angew. Chem., Int. Ed.* **2009,** *48*, 6524-6528.

34.   Guan, H.; Iimura, M.; Magee, M.; Norton, J.; Zhu, G., *J. Am. Chem. Soc.* **2005,** *127*, 7805-7814.

35.   Magee, M.; Norton, J., *J. Am. Chem. Soc.* **2001,** *123*, 1778-1779.

36.   Wu, X.; Xiao, J., *Chem. Commun.* **2007**, 2449-2466.

37.   Bubert, C.; Blacker, J.; Brown, S. M.; Crosby, J.; Fitzjohn, S.; Muxworthy, J. P.; Thorpe, T.; Williams, J. M. J., *Tetrahedron Lett.* **2001,** *42*, 4037-4039.

38.   Thorpe, T.*;* Blacker, J.; Brown, S. M.; Bubert, C.; Crosby, J.; Fitzjohn, S.; Muxworthy, J. P.; Williams, J. M. J., *Tetrahedron Lett.* **2001,** *42*, 4041-4043.

39.   Shende, V. S.; Deshpande, S. H.; Shingote, S. K.; Joseph, A.; Kelkar, A. A., *Org. Lett.* **2015,** *17*, 2878-2881.

40.	Ogo, S.; Abura, T.; Watanabe, Y., *Organometallics* **2002,** *21*, 2964-2969.

41.	Wu, X. F.; Li, X. G.; King, F.; Xiao, J., *Angew. Chem., Int. Ed.* **2005,** *44*, 3407-3411.

42.	Shende, V. S.; Shingote, S. K.; Deshpande, S. H.; Kelkar, A. A., *ChemistrySelect* **2016,** *1*, 2221-2224.

43.	Gutierrez, O.; Iafe, R. G.; Houk, K. N., *Org. Lett.* **2009,** *11*, 4298-4301.

44.	Yang, J.; List, B., *Org. Lett.* **2006,** *8*, 5653-5655.

45.	Zheng, C.; You, S. L., *Chem. Soc. Rev.* **2012,** *41*, 2498-2518.

46.	Zhou, S.; Fleischer, S.; Junge, K.; Beller, M., *Angew. Chem., Int. Ed.* **2011,** *50*, 5120-5124.

47.	McSkimming, A.; Bhadbhade, M. M.; Colbran, S. B., *Angew. Chem., Int. Ed.* **2013,** *52*, 3411-3416.

48.	Hohn, M.; Bornscheuer, U. T., *ChemCatChem* **2009,** *1*, 42-51.

49.	Savile, C. K.; Janey, J. M.; Mundorff, E. C.; Moore, J. C.; Tam, S.; Jarvis, W. R.; Colbeck, J. C.; Krebber, A.; Fleitz, F. J. *et al.*, *Science* **2010,** *329*, 305-309.

50.	De Lange, B.; Hyett, D. J.; Maas, P. J. D.; Mink, D.; van Assema, F. B. J.; Sereinig, N.; de Vries, A. H. M.; de Vries, J. G., *ChemCatChem* **2011,** *3*, 289-292.

51.	Kohls, H.; Steffen-Munsberg, F.; Hohne, M., *Curr. Opin. Chem. Biol.* **2014,** *19*, 180-192.

52.	Mitsukura, K.; Kuramoto, T.; Yoshida, T.; Kimoto, N.; Yamamoto, H.; Nagasawa, T., *Appl. Microbiol. Biotechnol.* **2013,** *97*, 8079-8086.

53.	Vaijayanthi, T.; Chadha, A., *Tetrahedron: Asymmetry* **2008,** *19*, 93-96.

54.	Iwaki, M.; Yagi, T.; Horiike, K.; Saeki, Y.; Ushijima, T.; Nozaki, M., *Arch. Biochem. Biophys.* **1983,** *220*, 253-262.

55.	Muramatsu, H.; Mihara, H.; Kakutani, R.; Yasuda, M.; Ueda, M.; Kurihara, T.; Esaki, N., *J. Biol. Chem.* **2005,** *280*, 5329-5335.

56.	Goto, M.; Muramatsu, H.; Mihara, H.; Kurihara, T.; Esaki, N.; Omi, R.; Miyahara, I.; Hirotsu, K., *J. Biol. Chem.* **2005,** *280*, 40875-40884.

57.	Mitsukura, K.; Suzuki, M.; Tada, K.; Yoshida, T.; Nagasawa, T., *Org. Biomol. Chem.* **2010,** *8*, 4533-4535.

58.	Rodriguez-Mata, M.; Frank, A.; Wells, E.; Leipold, F.; Turner, N. J.; Hart, S.; Turkenburg, J. P.; Grogan, G., *ChemBioChem* **2013,** *14*, 1372-1379.

59. Baskar, B.; Pandian, N.; Priya, K.; Chadha, A., *Tetrahedron* **2005,** *61*, 12296-12306.

60. Padhi, S.; Titu, D.; Pandian, N.; Chadha, A., *Tetrahedron* **2006,** *62*, 5133-5140.

61. Li, H.; Williams, P.; Micklefield, J.; Gardiner, J.; Stephens, G., *Tetrahedron* **2004,** *60*, 753-758.

62. Mulder, N.; Apweiler, R.; Attwood, T. K.; Bairoch, A.; Barrell, D.; Bateman, A.; Binns, D.; Biswas, M.; Bradley, P. *et al.*, *Nucleic Acids Res.* **2003,** *31*, 315-318.

63. Bateman, A.; Coin, L.; Durbin, R.; Finn, R. D.; Hollich, V.; Griffiths-Jones, S.; Khanna, A.; Marshall, M.; Moxon, S. *et al.*, *Nucleic Acids Res.* **2004,** *32*, D138-D141.

64. Cusa, E.; Obradors, N.; Baldoma, L.; Badia, J.; Aguilar, J., *J. Bacteriol.* **1999,** *181*, 7479-7484.

65. Graupner, M.; Xu, H.; White, R., *J. Bacteriol.* **2000,** *182*, 3688-3692.

66. Yew, W.; Gerlt, J., *J. Bacteriol.* **2002,** *184*, 302-306.

67. Mitsukura, K.; Suzuki, M.; Shinoda, S.; Kuramoto, T.; Yoshida, T.; Nagasawa, T., *Biosci., Biotechnol., Biochem.* **2011,** *75*, 1778-1782.

68. Leipold, F.; Hussain, S.; Ghislieri, D.; Turner, N. J., *ChemCatChem* **2013,** *5*, 3505-3508.

69. Aleku, G.; Man, H.; France, S. P.; Leipold, F.; Hussain, S.; Toca-Gonzalez, L.; Marchington, R.; Hart, S.; Turkenburg, J. P. *et al.*, *ACS Catal.* **2016,** *6*, 3880-3889.

70. Lenz, M.; Scheller, P.; Richter, S.; Hauer, B.; Nestl, B., *Protein Expression Purif.* **2017,** *133*, 199-204.

71. Li, H.; Tian, P.; Xu, J. H.; Zheng, G. W., *Org. Lett.* **2017,** *19*, 3151-3154.

72. Fademrecht, S.; Scheller, P.; Nestl, B.; Hauer, B.; Pleiss, J., *Proteins: Struct., Funct., Bioinf.* **2016,** *84*, 600-610.

73. Wetzl, D.; Berrera, M.; Sandon, N.; Fishlock, D.; Ebeling, M.; Muller, M.; Hanlon, S.; Wirz, B.; Iding, H. *et al.*, *ChemBioChem* **2015,** *16*, 1749-1756.

74. Lenz, M.; Meisner, J.; Quertinmont, L.; Lutz, S.; Kastner, J.; Nestl, B. M., *ChemBioChem* **2017,** *18*, 253-256.

75. Holm, L.; Sander, C., *Science* **1996,** *273*, 595-602.

76. Czekster, C.; Vandemeulebroucke, A.; Blanchard, J., *Biochemistry* **2011,** *50*, 367-375.

77. Schrittwieser, J. H.; Velikogne, S.; Kroutil, W., *Adv. Synth. Catal.* **2015,** *357*, 1655-1685.

78. Brändén, C. I.; Jörnvall, H.; Eklund, H.; Furugren, B., *The Enzymes*. 3rd ed.; Academic Press: New York and London, 1975; Vol. 11., pp 104-190.

79. De Smidt, O.; Du Preez, J.; Albertyn, J., *FEMS Yeast Res.* **2008,** *8*, 967-978.

80. Elleuche, S.; Fodor, K.; Klippel, B.; Von Der Heyde, A.; Wilmanns, M.; Antranikian, G., *Appl. Microbiol. Biotechnol.* **2013,** *97*, 8963-8975.

81. Oppermann, U.; Filling, C.; Hult, M.; Shafqat, N.; Wu, X. Q.; Lindh, M.; Shafqat, J.; Nordling, E.; Kallberg, Y. *et al.*, *Chem. Biol. Interact.* **2003,** *143*, 247-253.

82. Eklund, H.; Ramaswamy, S., *Cell. Mol. Life Sci.* **2008,** *65*, 3907-3917.

83. Eklund, H.; Nordstrom, B.; Zeppezauer, E.; Soderlund, G.; Ohlsson, I.; Boiwe, T.; Soderberg, B. O.; Tapia, O.; Brändén, C. I. *et al.*, *J. Mol. Biol.* **1976,** *102*, 27-59.

84. Auld, D. S.; Bergman, T., *Cell. Mol. Life Sci.* **2008,** *65*, 3961-3970.

85. Ryde, U., *J. Comput. Aided Mol. Des.* **1996,** *10*, 153-164.

86. Korkhin, Y.; Kalb, A.; Peretz, M.; Bogin, O.; Burstein, Y.; Frolow, F., *J. Mol. Biol.* **1998,** *278*, 967-981.

87. Persson, B.; Krook, M.; Jornvall, H., *Eur. J. Biochem.* **1991,** *200*, 537-543.

88. Kavanagh, K.; Jornvall, H.; Persson, B.; Oppermann, U., *Cell. Mol. Life Sci.* **2008,** *65*, 3895-3906.

89. Filling, C.; Berndt, K. D.; Benach, J.; Knapp, S.; Prozorovski, T.; Nordling, E.; Ladenstein, R.; Jornvall, H.; Oppermann, U., *J. Biol. Chem.* **2002,** *277*, 25677-25684.

90. Theorell, H.; Chance, B., *Acta Chem. Scand.* **1951,** *5*, 1127-1144.

91. Eklund, H.; Plapp, B. V.; Samama, J. P.; Brändén, C. I., *J. Biol. Chem.* **1982,** *2571*, 14349-14358.

92. Lee, C; Bedgar, D. L.; Davin, L. B.; Lewis N. G., *Org. Biomol. Chem.,* **2013***, 11,* 1127–1134.

93. Kleifeld, O.; Frenkel, A.; Bogin, O.; Eisenstein, M.; Brumfeld, V.; Burstein, Y.; Sagi, I., *Biochemistry* **2000,** *39*, 7702-7711.

94. Levy, H.; Loewus, F.; Vennesland, B., *J. Am. Chem. Soc.* **1957,** *79*, 2949-2953.

95. Hollmann, F.; Arends, I.; Holtmann, D., *Green Chem.* **2011,** *13*, 2285-2314.

96. Faber, K., *Biotransformations in Organic Chemistry.* 6th ed.; Springer: Berlin, 2011, pp 31-313.

97. Yamazaki, Y.; Uebayasi, M.; Hosono, K., *Eur. J. Biochem.* **1989,** *184*, 671-680.

98. Yamazaki, Y.; Hosono, K., *Tetrahedron Lett.* **1989,** *30*, 5313-5314.

99. Davies, J.; Jones, J., *J. Am. Chem. Soc.* **1979,** *101*, 5405-5410.

100. Lam, L.; Gair, I.; Jones, J., *J. Org. Chem.* **1988,** *53*, 1611-1615.

101. Irwin, A. J.; Jones, J. B., *J. Am. Chem. Soc.* **1977,** *99*, 556-561.

102. Lamed, R.; Keinan, E.; Zeikus, J., *Enzyme Microb. Technol.* **1981,** *3*, 144-148.

103. Goihberg, E.; Peretz, M.; Tel-Or, S.; Dym, O.; Shimon, L.; Frolow, F.; Burstein, Y., *Biochemistry* **2010,** *49*, 1943-1953.

104. Deamici, M.; Demicheli, C.; Carrea, G.; Spezia, S., *J. Org. Chem.* **1989,** *54*, 2646-2650.

105. Drueckhammer, D. G.; Barbas, C. F.; Nozaki, K.; Wong, C. H.; Wood, C. Y.; Ciufolini, M. A., *J. Org. Chem.* **1988,** *53*, 1607-1611.

106. Keinan, E.; Sinha, S. C.; Sinhabagchi, A., *J. Org. Chem.* **1992,** *57*, 3631-3636.

107. Barzegar, A.; Moosavi-Movahedi, A.; Pedersen, J.; Miroliaei, M., *Enzyme Microb. Technol.* **2009,** *45*, 73-79.

108. Hollmann, F.; Kleeb, A.; Otto, K.; Schmid, A., *Tetrahedron: Asymmetry* **2005,** *16*, 3512-3519.

109. Hollrigl, V.; Hollmann, F.; Kleeb, A. C.; Buehler, K.; Schmid, A., *Appl. Microbiol. Biotechnol.* **2008,** *81*, 263-273.

110. Otto, K., *Ph.D. Thesis,* **2001**, Hamburg University of Technology, Hamburg.

111. Poizat, M.; Arends, I.; Hollmann, F., *J. Mol. Catal. B: Enzym.* **2010,** *63*, 149-156.

112. Iyer, R.; Bachas, L., *J. Mol. Catal. B: Enzym.* **2004,** *28*, 1-5.

113. Eckstein, M.; Daussmann, T.; Kragl, U., *Biocatal. Biotransform.* **2004,** *22*, 89-96.

114. Kohler, V.; Turner, N., *Chem. Commun.* **2015,** *51*, 450-464.

115. Lo, H. C.; Fish, R. H., *Angew. Chem., Int. Ed.* **2002,** *41*, 478-481.

116. Lo, H. C.; Ryan, J. D.; Kerr, J. B.; Clark, D. S.; Fish, R. H., *J. Organomet. Chem.* **2017,** *839*, 38-52.

117. Maret, W.; Andersson, I.; Dietrich, H.; Schneiderbernlohr, H.; Einarsson, R.; Zeppezauer, M., *Eur. J. Biochem.* **1979,** *98*, 501-512.

118. Dietrich, H.; Maret, W.; Kozlowski, H.; Zeppezauer, M., *J. Inorg. Biochem.* **1981,** *14*, 297-311.

119. Maret, W.; Zeppezauer, M.; Desideri, A.; Morpurgo, L.; Rotilio, G., *FEBS Lett.* **1981,** *136*, 72-74.

120. Andersson, I.; Maret, W.; Zeppezauer, M.; Brown, R. D.; Koenig, S. H., *Biochemistry* **1981,** *20*, 3433-3438.

121. Bill, E.; Haas, C.; Ding, X. Q.; Maret, W.; Winkler, H.; Trautwein, A. X.; Zeppezauer, M., *Eur. J. Biochem.* **1989,** *180*, 111-121.

122. Bogin, O.; Peretz, M.; Burstein, Y., *Protein Sci.* **1997,** *6*, 450-458.

123. Zeppezauer, M.; Andersson, I.; Dietrich, H.; Gerber, M.; Maret, W.; Schneider, G.; Schneiderbernlohr, H., *J. Mol. Catal.* **1984,** *23*, 377-387.

124. Kleifeld, O.; Rulisek, L.; Bogin, O.; Frenkel, A.; Havlas, Z.; Burstein, Y.; Sagi, I., *Biochemistry* **2004,** *43*, 7151-7161.

125. Vanni, A.; Pessione, E.; Anfossi, L.; Baggiani, C.; Cavaletto, M.; Gulmini, M.; Giunta, C., *J. Mol. Catal. B: Enzym.* **2000,** *9*, 283-291.

126. Hult, K.; Berglund, P., *Trends Biotechnol.* **2007,** *25*, 231-238.

127. Hederos, S.; Broo, K.; Jakobsson, E.; Kleywegt, G.; Mannervik, B.; Baltzer, L., *Proc. Natl. Acad. Sci. U.S.A.* **2004,** *101*, 13163-13167.

128. Hederos, S.; Tegler, L.; Carlsson, J.; Persson, B.; Viljanen, J.; Broo, K., *Org. Biomol. Chem.* **2006,** *4*, 90-97.

129. Rosati, F.; Roelfes, G., *ChemCatChem* **2010,** *2*, 916-927.

130. Abe, S.; Ueno, T.; Reddy, P. A. N.; Okazaki, S.; Hikage, T.; Suzuki, A.; Yamane, T.; Nakajima, H.; Watanabe, Y., *Inorg. Chem.* **2007,** *46*, 5137-5139.

131. Deuss, P. J.; Den Heeten, R.; Laan, W.; Kamer, P. C. J., *Chem. Eur. J.* **2011,** *17*, 4680-4698.

132. Ringenberg, M. R.; Ward, T. R., *Chem. Commun.* **2011,** *47*, 8470-8476.

133. Wilson, M. E.; Whitesides, G. M., *J. Am. Chem. Soc.* **1978,** *100*, 306-307.

134. Wu, Z.; Hilvert, D., *J. Am. Chem. Soc.* **1990,** *112*, 5647-5648.

135. Toscano, M. D.; Woycechowsky, K. J.; Hilvert, D., *Angew. Chem., Int. Ed.* **2007,** *46*, 3212-3236.

136. Arnold, F. H.; Volkov, A. A., *Curr. Opin. Chem. Biol.* **1999,** *3*, 54-59.

137. Reetz, M. T., *Pure Appl. Chem.* **2000,** *72*, 1615-1622.

138. Bloom, J. D.; Meyer, M. M.; Meinhold, P.; Otey, C. R.; Macmillan, D.; Arnold, F. H., *Curr. Opin. Struct. Biol.* **2005,** *15*, 447-452.

139. Deuss, P.; Popa, G.; Botting, C.; Laan, W.; Kamer, P., *Angew. Chem., Int. Ed.* **2010,** *49*, 5315-5317.

140. Key, H.; Dydio, P.; Clark, D.; Hartwig, J., *Nature* **2016,** *534*, 534-537.

141. Pordea, A.; Creus, M.; Panek, J.; Duboc, C.; Mathis, D.; Novic, M.; Ward, T. R., *J. Am. Chem. Soc.* **2008,** *130*, 8085-8088.

142. Zimbron, J. M.; Heinisch, T.; Schmid, M.; Hamels, D.; Nogueira, E. S.; Schirmer, T.; Ward, T. R., *J. Am. Chem. Soc.* **2013,** *135*, 5384-5388.

143. Schwizer, F.; Kohler, V.; Durrenberger, M.; Knorr, L.; Ward, T. R., *ACS Catal.* **2013,** *3*, 1752-1755.

144. Yamamura, K.; Kaiser, E. T., *J. Chem. Soc., Chem. Commun.* **1976**, 830-831.

145. Kaiser, E. T.; Kaiser, B. L., *Acc. Chem. Res.* **1972,** *5*, 219-224.

146. Bakker, M.; Van Rantwijk, F.; Sheldon, R., *Can. J. Chem.* **2002,** *80*, 622-625.

147. Okrasa, K.; Kazlauskas, R., *Chem. Eur. J.* **2006,** *12*, 1587-1596.

148. Fernandez-Gacio, A.; Codina, A.; Fastrez, J.; Riant, O.; Soumillion, P., *ChemBioChem* **2006,** *7*, 1013-1016.

149. Jing, Q.; Okrasa, K.; Kazlauskas, R., *Chem. Eur. J.* **2009,** *15*, 1370-1376.

150. Key, H.; Clark, D.; Hartwig, J., *J. Am. Chem. Soc.* **2015,** *137*, 8261-8268.

151. Piazzetta, P.; Marino, T.; Russo, N.; Salahub, D. R., *ACS Catal.* **2015,** *5*, 5397-5409.

152. Creus, M.; Pordea, A.; Rossel, T.; Sardo, A.; Letondor, C.; Ivanova, A.; Le Trong, I.; Stenkamp, R. E.; Ward, T. R., *Angew. Chem., Int. Ed.* **2008,** *47*, 1400-1404.

153. Pordea, A.; Ward, T. R., *Chem. Commun.* **2008**, 4239-4249.

154. Durrenberger, M.; Heinisch, T.; Wilson, Y. M.; Rossel, T.; Nogueira, E.; Knorr, L.; Mutschler, A.; Kersten, K.; Zimbron, M. J. *et al.*, *Angew. Chem., Int. Ed.* **2011,** *50*, 3026-3029.

155. Monnard, F. W.; Nogueira, E. S.; Heinisch, T.; Schirmer, T.; Ward, T. R., *Chem. Sci.* **2013,** *4*, 3269-3274.

156. Trott, O.; Olson, A. J., *J. Comput. Chem.* **2010,** *31*, 455-461.

157. Robert, N.; Bonneau, A. L.; Hoarau, C.; Marsais, F., *Org. Lett.* **2006,** *8*, 6071-6074.

158. McSkimming, A.; Bhadbhade, M.; Colbran, S. B., *Dalton Trans.* **2010,** *39*, 10581-10584.

159. Miecznikowski, J.; Crabtree, R., *Polyhedron* **2004,** *23*, 2857-2872.

160. Musa, M.; Phillips, R., *Catal. Sci. Technol.* **2011,** *1*, 1311-1323.

161. Radianingtyas, H.; Wright, P., *FEMS Microbiol. Rev.* **2003,** *27*, 593-616.

162. Karabec, M.; Lyskowski, A.; Tauber, K.; Steinkellner, G.; Kroutil, W.; Grogan, G.; Gruber, K., *Chem. Commun.* **2010,** *46*, 6314-6316.

163. Man, H.; Gargiulo, S.; Frank, A.; Hollmann, F.; Grogan, G., *J. Mol. Catal. B: Enzym.* **2014,** *105*, 1-6.

164. Burdette, D.; Vieille, C.; Zeikus, J., *Biochem. J.* **1996,** *316*, 115-122.

165. Lavandera, I.; Kern, A.; Schaffenberger, M.; Gross, J.; Glieder, A.; De Wildeman, S.; Kroutil, W., *ChemSusChem* **2008,** *1*, 431-436.

166. Stampfer, W.; Kosjek, B.; Kroutil, W.; Faber, K., *Biotechnol. Bioeng.* **2003,** *81*, 865-869.

167. Hollrigl, V.; Otto, K.; Schmid, A., *Adv. Synth. Catal.* **2007,** *349*, 1337-1340.

168. Winograd, E.; Pulido, M.; Wasserman, M., *BioTechniques* **1993,** *14*, 886-890.

169. Grossman, T.; Kawasaki, E.; Punreddy, S.; Osburne, M., *Gene* **1998,** *209*, 95-103.

170. Ferreira-Silva, B.; Lavandera, I.; Kern, A.; Faber, K.; Kroutil, W., *Tetrahedron* **2010,** *66*, 3410-3414.

171. Sharkawi, M., *Toxicol. Lett.* **1979,** *4*, 493-497.

172. Al-Karadaghi, S.; Cedergrenzeppezauer, E.; Hovmoller, S.; Petratos, K.; Terry, H.; Wilson, K., *Acta Crystallogr., Sect. D: Biol. Crystallogr.* **1994,** *50*, 793-807.

173. Heifets, A.; Lilien, R., *J. Mol. Graphics. Modell.* **2010,** *29*, 93-101.

174. Robles, V.; Durrenberger, M.; Heinisch, T.; Lledos, A.; Schirmer, T.; Ward, T. R.; Marechal, J., *J. Am. Chem. Soc.* **2014,** *136*, 15676-15683.

175. Genz, M.; Kohler, V.; Krauss, M.; Singer, D.; Hoffmann, R.; Ward, T. R.; Strater, N., *ChemCatChem* **2014,** *6*, 736-740.

176. Pordea, A., *Curr. Opin. Chem. Biol.* **2015,** *25*, 124-132.

177. Jing, Q.; Kazlauskas, R. J., *ChemCatChem* **2010**, *2*, 953-957.

178. Dunn, M., F.; Dietrich, H.; Macgibon, A., K., H.; Koerber, S., C.; Zeppezauer, M., *Biochemistry* **1982,** *21*, 354-363.

179. Guy, J.; Isupov, M.; Littlechild, J., *J. Mol. Biol.* **2003,** *331*, 1041-1051.

180. Koerber, S. C.; Macgibbon, A. K. H.; Dietrich, H.; Zeppezauer, M.; Dunn, M. F., *Biochemistry* **1983,** *22*, 3424-3431.

181. Peris, E.; Crabtree, R., *Coord. Chem. Rev.* **2004,** *248*, 2239-2246.

182. Fabrello, A.; Bachelier, A.; Urrutigoity, M.; Kalck, P., *Coord. Chem. Rev.* **2010,** *254*, 273-287.

183. Gómez-Gallego, M.; Sierra, M. A., *Chem. Rev.* **2011,** *111*, 4857-4963.

184. Blaser, H.; Pugin, B.; Spindler, F.; Thommen, M., *Acc. Chem. Res.* **2007,** *40*, 1240-1250.

185. Jantke, D.; Cokoja, M.; Pothig, A.; Herrmann, W.; Kuhn, F., *Organometallics* **2013,** *32*, 741-744.

186. Albrecht, M.; Crabtree, R. H.; Mata, J.; Peris, E., *Chem. Commun.* **2002**, 32-33.

187. Azua, A.; Finn, M.; Yi, H. N.; Dantas, A. B.; Voutchkova-Kostal, A., *ACS Sustainable Chem. Eng.* **2017,** *5*, 3963-3972.

188. Gnanamgari, D.; Sauer, E.; Schley, N.; Butler, C.; Incarvito, C.; Crabtree, R., *Organometallics* **2009,** *28*, 321-325.

189. Mata, J. A.; Poyatos, M.; Peris, E., *Coord. Chem. Rev.* **2007,** *251*, 841-859.

190. Li, Y. J.; Lei, M.; Yuan, W.; Meggers, E.; Gong, L., *Chem. Commun.* **2017,** *53*, 8089-8092.

191. Kash, P.; Sun, D.; Xi, M.; Flynn, G.; Bent, B., *Abstr. Pap. Am. Chem. Soc.* **1994,** *207*, 251-COLL.

192. Hassan, J.; Sevignon, M.; Gozzi, C.; Schulz, E.; Lemaire, M., *Chem. Rev.* **2002,** *102*, 1359-1469.

193. Evano, G.; Blanchard, N.; Toumi, M., *Chem. Rev.* **2008,** *108*, 3054-3131.

194. Beletskaya, I. P.; Cheprakov, A. V., *Coord. Chem. Rev.* **2004,** *248*, 2337-2364.

195. Sambiagio, C.; Marsden, S. P.; Blacker, A. J.; Mcgowan, P. C., *Chem. Soc. Rev.* **2014,** *43*, 3525-3550.

196. Ma, D. W.; Cai, Q. A., *Acc. Chem. Res.* **2008,** *41*, 1450-1460.

197. Goldberg, I., *Ber. Dtsch. Chem. Ges.* **1906,** *39*, 1691-1692.

198. Ley, S.; Thomas, A., *Angew. Chem., Int. Ed.* **2003,** *42*, 5400-5449.

199. Beletskaya, I.; Cheprakov, A., *Coord. Chem. Rev.* **2004,** *248*, 2337-2364.

200. Raba, A.; Anneser, M.; Jantke, D.; Cokoja, M.; Herrmann, W.; Kuhn, F., *Tetrahedron Lett.* **2013,** *54*, 3384-3387.

201. Bittermann, A.; Harter, P.; Herdtweck, E.; Hoffmann, S. D.; Herrmann, W. A., *J. Organomet. Chem.* **2008,** *693*, 2079-2090.

202. Kascatan-Nebioglu, A.; Panzner, M. J.; Tessier, C. A.; Cannon, C. L.; Youngs, W. J., *Coord. Chem. Rev.* **2007,** *251*, 884-895.

203. Bittermann, A.; Baskakov, D.; Herrmann, W. A., *Organometallics* **2009,** *28*, 5107-5111.

204. Azua, A.; Mata, J. A.; Peris, E., *Organometallics* **2011,** *30*, 5532-5536.

205. Baskakov, D.; Herrmann, W. A.; Herdtweck, E.; Hoffmann, S. D., *Organometallics* **2007,** *26*, 626-632.

206. Scheller, P. N.; Fademrecht, S.; Hofelzer, S.; Pleiss, J.; Leipold, F.; Turner, N. J.; Nestl, B. M.; Hauer, B., *ChemBioChem* **2014,** *15*, 2201-2204.

Chapter 7 Appendices

Appendix 1 - *Thermus sp* ADH (TADH) Constructs

The TADH gene inserted into a derivative of the pET-11a vector was obtained from Dr. Frank Hollmann. The plasmid was constructed by inserting the TADH gene between the EcoRIand the BamHI sites of the pET11aEco vector. pET11aEco is a derivative of pET-11a from Novagen, containing an additional EcoRI site between the NdeI and the RBS sites.

CCTCTAGAATAATTTTGTTTAACTTTAAGAAGGA**GAATTC**CT**ATG**CGCGCAGTGGTTTTTGA
AAACAAAGAGCGCGTCGCCGTCAAGGAGGTCAATGCCCCTCGCCTACAACATCCCCTAGAT
GCCCTCGTGCGCGTGCACCTGGCCGGCATATGTGGCTCGGACTTGCACCTTTACCACGGCA
AAATACCTGTTCTCCCCGGAAGTGTACTGGGCCACGAGTTCGTGGGCCAAGTGGAAGCCGT
GGGCGAAGGTATCCAAGATCTTCAGCCAGGGGACTGGGTTGTTGGACCGTTCCACATCGCC
TGTGGCACCTGCCCCTACTGCCGAAGGCACCAGTACAACCTGTGTGAACGGGGAGGCGTCT
ACGGTTATGGCCCCATGTTTGGCAATCTCCAAGGAGCCCAGGCGGAAATCCTTCGGGTTCC
CTTCAGCAACGTCAATCTCCGGAAACTGCCTCCAAACCTAAGCCCAGAACGGGCCATCTTTG
CCGGCGATATCCTCTCCACAGCCATGGAGGACTCATCCAGGGCCAGCTCCGGCCCGGTGA
TAGCGTGGCTGTCATCGGAGCGGGGCCCGTGGGATTGATGGCCATTGAAGTAGCCCAGGT
ATTGGGTGCGAGCAAAATACTTGCCATAGATCGCATTCCTGAGCGATTGGAACGCGCCGCT
TCCCTCGGCGCCATCCCCATCAACGCCGAACAAGAAATCCTGTCCGGCGAGTTCGCTCTGA
AACCAACGATGAGGGGCCAGATTTGGTCCTCGAGGCTGTAGGCGGAGCTGCCACCCTCAG
CTTGGCCCTGGAGATGGTACGCCCTGGGGGGAAGGGTATCAGCTGTTGGGGTGGATAACGC
CCCCTCCTTTCCATTCCCTTTAGCATCGGGCCTGGTCAAGGACCTAACCTTCCGTATAGGTTT
GGCCAACGTCCACCTCTACATTGATGCGGTTCTGGCCCTTTTGGCTAGCGGCCGTTTGCAAC
CGGAGCGGATTGTTTCCCACTATCTCCCCTTGGAGGAAGCTCCTCGAGGGTATGAGCTTTTT
GACCGGAAAGAAGCGCTAAAAGTCCTTTTGGTTGTCAGGGGG**TGA**TGAAAGGTGTTAAGG
GAAGGGTTCCAAACAGCGCGGGTAGGCCTGAAGGACTCGTTTCCTCTCCAACTTTACCACA
AGGCAAAGAAGTACTTCTG**GGATCC**GGCTGCTAACAAAGCCCGAAAGAA

The TADH primary sequence is shown below (the five cysteines are highlighted in yellow.). Predicted properties: MW = 37194; pI = 6.32.

MRAVVFENKERVAVKEVNAPRLQHPLDALVRVHLAGI<mark>C</mark>GSDLHLYHGKIPVLPGSVLGHEFVG
QVEAVGEGIQDLQPGDWVVGPFHIA<mark>C</mark>GT<mark>C</mark>PY<mark>C</mark>RRHQYNL<mark>C</mark>ERGGVYGYGPMFGNLQGAQAE
ILRVPFSNVNLRKLPPNLSPERAIFAGDILSTAYGGLIQGQLRPGDSVAVIGAGPVGLMAIEVAQV
LGASKILAIDRIPERLERAASLGAIPINAEQENPVRRVRSETNDEGPDLVLEAVGGAATLSLALEM
VRPGGRVSAVGVDNAPSFPFPLASGLVKDLTFRIGLANVHLYIDAVLALLASGRLQPERIVSHYLP
LEEAPRGYELFDRKEALKVLLVVRG

Appendix 2 - Primer sequences of forward and reverse primers for introduction of desired mutations (shown in red), continued over the page.

Starting protein	Mutation	Primer name	Primer Sequence (5' to 3')
WT_TADH	C38A	t112g_g113c	5'-gtccgagcca**gc**tatgccggccaggtgcacg-3' 5'-cgtgcacctggccggcata**gc**tggctcggac-3'
WT_TADH	H59A	c175g_a176c	5'-ggcccacgaactcg**gc**gcccagtacacttc-3' 5'-gaagtgtactgggc**gc**cgagttcgtgggcc-3'
WT_TADH	D152A	a455c	5'-gctgtggagaggata**g**cgccggcaaagatgg-3' 5'-ccatctttgccggcg**c**tatcctctccacagc-3'
D152A_TADH	C38Y	g113a	5'-tccgagcca**t**atatgccggccaggtgc-3' 5'-gcacctggccggcatat**a**tggctcgga-3'
C38A_TADH	H59Y	c175t_c177t	5'-cttggcccacgaactc**a**ta**g**cccagtacacttccg-3' 5'-cggaagtgtactgggc**t**at**g**agttcgtgggccaag-3'
C38A_TADH	D152Y	g454t	5'-ctgtggagaggatat**a**gccggcaaagatggc-3' 5'-gccatctttgccggc**t**atatcctctccacag-3'
C38A_TADH	S40Y	t112g_g113c c119a_g120t	5'-tggtaaaggtgcaagtc**a**tagcca**gc**tatgccggccaggtgcac-3' 5'-gtgcacctggccggcata**gc**tggct**at**gacttgcacctttacca-3'
C38A_TADH	F85Y	t254a_c255t	5'-gccacaggcgatgtg**at**acggtccaacaaccc-3' 5'-gggttgttggaccgt**at**cacatcgcctgtggc-3'
C38A_TADH	V108Y	g322t_t323a_c324t	5'-catggggccataaccgta**ata**gcctccccgttcacacag-3' 5'-ctgtgtgaacggggaggc**tat**tacggttatggccccatg-3'

	Template	Mutation	Nucleotide changes	Primer sequences
	C38A_TADH	V268Y	g802t_t803a_g804t	5'-gaaaggaggggggcgttatc**ata**cccaacagctgatacccctt-3' 5'-aagggtatcagctgttggg**tat**gataacgccccctcctttc-3'
	D152A_TADH	C38D	t112g_g113a	5'-gtccgagcca**tc**tatgccggccaggtgcacg-3' 5'-cgtgcacctggccggcata**ga**tggctcggac-3'
	C38A_TADH	H59D	c175g_c177t	5'-ttggcccacgaactc**atc**gcccagtacacttcc-3' 5'-ggaagtgtactgggc**gat**gagttcgtgggccaa-3'
	C38A_TADH	S40D	t112g_g113c_t118g c119a_g120t	5'-gtggtaaaggtgcaagtc**atc**gcca**gc**tatgccggccaggtgcacg-3' 5'-cgtgcacctggccggcata**gc**tggc**gat**gacttgcacctttaccac-3'
	C38A_TADH	F85D	t253g_t245a_c255t	5'-actgggttgttggaccg**gat**cacatcgcctgtggcac-3' 5'-gtgccacaggcgatgtg**atc**cggtccaacaacccagt-3'
	C38A_TADH	V108D	t323a_c324t	5'-ggggccataaccgta**atc**gcctccccgttcac-3' 5'-gtgaacggggaggcg**at**tacggttatggcccc-3'
	C38A_TADH	V268D	t803a_g804t	5'-aggagggggcgttatc**at**ccccaacagctgatac-3' 5'-gtatcagctgttgggg**at**gataacgccccctcct-3'

Appendix 3 - Michaelis-Menten kinetics of cyclohexanol
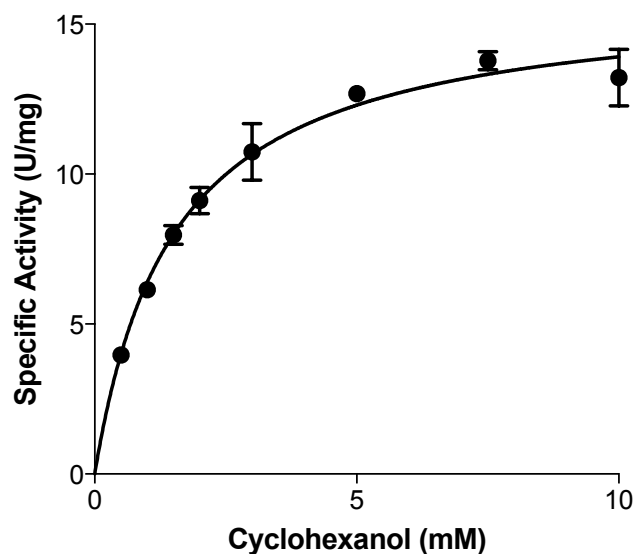
Oxidation assays were performed at 60 ^{o}C, using TADH (3 μg) cyclohexanol (0.5, 1, 1.5, 2, 3, 5, 7.5 and 10 mM) as substrate, NAD^{+} (1 mM) as cofactor, in 50 mM Glycine-NaOH buffer pH 9.0. The specific activities were determined from the slope calculated in the first 250 seconds of enzymatic activity plots and enzyme concentration. These values were used to plot the Michaelis-Menten graph. Assays were performed in triplicate with error bars shown over 1 % error.

Appendix 4 - Michaelis-Menten kinetics of cyclohexanone
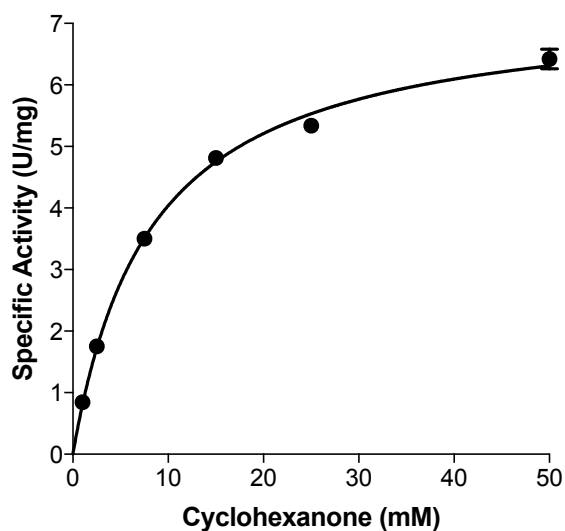
Reduction was performed at 60 ^{o}C, using TADH (1 μg), cyclohexanone (1, 2.5, 7.5 15, 25 and 50 mM) as substrate, NADH (0.1 mM) as cofactor, in 50 mM Bis-Tris buffer pH 6.0. The specific activities were determined from the slope calculated in the first 250 seconds of enzymatic activity plots and enzyme concentration. These values were used to plot the Michaelis-Menten graph. Assays were performed in triplicate with error bars shown over 1 % error.

Appendix 5 - Michaelis-Menten kinetics for cyclohexanone in the presence of different concentrations of 2-methyl-1-pyrroline, (1).
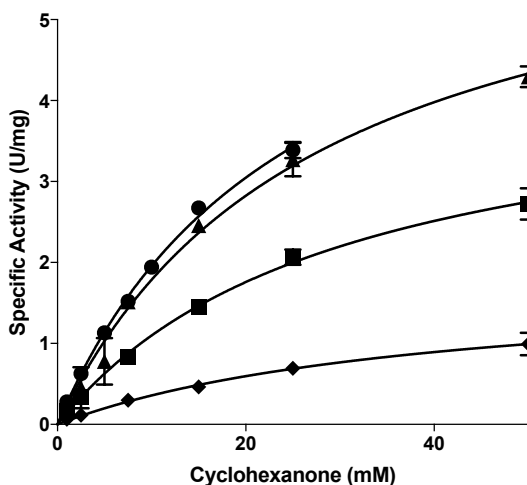
Reduction was performed at 60 ^{o}C, using TADH (1 μg), cyclohexanone (1, 2.5, 7.5 15, 25 and 50 mM) as substrate, NADH (0.1 mM) as cofactor, in 50 mM Bis-Tris buffer pH 6.0 Containing 2 % v / v ACN with containing 2-methyl-1-pyrroline, **1** as inhibitor at concentration: (●) 0 mM, (▲) 10 mM, (■) 25 mM, (◆) 50 mM. The specific activities were determined from the slope calculated in the first 250 seconds of enzymatic activity plots and enzyme concentration. Assays were performed in triplicate with error bars shown over 1 % error.

Appendix 6 - Michaelis-Menten kinetics for cyclohexanol in the presence of different concentrations of 1-methylpyrrolidine, (3).
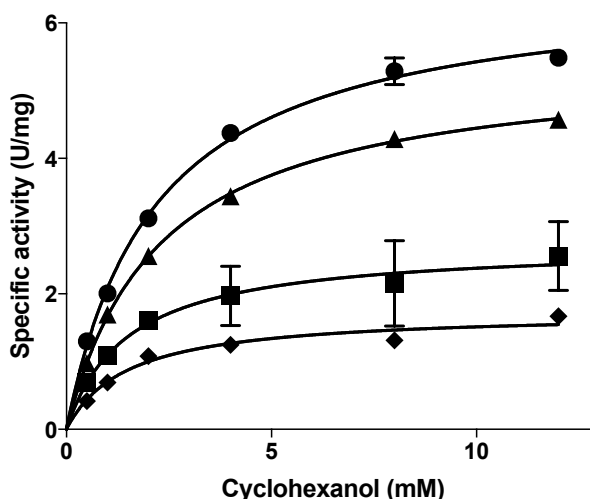
Oxidation assays were performed at 60 ^{o}C, using TADH (3 μg) cyclohexanol (0.5, 1, 2, 4, 8 and 12 mM) as substrate, NAD$^+$ (1 mM) as cofactor, in 50 mM Glycine- NaOH buffer pH 9.0 containing 5 % v / v ACN with 2-methylpyrrolidine, **3** as inhibitor at concentration: (●) 0 mM, (▲) 1 mM, (■) 5 mM, (◆) 10 mM. The specific activities were determined from the slope calculated in the first 250 seconds of enzymatic activity plots and enzyme concentration. These values were used to plot the Michaelis-Menten graph. Assays were performed in triplicate with error bars shown over 1 % error.

Appendix 7 - Michaelis-Menten illustrating the inhibitory effect of nicotinamide-functionalised ligand 21a in the reductive direction using NADH and cyclohexanone as substrates
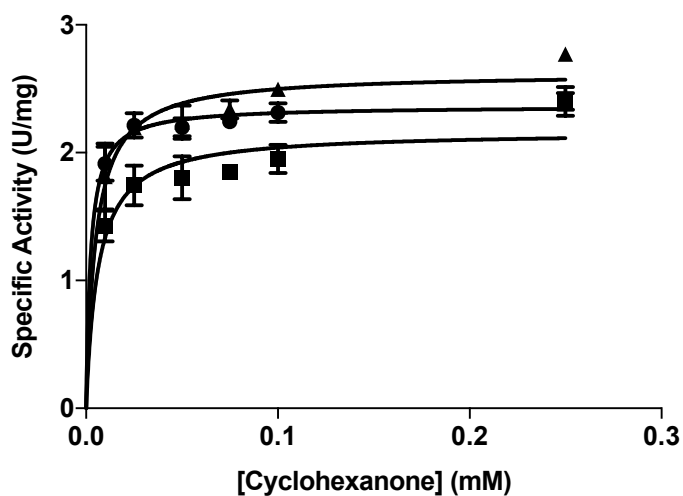
Specific activities were determined in the reductive direction at 60 ^{o}C, using TADH (5.6 μg), NADH (0.01, 0.025, 0.05, 0.075, 0.1, 0.25 mM) as substrate, cyclohexanone (20 mM) as secondary substrate, in 50 mM Bis-Tris buffer pH 6.0 containing 2 % v / v DMF with nicotinamide-functionalised ligand, **21a** as inhibitor at concentration: (●) 0 mM, (▲) 0.1 mM, (■) 0.25 mM.

Appendix 8 - Michaelis-Menten illustrating the inhibitory effect of Ir complex 24a in the reductive direction using NADH and cyclohexanone as substrates

Specific activities were determined in the reductive direction at 60 ^{o}C, using TADH (5.6 μg), NADH (0.01, 0.025, 0.05, 0.075, 0.1, 0.25 mM) as substrate, cyclohexanone (20 mM) as secondary substrate, in 50 mM Bis-Tris buffer pH 6.0 containing 5 % v / v ACN with Ir complex, **24a** as inhibitor at concentration: (●) 0 mM, (▲) 0.05 mM, (■) 0.1 mM.

^{1}H-NMR 5-chloro-*N*,*N*-diisopropylnicotinamide, 16a

^{13}C-NMR 5-chloro-*N*,*N*-diisopropylnicotinamide, 16a

¹H-NMR 4-chloro-*N*,*N*-diisopropylnicotinamide, 16b
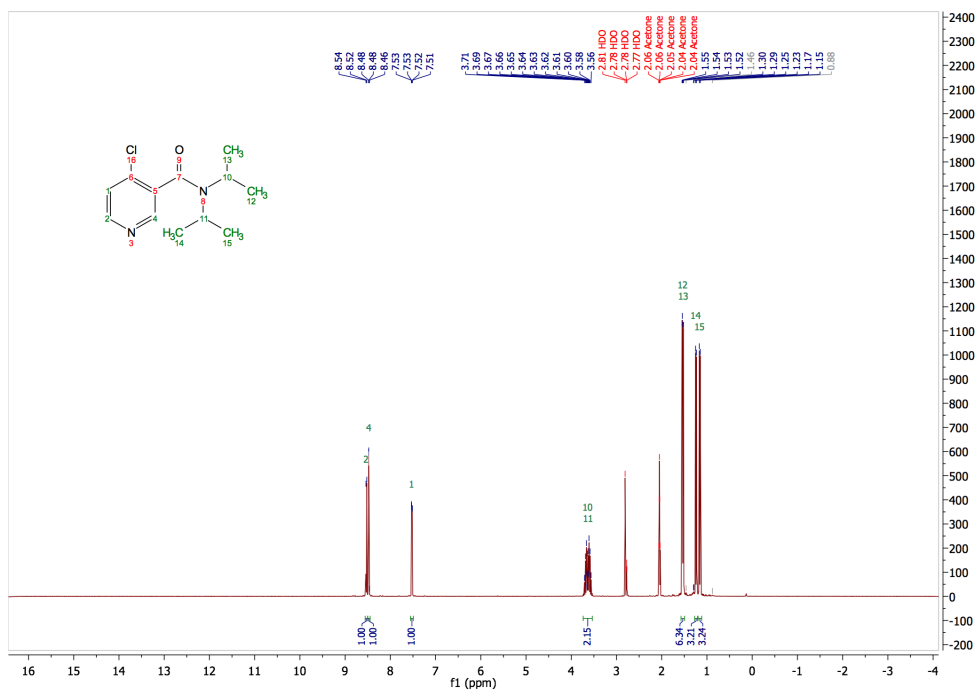
¹³C-NMR 4-chloro-*N*,*N*-diisopropylnicotinamide, 16b
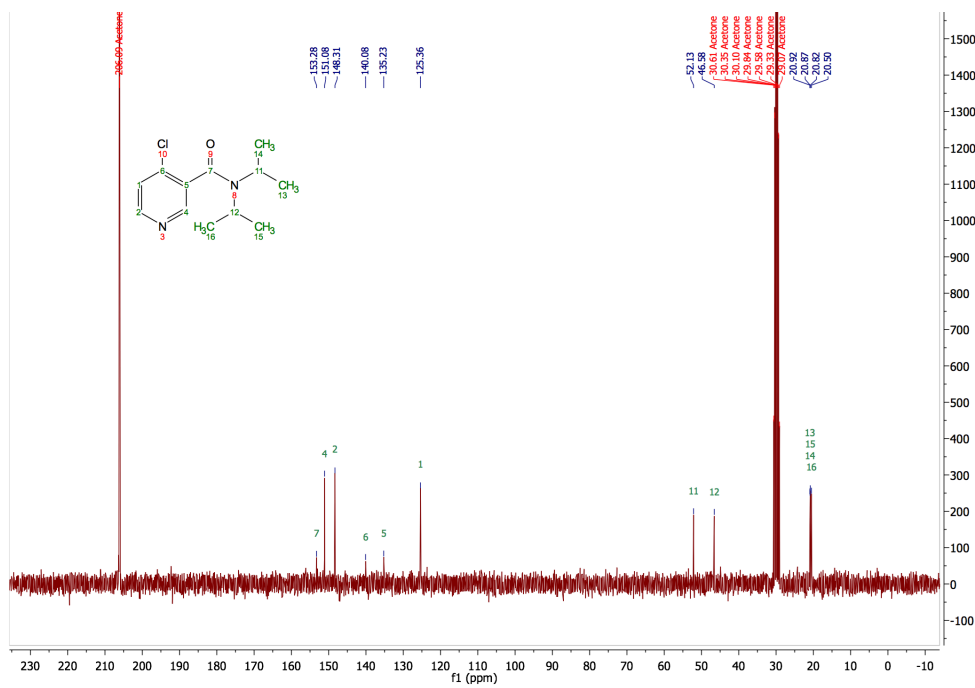
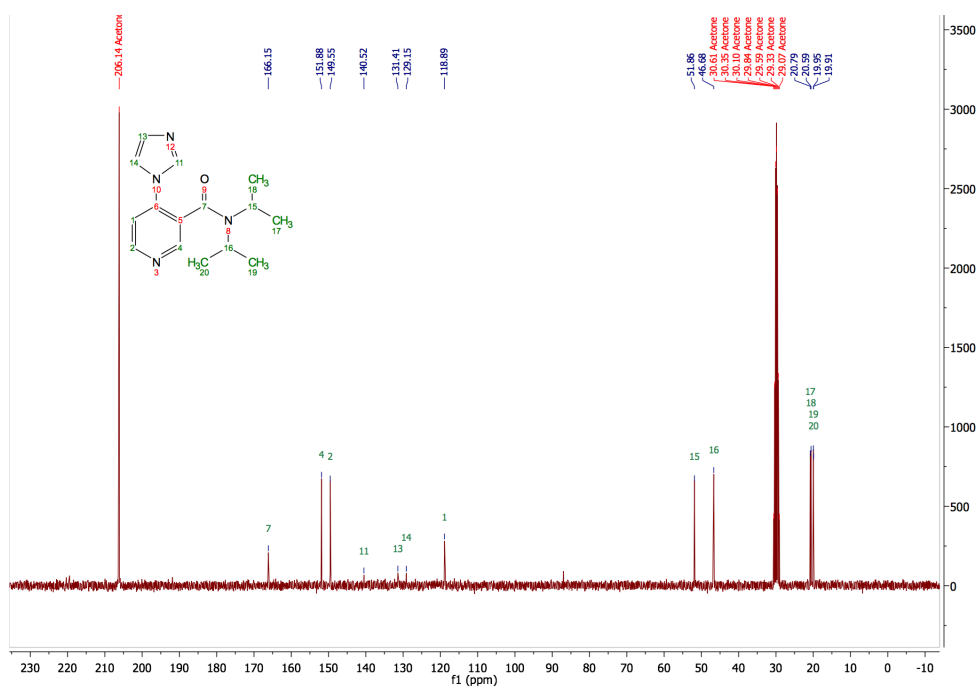# ^{1}H-NMR 5-(1 *H*-imidazol-1-yl)-*N*,*N*-diisopropylnicotinamide, 17a
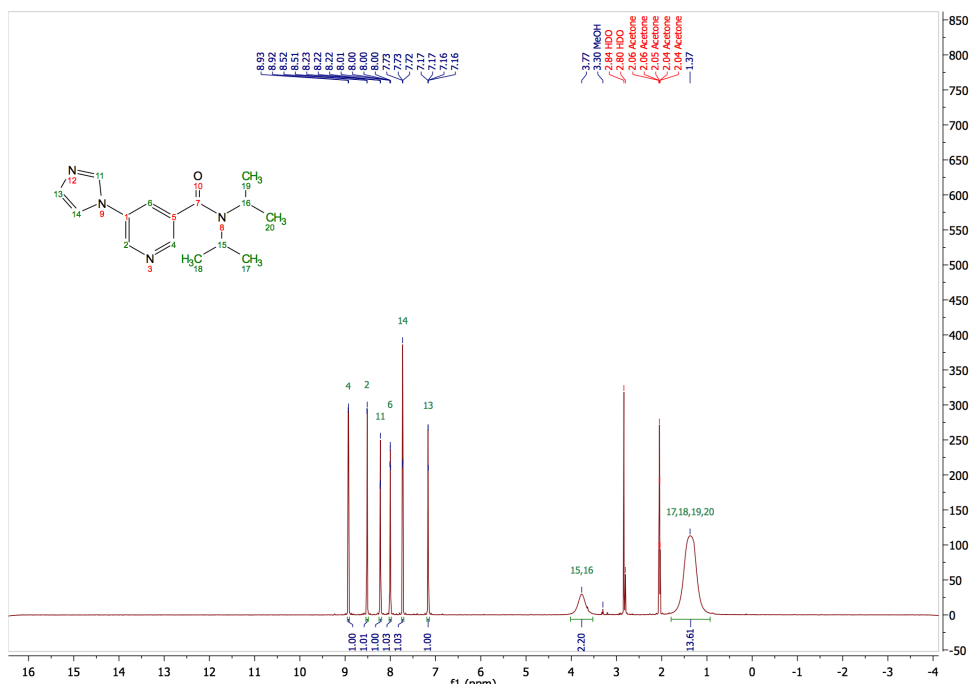
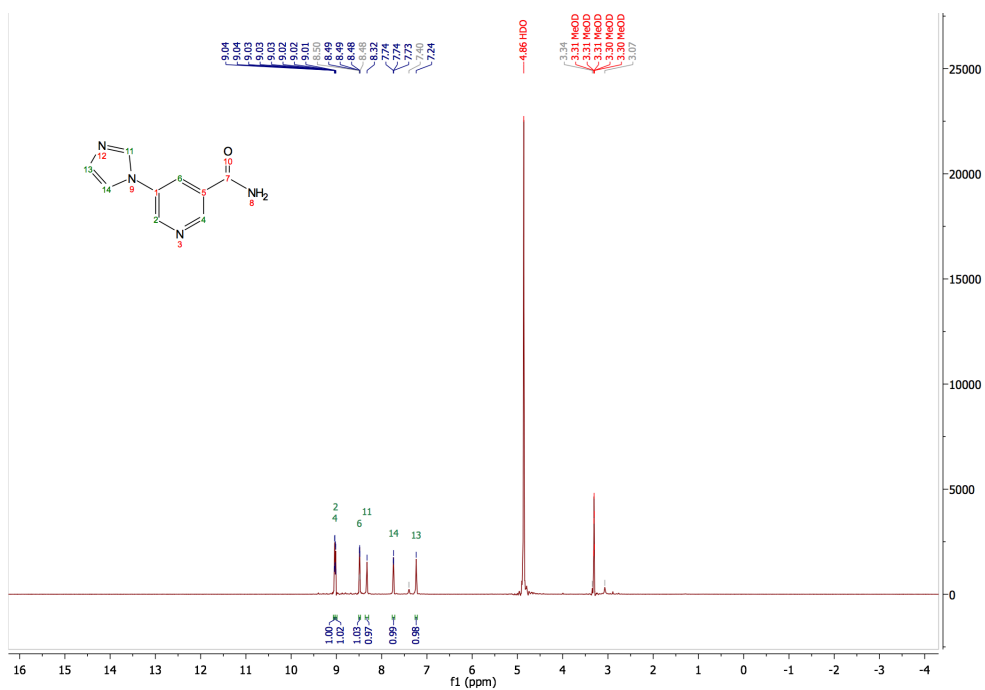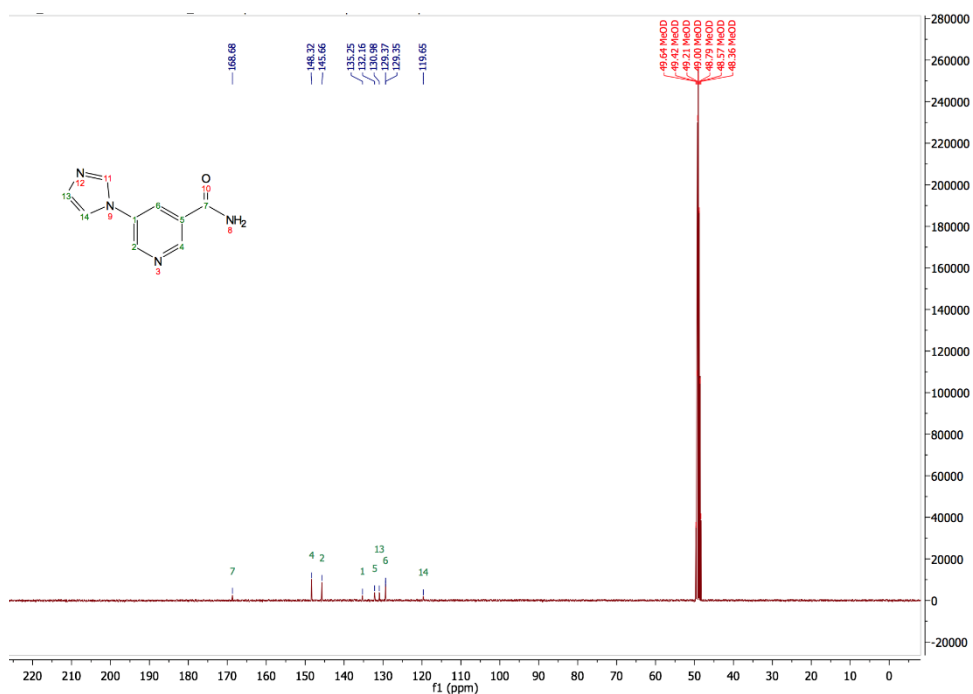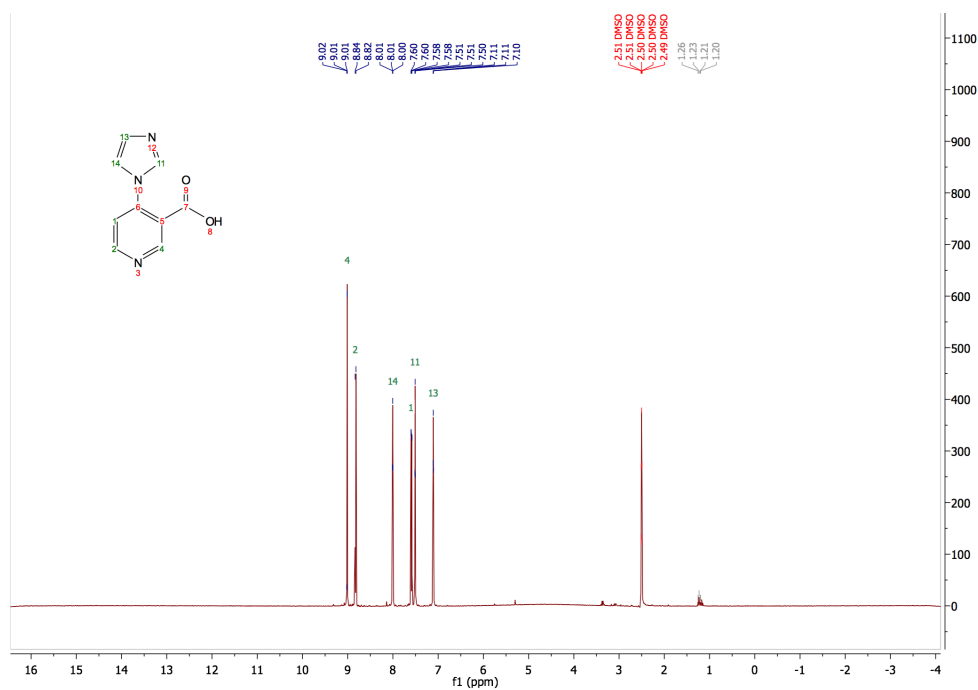# ^{13}C-NMR 5-(1 *H*-imidazol-1-yl)-*N*,*N*-diisopropylnicotinamide, 17a

a_net.PR2AN4 2.2.fid — Slot No. 56 Sample ID c SupervisorID gstep Lab Phone No. x UserID a_net
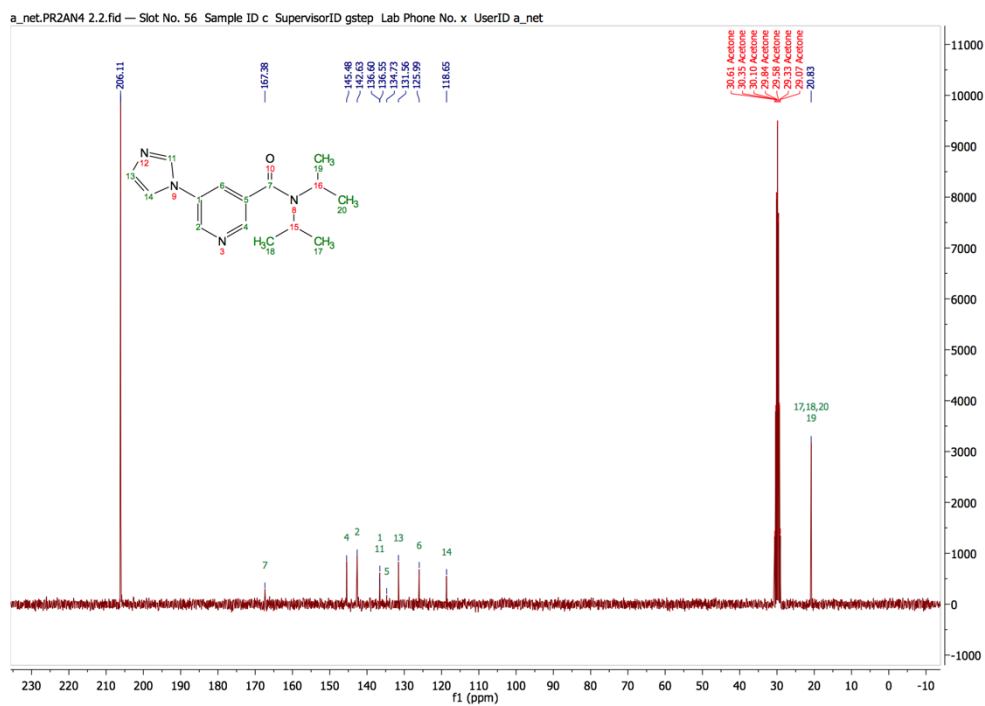
¹H-NMR 4-(1*H*-imidazol-1-yl)-*N*,*N*-diisopropylnicotinamide, 17b
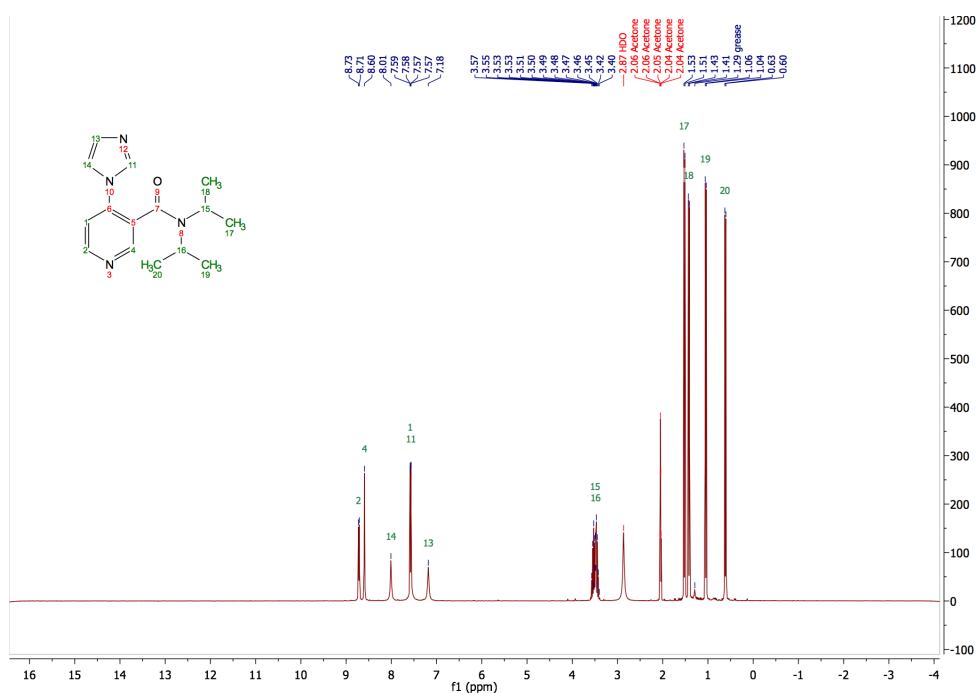
¹³C-NMR 4-(1*H*-imidazol-1-yl)-*N*,*N*-diisopropylnicotinamide, 17b

^{1}H-NMR 5-(1*H*-imidazol-1-yl)nicotinamide, 20a

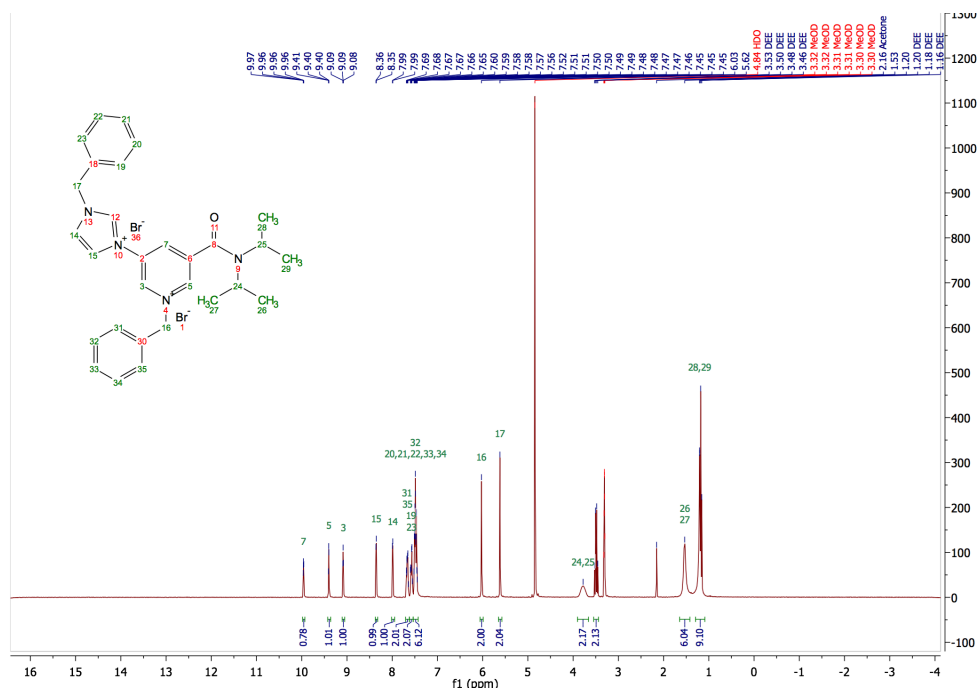# ^{13}C-NMR 5-(1*H*-imidazol-1-yl)nicotinamide, 20a

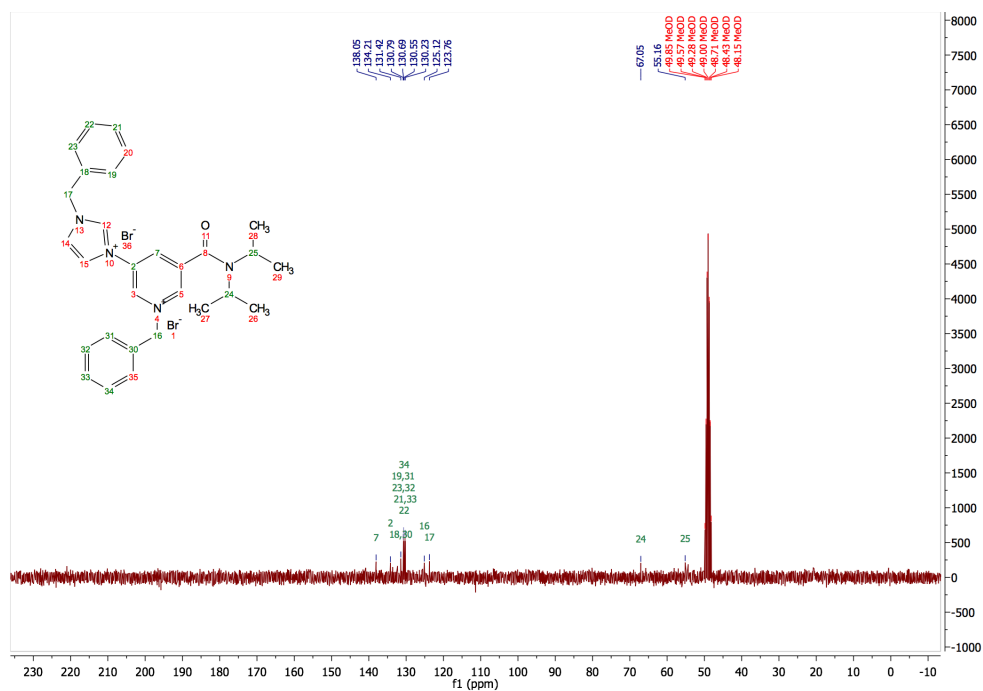# ¹H-NMR 4-(1*H*-imidazol-1-yl)nicotinic acid, 23

¹³C-NMR 4-(1*H*-imidazol-1-yl)nicotinic acid, 23
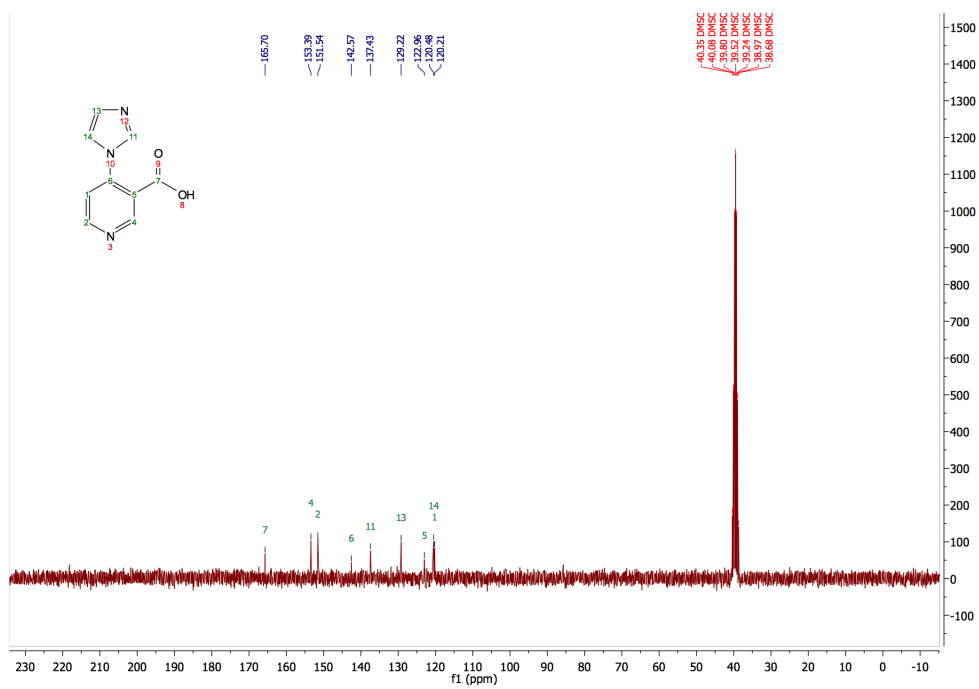
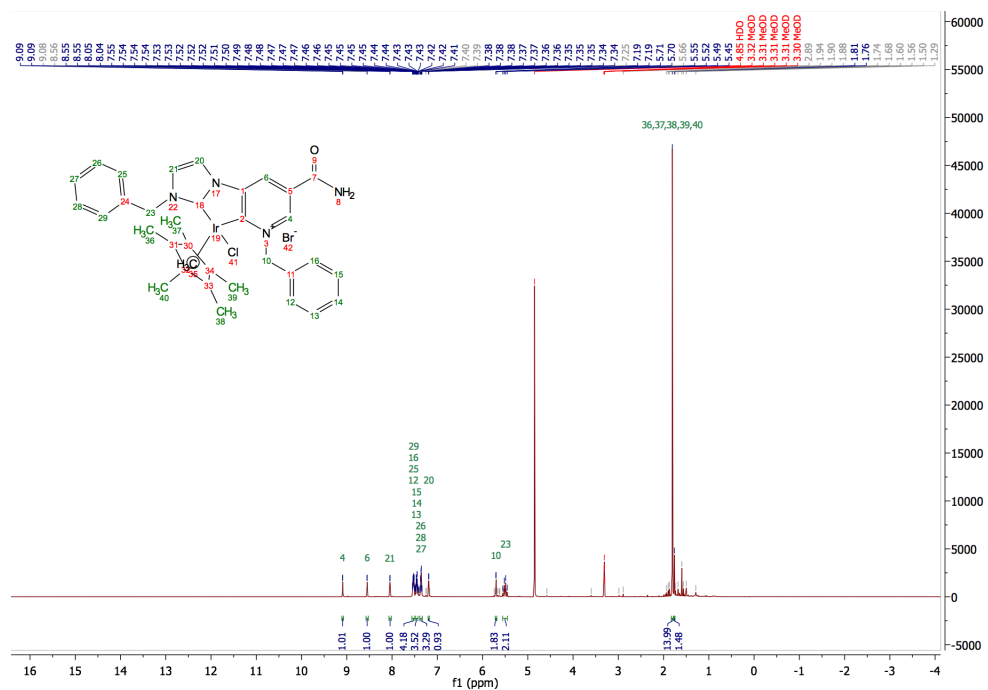## ^{1}H-NMR 1-benzyl-3-(*N*-benzylimidazol-1-yl)-5-(diisopropylcarbamoyl)pyridinium bromide, 18a

^{13}C-NMR 1-benzyl-3-(*N*-benzylimidazol-1-yl)-5-(diisopropylcarbamoyl)pyridinium bromide, 18a

^{1}H-NMR 1-benzyl-4-(*N*-benzylimidazol-1-yl)-3-(diisopropylcarbamoyl)pyridinium bromide, 18b

^{13}C-NMR 1-benzyl-4-(*N*-benzylimidazol-1-yl)-3-(diisopropylcarbamoyl)pyridinium bromide, 18b
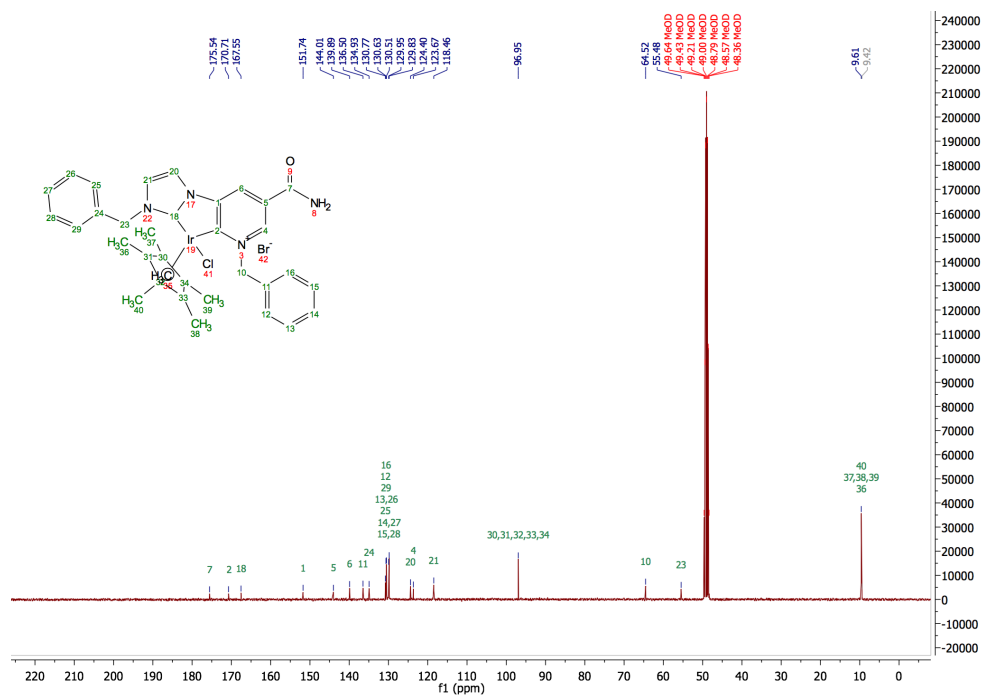
^{1}H-NMR 1-benzyl-3-(*N*-benzylimidazol-1-yl)-5-carbamoylpyridinium bromide, 21a: (or Ligand 21a)

^{13}C-NMR 1-benzyl-3-(*N*-benzylimidazol-1-yl)-5-carbamoylpyridinium bromide, 21a: (or Ligand 21a)

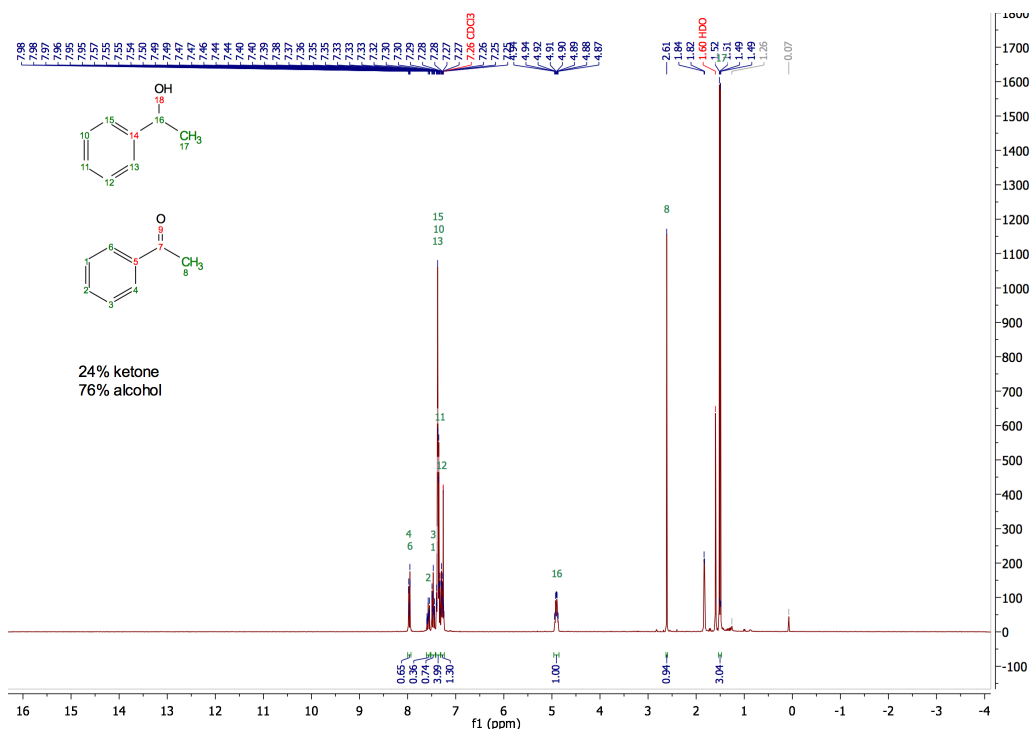# ^{1}H-NMR iridium NHC functionalised complex, 24a (or Ir complex 24a)

^{13}C-NMR iridium NHC functionalised complex, 24a (or Ir complex 24a)

¹H-NMR Transfer hydrogenation reaction with 24a showing conversion of acetophenone to 1-phenylethanol

¹H-NMR Transfer hydrogenation reaction with 24a showing conversion of 3,4-dihydroquinoline to 1,2,3,4-tetrahydroisoquinoline